

# **Structure-property relationships of polystyrene-based bead foams**

---

von der Fakultät für Ingenieurwissenschaften  
der Universität Bayreuth  
genehmigte Dissertation  
zur Erlangung des Grades

**Doktor-Ingenieur**

vorgelegt von:

Dipl.Ing. Daniel Raps

**Fachgutachter:**

Professor Dr.-Ing. Volker Altstädt  
Professor Dr. Hans-Werner Schmidt

## **Für die Nutzung dieser Dissertation gelten folgende rechtliche Bestimmungen**

- Die vorliegende Dissertation darf von der Universität Bayreuth frei im Internet angeboten werden. Eine weitere Verbreitung oder öffentliche Wiedergabe ist nicht gestattet und kann nur mit ausdrücklicher Genehmigung des Autors (Promovierten) geschehen.
- Die Vervielfältigung ist nur im Rahmen des privaten und eigenen wissenschaftlichen Gebrauchs (§ 53 UrhG) erlaubt.
- Die Publikation darf nicht bearbeitet oder in anderer Weise verändert werden.
- Der Autor hat das Recht, sein Werk, auch auszugsweise, anderweitig verfügbar zu machen und zu verbreiten.
- Für den Inhalt des Dokuments ist allein der Autor verantwortlich.
- Die Dissertation wird vertrieben durch TuTech Innovation GmbH

## **This publication (dissertation) is subject to the following terms of use:**

- The University of Bayreuth is entitled to give open access to this publication. Further publication or public broadcasting needs explicit authorization of the copyright owner (doctor).
- Copying is permitted only for private or the own scientific purposes of the person who performs copying (according to § 53 of the German Copyright Act). The copyright owner grants production of complete single copies of this publication by means of a print on demand service.
- This publication may not be edited or changed otherwise.
- The copyright owner has got the right to publish or broadcast this publication as a whole or parts thereof elsewhere.
- The author is exclusively responsible for the content of this publication.
- The dissertation is sold by TuTech Innovation GmbH

## **Vorwort**

Die vorliegende Dissertation entstand während meiner Zeit als wissenschaftlicher Mitarbeiter am Lehrstuhl für Polymere Werkstoffe der Universität Bayreuth.

Herrn Prof. Dr.-Ing. Altstädt danke ich für die Betreuung meiner Arbeit, während welcher ich unzählige wertvolle Erfahrungen in den Bereichen Kunststofftechnik, Polymerphysik und wissenschaftlichem Arbeiten sammelte. Mein Dank geht auch an Herrn Prof. Dr. Schmidt für die freundliche Übernahme des Zweitgutachtens.

Meinen Freunden und Weggefährten Dr.-Ing. Markus Brandmeier, Clemens Hanschcow, Dr.-Ing. Johannes Popp, Dr.-Ing. Thomas Köppl, Clemens Keilholz, Nick Weingart, Dominik Dörr, Tobias Standau, Dr. Aline Sanchez-Vazquez, Dr.-Ing. Kalaivani Subramaniam und Martin Demleitner danke ich für unzählige wissenschaftliche und natürlich nichtwissenschaftliche Diskussionen und eine wunderbare gemeinsame Zeit mit vielen schönen Erinnerungen.

Für die hilfreiche Unterstützung im Labor und Technikum im Rahmen meiner Dissertation und vielen weiteren Projekten richte ich meinen herzlichen Dank an Anne Lang, Marco Weniger, Alexander Brückner, Andreas Mainz, Jacqueline Uhm, Ute Kuhn, Annika Pfaffenberger, Max Löhner, Christian Brunner, Sebastian Gröschel und Markus Schirmer.

Auch meinen Bachelor- und Masterstudenten, die bei mir in zahlreichen Projekten die Welt der Kunststoffe entdeckten, gebührt mein Dank. Diese sind Georg Tauer, Holger Deutges, Florian Dresel, Dominik Dörr, Shuan Xu und Wanlu Cheng.

Schließlich möchte ich mich bei der BASF SE für die Finanzierung des Promotionsprojektes bedanken. Meinen Projektpartnern Dr. Hingmann, Dr. Däschlein, sowie Dr. Löffler gebührt in diesem Rahmen mein spezieller Dank. Ein ganz besonderer Dank geht an Dr.-Ing. Peter Gutmann für viele Diskussionen, das Lesen der Dissertation sowie viele hilfreiche Vorschläge während der Forschungstätigkeit.

Schließlich gilt mein herzlicher Dank meinen Eltern Uwe und Sylvia und meinem Großvater Hans für die immerwährende Unterstützung und Hilfe in allen Lebenslagen sowie die motivierenden Worte während der Erarbeitung meiner Dissertation.

---

## Kurzfassung

Expandierbares Polystyrol (EPS, ugs. "Styropor", "Unicell", "Styrofoam") ist einer der meist genutzten Schäume. Mehr als ein Viertel der weltweiten Schaumproduktion bezogen auf das Volumen geht in EPS. Als Partikelschaum hat EPS eine mehrskalige Morphologie aus Zellwänden und -stegen, den Zellen, den Schaumpartikeln und schließlich dem Bauteil. In diesem Zusammenhang bedingt eine Änderung der Partikelgröße auch eine Änderung der zu verschweißenden Fläche, wohingegen kleinere Zellen zu einer anderen Mikromorphologie (Zellstege und -wände) führen. Jedoch ist der Wirkzusammenhang der Morphologie und der Schaumteileigenschaften noch nicht umfassend untersucht worden. Deshalb ist es das Ziel der Arbeit Struktur-Eigenschaftsbeziehungen aufzuzeigen und deren zu Grunde liegende Mechanismen aufzuklären. Dafür werden EPS und ein Partikelschaum aus einem Blend aus Polystyrol und Polyethylen bezüglich des Einflusses der Zellgröße, Partikelgröße und Dichte auf die Mechanik sowie die Isolationseigenschaften untersucht. Daneben, wird die Verteilung des Polymers innerhalb eines Partikels durch eine variabel dicke Partikelhaut gesteuert.

Wie erwartet stellt sich die Dichte als wichtigste Einflussgröße auf die Schaumeigenschaften dar. Jedoch führt eine kleinere Zellgröße zu mehr Orientierung der Polymerketten sowie einem stärkeren Tempereffekt, was wiederum Modul, Festigkeit und Zähigkeit erhöht. Des Weiteren bestimmt die Domänengröße der Polystyrol-domänen die Zähigkeit maßgeblich, da kleinere Domänen (durch dünnere Wände oder durch einen Blend) größere plastische Deformation erlauben. Auch die Wärmeleitfähigkeit profitiert von kleineren Zellen, da der Energietransport durch IR-Strahlung reduziert wird, falls die Zellwände und Stege nicht zu dünn sind. Im Gegensatz dazu beeinflusst die Partikelgröße die Mechanik indirekt durch einen Einfluss auf die Verschweißungsqualität oder Makroporosität. In Rahmen der Untersuchung zum Einfluss der Wandstärke der Partikelhaut wurde eine Methode entwickelt mit welcher 25-mal dickere Partikelwände (nicht Zellwände!) im Vergleich zu „Standard-EPS“ erzielt werden können um einen inneren Sandwicheffekt hervorzurufen. Leider wurde aber eine geringe Verschlechterung der Eigenschaften mit dickerer Schaumhaut beobachtet.

Die gefundenen Erkenntnisse sind ein wertvoller Leitfaden um bessere Schaumeigenschaften zu erreichen. So zeigt sich, dass eigentlich spröde Kunststoffe durch dünne Zellwände und Stege oder durch Blenden inhärent zähmodifiziert werden können. Die Partikelgröße muss in einem bestimmten Bereich (EPS: 3 – 4 mm) liegen um gute Eigenschaften zu erhalten. Obwohl sich der Weg zu einem inneren Sandwicheffekt als nicht wirksam erwies, zeigte sich im Rahmen der Untersuchung, dass eine lokale Plastifizierung der Schaumhaut durch ein Lösungsmittel vor dem Formsäumen die Verschweißungsqualität und damit die Produkteigenschaften verbessert.



## Abstract

Expandable polystyrene (EPS, *coll.* “Styropor”, “Unicell”, “Styrofoam”) is one of the most used foams. It accounts for one quarter of the current foam production in terms of volume. EPS has a multi-scale morphology since EPS parts consist of many fused foamed beads. The foamed beads themselves contain cells, which are formed of walls and struts as well as the cell gas. In this frame, a variation in bead size causes a significant change of surface area, which needs to be moulded, whereas the variation in cell size leads to an altered micro-morphology (cell walls and struts). However, the effect of the multi-scale morphology on the properties has never been studied in a comprehensive manner to the knowledge of the author. Hence, the aim of the work is the establishment of structure-property relationships as well as the clarification of their fundamental mechanisms for the purpose to be able to tailor the structure for a specific application. Thus, further material and cost savings could be possible. EPS and a bead foam made from a blend of polystyrene and polyethylene were studied regarding the effects of cell size, bead size and density on the mechanical and thermal behaviour. Furthermore, the distribution of polymer within a single bead was controlled by the introduction of a solid skin around the beads.

As expected, density is the most important parameter for the foam’s properties. However, a smaller cell size at constant density in EPS leads to more orientation and annealing, which improves the modulus, strength and toughness. Furthermore, the size of polystyrene domains determines the fracture toughness as smaller domains (from smaller cells or a blend) enable more pronounced plastic deformation. Also, the thermal conductivity is improved by smaller cells as the radiative energy transfer is decreased (if the cell walls and struts are not too thin). The bead size at constant density changes the mechanical properties indirectly by affecting the moulding quality and macro-porosity. In terms of beads with a compact thick skin, a method to obtain beads with a 25 times thicker skin compared to “standard EPS” was successfully established to facilitate an internal sandwich effect. Unfortunately, a slight deterioration of the mechanical properties was observed with thicker skins.

These insights provide valuable guidelines to enhance the properties of foams. For example, brittle polymers can be inherently toughened, if the domain size is decreased sufficiently, *e.g.* by smaller cells or by blending with other polymers. The bead size should be in a suitable range (EPS: 3 – 4 mm) as both too large and too small beads result in deteriorated mechanics. Although, the approach to facilitate an internal sandwich effect was not successful, the study shows that a local plasticisation of the beads’ surfaces with a solvent can enhance the moulding quality and thus the mechanics of the product.

---

**Table of contents**

<b>1</b>	<b>Introduction and motivation</b> .....	<b>12</b>
<b>2</b>	<b>Literature-review and state-of-the-art</b> .....	<b>15</b>
	2.1 <i>Physical basics for the foaming of polymers</i> .....	15
	2.2 <i>Historical milestones in the industrial evolution of bead foams</i> .....	17
	2.3 <i>Bead foams in scientific literature</i> .....	19
	2.4 <i>The production chain of bead foams</i> .....	21
	2.5 <i>Mechanical properties of foams and bead foams</i> .....	34
	2.6 <i>Thermal conductivity</i> .....	39
	2.7 <i>Summary of the state of the art</i> .....	43
	2.8 <i>Open scientific questions</i> .....	44
<b>3</b>	<b>Aims and concept of the thesis</b> .....	<b>45</b>
<b>4</b>	<b>Materials and methods</b> .....	<b>48</b>
	4.1 <i>Materials</i> .....	48
	4.2 <i>Methods</i> .....	51
<b>5</b>	<b>Results and discussion</b> .....	<b>61</b>
	<b>Part I: Influence of foam morphology on the mechanical and thermal behaviour</b> .....	<b>61</b>
	5.1 <i>Morphological features of the studied bead foams</i> .....	61
	5.2 <i>Mechanical and fracture mechanical properties</i> .....	74
	5.3 <i>Interplay of the bead foam structure with its thermal conductivity</i> .....	110
	<b>Part II: Creation and exploration of a novel length scale in EPS: a thick skin around the beads</b> .....	<b>122</b>
	5.4 <i>The unknown morphological parameter of a thick bead skin</i> .....	122
	5.5 <i>Development of a process to create beads with a thick skin</i> .....	124
	5.6 <i>Interplay between the bead skin thickness and the morphology</i> .....	138
	5.7 <i>Effect of the bead-skin thickness on the mechanical properties</i> .....	146
	5.8 <i>Summary of the novel length scale of bead skin thickness</i> .....	156
	5.9 <i>An experimental outlook: Improvement of the steam-chest moulding process by a second ethanol treatment</i> .....	157
<b>6</b>	<b>Summary</b> .....	<b>161</b>
<b>7</b>	<b>Outlook</b> .....	<b>164</b>

---

## Table of contents

---

<b>8 Ausführliche deutsche Zusammenfassung .....</b>	<b>166</b>
<b>Appendix .....</b>	<b>176</b>
<b>References .....</b>	<b>182</b>

---

## Abbreviations

### Abbreviations

(E)PS	(Expandable) Polystyrene
EPS	EPS from extrusion with pentane and subsequent under-water pelletisation
sEPS	EPS from suspension polymerisation under presence of pentane
E-Por	Expandable bead foam made of a PS/PE-blend (PS matrix phase, PE dispersed phase)
(E)PP	(Expanded) Polypropylene
(E)PE	(Expanded) Polyethylene
(E)PBT	(Expanded) Polybutylene terephthalate
(E)TPU	(Expanded) Thermoplastic Polyurethane
(E)PC	Polycarbonate-based bead foam, possibly either expandable or expanded
(E)PEI	Polyetherimide-based bead foam, possibly either expandable or expanded
PLA	Polylactic acid
PBAT	Polybutylene adipate terephthalate
PVDF	Polyvinylidene fluoride
PVC	Polyvinylchloride
PMI	Polymethacrylimide
SCM	Steam-chest moulding
RTM	Resin transfer moulding
SEM	Scanning electron microscopy
TEM	Transmission electron microscopy
DSC	Differential scanning calorimetry
TGA	Thermo-gravimetric analysis
DMA	Dynamic mechanical analysis
CS	Cell size [ $\mu\text{m}$ ] (same as $d_c$ )
CSD	Cell size distribution (same as $d_B$ )
BS	Bead size [mm]
BSD	Bead size distribution
$d_c$	Cell diameter [ $\mu\text{m}$ ]

## Abbreviations

$d_B$	Bead diameter [mm]
$t_s$	Strut thickness [ $\mu\text{m}$ ]
$t_w$	Wall thickness [ $\mu\text{m}$ ]
$\phi_S$	Volume fraction of cell struts [%] or [1]
$\phi_W$	Volume fraction of cell walls [%] or [1]
$\rho$	Density [g/l]
$\rho_{rel}$	Relative density [%] or [1]
$F$	Force [N]
$\sigma$	Stress [MPa] or [kPa]
$\sigma_{x\%}$	Strength“ at x % strain [MPa] or [kPa]
$\varepsilon$	Strain [%]
$E$	Young’s modulus [kPa] or [MPa]
$n$	Exponent in power law relations, represents the sensitivity
$J$	J-Integral (fracture toughness) [ $\text{J}/\text{m}^2$ ]
COD	Crack opening displacement
CTOD	Crack tip opening displacement
$\dot{Q}$	Heat flow signal in DSC (per sample weight) [W/g]
$\Delta H$	Enthalpy (per sample weight) [J/g]
$T_G$	Glass transition temperature [ $^{\circ}\text{C}$ ] or [K]
$T_m$	Melting temperature [ $^{\circ}\text{C}$ ] or [K]
$\lambda$	Thermal conductivity [W/mK]
$\lambda_{tot}$	Total thermal conductivity
$\lambda_{gas}$	Gaseous contribution (conduction) of the thermal conductivity
$\lambda_{conv}$	Convective contribution of the thermal conductivity
$\lambda_{rad}$	Radiative contribution of the thermal conductivity
$\lambda_{solid}$	Solid contribution of the thermal conductivity
Mt	Megaton
Ref	Reference

## 1 Introduction and motivation

We have contact with foams everywhere in our daily life: we usually wake up on a PUR-foam mattress, we sit on car or train seats made of polymeric foam for a comfortable trip. Back home we clean our apartment with foamed cloths or sponges. We eat food packed in foams. It is evident how many polymeric foams we use each day, but do not really recognise it. Also, in the car industry, besides seats, foams are widely used in dashboards, crash absorbers or sound insulation. In aerospace, foam is needed for lightweight building and again insulation.

The characteristic properties of the foams, like superb acoustical and thermal insulation, low density and high energy absorbency for impacts enable engineers to produce more efficient, cost effective and comfortable products. Due to reduced material consumption and weight reduction, cars can both be produced and drive more efficiently. This is enabled by a reduced fuel consumption, which both saves costs and protects the environment by fewer emissions of greenhouse gases.

Those properties also express themselves in market numbers: from a perspective of weight, foams account for about 10 % of the U.S. plastic consumption. However, looking at this from a volumetric viewpoint the share is totally inverse: about 50 % of the total volume of polymers are foams assuming an average expansion ratio of 10. In terms of market volume, it is expected that the foam market will grow from 94.86 billion USD in 2017 to 126.08 billion USD in 2022 [1]. The individual market shares for various foams in the U.S. are plotted in Figure 1.

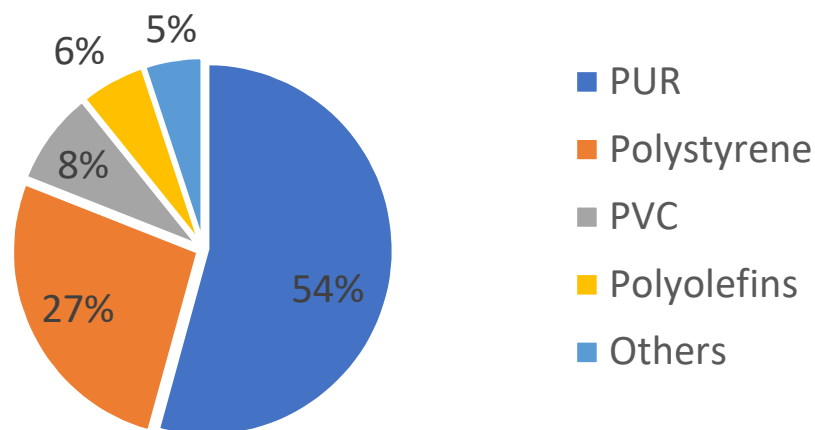


**Figure 1: Monetary market shares of various foams. EPS has about one quarter of the total market in the U.S. in 2015.**

From the polystyrene-based foams, about two thirds are covered by EPS, one third by XPS. Thus, EPS is the most widely used thermoplastic foam material and only second to polyurethane foams.

More recent surveys show that EPS has a consumption of 6.4 Mt in 2017 due to its low price (about \$ 1400 per metric ton in the U.S. and Europe) and high availability. The shares according to application are plotted in Figure 2. It can be seen that the biggest application is construction, which accounts for 59 % of the total volume in 2017, while packaging accounts for more than one quarter of the share and other applications for about 6 % [2]. Moreover, the predicted market growth is impressive. From 2017 to 2022, the average growth rate is predicted to be 2 % per year. This would result in a world-wide consumption of 7.1 Mt in 2022.

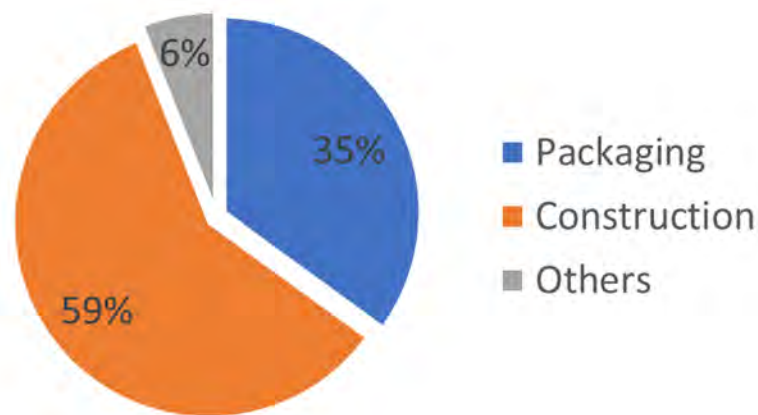


**Figure 2: Shares of EPS by application in 2017.**

EPS is widely used for the insulation of houses in the form of blocks in the construction sector thanks to its competitive thermal insulation performance. It has the second highest market share of insulation materials after glass wool [3]. Furthermore, EPS is used for acoustic insulation, for example against footfall sound. The market for insulation looks very promising in terms of growth as EPS will become important in the construction industry in large developing countries as China and India. From 2007 to 2017 it was growing by about 3 % per year. In the future, growth is predicted to be more than 2 % per year. One at the moment intensively discussed issue of EPS is its flammability. This especially became true after the fire of the Grenfell tower in the city of London in 2017 with 71 inhabitants dead and as many injured, where the polyethylene foam between aluminium sheets fuelled the ongoing fire [4]. To prevent such events, EPS is commonly equipped with flame retardants (FR), which, of course, raise the price of the product and are even harmful or dangerous themselves. For example, hexabromocyclododecane (HBCD) was a standard FR for EPS. Now it is banned worldwide as a FR due to its toxicity and costlier alternatives must be used.

In terms of packaging, EPS is generally well known for the protection of electronic devices from transport-damage (EPS crash absorbers or spacers). For the cooling of perishable goods such as drugs, food, especially fish, or human blood, EPS contributes to keep energy costs low and makes the transportation of such goods affordable and practical. However, the growth rate for packaging is lower than for construction, namely below 2 % per year. Also in areas where rigorous safety restrictions exist, such as helmets for cyclists or motor-bikers or car-seats for children, EPS is often used [5].

Other applications like the cups for beverages or loose fillings are predicted to grow even less, namely by less than 1.5 % per year. EPS is also widely used for lost-foam casting, where it is used as the core material [6]. The lost-foam casting technique allows the production of complex parts, mainly from aluminium and iron, for the automotive industry ranging from cylinder heads to motor blocks [7], [8].

In the research sector, EPS is often used to investigate the thermal properties of foams in general [3], [9], [10]. However, the special particle-structure of bead foams has never been investigated in detail until now.

It is clear, that EPS is one of the most important foam products worldwide and likely will remain so for years to come. However, resource efficiency and global warming dictate a more responsible handling of EPS. Every small effort in the improvement of the material can have a big impact on the material consumption and its life cycle. Furthermore, different applications require different material characteristics. Subsequently, the question of how the material properties can be controlled is to be answered in this work. Thus, it is paramount to understand the governing mechanisms of the mechanical and insulation properties of EPS to use this material to its full potential and to give also valuable knowledge for the development of novel amorphous bead foams such as E-PC or E-PEI.

In order to drive the research and knowledge further, the work at hand aims to contribute to the better understanding of the dependency of the properties on the morphology.

The following literature review will lay the groundwork of the thesis by identifying main open scientific questions on EPS and related products.



## **2 Literature-review and state-of-the-art**

The following chapter will critically review the existing state-of-the-art and scientific literature on foams and more specifically on bead foams. It is aimed to provide the reader with a comprehensive and concise overview on the production and processing of bead foams to establish a basic understanding of this category of foams. Subsequently, the literature on the mechanical behaviour of foams with an emphasis on bead foams is reviewed. This section also includes the subject of fracture mechanics. Finally, the literature of thermal conductivity is critically examined. Please note, that parts of this chapter were already published in [48].

### **2.1 Physical basics for the foaming of polymers**

In order to understand the morphological development of bead foams and their processing techniques, knowledge of the general background of foaming of thermoplastics is necessary. This is explained in several publications [11], [12], so the subject will be explained only briefly. The foaming process can be divided into four steps:

1. Creation of a homogeneous polymer/gas mixture
2. Nucleation of cells
3. Cell growth
4. Cell stabilisation

The first step, the homogenisation of the polymer with the blowing agent, is mainly determined by mass-transport processes. During this step, the blowing agent has to diffuse into the melt or solid bead and remain in the polymer-gas solution. The well-known second Fick's law can describe the temporal and spatial dependency of this transport. Besides temperature, diffusion also depends on pressure and gas-concentration in the polymer [13]. Consequently, diffusion is also dependent on time and space. The free volume of the polymer is important for diffusion [14] as with increasing free volume the diffusivity is increased. In contrast to diffusion, the solubility of the gas in the polymer is highly dependent on pressure. Henry's law describes the pressure dependent concentration of a dissolved blowing agent in a polymeric melt [15]. The solubility decreases exponentially with temperature for most gases. In other words, increasing temperature leads to a reduced solubility. Furthermore, high shear-rates reduce the solubility of the blowing agent in the polymer melt due the decrease in free volume caused by aligning the polymer chains [16].

The second step of the foaming process is the nucleation of cells. These nuclei then act as centre for cell growth. A sudden pressure drop causes a reduction of solubility

(the melt becomes super-saturated), thus creating a driving force to reduce the gas-content of the polymer-gas-mixture. Alternatively, a sudden drop in solubility can also be achieved by a temperature jump. Nucleation can be either homogeneous or heterogeneous. The latter mechanism dominates the nucleation process, if a solid second phase exists (*e.g.* a particle or surface of the processing equipment) and gas will diffuse to micro-voids on this surface and form a bubble.

According to nucleation theory, nucleation starts at clusters of gas-molecules inside the melt [17]. Those voids act as nucleating sites. The homogeneous nucleation rate is heavily dependent on the pressure drop. A high pressure drop leads to a high nucleation rate. This is dependent on the surface tension between polymer-melt and gas. Another nucleation process is stress, both in elongation and shear [18], [19]. Extensional stress around growing cells is responsible for pressure fluctuations, which reduces solubility and thereby increases super-saturation [20]. On the other hand, shear fields cause micro-voids within the polymer. Those mechanisms lead to an increased nucleation rate and higher cell densities.

After nucleation, cell growth takes place. During cell growth, the stored gas diffuses out of the melt to the nucleation sites. The driving force behind this process is super-saturation caused by the pressure drop or temperature increase. Typical quantities that control this process are temperature, which influences diffusion, the pressure drop rate and the actual pressure, as they change the degree of supersaturation [20]. Another important factor for foaming are the visco-elastic properties of the melt as the melt is subjected to elongational deformation during bubble growth [21].

To obtain foams with a favourable average cell size, cell size distribution and thereby desired physical properties (*e.g.* mechanical behaviour or thermal transport properties), the morphology must be stabilised and cell growth has to stop. Otherwise cell coalescence or coarsening (large cells grow at the expense of small ones) takes place and deteriorates the final foam morphology. The main factor for stabilisation is a reduction of the polymer's temperature due to which the melt's viscosity increases. As the blowing agent is diffusing out of the polymer, the viscosity increases even further, because dissolved gas in a polymer acts as a plasticising agent [15], [22]. At large elongations strain-hardening is important. Strain hardening means the rise of the transient elongational viscosity  $\eta_E(t)$  above the zero-rate elongational viscosity  $\lim_{\dot{\epsilon} \rightarrow 0}(\eta(\dot{\epsilon}))$  [23], [24]. Due to strain hardening thin sections of a cell wall are more difficult to extend than thicker ones (thinner sections are subjected to higher strains and thereby a higher

degree of stretching of chains). So the thick sections are extended preferentially, the so called self-healing effect takes place [25].

Strain-hardening can be introduced by long chain branching [26]–[29], additives with high-aspect-ratio, *e.g.* nano-particles [30]–[33] or by blends having a fibril morphology [34]. Effects countering cell stabilisation are the creation of crevices by large and fast deformations and the rupture of cell walls [12].

## **2.2 Historical milestones in the industrial evolution of bead foams**

It is noteworthy, that the sign for a registered trade name, “®”, will be left out for simplicity hereafter. The first bead foam, expandable polystyrene (EPS), was invented by Dr. Fritz Stastny in the laboratories at BASF SE and ultimately patented in 1950 [35]. EPS is used in packaging applications, *e.g.* for electronic devices, as an insulation material. A more recent (since the end of the 1990s) development is the so-called “grey” EPS, which contains graphite for lower thermal conductivity, or for sports, *e.g.* as a crash absorber in helmets. EPS can be expanded to densities between 15 g/l (packaging) and 90 g/l (crash absorbers in helmets). For thermal insulation, densities between 40 and 60 g/l proved beneficial.

More than 20 years later, namely in the mid-1970s, expanded polyethylene (EPE) was introduced to the market. EPE is used for a variety of applications, ranging from sport mats (crosslinked Neopolen E) to cushions for highly dynamic transports (*e.g.* with high amplitudes of vibrations). It can be expanded to densities between 20 and 50 g/l.

EPE was followed by expanded polypropylene (EPP) ten years after, which allows the production of parts with a density ranging between 20 and 120 g/l [36]. EPP offers superior multi-impact capabilities compared to EPS, which is the reason why it is preferably used for transport boxes/reusable packaging, *e.g.* for pizza, to ensure a long life cycle. The disadvantage of EPP compared to EPS is, that it cannot be produced as expandable beads (*e.g.* micro-granules), but only in expanded form. Hence, large volumes of “air” need to be transported (bulk density of EPP 12 – 100 g/l, bulk density EPS 700 g/l). Furthermore, the part producer cannot set a broad range of densities with EPP, which is possible for EPS in the pre-expansion step. Recently, so called “light pre-foamers” are also available for EPP, which allow the transport of beads with higher density and the adjustment of the final density at the part producer [37].

At the same time, also bead foams made of a mixture of PS and PE were developed [5]. The aim was to combine the higher chemical resistance and mechanical resilience of EPE with the processability of EPS. Similar densities as EPS can be accessed with this type of blend.

Most recently (in 2013), BASF SE introduced Infinergy, a TPU-based bead foam with part densities between 200 and 300 g/l [38]. It became widely known from the adidas Boost shoes, where ETPU is used in the midsoles in order to increase the energy-return and thus the running efficiency. Similar to EPP, it is also delivered as already expanded bead.

Due to the high density of ETPU, a complimentary bead foam with significantly lower part density (90 – 150 g/l), but a higher modulus at the cost of reduced elasticity/“energy return” was developed. It was entitled “Boost light” [39] and firstly used in the Tokyo marathon by the well-known athlete Wilson Kipsang in 2017 [40].

Besides the widely known bead foams EPS, EPE, EPP and ETPU, also two niche products exist, which, however, are rather unique. One is E-PVDF, a highly flame-retardant bead foam, which was introduced into the market for aerospace applications by Solvay in 2012 (Solef 80000 Series). The other is Rohacell TripleF, a PMI-based bead foam for applications with high mechanical and thermal requirements (*e.g.* foam cores for high-pressure RTM) with a density ranging between 70 and 200 g/l. It was introduced into the market in 2014.

As can be seen, the progress of bead foams was rather slow at the time of their invention, however, recently it has accelerated significantly and points towards the direction of technical thermoplastics such as Polybutyleneterephthalate (PBT), which was developed at the University of Bayreuth [41].

At the moment (at least partially) especially bio-based or bio-degradable bead foams are of high industrial interest. In this frame, bead foams made of pure PLA were introduced into the market, *e.g.* “BioFoam” by Symbra in 2009. Another commercially available example is Ecovio EA from BASF SE, which is made of a mixture of bio-based PLA and petrol-based but bio-degradable Ecoflex (PBAT). It is intended to substitute EPS.

In summary, the future of bead foams is very dynamic and promises very interesting and diverse applications in years to come. An overview of the current commercially available bead foam with the largest manufacturers is given Table 1.

**Table 1: List of commercially available bead foams with their density specifications, trade names, producers and their year of invention or market release.**

Bead foam	Base polymer	Minimum density / g/l	Maximum density / g/l	Trade names	Producers	Invention
EPS	PS	10	90	Stryopor, unicell, airpop,	BASF SE	1949
EPE	PE			EPERAN PE	Kaneka	1970s
-	PS/PE	12	60	Arcel, PICO-CELAN, E-Por	Nova Chemicals, Sekisui Alveo, BASF SE	1980s
EPP	EPP	20	120	Neopolen P, ARPRO, E-PERAN-PP	BASF, JSP, Kaneka	1980s
E-PMI	PMI	70	200	Rohacell Triple F	Evonik	2014
E-PVDF	PVDF	60	140	Solef 80 000	Solvay	2012
E-TPU	TPU	200	300	Infinergy	BASF SE	2013
E-PLA	PLA, PLA/PBAT	16	-	BioFoam, Eco-vio EA	Symbra, BASF SE	2009

### 2.3 Bead foams in scientific literature

Although bead foaming is an already well-established technology to produce foams, its impact in scientific literature is scarce. A literature review in the “Web of Knowledge” for the key words in the title “bead foam”, “particle foam”, “EPP” and “EPS” reveals only 75 hits in the time between 1998 and 2017. In Figure 3 a) the number of publications per year and b) the number of citations per year are plotted for the last two decades. A trend towards more research on this topic in the last five years can be observed as the number of publications now remains steadily above five per year. One reason behind this observation is the increased scientific and industrial interest in novel bead foams, *e.g.* E-PBT. As the number of publications increases also the number citations per year increases naturally as the potential for citations increases.

In literature, bead foams are usually studied with focus on their moulding conditions and at varying densities [42]–[47]. However, bead foams possess a unique multi-scale morphology, which consists of the cellular scale, bead scale and the part scale [48]. To the best knowledge of the author, these properties have never been studied in the literature until now. In order to obtain beads with variable morphology, the processing conditions during bead production have to be varied. It can be expected, that by applying different processing conditions, different orientations of the polymer chains could be induced, which should lead to different properties.

Bead foams are often used as “model-foams” to derive statements for foams in general [49], [50]. Thus, it is important to study the applicability of bead foams as “model foams” by a thorough study of their unique morphological features in order to validate this approach in the literature.

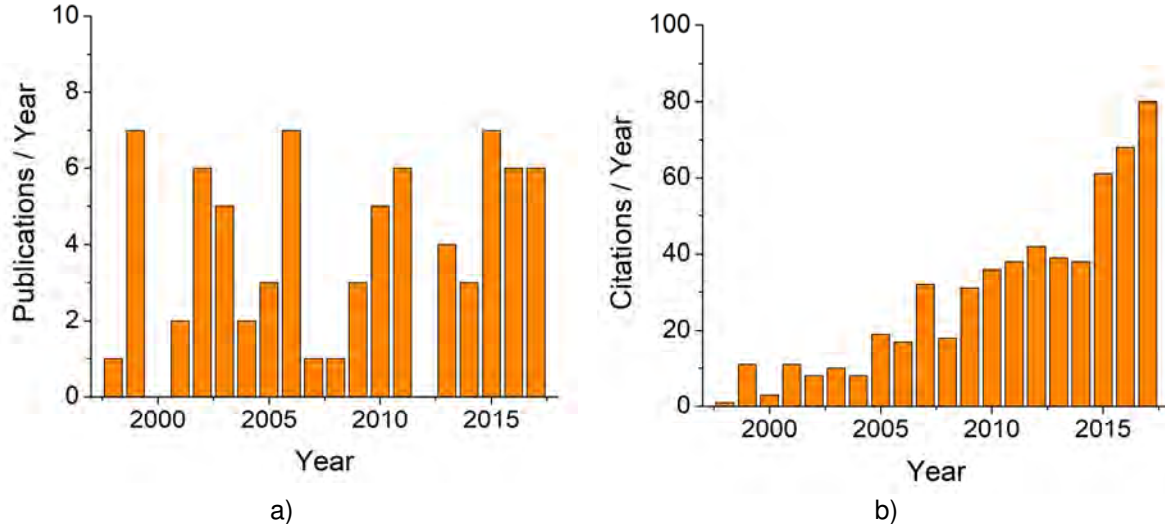


**Figure 3: Results of a literature research by year in the Web of Knowledge by using the key words “EPS”, “EPP”, “bead foam” and “particle foam” in the title: a) published items in each year and b) citations each year.**

When cell size is studied in the literature, it is usually done on foams with different density [51], [52], so it becomes very difficult, if not impossible, to distinguish between density-induced and cell size-induced changes. The currently available studies on the effect of cell size at “similar” density are conducted either at a too low expansion ratio, *i.e.* only 1.1 to 1.5 [53], or are not conclusive or incomplete, *i.e.* no information about the density at varying cell size is given [54]. Fortunately, expandable bead foams permit the variation of cell size at constant density allowing the investigation of this parameter in a separated manner. In terms of fracture behaviour, bead foams remain scarcely studied as well. For example, Stupak [43] explored the fracture toughness as a function of processing and density. However, he ignored the morphological dependencies. It is clear, that the dependency between the morphology and properties of bead foams still remains unknown in literature. This highlights the necessity of a thorough study on this topic.

The investigation of the morphological and processing properties of bead foams is important not only from a scientific standpoint. From an economical point, an optimised process would allow a more efficient production with reduced material input as well as the tailoring of the product. Therefore, it is essential to understand the effect of process-

variations on the morphology and then subsequently on the properties. The most influencing parameters must be identified in order to assess their impact on process stability.

## **2.4 The production chain of bead foams**

### **2.4.1 Production of beads**

In principle, two approaches for the production of foamed beads exist: a) the creation of expandable beads, which must be pre-expanded and b) the production of already expanded beads. Expandable beads are polymer granules in which a blowing agent (*e.g.* pentane) is trapped and the impregnated polymer granules are expanded in a separate step (*i.e.* pre-expansion step) before the actual welding-process (*i.e.* sintering). Efficient transport of the unfoamed impregnated polymer micro-granules and the control of density by the part-manufacturer are the main advantages compared to expanded beads [55]. This first approach can be applied only for amorphous thermoplastic resins, *e.g.* polystyrene, since only amorphous thermoplastics retain a blowing agent over sufficiently long durations. This arises because the storage temperature is required to be significantly below the glass transition temperature  $T_G$  of the polymer-blowing agent mixture to prevent the loss of the blowing agent due to diffusion. Pentane is a preferred blowing agent due to its high solubility and slow diffusion compared to other gases as carbon dioxide or nitrogen.

Expanded beads are produced from semi-crystalline thermoplastics, since the presence of crystalline domains prevents the storage of a blowing agent inside the solid bead as no blowing agent is stored inside the crystalline domains [56], which are also impenetrable for gases. Furthermore, semi-crystalline polymers have a rather high diffusivity of the blowing agent as the common storage temperatures are usually above the glass transition temperature  $T_G$  of the polymer-blowing agent mixture. An overview of the possible methods for producing polymer bead foams is given in Figure 4.

The standard method to produce expandable beads of polystyrene is suspension-polymerisation method with a blowing agent [57]. This process consists of two steps, namely the polymerisation, where the granules are formed, and the addition of pentane and/or other blowing agents, which diffuse into the granules [58]. After this process the beads are sieved to several fractions with a narrow size distribution and coated with antistatic agents to prevent agglomeration [57] as well as electrical discharges and thus explosions. Problems arise with the use of additives, since the additives have to meet strict requirements as they should not alter the polymerisation process and the

interfacial tension between water and styrene [59]. Another drawback is that not all polymers can be synthesised *via* suspension-polymerisation. Hereafter, EPS produced from suspension polymerisation is referred to as “sEPS”.

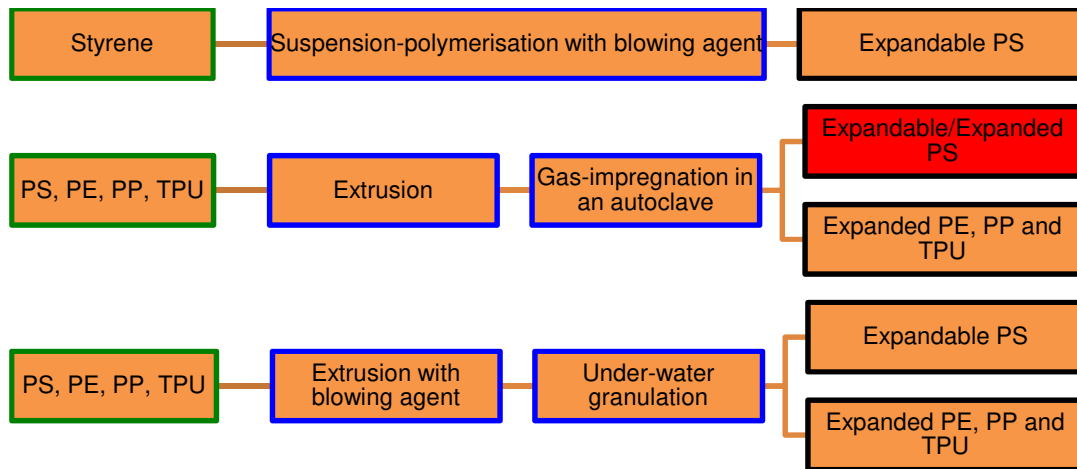


**Figure 4: Methods for the production of expandable and expanded beads. The base-material is highlighted by a green frame, the processing steps by a blue and the final bead by a black frame. Impregnation of PS in an autoclave is a time-consuming procedure and thus not applied in industry. Hence, this technique is highlighted in red [48].**

As for expanded beads, their production can be achieved *via* the impregnation of micro-granules (which contain all required additives) with the blowing agent in an autoclave. This is the main production process for expanded poly-propylene (EPP) [60]. In a first impregnation vessel, the solid PP-beads are saturated with the blowing agent close to the melting point of PP (*i.e.* 150 °C for 30 - 90 min). After the saturation step, the beads with blowing agent are released into an expansion vessel in which foaming takes place due to the pressure drop [60]. Finally, the beads are washed to remove any residual suspension stabilizer, which would inhibit proper welding of the beads [55]. For amorphous polymers, expandable beads could be produced as well by this process, if the saturation step takes place at a temperature below the glass-transition of the polymer-blowing agent-solution.



Alternatively, foam extrusion with under-water pelletizing allows the production of expandable as well as already expanded beads [61]. Throughputs up to 3000 kg/h can be realised [62]. It is schematically shown in Figure 5. In this method, a gas-loaded polymer melt is extruded through a hole-plate (or also breaker plate) into a water-stream and cut by rotating knives. If the water-pressure is above the vapour pressure of the blowing agent (for example 10.1 bar for pentane at 125 °C), the blowing agent is trapped within the solidifying polymer during cooling and expandable beads are produced. At low pressure, the dissolved gas evaporates and forms bubbles resulting in expanded beads. Advantages of this method are the exact dosing of the blowing agent(s) into the melt, a continuous and flexible process and the applicability of additives that cannot be used in suspension polymerisation [57], [60]. Also polymer blends can be processed, *e.g.* PS/PE-blends as “E-Por” from the BASF SE. Consequently, it theoretically allows the processing of any thermoplastic polymer with additives. Furthermore, the bead size is rather uniform [57]. A challenge is maintaining the required temperature, since a deviation by only a few degrees might lead to unusable products [60]. Other process parameters are the temperature and pressure of the water, the rotational speed of the knives and the temperature of the breaker plate.

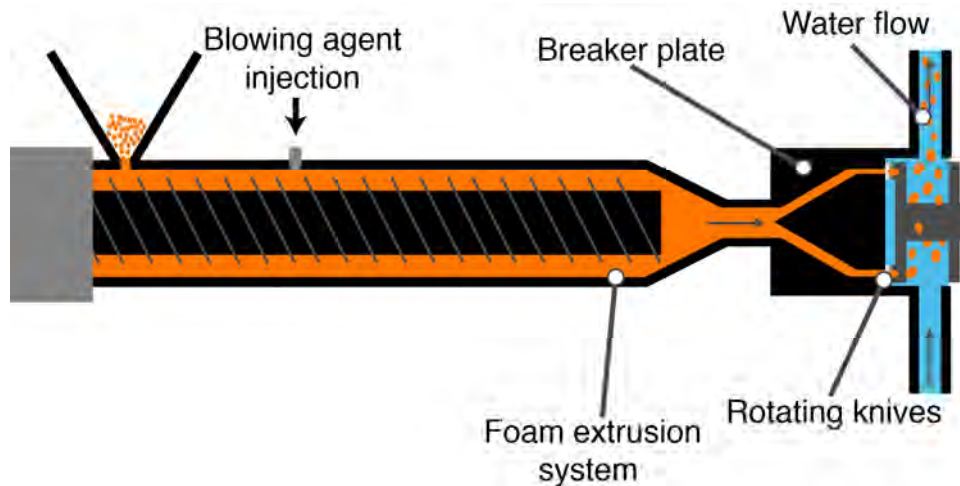


**Figure 5: Schematic of under-water pelletisation as a following unit of a foam extrusion system. For expandable beads, the water pressure is set above or at least close to the vapour pressure of the blowing agent, for expanded beads it lies at atmospheric pressure [48].**

#### 2.4.2 Processing of bead foams

In the case of EPS, the processing of bead foam parts consists of two steps. The expandable micro-granules have to be pre-expanded first and subsequently moulded to a part. In contrast already expanded beads, as EPP, only require the moulding. However, special steam-chest moulding machines must be used for EPP.

### **2.4.2.1 Pre-foaming**

During pre-foaming, the expandable micro-granules are expanded (but not yet fused) by hot steam to their desired density in a so-called pre-foamer. This process takes place at steam temperatures above the glass transition of EPS. Thus, the micro-granules are softened and foamed by the stored pentane [63].

Two types of pre-foamers are usually used in industry, a continuous and a discontinuous one. The discontinuous pre-foamer consists of a closed vessel through which steam flows. The density of the expanded beads can be adjusted by the steam pressure/temperature and the exposure time to the steam. Often an optical system in combination with gravimetric dosing is used to automatically adjust the steaming time in order to expand the beads to a certain density. After steaming, the beads are dried in a fluidised bed. The advantage of a discontinuous pre-foamer is that higher pressures compared to a continuous one can be applied. Throughputs between 85 and 3,500 kg/h at a density of 15 g/l can be achieved.

In contrast, continuous pre-foamers consist of an open container, through which steam runs in a continuous manner. The beads are conveyed into the container by a screw and transported upwards by the steam while expanding. The density of the beads is controlled *via* the residence time of the beads in the steam flow, which in turn is adjusted by the height of the pre-foamer. Subsequently, the beads are dried in a fluidised bed as well. Continuous pre-foamers require less energy and have a simpler structure compared to the discontinuous version [64]. Recently, IR-based processes have been applied to pre-foam EPS. This procedure promises smaller cells and thus better insulation as well as mechanical properties [65].

After the pre-expansion and drying, the beads cool back to room temperature. Hence, the pentane inside the cells condenses, which leads to a negative pressure compared to the ambient conditions. The beads are easily damageable in this state. Thus, it is of utmost importance, that air can diffuse into the beads (and some pentane out) to equilibrate the pressure difference. This process is called intermediate storage and takes 4 to 24 h [66] depending on the expansion ratio and EPS type. After the intermediate storage, a second or even third pre-expansion can be conducted in order to achieve lower density [64].

### 2.4.2.2 Steam-chest moulding

Parts from bead foams are made in a complex, yet efficient process, which allows the production of parts with a high geometrical degree of freedom with very low density. For the production of parts, foamed beads are welded together in a steam-chest moulding machine. The surface of the beads is molten or softened [60], using high pressure (*i.e.* high temperature) steam, which leads to an inter-diffusion of polymer chains between different beads resulting in a cohesion of the beads [44].

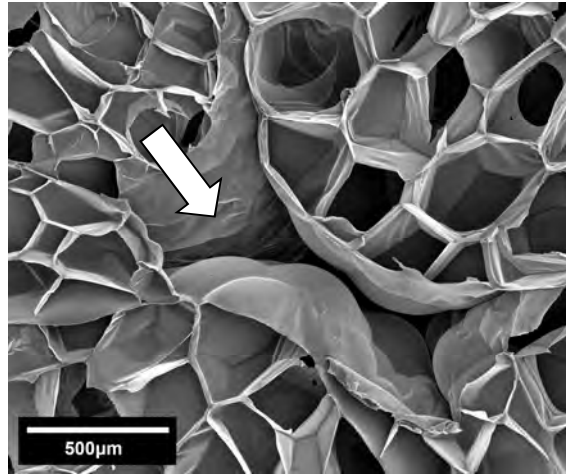


**Figure 6: Macro-voids in bead foams at the intersection of several beads [48].**

Good cohesion between the beads and a low content of macro-voids (marked with arrow in Figure 6) are necessary to ensure favourable mechanical properties [42], [43]. Macro-voids are the interstitial volume between the beads. They occur when pre-expanded beads cannot expand enough during steam-chest moulding to close the space at bead-bead intersections.

The steam-chest moulding process to fuse the pre-expanded or expanded beads together takes place in five steps. The principle steps are shown on Figure 7 and will be explained in more detail subsequently.

#### 1. Closing of the mould

The first step in the steam-chest moulding cycle is the closing of the mould.

#### 2. Filling of the mould

Foamed beads are drawn by air pressure out of a container and blown into the mould by an injector, which usually functions according to the Venturi principle. This step is critical to achieve a homogenous distribution of the beads inside the mould and is considered the most important step [67]. It is noted, that for EPP, special filling techniques (the pressure and the crack filling technique) are necessary, which are explained in more detail in [48].

### 3. Welding of the beads

After the filling process, the beads are fused together by hot steam flowing through the mould. During steaming, the beads form physical links between each other due to inter-diffusion of chains with the neighbouring beads. To ensure a high quality of welding between the beads, elevated temperatures and a sufficient steaming time are necessary [63]. Furthermore, a large contact area and high contact forces between the beads are also important to achieve good bonding. With a low contact area, force is transferred only at a few points, which leads to bad mechanical properties. On the other hand, if the contact force is low, the beads might not touch sufficiently leading to poor welding.

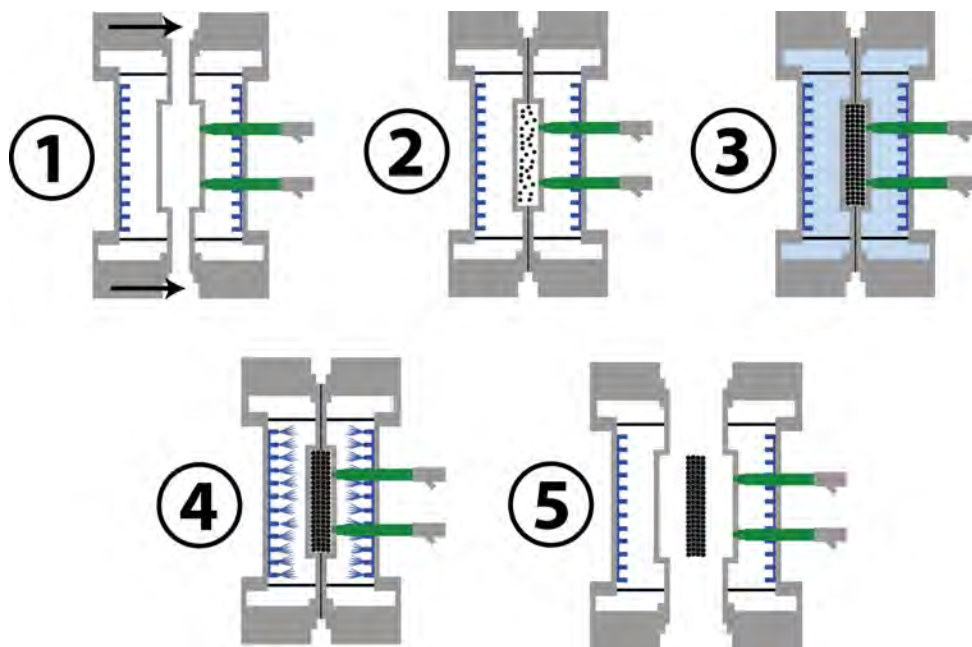


**Figure 7: Bead foam processing steps in a steam-chest moulding machine: 1: closing the mould 2: filling, 3: steaming, 4: cooling and 5: ejection of moulded part [48].**

The steaming process through the mould consists of three steps, which are shown in Figure 8. At first, the air between the beads is purged out and the mould is pre-heated. During this step, steam is flowing parallel to the mould with all the valves open (Figure 8 - 1). In the second step, the steam flows through the mould, which is called cross steaming (Figure 8 - 2). During this step, the supply and exit valves opposite to each other are open. To ensure a homogeneous temperature distribution and uniform quality of welding throughout the entire part, the mould is steamed from both sides subsequently. For EPS, steam pressures of about 1.2 bar are common, which corresponds to a steam temperature of 105 °C. In contrast to EPS, EPP requires an inlet pressure of the steam between 7 and 8 bar for EPP [68]. However, the pressure inside the mould

is lower as pressures between 2.5 and 4 bar are common [68]. Thus, a steam-temperature of up to 150 °C is achieved corresponding to steam pressure of 4 bar. Finally, steam is guided into the steam chamber while the exit valves are closed to improve surface quality by the creation of a skin (autoclave steaming, Figure 8 - 3) [69].

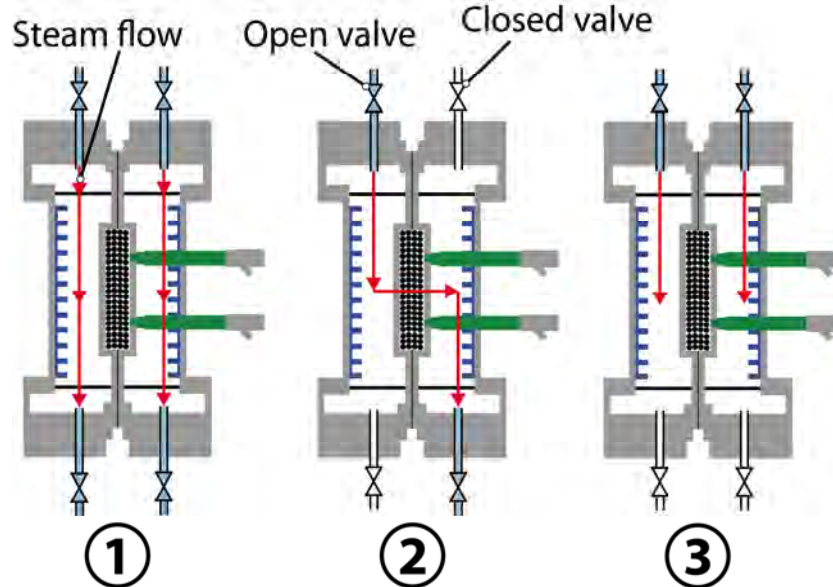


**Figure 8: Steps for steaming bead foams: 1: purging, 2: cross-steam, 3: autoclave steam [48].**

During steaming, the characteristic imprints of the steam nozzles on the part's surface are formed. The nozzles and imprints are depicted in Figure 9.

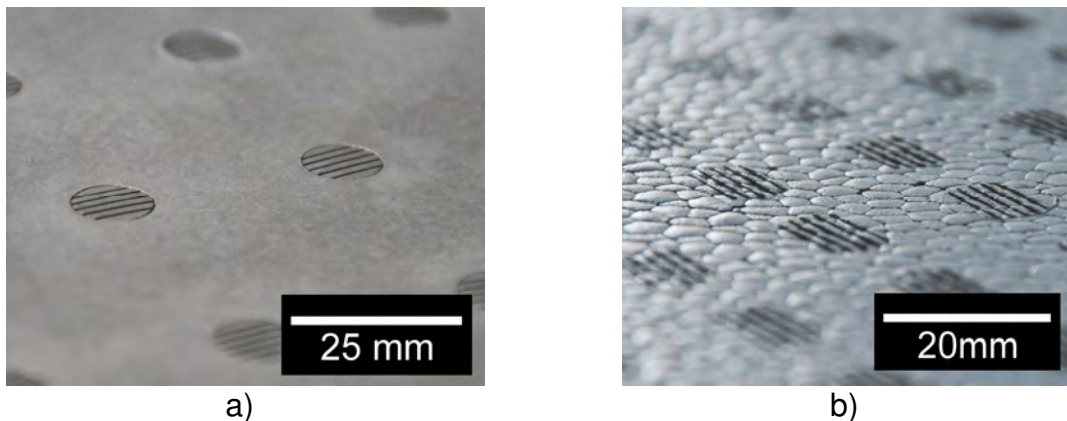


**Figure 9: a) Steam nozzles to allow the flow of steam from the steam chamber into the mould and b) their imprints on the final part (EPS) [48].**

#### 4. Cooling and stabilisation

For dimensional stability of the part, the cooling of the mould is a crucial step. For cooling, the mould is sprayed with water until a temperature of around 80 °C is reached [67]. If the part is ejected without cooling, further expansion of the beads is possible, which leads to a deviation of the original size.

### 5. Ejection of the moulded part

After moulding and cooling, the part is finally ejected. Pressurized air and mechanical ejectors are used to eject the part.

### 6. Post-processing of the final part

Shrinkage can be a major challenge at low part density. For example EPP at a density of 22 g/l can have a shrinkage up to 2.8 % [70], which comes from the condensation of steam inside the beads that leads to a lower pressure compared to the outer atmosphere. For components requiring high dimensional accuracy, a tempering step of the parts is necessary, *e.g.* at a temperature of 80 °C [71]. In this step, the original shape is restored, since air diffuses quickly into the part at this elevated temperature thus reducing the vacuum inside the beads and leading to a volume expansion. Furthermore, condensed water from the steaming step is removed as well [55].

#### **2.4.2.3 Other methods**

Instead of steam, microwaves can also be used to both pre-expand and weld beads to a foamed part [72] with a reduced energy consumption [73]. Since the polymers commonly used for bead foaming are transparent for microwaves, the beads must be coated with a microwave active substance or a microwave active blowing agent must be used for expansion. With this approach the volatile organic blowing agent n-pentane could be substituted with 2-propanol for EPS [74]. Starch-based bead foams were also prepared in the past using this method [75]–[78]. Microwave-based bead foam processing is a promising approach, especially for polymers requiring elevated temperatures for sintering, to achieve good welding without the investment in high-temperature steam-chest moulding technology, which is not a state-of-the-art technology. However, problems due to inhomogeneous moulding can occur as the intensity of the radiation drastically drops towards the thickness direction of the part. Besides micro-waves, also radio waves can be applied to mould foamed beads as described by the Kurtz GmbH [79].

Recently methods based on the rapid heating of a mould are also applied [65], which is believed to be more efficient and can be applied also for polymers requiring elevated fusion temperatures as for example PBT.



#### 2.4.2.4 Physical processes during moulding

##### Amorphous polymers

The working mechanism of inter-bead bonding is similar to a sintering process. The major difference between the two processes is that the former uses high temperature steam as an effective heating/cooling medium [44], [80], while the latter normally uses hot air [81]–[83]. During the steam-chest moulding process [84], [85], high temperature steam is injected into the mould in the three cycles explained in the previous section to soften and fuse the beads. In the case of EPS, the steam vaporises the volatile gas present in the beads and hence causes an expansion in volume. In the case of EPP, the beads need to be compressed prior to moulding. Through this process of steam-chest moulding, the empty space between the beads is filled and the inter-bead fusion is created. To improve bead foaming technologies and bead-moulded products, many researchers performed mechanical property tests of bead-moulded products based on commercially available beads, such as EPS and EPP. The formation of inter-bead bonding in EPS beads involves the diffusion of polymer chains across the bead-bead interface during the heating process in steam-chest moulding. The cooling cycle freezes the physical entanglement of the polymer chains at the bead-bead interfaces and results in the bonding of the EPS bead foams.

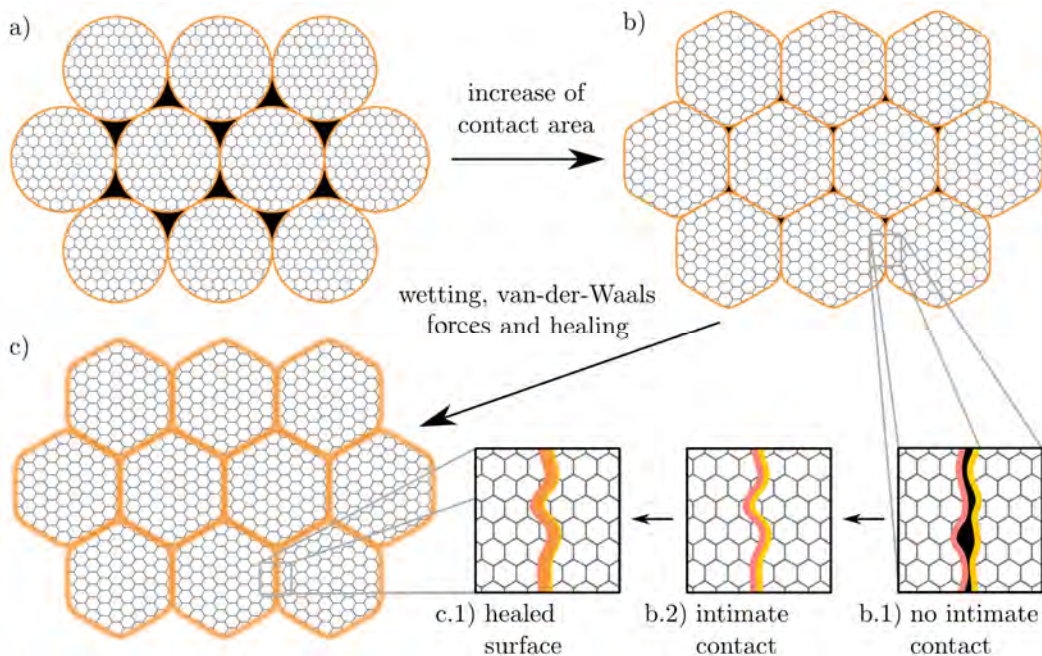


**Figure 10: Overview on the processes and mechanisms during the fusion of the beads in steam-chest moulding [88].**

Steam temperature and moulding time are two critical parameters affecting the extent of bead fusion, which significantly affects the overall mechanical properties of the moulded EPS bead foam samples [42], [44], [86], [87]. The fusion process consists of the establishment of intimate contact between the beads (Figure 10 a) and b)) and the healing/fusion of the beads (Figure 10 c)).

The establishment of an intimate contact means the reduction and removal of macro- and micro-roughness as well as cavities between the beads, as shown in Figure 11. The temporal evolution of intimate contact is dependent on pressure, temperature, time and the surface topography [89], [90]. Either the establishment of the intimate contact of the surfaces or the healing can be the limiting mechanism for bead fusion [91]. The correct choice of processing settings can not only reduce the macro-porosity in the final part, but also leads to good bonding strength between the beads.

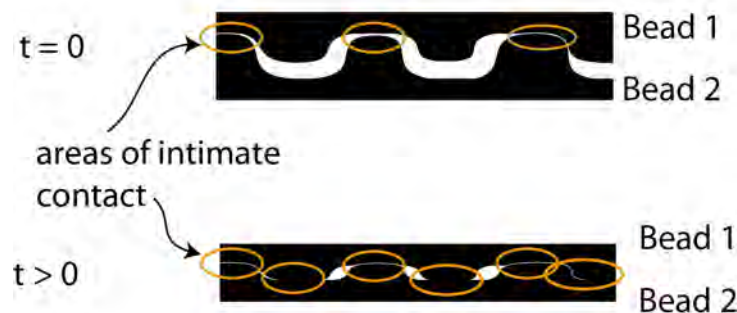


**Figure 11: Schematic process of the formation of intimate contact between the beads during steam chest moulding. Initially, the contact is limited to a few points. When the beads expand further, the contact area where inter-diffusion can occur is increased [48].**

During steaming, the beads' surfaces soften or melt. At first, only wetting and van-der-Waals-forces dominate the welding process, which would result only in weak bonding. These are followed by the actual healing by inter-diffusion of polymer chains across the interfaces between the beads [90] as depicted in Figure 12. The diffusion step is described well by several authors in the context of welding, healing of interfaces/cracks or novel measurement techniques to quantify the inter-diffusion across a surface [89], [90], [92]–[97]. A brief summary of the underlying processes, their time-scales and ultimately their relevance for bead foaming is given here.

The most well-known type of diffusion is the Fickian diffusion, which applies to small molecules (like a blowing agent) diffusing in a homogeneous matrix without entanglements. Small molecules diffusing and dissolving in a network of entangled chains cause swelling, which leads to an increased entanglement density and changes the



relaxation mechanism of the polymer resulting in non-Fickian behaviour (case II diffusion) [92].

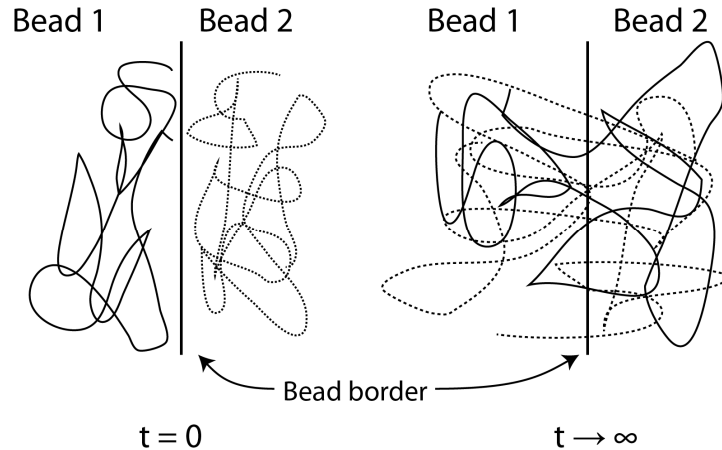


**Figure 12: The molecular arrangement before and after steam-chest moulding. A sharp interface between the beads exists at the initial state, when the beads are just touching. After sufficient steaming, polymer chains diffuse through the interface thus forming a bond [48].**

The inter-diffusion of polymers across an interface is complex and depends on molecular weight, the distribution of chain ends and temperature history [89]. It can be modelled from the reptation theory taking the so-called minor chain segments into account, which are the non-constrained segments outside of their original confining tube. At the initial stage, all chains are constrained to a tube and can move along this tube due to Brownian motion. After some time, the ends of the chain escape the tube, which are then called minor chains. This process is illustrated in Figure 13.

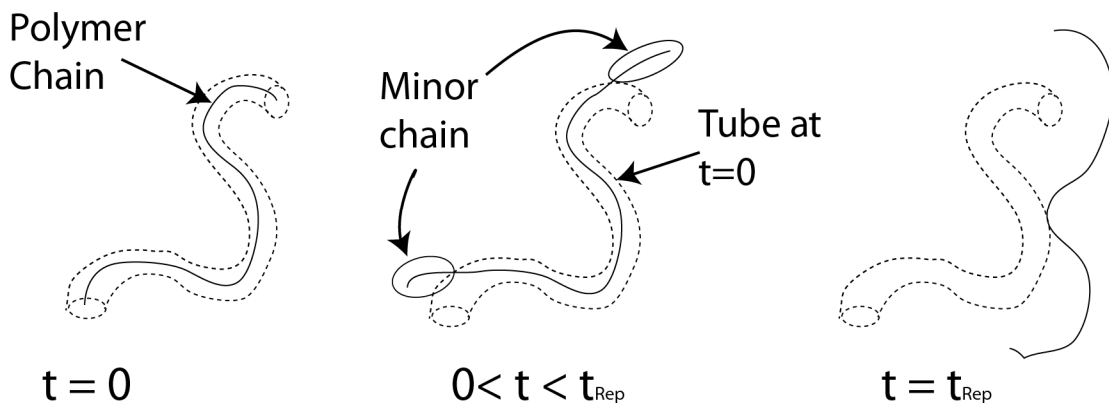


**Figure 13: Formation of minor chains by diffusion of chain ends out of their former constraining tube into a new one in the time scale of the reputation time  $t_{Rep}$  [48].**

The minor chains grow in length with time  $t$  since more segments of the chain are moving out of the constraining tube. The minor chains can move across the bead boundary, since this is a thermodynamically more favourable state, thus leading to a polymer network across the interface. For interfaces without an excess of chain ends,

which is the case in bead foaming, the time scale for the bond strength varies with  $(t/t_{Rep})^{1/2}$ , where  $t_{Rep}$  (reptation time) is the time necessary for the chain to move completely out of its original tube. This is also depicted in Figure 14. In contrast, fractured surfaces with an excess of chain ends vary with  $(t/t_{Rep})^{1/4}$ . The temperature dependency of the process follows the Arrhenius-equation. Bousmina et al. [92] observed a transition of the time scaling laws: at short times the  $t^{1/2}$ -law holds, at longer times the  $t^{1/4}$ -law. Healing is also dependent on molecular weight ( $M_w$ ) of the polymer. For a linear and mono-disperse polymer, the reptation time scales to  $t_{Rep} \sim M_w^3$  and the diffusion coefficient to  $D \sim M_w^{-2}$  [91]. Therefore, melts with lower molecular weight exhibit faster healing.

Those dependencies emphasize that both steaming time and temperature respectively must be sufficiently long and high for a given material to achieve good bonding.

Stupak et al. [43] conducted fracture toughness experiments on EPS samples, which were moulded at different temperatures and steaming times. He observed that fracture toughness varied with moulding time by  $t^{1.25}$  and moulding pressure (equivalent to steam temperature) by  $p^{6.7}$ . The time-scales differ from the ones shown above, which can be attributed to several factors. Firstly, the contact area between the beads is highly time-dependent, which changes the flow resistance of the beads for the steam and makes the degree of healing inhomogeneous. Secondly, the polymer chains are neither mono-disperse nor in thermo-dynamic equilibrium at the initial condition.

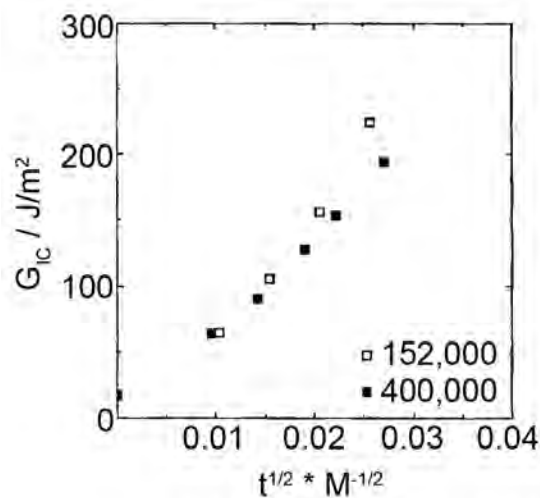


**Figure 14:** The strain energy release rate  $G_{1c}$  as an indicator of bond strength.  $G_{1c}$  is plotted vs.  $t^{1/2} * M^{-1/2}$  for the welding of polystyrene with the molecular weights 152,000 and 400,000 (Pressure Chemical) at 115 °C [90].

Rossacci et al. [48] investigated the effects of varying moulding pressure and moulding time on the tensile property of EPS parts with densities ranging from 19 to 34 kg/m<sup>3</sup>.

The EPS beads were sintered in a mould with a thickness of 60 mm. They reported that the steam temperature and moulding time are two critical parameters affecting the extent of bead fusion, which significantly affected the overall mechanical properties of the EPS moulded bead foam samples [48]. Furthermore, Zhai et al. [42], [86] showed that at high steam pressure, the tensile properties of EPP moulded parts with a thickness of 10 cm were much higher than the samples moulded at lower pressure due to improved bead-to-bead bonding. However, experience and literature shows that if the foamed beads are steamed for too long, their cell structure might collapse and deteriorate the surface property of the moulded product [63].

### Semi-crystalline polymers

It is widely believed that a good fusion of beads from semi-crystalline polymers, such as EPP, requires a double melting peak [48], [98]–[100] or at least a broad melting range [101]. The double melting peak derives from two fractions of crystals, a less perfect fraction (melting peak at lower temperature) and a perfected fraction (melting peak at higher temperature).

The higher melting peak serves the purpose of stabilising the foam structure during steam-chest moulding as it does not melt during processing and thus gives the structure sufficient strength to withstand the steam pressure. The less perfect crystals (lower melting peak) are molten during steam-chest moulding, which enables the interdiffusion of polymer chains across neighbouring bead surfaces. During the cooling step, crystallization occurs, as shown by Gensel et al. [102]. Hence, the desired steam-temperature lies between the two peaks as shown in by the grey area in Figure 15 [103]–[110].

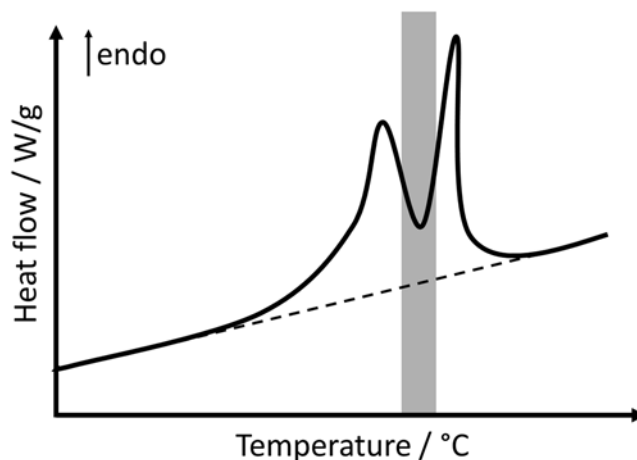


**Figure 15: Schematic representation of the first DSC heating curve of EPP showing a double melting peak.**

## 2.5 Mechanical properties of foams and bead foams

After presenting the processing cycle of bead foams, the mechanical properties of foams in general are presented briefly to lay the foundation for the understanding of the structure-property relationship of bead foams. In this frame, the most important aspects of their mechanical properties are summarised below.

### 2.5.1 Effect of the density and micro-structure on the mechanical response

#### Dependency on the density

The effect of density on the mechanics of foams is well understood in the scientific literature. The well-known Gibson-Ashby-model [111] explains the mechanical response in compression by assuming a cubic unit cell, which deforms by bending and buckling of the cell walls and struts in the linear region and by yielding and breaking phenomena in the non-linear region. In literature, a power-law function ( $y = Ax^n$ ) is also applied to describe the dependence of the foams mechanical properties on density [53]. In addition, Deschanel et al. [112] studied PU-foams in tensile mode in combination with acoustic emission analysis. It was found, that probability-density functions of time-intervals and energies of the acoustic signals also obey power-law probability distributions.

In strong contrast to the impact of foam density, the effect of the foam's morphology at a constant density is almost never studied in the scientific literature. In most publications the foam density and thus also the cell size vary [51], [52]. This indicates that there is a lot to be learned and understood as it remains an unstudied topic to the knowledge of the author.

#### Dependency on the cell size

Most publications only find a limited effect of cell size on the mechanical properties. Liu, Han and Dong [53] observed for poly( $\epsilon$ -caprolactone), that the relative modulus in uniaxial compression is independent of cell size in a range between 60 and 160  $\mu\text{m}$ . Interestingly, a significant increase in specific modulus was found for a cell size of 40  $\mu\text{m}$ . Generally, the relative modulus was affected by the cell wall thickness and cell density. However, the cell size in the studied range is less influential.

Gong et al. [54] studied a high-density (about 800  $\text{kg/m}^3$ ) micro-cellular PP-foam for its dependency of tensile and impact properties on cell size (range between 20 and 70  $\mu\text{m}$ ) as well as its cell size distribution. They found, that the strength decreases with broader cell size distribution. Furthermore, the strength increased with a reduced cell size at a constant width of the cell size distribution.

### Dependency on other micro-structural parameters

Besides the cell size, also the properties on the microscopic scale of the cell wall can affect the foam's mechanical response. Therefore, Grenestedt et al. [113]–[115] studied the effect of wavy cell walls and struts, inhomogeneously thick cell struts and an inhomogeneous cellular structure by theoretical approaches and FEM-based computer models. They found, that the modulus is decreased by an inhomogeneous cellular structure. The distribution of cell wall thicknesses only exhibited a minor effect on this property. In contrast, a waviness of the cell walls causes a distinctly reduced modulus as wavy walls can bend or buckle more easily.

### Dependency on deformation speed

Regarding the effect of deformation speed on the mechanical behaviour the work of Sorrentino *et al.* is noteworthy [116]. They studied an open-cellular PU-foam under compressive loading. They found that visco-elastic properties and the effect of cells superimpose. The effect of the gas inside the cell is important for open-cell foams above a critical rate of deformation, at which the gas has not enough time to flow out of the foam. The open-cellular foam will then have the characteristics of a closed-cell one. The interdependency between density and the speed of deformation is not conclusively shown in literature. Juntunen *et al.* [117] found increasing impact resistance with relative density, while other authors observed a maximum [52], [118].

## **2.5.2 Mechanical behaviour of bead foams**

Bead foams are often used as “model-foams” to derive generalised statements for all classes of low-density foams [49], [50]. Due to this fact, it is important to study the applicability of bead foams as “model foams” by a thorough study of their unique morphological features in order to validate this approach in the literature.

Bead foams exhibit a more complex behaviour than homogeneous foams, since additional factors affect the mechanical response and thermal properties of this class of foams. Firstly, the additional characteristic length scale of the bead size comes into play [119]. Additionally, macro-voids as interstitial volume, where three or more beads come into contact, can impair the mechanical properties. Thirdly, the unique processing of bead foams, namely steam-chest moulding, causes a gradient of density within the part [120]. Furthermore, the strength of the bead-bead interface (the welding quality), which is also controlled by steam-chest moulding, is highly influential on the mechanical properties of the moulded part.

The effect of steam-chest moulding conditions on the mechanical properties is quite well understood, as it has been studied extensively in the literature [42], [44], [46], [47], [63], [121]. With an improved quality of fusion, the tensile strength [44] as well as the fracture toughness [63] increase distinctly. The quality of fusion can be assessed from the fracture surfaces of the samples. In principle, bead foams can fail by two mechanisms: 1) fracture through one bead, which is called cellular- or intra-bead fracture, and 2) fracture along the interface of two adjacent beads, also called inter-bead fracture. These two mechanisms are shown in Figure 16.

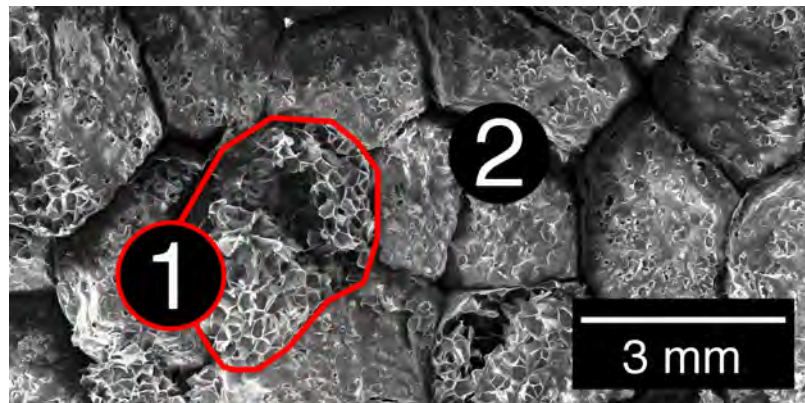


**Figure 16: Fracture pattern in bead foams: 1) intra-bead or cellular fracture and 2) inter-bead or interfacial fracture.**

Usually, damage from both mechanisms is found simultaneously in the fracture surface of a moulded part. According to the quality of fusion, their relative fractions differ. Better fusion leads to an increased degree of intra-bead fracture, whereas bad fusion with a weak interface fails in inter-bead mode. The relative fraction of intra-bead fracture is also referred to as the degree of fusion (DOF) [44]. Rossacci and Shivkumar [44] found, that the degree of fusion is indirectly proportional to the foam's density and the molecular weight of the polymeric matrix. Furthermore, the quality of fusion is dependant on the location within the moulded part.

One of the few works, where the effect of different cell sizes at a relatively constant density is studied, was conducted by Doroudiani and Kortschot [51], [52]. They studied the interdependency between the microstructural properties and the tensile and impact-behaviour of EPS. The density exhibited the highest effect on the mechanical response, whereas a reduced cell size (at a more or less constant density) lead only to minor changes in the tensile modulus and strength. The modulus showed a more pronounced dependency on cell size than strength. In contrast, smaller cells did not improve the impact behaviour.

Also, the works from Viot et al. are noteworthy, since the microscopic deformation of bead foams is examined in their work and also fast deformation speeds are applied. They studied expanded polypropylene (EPP) under impact loading [122], [123]. The impact was applied in multiple stages. The sample was scanned by computer tomography after each stage. They studied the local deformation of the beads by the change of their outer surface. From the outer surface, the volume was calculated. In contrast, the density was calculated from their average grey-value, since the absorption of radiation by matter correlates with density according to the Beer-Lambert law [29]. They observed layers of localised deformation perpendicular to the force direction. No correlation of local deformation with density was observed. In their second publication, the bead size was automatically evaluated with an algorithm. The density was again measured from the average grey-value of the bead. A strong correlation between bead density and local deformation was found [30].

To summarise, the mechanical behaviour of bead foams is very complex. It is dependent on the bead and part morphology as well as the processing conditions in steam-chest moulding (*i.e.* time and temperature). In the literature, mainly the effect of the moulding conditions on the mechanical and insulation properties was studied. In contrast, the morphological dependency remains unstudied. Furthermore, interdependencies between the morphology, especially the bead size, and processing conditions are yet to be studied, and are also likely to have a pronounced effect on the material properties.

### 2.5.3 Fracture mechanics of foams and bead foams

In contrast to bulk materials, the fracture toughness of foams remains relatively unexplored. Some results exist for metallic foams. Motz and Rippan studied an Al-alloy-foam (density 250 – 500 kg/m<sup>3</sup>) obtaining very interesting results [124]. They compared the critical stress intensity factor  $K_{Ic}$  with the J-Integral and the crack opening displacement (COD), showing that the first is invalid, while the latter two deliver sensible results. However, COD is deemed superior due to lower data-scatter. They also concluded, that for the fracture two length scales are relevant, namely the cell wall and edge thickness on the lower scale and the fracture process zone in the scale of several cell sizes. Using *in-situ* SEM-analysis, they also observed highly localised deformation behaviour within the cell walls, as shown on Figure 17.

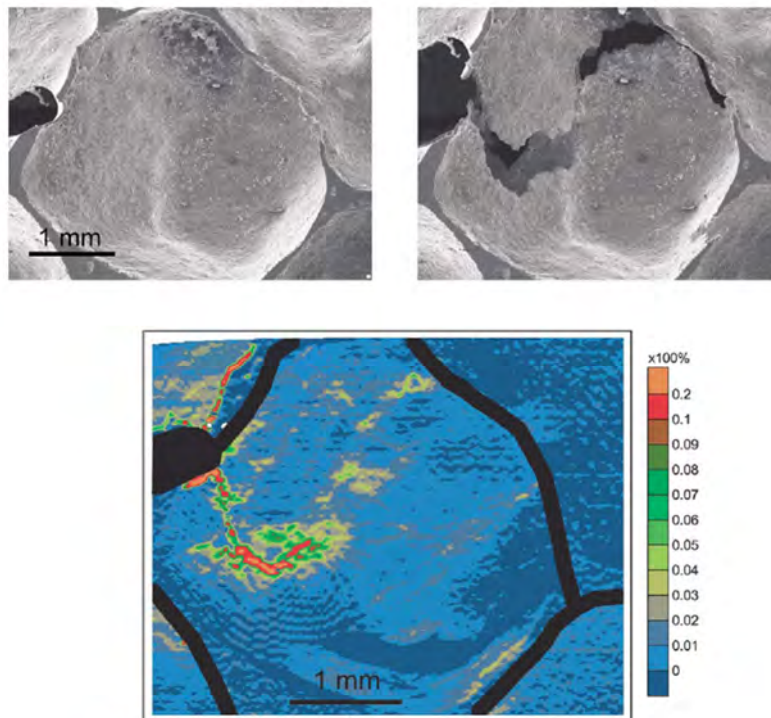


**Figure 17:** *In-situ* observed fracture of an Al-foam showing the cell before fracture (upper left) and after (upper right), as well as the local strain shortly before crack extension (lower picture) [124].

The fracture behaviour of polymeric foams is mostly deduced from impact data, as for example for epoxy-impregnated PUR-Foam [125]. Also linear elastic fracture mechanics (LEFM) is applied [126]–[129]. However, linear approaches are questionable for low density foams as often they do not exhibit brittle fracture [63], which is a requirement for LEFM.



In terms of elastic-plastic fracture mechanics (EPFM), the “Essential Work of Fracture” (EWF) method was applied once [130] for polypropylene foam sheets. However, EWF has not been used for bead foams due to its limitation in sample thickness, which is one order of magnitude below the highly relevant length scale of bead size. Also computer aided fracture mechanics is a method to study the fracture processes in foams [131], [132].

Bead foams were studied by Stupak et al [43] with regards to their quality of fusion and density ( $23.2 - 29.2 \text{ kg/m}^3$ ). They used the J-integral showing that steaming pressure has, by far, the highest influence on fracture toughness, whereas steaming time only has a minor influence. Density increased the fracture toughness. Furthermore, they correlated the J-Integral with the fracture pattern. It was found, that the J-Integral correlates very well with the amount of intra-bead fracture. The higher the intra-bead (or cellular) fracture, the higher is the fracture toughness. Furthermore, an additional type of fracture can occur as shown by Mills and Kang [133]. They found, that the crack can propagate along just slightly below the border of the beads through the cellular structure. Hence, the bead is “scalped”.

In summary, the available literature gives only a preliminary understanding on the fracture mechanics of foams. It is obvious, that only methods taking plasticity into account, as EWF or the J-Integral, deliver sensible results for low density foams. Bead foams are a scarcely studied topic. Only one work deals with this class of materials and only the effect of processing is studied. In contrast, the effect of the bead foam’s morphology remains unstudied. However, it is expected that the morphology of the beads plays a crucial role in the foams fracture behaviour.

## **2.6 Thermal conductivity**

At first, an overview on the physical mechanisms of thermal transport of foams is given, which is followed by a brief overview on the studies about the thermal conductivity of EPS.

A thorough understanding of the thermal transport phenomena in foams is crucial to improve the insulation properties of such materials. Thermal energy transport in foams is a complex topic, since all contributions of heat transport can be involved, namely conduction of energy through the solid polymer or the cell gas, convection of the cell gas, and radiation. This is shown in Figure 18 and mathematically expressed by equation (2-1). The relevant factors for bead foams are conduction both in the solid polymer ( $\lambda_{sol}$ ) and cell gas ( $\lambda_{gas}$ ), as well as the radiation term ( $\lambda_{rad}$ ).

$$\lambda_{tot} = \lambda_{rad} + \lambda_{sol} + \lambda_{gas} + \lambda_{conv} \quad (2-1)$$

Gaseous convection ( $\lambda_{conv}$ ) can be neglected for cells smaller than 3 mm [134]. Thus, this mechanism does not contribute to the total heat conductivity of conventional insulating foam materials. In the following section, the individual contributions to the foams' thermal conductivity will be discussed.

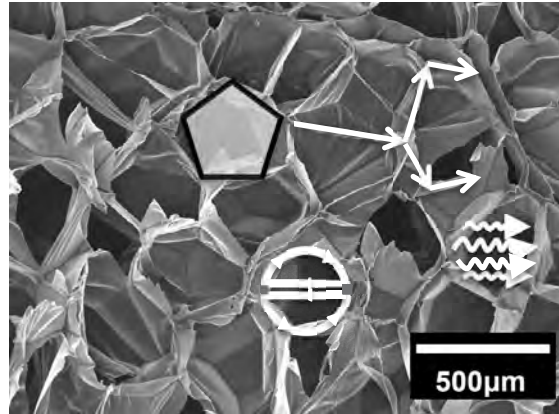


**Figure 18: Mechanisms of thermal transport in foams: gaseous conduction (upper left), solid conduction (upper right), convection (lower left) and radiation (lower right).**

#### Conductive energy transport in foams

Thermal energy is transported in polymers by thermal excitation of the chains and their interactions. The thermal conduction of polymers is a complex matter for itself, since it is affected by crystallinity and chain orientation [135]–[137]. Polymers normally possess heat conductivities in the order of magnitude of several 100 mW/mK.

In contrast to solid bodies, conduction in gases takes place by random collision of gas molecules. Compared to the heat conductivity of polymers, the heat conductivity of gases is around one order of magnitude lower (in the order of 10 mW/mK). However, the respective contribution of each phase (solid and gaseous) in foams is highly dependent on the foam density. For low density foams (Volume polymer  $\ll$  Volume gas), gaseous conductivity in the cells is the dominant factor, although  $\lambda_{solid} \gg \lambda_{gas}$ . When the relative polymer volume increases, solid conductivity becomes the dominant factor. As mentioned above, the entrapped gas is the major contributor to conduction at temperatures relevant for low-density foams (room temperature and below).

#### Radiative energy transport in foams

Besides conduction, radiation is a very important transport mechanism of thermal energy in foams. Its effect is mainly dependent on foam cell morphology and temperature.

Many works in literature have tried to separate the total heat conductivity into its individual components, namely radiation and conduction [10], [134], [138]–[142]. However, those contributions are difficult to be measured separately using ordinary techniques without the aid of analytical modelling [143].

From the model of Progelhof et al. [144], it can be seen that larger cells better promote radiation compared to smaller cells, since the temperature difference across one cell is larger. Furthermore, it was seen that the distribution of material between cell struts, walls and vertices is distinctly affecting the propagation of radiation in the foams [140], [145].

In their theoretical work, Ferkl et al. [134] found that radiation is indeed a very important factor in thermal transport in foams, which has higher contribution at lower density and large cell foams. For example, for PS-foams with a density 40 g/l and a cell size of 200  $\mu\text{m}$ , radiative transport accounts for 14 % of the thermal conductivity [146].

In summary, it was found, that the thermal transport through the gaseous matrix and by radiation are the most influential factors. To our knowledge, there is no literature studying the effect of the unique morphology of bead foams on the thermal conductivity. Also, the available experimental literature studying the effect of cell size at constant density only relies on a limited dataset. Hence it is concluded, that a study on the effect of bead and cell size at constant density is a missing link to the understanding of bead foam behaviour.

#### Literature on the thermal conductivity of EPS

Although EPS is a common insulation material used in many buildings, only very few scientific publications focus on this material [3], more can be found in brochures and flyers from EPS-producers as the BASF SE [147]. Especially, the so-called “grey EPS” is promoted. “Grey EPS” refers to EPS with graphite as an additive in order to reduce thermal energy transport by infrared radiation. However, graphite also acts as a nucleation agent thus reducing the cell size of the foam. This might also significantly affect the thermal conductivity. Unfortunately, this has never been scientifically discussed and proved by the respective producers.

In scientific literature, EPS is sometimes used as model material. An example is the work of Coquard et al. [148], in which the researchers studied the hot-wire method with the aim to make it applicable to low-density insulators. They found, that classical set-ups with short and thick wires are not suitable for low-density foams.

The same researchers also carried out a study, in which they developed a numerical model for coupled radiative and conductive heat transfer and compared it to several EPS-samples. The model delivered satisfactory agreement to the experimental results. Interestingly, the assumption of cubic unit cells led to better results as compared to dodecahedral unit cells.

More modelling work was also carried out by Placido et al. [10], who developed an analytical model to quantify the radiative component of the thermal conductivity based on geometrical information of the foam cell (*i.e.* cell size, wall- and strut-thickness). They found, that the “total conductivity can be improved for a fixed density by modifying suitably wall thickness, strut diameters and most cell diameters”. The drawback of the cited work is an inadequate description of the materials used for experimental validation, as only the density of the investigated EPS is given in the material information, but nothing on the other foams.

In contrast to the more theoretical works described before, Schellenberg and Wallis [9] studied three grades of EPS (fine, medium and coarse cells) per density. Thus, it was attempted to separate the effect of density and cell size. It was found that larger cells lead to better insulation properties (*cp.* Figure 19 a)), which is quite in contrast to models [134], [146] and a study on metallic foams [143], [149]. The reason for this observation might be a non-uniform cell size distribution as shown in Figure 19 b).

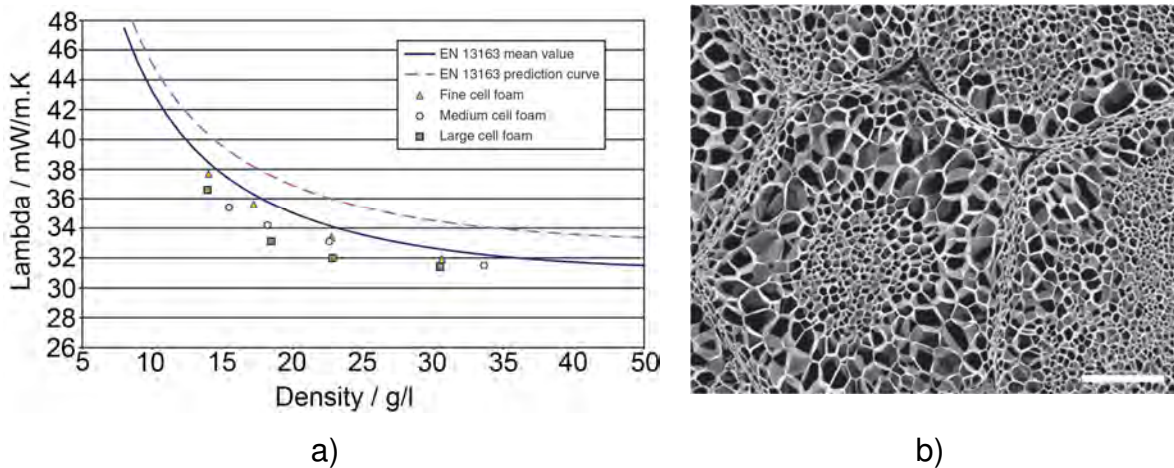


**Figure 19: a) Thermal conductivity of EPS-foams as function of density and cell size and b) the cellular structure of a “Large cell foam” (modified from Schellenberg and Wallis [9]).**

## 2.7 Summary of the state of the art

Bead foams are the only class of foams combining a comparatively free choice of geometry with a low density below  $15 \text{ kg/m}^3$ . This is possible due to its unique processing route. At first, foamed beads have to be created, which itself is either a two-step process as in the case of EPS (production of expandable beads followed by pre-foaming) or a direct, one-step- process as for EPP (gas-saturation and expansion in an autoclave process). Subsequently, the bead foams are joined together to form the final geometry using the steam-chest moulding process. The foamed beads can fill nearly any geometry, which is the reason for the design freedom.

The literature on bead foams is rather scarce, especially compared to more fashionable subjects as *e.g.* nano-composites. The main research topic is the effect of steam-chest moulding conditions on the mechanical response. Better fusion leads to better mechanical properties, as for example increased impact and fracture toughness. Usually, the quality in moulding is assessed from its fracture surface by the fraction of inter- and intra-bead fracture.

EPS is also occasionally used as a model material for studies on the insulation properties of cellular materials. Interestingly, only very few works on EPS are available in the scientific literature; more can be found in brochures and flyers from EPS-producers like BASF SE.

In this frame, the topic of thermal conductivity is studied to some extent. However, the information from the materials producers has a lack of scientific content, whereas the scientific studies available are not completely conclusive. A similar statement can be drawn for the studies on the mechanical behaviour of EPS as mainly the effect of moulding parameters on the mechanics and fracture pattern is examined. However, no work deals with the effect of the morphological parameters at constant moulding conditions. Thus, a thorough basis for further research is missing. Additionally, it is widely believed that a double-melting peak is a requirement for good fusion of semi-crystalline polymers as EPP. Hence, the formation and effect of this feature is investigated extensively also with the aim to transfer the obtained knowledge on novel bead foams, as for example PLA.

From the reviewed literature, the open scientific questions as foundation of the work are identified and presented as follows.

## 2.8 Open scientific questions

Three main open topics are thus identified from the literature review:

1. First and foremost, the **effect of the multi-scale morphology on the mechanical behaviour** of bead foams is of fundamental interest. Since EPS is often used as a model material for cellular solids in general, it is necessary to ascertain the interplay of the different morphological features of the bead foam's multi-scale morphology with the mechanical response and the micro-deformation mechanisms. As a benefit, bead foams theoretically allow the separate study of single morphological features (as the cell or bead size) at a constant density by a clever variation of the processing conditions. In this frame, also the effect of blending (*e.g.* PS with PE) is of interest, as it is known from practical experience that blending improves the elasticity of the foams. Furthermore, the interplay between the morphology and the fracture behaviour of bead foams is only scarcely explored, although it is of high industrial relevance, *e.g.* to ensure the safety of cycling helmets or the effectiveness of packaging. For these applications, the knowledge of the mechanical performance as function of deformation speed is highly important for designs that are more efficient. Literature does not provide conclusive data on foams in general, let alone bead foams.
2. Besides the mechanics of bead foams, their **thermal insulation properties** are also of high industrial relevance, as EPS and EPP are common insulation materials. Unfortunately, the literature gives contradictory results on the interplay of cell size with thermal insulation. Furthermore, combinations of multiple effects are studied together (*e.g.* varying density and cell and bead size).
3. In contrast to the influence of cell and bead size, for which at least some scientific literature exists, a **compact and thick skin around expanded EPS beads** remains uncharted territory on the map of materials science. Not even a method to create (and control) this morphological feature is established in literature, let alone its effect on properties studied.

The aim of this thesis is to contribute to answering these three open questions and contribute to a more comprehensive understanding of the influence of the bead foam morphology on their properties.

### 3 Aims and concept of the thesis

From the previous chapters the aims for the thesis are derived and a research strategy was developed.

#### Aims

From an economical viewpoint it becomes clear, that it is of paramount importance to a) further tune the properties of EPS and b) to be able to adjust it with regards to its final application. From a scientific perspective, a major gap exists in the understanding of the dependency between the morphology of EPS parts and the mechanical and insulation properties. Consequently, the overall aim of the study is to provide an understanding of this open scientific topic. In this frame, **structure-property relationships** are to be established. Therefore, the morphological features (*e.g.* cell size, bead size and density) exhibiting significant effects on the mechanical response and insulation properties of the parts must be identified. It is important to note, that this work does not include the effects of steam-chest moulding as these were already subject of numerous studies. From practical experience it is known that the introduction of a blend partner leads to superior elasticity, which is important for shock absorption in packaging. Thus, the mechanisms behind the improved elasticity are to be clarified exemplarily for a PS/PE-blend (E-Por®) in comparison to EPS, which is made solely of polystyrene. Subsequently, the relevant parameters affecting the local deformation and fracture behaviour are to be identified and correlated to the failure mechanism of the materials (inter or intra-bead failure).

Furthermore, the skin around single EPS beads is of great scientific as well as industrial interest, as this feature could enable an internal sandwich effect between the beads inside EPS parts. However, the influence of this morphological feature remains unknown for EPS until now. In this frame, a method has to be developed and studied in order to create beads with a homogeneous solid skin, at least one order of magnitude thicker than for standard beads. Secondly, its interdependency on the other morphological features, especially cell size, has to be studied as basis for the structure-property relationships. Due to the initial idea of an internal sandwich effect, solely the mechanical properties are investigated in this study.

#### Concept and research strategy

The research strategy is divided into two parts as shown in Figure 20. **Part I** aims to shed light into the dependency of the mechanical and insulation properties on morphological features found in moulded parts such as density, cell size and bead size. Three



main morphological features are present in bead foam parts, which might affect the properties: 1) the (possibly not perfect) interfacial area between two neighbouring beads (controlled by bead size), 2) the micro-morphology in form of cell struts and walls (controlled by cell size) and 3) the fraction of polymer in the foamed core volume, which is basically the foam density. Furthermore, the influence of the properties of the polymeric matrix on the properties of the final part has to be studied by comparing EPS with the PS/PE-blend bead foam designated as E-Por®. The investigation of these factors allows a thorough characterisation of the length scales in bead foams. It is noteworthy, that in order to obtain parts with different morphological features only the processing procedure of the beads was varied in part I of the study. In contrast, both the process parameters for pre-foaming (except for the varying density) and steam-chest moulding were kept almost constant in order to assure that the quality of bead-fusion remains constant.

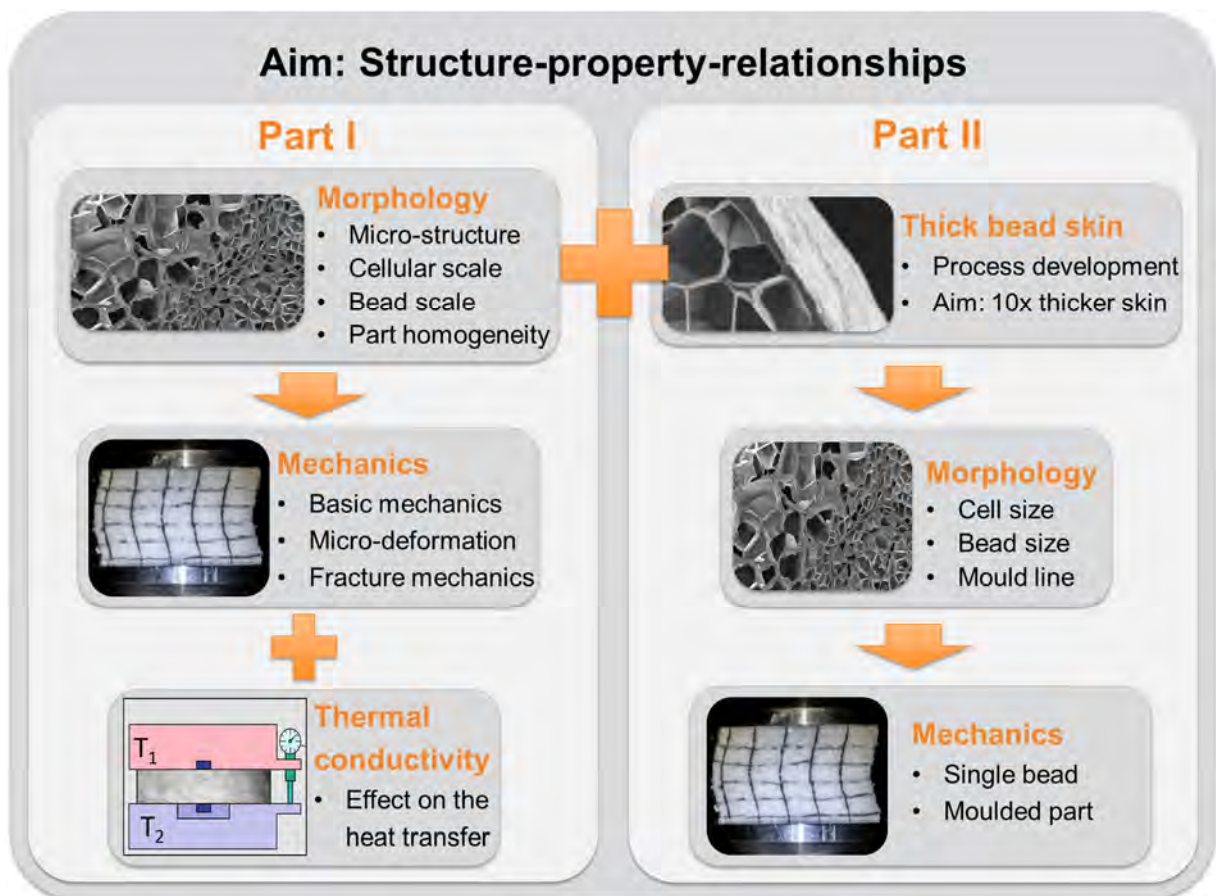


Figure 20: Overview on the structure of the research and the thesis.

In addition to part I, **part II** of the thesis will explore uncharted territories of the bead foam morphology. It will be studied how the thickness of the skin around beads affects



the other morphological parameters (*e.g.* cell size) and ultimately the mechanical properties. Therefore, a method to obtain a thick and homogeneous skin around the beads in a reproducible manner has to be developed and studied.

This task appears to be sensible from a scientific as well as from a didactic standpoint due to the different nature and pathway of the research. Moulded parts for the testing in part I are gratefully provided by BASF SE and are produced by standard industrial processes, *i.e.* extrusion with under-water pelletisation or suspension polymerisation in the presence of pentane, pre-foaming and steam-chest moulding. In contrast, part II requires a novel method to create samples with a thick bead skin. The exploration of the said method is thus a major subject in part II.

## 4 Materials and methods

### 4.1 Materials

In order to be able to distinguish effectively between the numerous materials investigated in this work, an easy nomenclature is required. Thus, all samples are named according to the following system:

*Material\_Density[g/l]\_AverageCellSize[ $\mu$ m]\_AverageBeadSize[mm].*

Moulded disks from three kinds of expandable beads are investigated: EPS from suspension polymerisation (“sEPS”) as benchmark, EPS produced *via* extrusion (“EPS”) and “E-Por”, which is a PS/PE-blend. For example, sEPS\_25\_70\_2.8 is an EPS from suspension polymerisation with a density of 25 g/l, an average bead size of 2.8 mm and an average cell size of 70  $\mu$ m. BASF SE, Ludwigshafen, Germany, provided foam plates (disks) with a dimension of 300 x 50 mm (diameter x height) for the study. The volume yields about 3500 cm<sup>3</sup>. A plate weights about 90 g at a density of 25 g/l.

#### 4.1.1 EPS

##### EPS produced by suspension-polymerisation (Benchmark systems)

Expandable Polystyrene produced from suspension polymerisation (“sEPS”) with different bead sizes (P226C, P326, P426) is used as benchmark. All three grades are produced in one batch. The three sizes are fractions obtained from a sieving process.

**Table 2: Overview on the studied EPS samples from suspension polymerisation (“eEPS”). The bead size represents the size of the beads within the moulded part. This is also true for the cell diameter. The error does not represent the experimental error, but the width of the respective distribution.**

Material name	Density / g/l	Bead diameter / mm	Cell diameter / $\mu$ m
<b>sEPS_25_70_2.8 (P226C)</b>	25 (25.4 $\pm$ 0.1)	2.8 $\pm$ 0.6	70 $\pm$ 34
<b>sEPS_25_57_2.3 (P326)</b>	25 (25.5 $\pm$ 0.1)	2.3 $\pm$ 0.4	57 $\pm$ 29
<b>sEPS_25_66_2.1 (P426)</b>	25 (25.3 $\pm$ 0.1)	2.1 $\pm$ 0.3	66 $\pm$ 30

##### EPS produced by extrusion

Expandable Polystyrene (EPS) produced from foam extrusion with attached underwater pelletisation is the main material of the study at hand. The major scientific advantage of foams from expandable beads is that the morphological parameters like cell and bead sizes can be varied independently (within a certain range) of foam density by an appropriate variation of the processing parameters (production of expandable beads).

The investigated parameters are density (with variable cell and bead size), foam cell size (at a constant set density of 25 g/l and constant bead diameter of around 3.5 mm), and bead size (at constant density of 25 g/l and constant average cell size).

**Table 3: Overview of the studied EPS samples from extrusion. The bead size represents the size of the beads within the moulded part. This is also true for the cell diameter. The error does not represent the experimental error, but the width of the respective distribution.**

Material name	Density / g/l	Bead diameter / mm	Cell diameter / $\mu\text{m}$
<b>1. Variation of cell size</b>			
EPS_25_160_2.8	25 (24.8 $\pm$ 0.2)	2.8 $\pm$ 0.7	160 $\pm$ 30
EPS_25_170_2.8	25 (25.1 $\pm$ 0.2)	2.8 $\pm$ 0.7	170 $\pm$ 35
EPS_25_215_3.2	25 (24.5 $\pm$ 0.1)	3.2 $\pm$ 0.8	215 $\pm$ 65
EPS_25_235_3.1	25 (24.5 $\pm$ 0.1)	3.1 $\pm$ 0.8	235 $\pm$ 65
EPS_25_250_2.9	25 (24.2 $\pm$ 0.2)	2.9 $\pm$ 0.7	250 $\pm$ 85
EPS_25_300_3.0_Ref	25 (24.7 $\pm$ 0.2)	3.0 $\pm$ 0.6	300 $\pm$ 75
EPS_25_310_3.0	25 (24.5 $\pm$ 0.1)	3.0 $\pm$ 0.7	310 $\pm$ 50
EPS_25_335_3.0	25 (23.9 $\pm$ 0.1)	3.0 $\pm$ 0.7	335 $\pm$ 60
EPS_25_385_2.9	25 (23.8 $\pm$ 0.2)	2.9 $\pm$ 0.8	385 $\pm$ 75
EPS_25_410_3.0	25 (24.5 $\pm$ 0.1)	3.0 $\pm$ 0.7	410 $\pm$ 90
<b>2. Variation of bead size</b>			
EPS_25_310_2.7	25 (23.2 $\pm$ 0.1)	2.7 $\pm$ 0.8	310 $\pm$ 55
EPS_25_380_2.9	25 (24.2 $\pm$ 0.2)	2.9 $\pm$ 0.8	375 $\pm$ 80
EPS_25_300_3.0_Ref	25 (24.7 $\pm$ 0.2)	3.0 $\pm$ 0.6	300 $\pm$ 75
EPS_25_420_3.5	25 (23.8 $\pm$ 0.1)	3.5 $\pm$ 0.6	420 $\pm$ 75
<b>3. Variation of foam density</b>			
<b>3.1. Small cells</b>			
EPS_20_270_3.0	20 (17.1 $\pm$ 0.1)	3.0 $\pm$ 0.8	270 $\pm$ 90
EPS_25_250_2.9	25 (24.2 $\pm$ 0.2)	2.9 $\pm$ 0.7	250 $\pm$ 85
EPS_30_240_2.8	30 (29.9 $\pm$ 0.4)	2.8 $\pm$ 0.8	240 $\pm$ 80
EPS_40_200_2.3	40 (40.4 $\pm$ 0.4)	2.3 $\pm$ 0.7	200 $\pm$ 50
<b>3.2. Large cells</b>			
EPS_20_340_3.1	20 (18.1 $\pm$ 0.2)	3.2 $\pm$ 0.8	340 $\pm$ 90
EPS_25_300_3.0_Ref	25 (24.7 $\pm$ 0.2)	3.0 $\pm$ 0.6	300 $\pm$ 75
EPS_30_275_2.7	30 (29.6 $\pm$ 0.2)	2.7 $\pm$ 0.8	275 $\pm$ 75
EPS_40_250_2.4	40 (41.0 $\pm$ 0.4)	2.4 $\pm$ 0.6	250 $\pm$ 60

#### 4.1.2 E-Por (PS/PE-blend)

The studied material E-Por is a polystyrene-based bead foam, toughened by an additional polyolefin component [150]–[152]. BASF SE (Ludwigshafen, Germany) provided moulded disks with a diameter of 30 cm and a thickness of 5 cm with different morphological properties. The investigated parameters are density (with variable cell and bead size), foam cell size (at a constant density of 25 g/l and constant bead diameter of around 3.5 mm), and bead size (at constant density of 25 g/l and constant average cell size).

**Table 4: Overview of the studied E-Por samples. The bead size represents the size of the beads within the moulded part. This is also true for the cell diameter. The error does not represent the experimental error, but the width of the respective distribution.**

Material name	Density / g/l	Bead diameter / mm	Cell diameter / $\mu\text{m}$
<b>1. Variation of cell size</b>			
EPor_25_140_3.5	25 (25.7 $\pm$ 0.1)	3.5 $\pm$ 0.7	140 $\pm$ 70
EPor_25_160_3.7	25 (24.9 $\pm$ 0.1)	3.7 $\pm$ 0.6	160 $\pm$ 70
EPor_25_160_3.3	25 (25.2 $\pm$ 0.3)	3.3 $\pm$ 0.8	160 $\pm$ 80
EPor_25_160_3.5	25 (25.3 $\pm$ 0.1)	3.5 $\pm$ 0.7	160 $\pm$ 80
EPor_25_170_3.7	25 (24.9 $\pm$ 0.1)	3.7 $\pm$ 0.7	170 $\pm$ 90
EPor_25_180_3.8	25 (25.6 $\pm$ 0.1)	3.8 $\pm$ 0.8	180 $\pm$ 80
EPor_25_190_3.7_Ref	25 (24.8 $\pm$ 0.1)	3.7 $\pm$ 0.6	190 $\pm$ 80
EPor_25_190_3.4	25 (25.0 $\pm$ 0.2)	3.4 $\pm$ 0.7	190 $\pm$ 90
EPor_25_200_3.5	25 (23.9 $\pm$ 0.1)	3.5 $\pm$ 0.8	200 $\pm$ 90
EPor_25_210_3.6	25 (24.9 $\pm$ 0.2)	3.6 $\pm$ 0.9	210 $\pm$ 80
EPor_25_270_3.5	25 (23.0 $\pm$ 0.1)	3.5 $\pm$ 0.9	270 $\pm$ 90
EPor_25_570_3.4	25 (25.9 $\pm$ 0.1)	3.4 $\pm$ 0.9	570 $\pm$ 170
<b>2. Variation of bead size</b>			
EPOR_25_180_3.0	25 (25.3 $\pm$ 0.1)	3.0 $\pm$ 0.8	180 $\pm$ 90
EPor_25_190_3.7_Ref	25 (24.8 $\pm$ 0.1)	3.7 $\pm$ 0.6	190 $\pm$ 80
EPOR_25_220_4.6	25 (24.8 $\pm$ 0.3)	4.6 $\pm$ 0.6	220 $\pm$ 80
<b>3. Variation of density</b>			
E-Por_12_360_3.5	12 (12.1 $\pm$ 0.1)	3.5 $\pm$ 0.9	360 $\pm$ 130
E-Por_15_290_3.0	15 (15.5 $\pm$ 0.1)	3.0 $\pm$ 0.7	290 $\pm$ 110
E-Por_20_310_3.1	20 (18.4 $\pm$ 0.1)	3.1 $\pm$ 0.8	310 $\pm$ 90
E-Por_25_280_3.4	25 (23.9 $\pm$ 0.2)	3.4 $\pm$ 0.8	280 $\pm$ 110
E-Por_40_240_3.2	40 (38.0 $\pm$ 0.8)	3.2 $\pm$ 0.8	240 $\pm$ 100
E-Por_60_200_2.1	60 (57.6 $\pm$ 1.3)	2.1 $\pm$ 0.4	200 $\pm$ 70
E-Por_80_170_1.9	80 (72.7 $\pm$ 3.7)	1.9 $\pm$ 0.3	170 $\pm$ 60
E-Por_100_120_1.6	100 (99.0 $\pm$ 2.3)	1.7 $\pm$ 0.4	120 $\pm$ 50

## 4.2 Methods

### 4.2.1 Analysis of the foam morphology

#### Density

The density was determined according to the Archimedes principle based on buoyancy. Therefore, the mass of the sample immersed in air  $m_L$ , as well as in water  $m_W$  with a density  $\rho_W(T)$  is measured. The density is calculated from the sample's buoyancy according to equation 1.

$$\rho = \rho_W(T) \frac{m_L}{m_L - m_W} \quad \text{Equation 1}$$

Cubic samples with an edge length of 10 mm are used. Possible sources of experimental errors are macro-porosity between beads and open cell structures. The latter is virtually non-existent as numerous SEM-pictures prove. Macro-porosity is also not an issue as the inter-bead volumes are tightly sealed as the moulded beads are well fused and microscopic channels cannot transport significant amounts of water into the structure.

#### Bead size

In order to measure the average bead size and its distribution of the moulded beads, the moulded EPS disks were cut into about 1 mm thick sheets with a bread slicer. This thickness of the slices equals about one half to one third of the bead diameter. The sheets were then placed on an illuminated table and photos were taken perpendicular to the surface of the sheets (*cp.* Figure 21). Subsequently, the photos were analysed by the public-domain image analyser software ImageJ in order to measure the cut area of the individual beads. Subsequently, the diameter of the circle with the same area was calculated. The results are presented as the number-averaged bead-diameter with the respective standard deviation as indication for the distributional width.

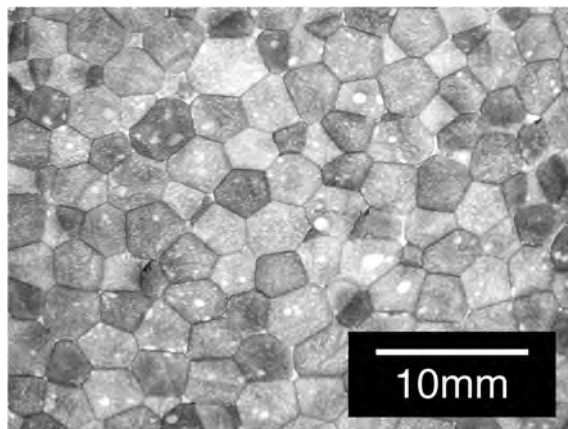


Figure 21: Example of a thin slice of EPS for the purpose of bead size evaluation.

### Macro-porosity

Macro-voids were tried to be identified from thin slices with thickness of about 1 mm. These slices were prepared with a bread slicing machine. In order to make the macro-voids visible, the slices were put on an illuminated table. Images were then taken (Nikon D5100 with Nikkor 18-55 mm lens (F3.5 - 5.6)) and analysed with respect to the number holes (macro-voids) between the beads per area.

### Cell size

The cell size, cell walls and struts thickness of various beads in the foam parts have been visualized by Scanning Electron Microscopy (Jeol JSM-6510) on samples sputtered with a layer of gold. An acceleration voltage of 10 kV was used.

The average cell size was determined from the micrographs of five to ten beads to obtain a representative value using ImageJ. The cell size ( $d_c$ ) of every individual cell was calculated according to Equation 2.

$$d_c = 2 \times \sqrt{\frac{A_c}{\pi}} \quad \text{Equation 2}$$

$A_c$  denotes the cross-section area of an individual cell. The average cell size was then calculated as the number-averaged of the individual cell sizes of the moulded part. For each material two disks combined with at least 1000 individual cells were evaluated.

### Cell wall- and strut thickness

The cell-wall thickness was calculated as the average thickness of the walls at different positions (Figure 22) for several beads. The strut thickness is given by the diameter of a circle area-equivalent to an ellipse fitted into the strut (Figure 22).

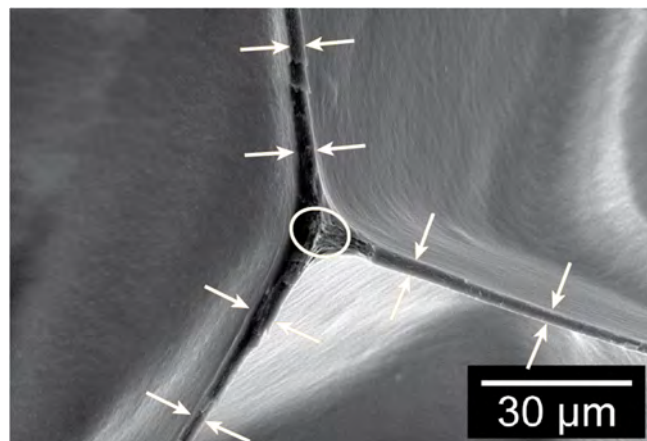


**Figure 22: Example for the evaluation of the cell walls and struts.**

### Study of the blend morphology of E-Por (TEM)

TEM imaging was conducted to determine the blend morphology of E-Por, which consist of polyethylene and polystyrene. Therefore, thin slices of the material with a thickness of about 50 nm were prepared with a Leica EM UC7 ultramicrotome, which had a diamond blade from the company Di-atome with a cutting angle of 35°. The cutting speed was 0.6 mm/s. The slices were placed on a carbon-sputtered copper grid. The samples were stained with ruthenium (VIII) tetroxid (RuO<sub>4</sub>) to enhance the contrast between the blend partners. A Zeiss 922 Omega transmission electron microscope with an acceleration voltage of 200 kV was used for the imaging.

### **4.2.2 Mechanical testing**

#### Compression test (quasi-static)

Compression tests were performed according to the DIN 53421, with the exception of a higher maximum deformation. No special treatment of the samples took place before testing. A 2.5 kN force transducer was used. Samples of 50 x 50 x 50 mm were used. A pre-force of 5 N was applied prior to the compression step. The samples were compressed to a maximum strain of 72 % at a rate of 5 mm/min followed by an unloading step at the same rate in order to obtain a hysteresis-loop.

From the stress-strain-diagrams the compressive modulus, the strength at 10 % strain and recovery are evaluated. The modulus is calculated from a secant between 1.7 and 2 % strain. The recovery is calculated according to Equation 3.

$$R = \frac{h_0 - h_{hyst}}{h_0} \quad \text{Equation 3}$$

This equation contains the initial height of the sample ( $h_0$ ) and the residual height at a stress of 0.005 MPa in the hysteresis ( $h_{hyst}$ ) after one load cycle.

#### Short-time dynamic testing (high speed compression)

Short-time dynamic testing was conducted in compression mode, since this mode is highly relevant for practical applications. Therefore, a novel procedure was applied. It comprises of a high-speed compression test in a servo-hydraulic test machine. The set-up and an exemplary photo during the experiment are given on Figure 23 a) and b).

Compression tests took place at deformation-speeds of 400 mm/s to a maximum strain of 70 %. A 16 kN force transducer was used to measure the force as function of time with a measurement interval of 0.2 ms.

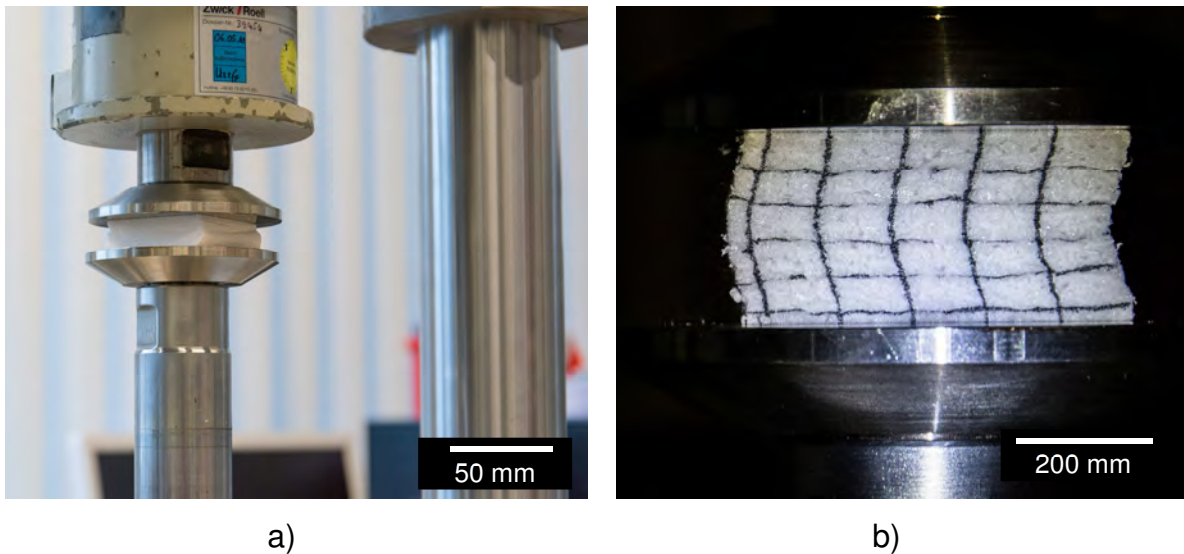


**Figure 23: a) Set-up of the high-speed compression test and b) photograph during compression.**

The same 50 x 50 x 50 mm samples as for standard compression tests were used. The force data were written into a ring-buffer. When the data-acquisition indicates that the beginning of the characteristic stress-strain-curve of the foam is at the “end” of the ring buffer, the whole ring buffer was saved and the data evaluated.

#### In-situ SEM (Compression test in a SEM)

For the *in-situ* SEM measurements cubic samples with an edge length of 10 mm were prepared using a circular saw. Those cubes were sputtered on one side perpendicular to the direction of deformation with a layer of gold. The *in-situ* SEM experiments were conducted on a Zeiss EVO MA 15 operating at 5 kV. An *in-situ* loading module from Kammrath & Weiss GmbH was used. A deformation rate of 10  $\mu\text{m/s}$  was applied until 50 % compression of the sample was reached.

#### Bending test (quasi-static)

Three-point-bending tests were performed according to DIN 53423. A 0.5 kN force transducer was used to assure accurate force-measurement. The samples had a dimension of 120 x 25 x 20 mm (l x w x h). The surface of the moulded disk was removed (by at least 4 mm). This side was chosen to be subjected to compressive stress (upper side). The centres of the lower supports have a distance of 100 mm. The supports possess a radius of 5 mm. A pre-force of 1 N is applied as initial condition. The subsequent test takes place at a speed of 10 mm/min until complete failure. The modulus is calculated from a secant between 0.25 and 0.5 % strain.



### Dynamic mechanical analysis

Cylindrical samples with a height of 5 mm and a diameter of 10 mm were studied in compressive deformation. The experiments were conducted on a Mettler Toledo DMA/SDTA 861e. Measurements were done at a frequency of 1 Hz with a strain amplitude of 20  $\mu\text{m}$ , an initial normal force of 5 N and auto-offset of 120 %. A temperature range from 25 to 110 °C was covered at a heating rate 3 K/min. Samples were taken parallel to the surface of the moulded plates in a depth of approximately 20 mm. The onset of glass transition was evaluated from the storage modulus  $G'$ .  $G'$  was averaged before the easily observable drop-off. The temperature at which  $G'$  drops by 5 % from this value is then defined as the onset of the glass transition.

### Compression test of individual beads

Compression test for individual beads were conducted using a rotational rheometer MCR 702 (Anton Paar, Austria). Initially, the parallel plates were set to a distance of 3.5 mm and the bead was placed between the plates. The testing speed was 3.5 mm. When the moving upper plate contacts the bead, a force is detected. Thus, the diameter of the bead was measured. After the compression, the bead's weight was measured. By the ratio of the weight and volume calculated from the bead diameter the density of the bead yields. The "stress" is calculated from the ratio of the normal force and the original cross-section area of the beads, the "strain" is calculated from the height of the gap and the original cross section. Compressive strengths at 5 %, 10 %, 25 % und 50 % "strain" were calculated.

### Fracture mechanics and analysis

#### a) *J-Integral measurement*

Single edge notched bending (SENB) specimens with the geometry shown in Figure 24 were cut from the foam plate with a circular saw. The upper surface is also the original surface of the moulded disk. A multi-specimen approach was pursued with initial crack lengths of 20, 24, 26, 28 mm, which were introduced using a razor blade. For each crack length five SENB specimens were prepared. Thus, a total of 20 specimens was tested per material.

By using the three-point bending test, load-displacement ( $F$ - $\delta$ )-diagrams are obtained. The experiments were carried out at a traverse speed of 10 mm/min, the force was measured using a 0.5 kN force transducer.

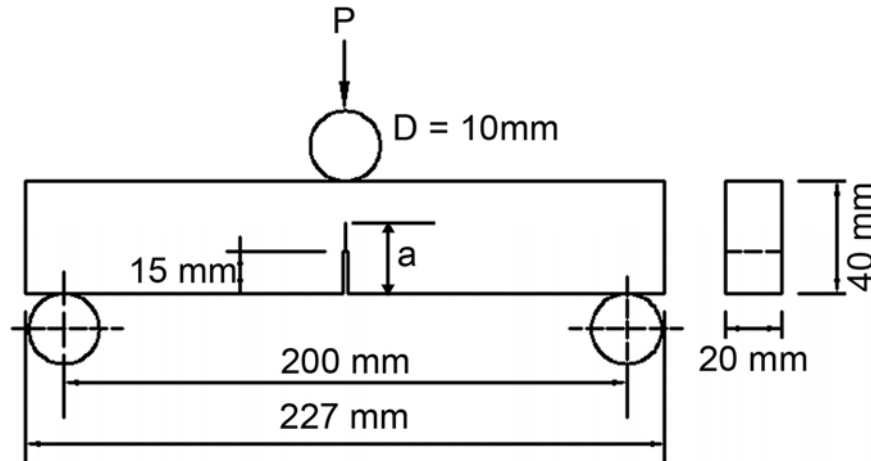


**Figure 24: Geometry of the three-point notched bend (SENB) specimens used to determine the J-Integral [43].**

The critical J-Integral represents the onset of fracture, *i.e.* when a crack grows by an infinitesimal length  $da$ . Since the onset of fracture cannot be determined accurately for polymeric foams in contrast to metals (electrical conductivity too low to measure the sample width, acoustic emission not reliable), an alternative method to characterize the onset of fracture must be used. Therefore, the point of the onset of fracture is defined as the maximum in the load-deflection curve. This point can be determined accurately, thus allowing a reproducible evaluation of J. For simplicity, henceforth J at the maximum load is referred to as J. J is evaluated according to Equation 4.

$$J = \frac{2U}{B(W - a)} \quad \text{Equation 4}$$

with the width,  $B$ , being equal to 20 mm, the height,  $W$ , being equal to 40 mm.  $a$  is the crack-length and  $U$  is the total stored energy until the onset of fracture, which is the area of the load-displacement-curve from the start of the experiment to the displacement at maximum Force  $\delta(F_{max})$ , according to Equation 5.

$$U = \int_0^{\delta(F_{max})} F(\delta) d\delta \quad \text{Equation 5}$$

$U$  was obtained *via* numerical integration from the experimental data. Figure 25 shows a typical load-displacement-curve from J-integral measurements with EPS, the hatched area represents the region of integration according to Equation 5.

#### **b) Evaluation of fracture surfaces**

In order to investigate the failure behaviour of each material, one representative sample is selected and investigated regarding its failure mechanism, namely inter- or intra-bead failure. Therefore, the whole fracture surface of the J-Integral sample is recorded by multiple, overlapping SEM-images, which are stitched together to a panorama using

an automatic algorithm implemented in Photoshop. The area of inter-bead fracture is manually evaluated in the resulting panorama and measured in ImageJ. It is normalised by the complete sample area to obtain the *relative* fraction of inter-bead failure.

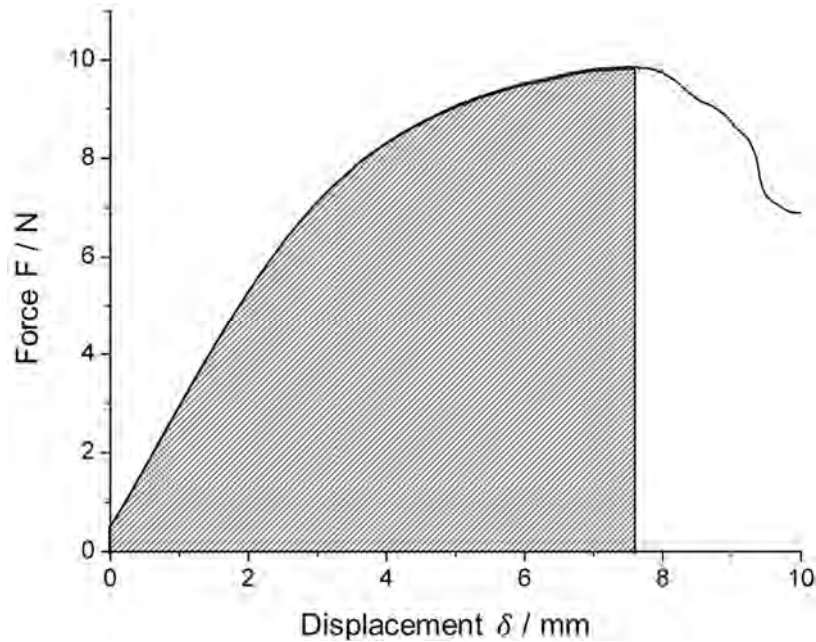


**Figure 25:** A typical load-displacement-curve from J-integral measurements of EPS. The hatched area represents the region of integration according to Equation 5.

### 4.2.3 Thermal conductivity

The thermal conductivity of the foam samples was measured using a heat flow meter (Fox 50, Lasercomp, USA). Therefore, circular foam specimens are placed between two plates in the test stack and a linear temperature gradient is established over the thickness of the material. The upper plate remains stationary, while a pneumatic drive positions the lower stack to assure a contact force pressure to the sample. A certain power per area is required to keep the set temperature gradient constant during the test. This power is proportional to the temperature gradient with the proportionality factor being the heat conductivity. All experiments were conducted at an average temperature between the plates of 23 °C and a temperature difference of 10 °C.

Cylindrical samples with a radius of 60 mm were drilled out of the foam plates. For the high-density foams, drilling was not possible and therefore the cylinders were machined out of the foam blocks. Afterwards, the cylindrical samples were cut to 15 mm thick disks using a circular saw. In order to avoid cell crushing, the contact pressure of the plates was varied with density: 1.2 – 1.5 bar for samples with a density below 40 g/l, and 2 bar for disks with higher density.

#### 4.2.4 Further methods to explore the foam properties

##### Tempering

In order to test the effect of annealing, the respective samples were stored close to the tabulated glass transition temperature for polystyrene at 90 °C for fourteen days in a convection oven (Memmert Modell 400) to facilitate physical ageing (*e.g.* relaxation of the polymer).

##### Thermo-gravimetric analysis (TGA)

Isothermal TGA-experiments were carried out on a Mettler-Toledo TGA/SDTA 851e to test the diffusion of pentane out of the expandable beads. Therefore, 20 mg of EPS-beads were kept at isothermal conditions at 60°C for 9 h.

In order to check for a possible residual pentane content of moulded samples, TGA experiments on a Netzsch TG209 F1 Libra were carried out. Samples weights between 4 and 5 mg were investigated. The temperature was raised from 25 °C to 200 °C at a heating rate of 5 K/min.

##### Shrinkage experiments

In order to explore the residual orientation of EPS, five beads of each EPS type were stored in an oven at a temperature above the glass transition (120, 125 or 130 °C). Their transient diameter was monitored for 90 minutes. Images were taken at regular intervals with a Nikon D7100 Camera mounted on a tripod. The camera was equipped with a Sigma 17 – 50 mm F2.8 lens. A spotlight was used to provide sufficient illumination. Reflections in the glass window of the oven were reduced with the aid of a polarising filter. The measurement setup is depicted in Figure 26. The evaluation of the bead size from the images was done with the program ImageJ. The resulting diameters were used to calculate the evolution of the beads' volume over time.



a)



b)

**Figure 26: a) Setup of the shrinkage experiment and b) resulting photos of the beads in the oven at the beginning and end of the experiment, T = 125 °C.**

#### **4.2.5 Methods used for the creation of a thick skin around beads**

##### Degassing of the expandable beads

In order to obtain a thick skin, the expandable beads have to be depleted of pentane in their outer region. Two approaches are pursued to obtain the pentane-depleted beads: a) in lab scale and b) in industrial scale. In lab-scale, a Memmert VO400 oven is used, which is continuously purged with nitrogen. The expandable beads are stored for various times at 60 °C in an aluminium-pan. They are mixed every 30 min. In industrial scale, a Vötsch VTU 75/100 convection oven is used. The beads are put into a pre-heated plastic tub with a filling height of maximum 5 cm. The same temperature as in lab-scale (60 °C) is applied and every 30 min a mixing step takes place. After the pentane depletion in the oven, the surface of the beads is treated with ethanol (Roth, Germany, with 1 % MEK) to locally plasticise it. As the exact time for plasticisation was studied extensively, this is presented in the results section.

##### Pre-foaming of the pentane-depleted beads and intermediate storage

Two approaches are followed to pre-foam the pentane-depleted beads: a) in lab scale and b) in industrial scale for the later steam-chest moulding. For lab-scale pre-foaming a glycerol-bath of a temperature of 120 °C is used, which is controlled by a VWR VT 5 thermostat and has a stirring unit IKA RCT classic. The industrial scale pre-foaming is conducted on a X-Line 3 unit from Kurtz GmbH (Germany). The pre-foaming is stopped by an optical sensor within the steam-chamber, when a certain volume is reached. The temperature of the pre-foamer before foaming is 70 – 75 °C. The pre-pressure of the steam lies between 800 and 1200 mbar, the steam-pressure between 100 mbar and 300 mbar. The target bulk density is 40 g/l. If not stated otherwise, the admissible deviation was  $\pm 3$  g/l. The intermediate storage is carried out in large plastic barrels for 20 to 24 h.

##### Steam-chest moulding

The steam-chest moulding machine TVZ 162/100PP (Teubert Maschinenbau GmbH, Germany) is used to mould the pre-expanded beads. Parts with a dimension of 287 x 196 x 54 mm are moulded. The filling time of the mould was 10 s, the pressure of the silo 0.5 bar and the dynamic pressure 0.5 bar. The moulding parameters read as follows: cross steaming from the static plate to the moving plate with a steam pressure of 1.1 bar for 1.9 s, then the direction is reversed with a pressure of 1.0 bar for 1.7 s. Thereafter, a autoclave steaming with 1.1 bar (static plate) and 1.0 bar (moving plate) steam pressure is applied for 1.6 s. Ultimately, vacuum is applied (up to 0.4 bar

pressure). The overall cycle time lies between 580 and 800 s, depending on the pre-expanded beads. For the trials in the outlook on the effect of a second ethanol treatment, another mould was used. This mould had a size of 160 × 140 × 90 mm and was hand-filled with about 2.3 l of pre-foamed beads. The same steaming parameters were used for both moulds.

## 5 Results and discussion

The results are presented and discussed in two parts as this structure appears clearer from a didactic as well as scientific viewpoint. *Part I* of the work presents the effect of different morphological features on the properties of EPS and E-Por. Therefore, at first the morphology of the studied parts is analysed and conclusions for the later work are drawn. Subsequently, the mechanical properties in dependency of the morphology with a focus on the fracture toughness are investigated. Finally, the insulation properties are examined. In contrast, *Part II* is dedicated to the study a compact and thick skin around the bead like Ping-Pong balls. Thereby, polymer is “shifted” out of the foam structure into the surface layer of the bead at a given density. At first, a novel method to create this morphological feature is presented. Subsequently, the effect of the bead skin thickness on the mechanical response of the single beads and a part made of them is studied.

### **Part I: Influence of foam morphology on the mechanical and thermal behaviour**

#### **5.1 Morphological features of the studied bead foams**

##### **5.1.1 Overview of the multi-scale morphology of moulded bead foam parts**

Parts made of bead foams consist of three primary length scales, the part scale, the morphological scale and the molecular scale, as shown in the upper pictures in Figure 27. The part scale is in the order of magnitude of several centimetres up to meters.

The morphological scale itself can be sub-divided into three distinctly different length scales, namely the bead-scale, the cellular scale and the sub-cellular scale. This is shown in the lower pictures in Figure 27. Hence, the morphology has a multi-scale character. The bead scale arises from the unique manufacturing, where foamed beads are welded together in steam-chest moulding. The beads size is in the range of several millimetres. One scale below is the cellular level, with cells ranging in size between several hundreds and tens of micrometres. In this size scale, macro-voids are found as well, which are the interstitial volume between beads, as shown in the centre of the lower centre picture of Figure 27. The smallest length scale of the morphology is found even below the level of the cells. It consists of their structural elements, namely the cell walls, struts and knots. Their dimension is in the range of several microns or even below one micron. Below the morphological scale lies the molecular level, including

the size scale of crystals (for the semi-crystalline polymers) and the dimension of the chains.

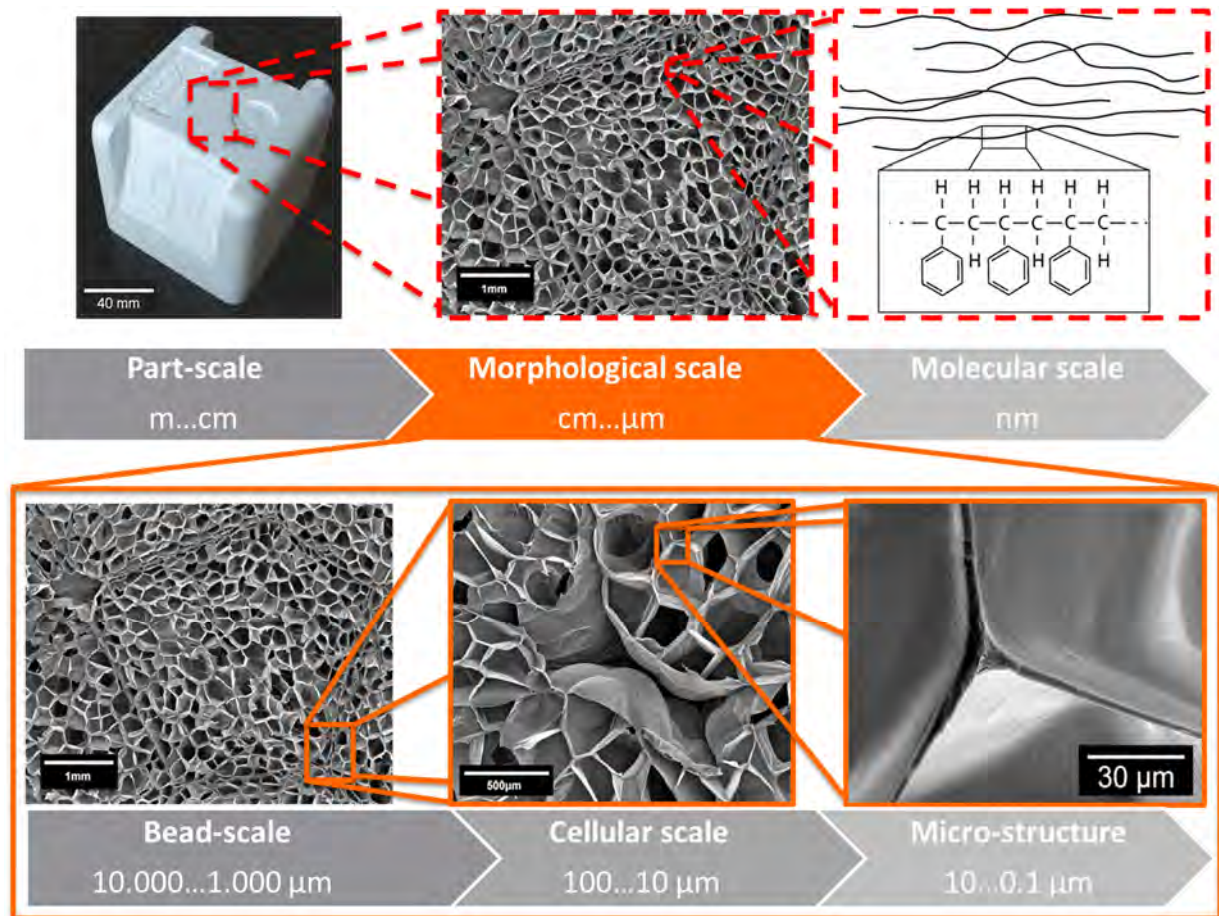


**Figure 27: Size scales of bead foam parts: from part scale down to the molecular scale.**

Another length scale is the solid skin around the beads. The maximum thickness of the skin is in the order of magnitude of several tens of microns at relevant densities for EPS. A solid skin at the bead boundary leads to an altered distribution of the polymer inside the beads (at constant bead size and density) as polymer contributing to the cellular morphology is located at bead border, which also affects the fusion of the beads. Also different cell sizes as well as struts and wall thickness are expected.

It became clear, that the morphology of bead foams consists of several length scales. For an appropriate description of the mechanical and thermal behaviour it is of utmost importance to consider these. Without the knowledge of the inter-dependency of the bead foams' morphology with processing and the resulting mechanical response, the optimisation of this class of material is impossible.



### 5.1.2 Characteristics of the investigated moulded parts

It is noteworthy, that the following calculations are based on a dodecahedral bead and cell model as this body reflects the shape of the moulded beads and cells well. Assuming an average bead diameter of 3 mm, then 750,000 beads are required for one part as shown in Figure 28: a) Picture of two moulded samples (one already cut and one only labelled) used for the work and b) their sketch including the dimensions. Thus, during moulding an area of about 11.4 m<sup>2</sup> must be fused. When the foam cells are considered, the numbers become even more impressive. More than 750 million cells are located within the plate at an average cell diameter of 300 μm. This results in an inner surface of 235 m<sup>2</sup> for only 90 g polymer.

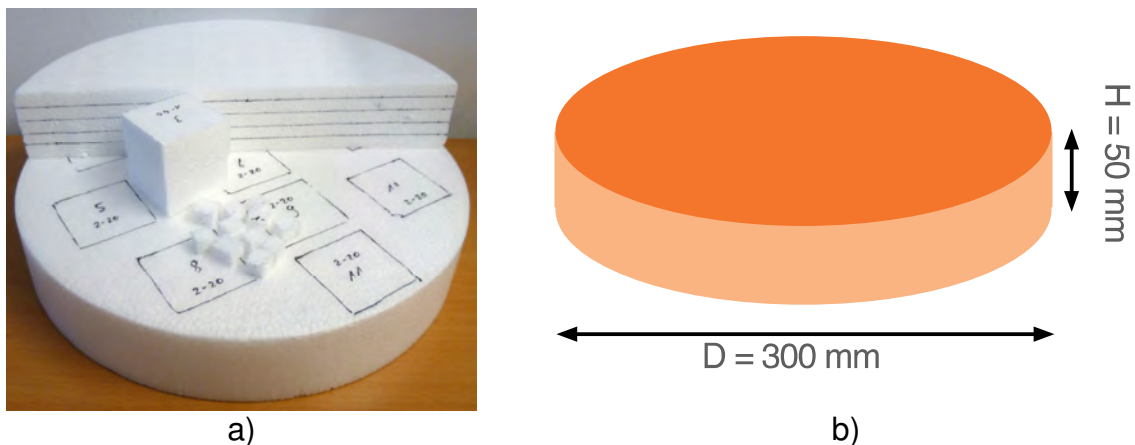


**Figure 28: a) Picture of two moulded samples (one already cut and one only labelled) used for the work and b) their sketch including the dimensions.**

Due to these big numbers, it is necessary to study the plates regarding their homogeneity. Otherwise, every tested plate would have to be studied for its morphology in every position, which is simply not possible due to practical reasons. Thus, their homogeneity in terms of cell size and density was studied a) in thickness direction in the middle of a plate and b) in the centre at various positions across the plate.

#### Homogeneity in thickness direction

The density and cell size as function of the thickness direction of moulded plates are shown in Figure 29. Thickness dependent densities from 11 positions across the plates were evaluated. It is observed, that an almost parabolic density gradient through the thickness of the part exists. The average density deviates by about 3 % from the desired value 25 g/l, at the extremes (inside and surface) by ± 15 %. Thickness dependent cell sizes were evaluated from the center position of the plate at the surface and in about 10 mm depth and the middle (25 mm depth). The cell size exhibits hardly any

variation with the thickness coordinate. Close to the surface, the cells are slightly smaller than in the centre of the moulded part.

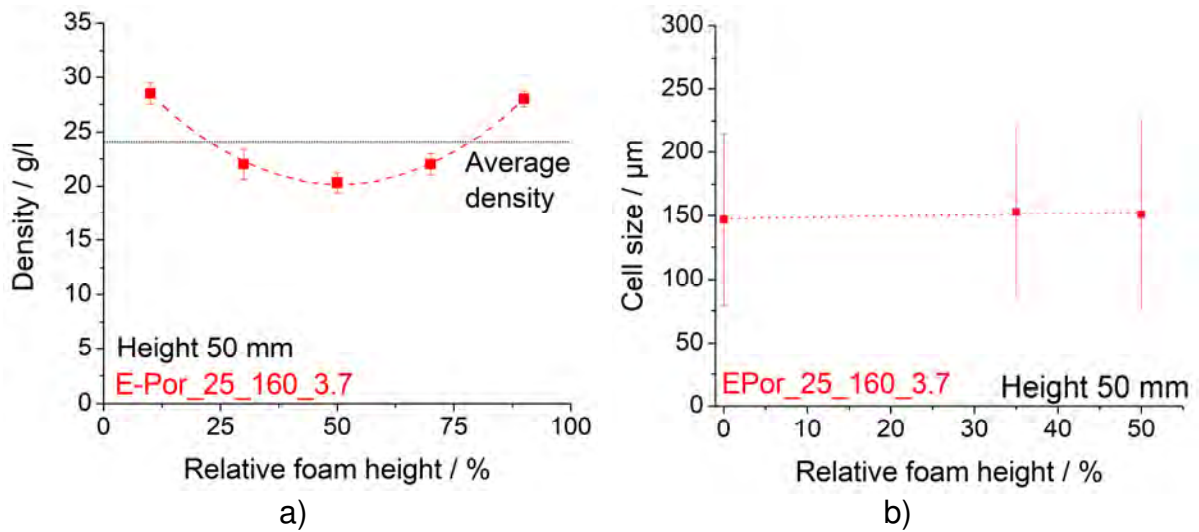


**Figure 29: Examples for the homogeneity in thickness direction of the foam plates: a) density gradient and b) cell size. The error bars do not represent the error of quantification, but the width of distribution.**

#### Homogeneity in the lateral dimension

The homogeneity across the plate was studied at various positions, which are highlighted in the sketch in Figure 30. It is noteworthy, that the position of the injector is at position 1. The effect of location on the plate on density and cell size is shown in Figure 31. The error bars do represent the width of distribution.

In terms of density, only the location at the injector leads to increased values as the beads are slightly compressed at the end of the filling step in this location (*cp.* Figure 31 a)). All other positions have an almost constant density, slightly above the desired value (< 5 %). In terms of cell size, no dependency on the location on the plate can be reported as can be seen in Figure 31 b).

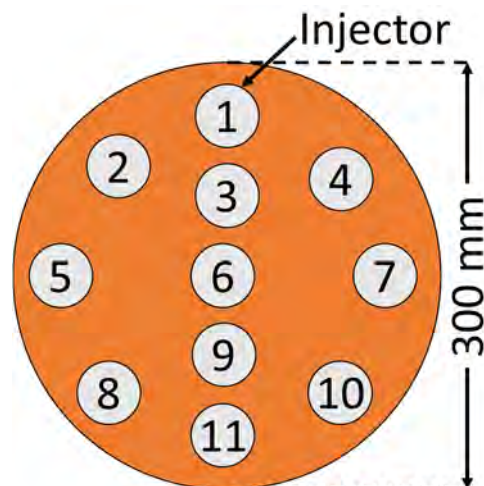


**Figure 30: Sketch of the location of the positions for density and cell size testing.**

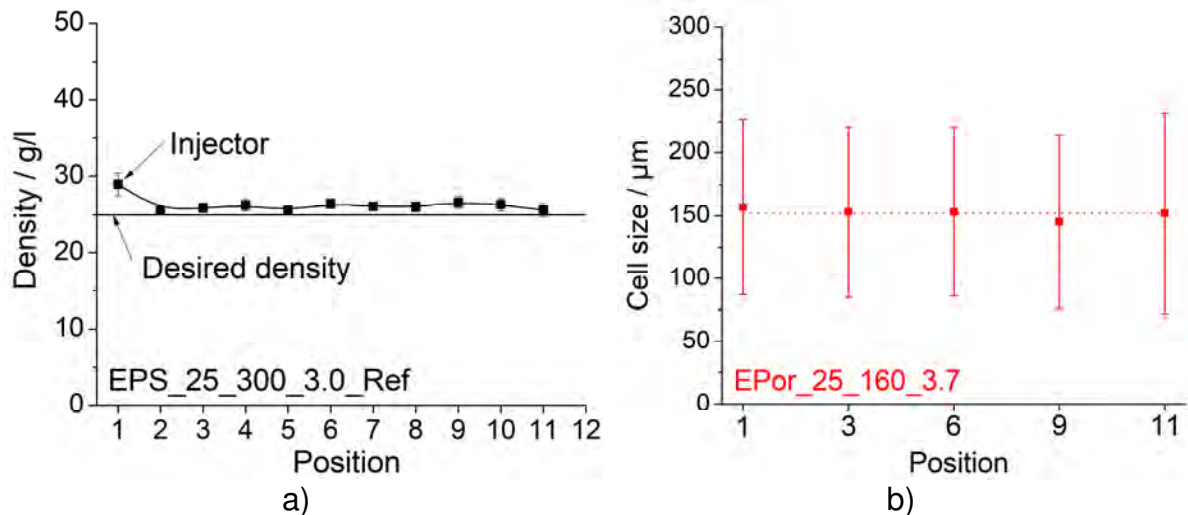


**Figure 31: Examples for the homogeneity of the foam plates in the lateral direction (positions indicated in Figure 30): a) density and b) cell size.**

### Summary and conclusion

The foam plates possess a density gradient along the thickness direction, which is a common feature of bead foam parts. Since the gradient is rather flat, only the average density is given in the following sections for ease of writing and better clarity. This density gradient only affects the cellular morphology to a very minor degree as it hardly varies in thickness direction of the plates.

In terms of homogeneity across the plate, almost no change of density can be observed. However, the average density deviates significantly at the location of the injectors. Thus, no samples were taken closer than 20 mm to the injector. The cellular morphology (cell size and cell size distribution) also remains constant across the part of the sample.

### **5.1.3 Interdependencies of morphological properties**

#### Dependency of the micro-morphology on the cell size at constant density

When the cell size at a constant density is varied, the cell walls and struts are expected to become thinner, as the internal surface increases. The resulting wall and strut dimensions of EPS and E-Por are shown in Figure 32.

Indeed, both the cell walls as well as the struts become thinner when the cell size reduces. It is interesting to note, that EPS has thinner walls but thicker struts compared to E-Por. The reason are the different visco-elastic properties of PS (EPS) and the PS-PE-Blend (E-Por). The EPS micro-granules will be completely in rubbery state during pre-expansion, whereas the PE-phase in E-Por is not molten at normal pre-foaming temperatures. The stabilisation caused by the PE-phase of E-Por leads to a lower difference in thickness between walls and struts compared to EPS.

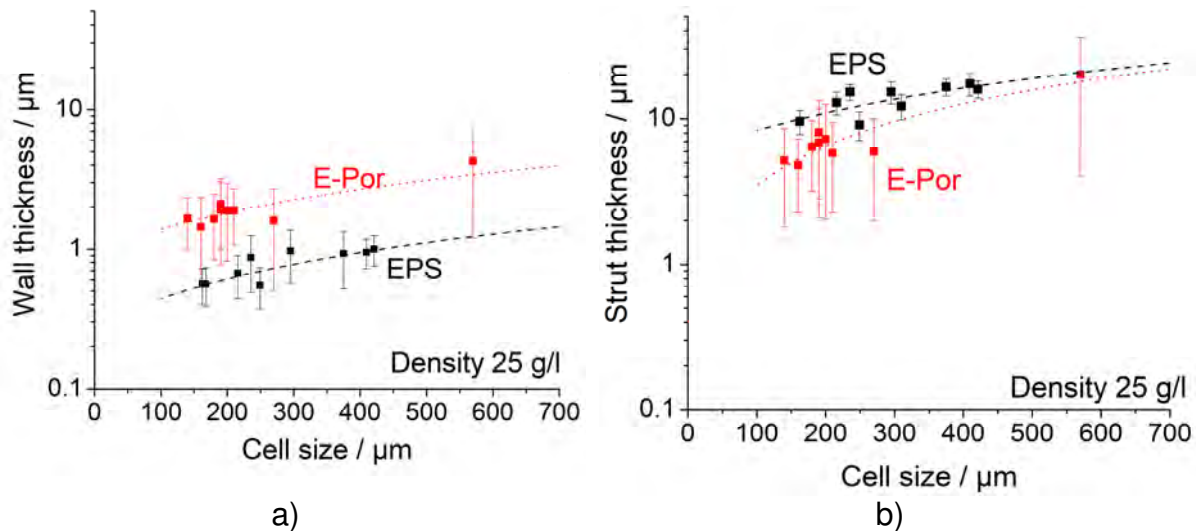


**Figure 32: a) Wall and b) strut thickness of EPS and E-Por as function of cell size at a density of 25 g/l. The error bars do not represent the error of quantification but the width of distribution.**

Impact of the bead size variation on the smaller length scales at constant density

Almost no dependency of cell size on bead size is expected when the bead size is varied, because the nucleation of cells should not be dependent on the dimensions of the expandable beads. This is indeed true for E-Por, but not for EPS as shown in Figure 33.

As reason it can be suggest that due to an increased knife-speed (standard parameter to adjust the bead size) for smaller beads, shear-induced nucleation takes place. Alternatively, the increased knife-speed can increase the pressure drop of the melt, which also increases the nucleation density. In contrast, the micro-cavities in E-Por occur at the boundary between the polystyrene and the polyethylene phase. Hence, an almost constant cell size as function of bead size yields.

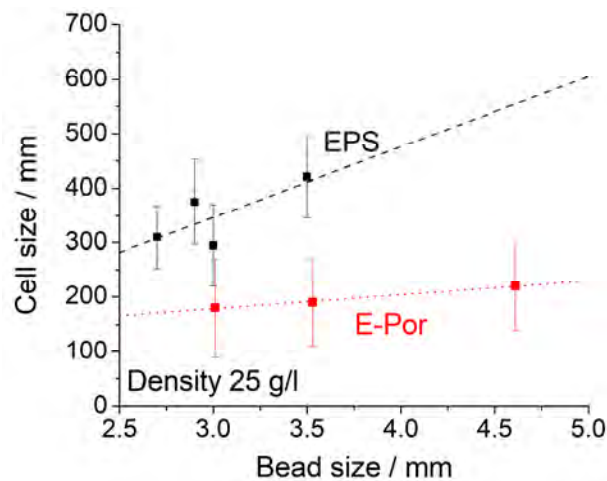


**Figure 33: Cell size in dependency of bead size for EPS and E-Por at a density of 25 g/l. The error bars do not represent the error of quantification but the width of distribution.**

In Figure 34 the dependency of the wall and strut thickness is plotted as function of bead size. For EPS only minor changes are observed. This is coherent with the observation of the cell size dependency. The studied EPS-parts possess cells with an average diameter between 300 to 400  $\mu\text{m}$ . In this range only a weak dependency of wall and strut thickness on cell size is observed (*cp.* Figure 32).

In contrast, E-Por exhibits a trend of smaller wall and strut thickness with increasing bead size, although cell size remains constant. However, the cell size distribution changes, which can cause this effect.

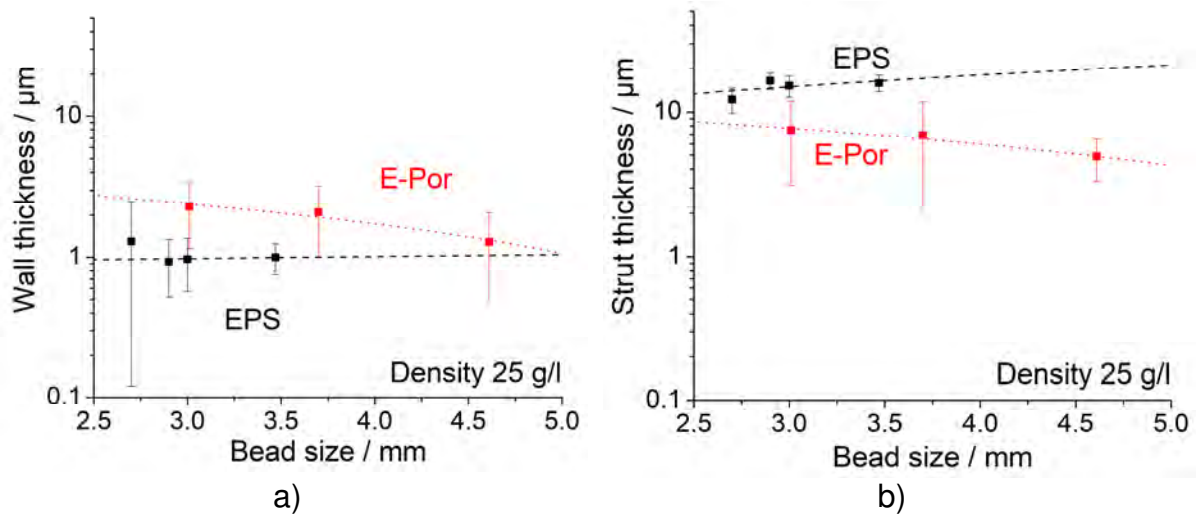


**Figure 34: a) Wall and b) strut thickness of EPS and E-Por in dependency of bead size at a density of 25 g/l. The error bars do not represent the error of quantification but the width of distribution.**

#### Effect of the density on the morphology of bead foams

For the variation of density, the pre-foaming conditions were adjusted to obtain the desired bead density. A reduced density by prolonged pre-expansion time or increased steam pressure for pre-expansion supposedly causes both larger cells as well as larger beads. Indeed, these trends can be observed for both EPS as well as E-Por in Figure 35. Although the same trend for both cell and bead size is observed, different curvatures of the dependencies yield. The cells become significantly larger with lower density, whereas almost a plateau is encountered for the bead size at low density.

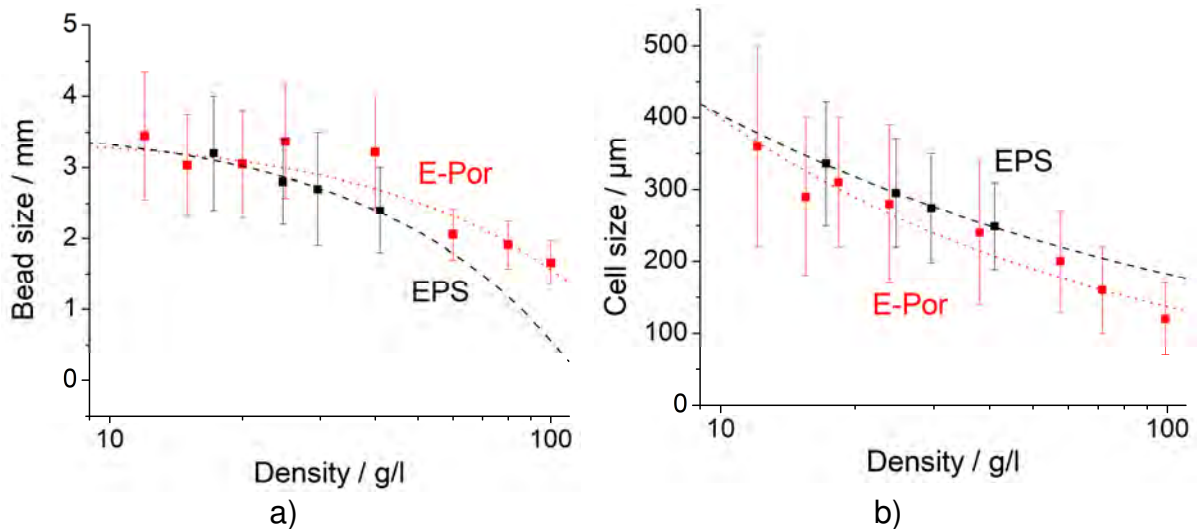


**Figure 35: a) Bead and b) cell size as function of density for EPS and E-Por. The error bars do not represent the error of quantification but the width of distribution.**

As for the cell and bead size, the density has a pronounced effect on the micro-morphology as shown in Figure 36. In the case of E-Por both wall and strut thickness increase with increasing density, which implies that the effect of more polymer is more pronounced than the reduction of cell size. In the case of EPS the wall thickness remains constant analogously to the previously shown effect of bead size. However, the strut thickness increases.

From the observed morphological changes in density it is not possible to draw definitive conclusions as too many parameters change simultaneously with density.

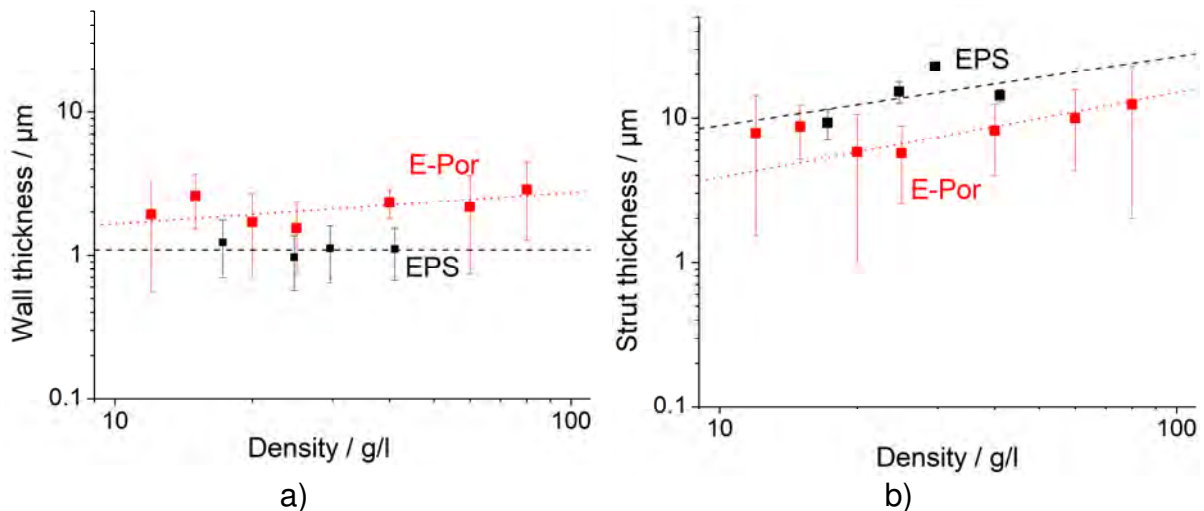


**Figure 36: a) Wall and b) strut thickness of EPS and E-Por as function of density. The error bars do not represent the error of quantification but the width of distribution.**



### Blend morphology of E-Por

In contrast to EPS, E-Por is a blend system with polystyrene as major and polyethylene as minor phase. The phases are studied regarding their orientation and total volume fraction using transmission electron microscopy due to their small size. Furthermore, the orientation probably depends on the location, *i.e.* cell walls, cell struts.

An example of a TEM image of E-Por is shown in Figure 37. A distinct orientation of the bright PE-phase can be observed in the cell wall. The dark PS-phase is the major phase. No co-continuous morphology is observed. The orientation is expected due to the equi-biaxial deformation during expansion. In contrast to the cell wall shown in Figure 37 a), the PE in the struts is elongated only in uniaxial mode. Thus, the PE domains in the struts appear more spherical in a cross-section image as shown in Figure 37 b).

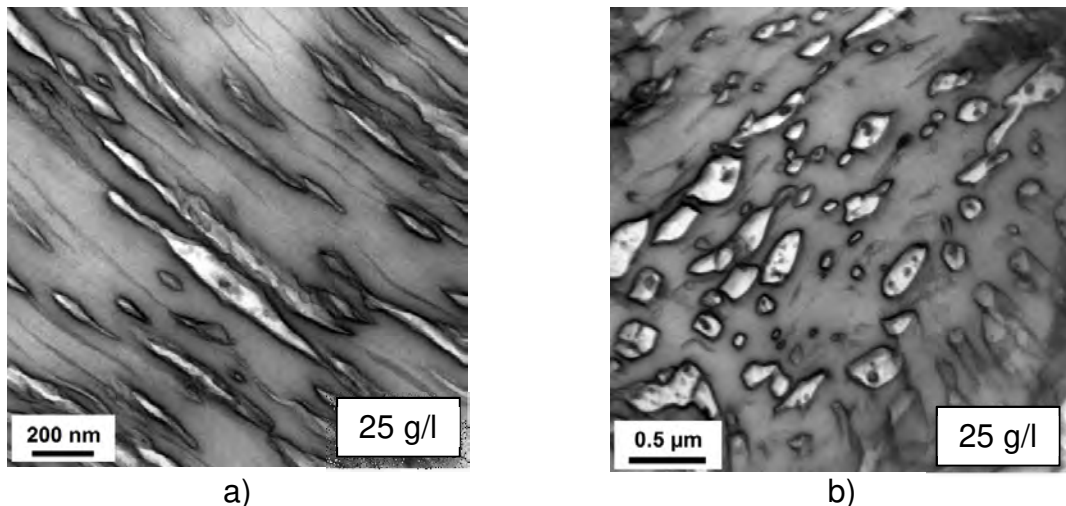


**Figure 37: Example of a TEM-image of a) a cell wall and b) a cell strut of E-Por (EPor\_25\_140\_3.5). The PE phase appears bright, PS-phase dark.**

An exemplary image and the corresponding result of the detection of the domains is shown in Figure 38. The average content of polyethylene was evaluated from numerous of TEM-pictures and yields 22.5 vol-%. The samples were also analysed regarding the domain size of PE in dependency on density and cell size. No correlation between the average value of domain size and neither density nor cell size found. This indicates, that the domain size of PE is independent on the foam morphology and expansion ratio, as the domain-morphology of the PS/PE-blend would be determined by the processing parameters (*e.g.* screw design and speed) and the volume fraction of PE. However, these results have to be regarded with care as the number of useable images for the analysis was rather limited due to the challenging sample preparation (cutting a usable thin slice of a cell wall or strut has only a chance of success of about 15 %).

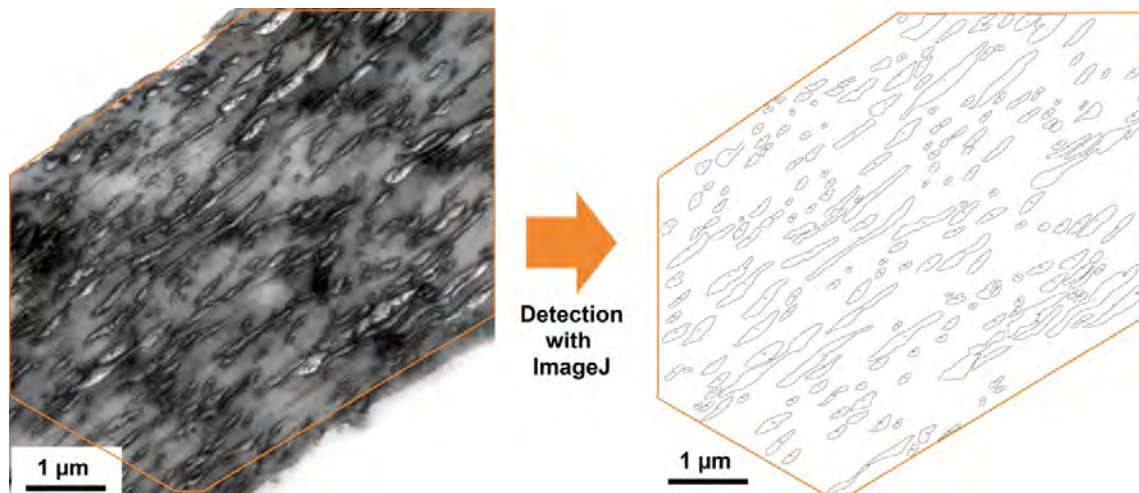


Figure 38: Example for the evaluation of the morphology of a cell wall (EPor\_25\_140\_3.5).

#### 5.1.4 Comparison of EPS from suspension polymerisation and extrusion

Although under-water pelletisation has many advantages in terms of processing, the main production method for EPS is still suspension polymerisation. Therefore, it is required to quantify and understand the differences in terms of morphology between the materials before relating them to changes in properties. In the study, three materials with different bead size from suspension polymerisation (“sEPS”: P226C, P326 and P426) are compared to the reference EPS produced by extrusion with under water-pelletisation (for better distinguishability: “eEPS”, EPS\_25\_300\_3.0\_Ref).

In terms of morphology, the bead size of the UWG-beads is in the same range as the suspension-beads, as can be observed in Figure 39 a).

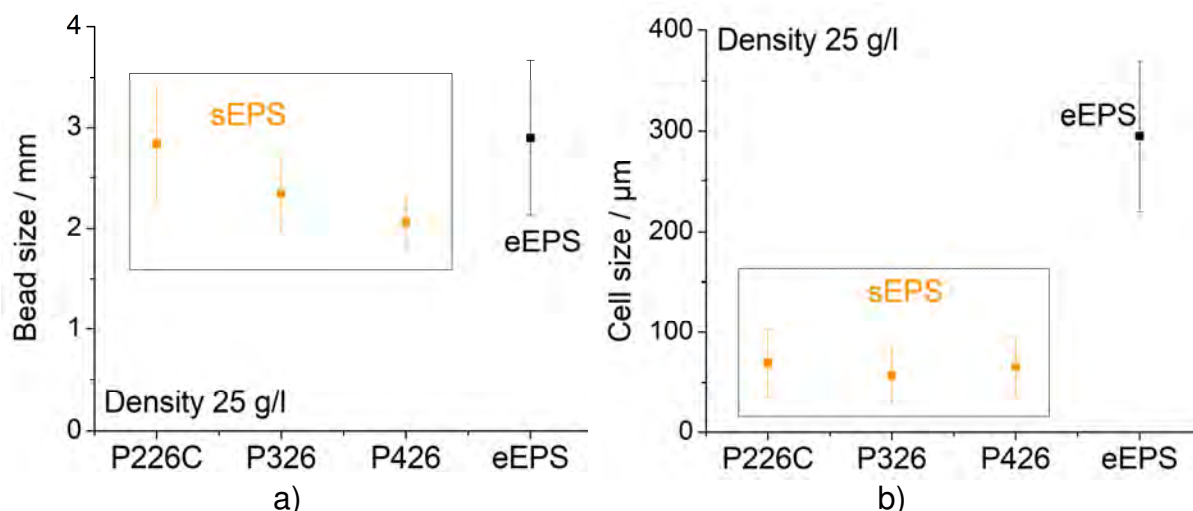


Figure 39: Comparison of a) bead size and b) cell size of sEPS and the reference EPS from extrusion. The error bars do not represent the error of quantification but the width of distribution.

The distribution of the bead size of extruded EPS is wider though, which is logical since the tested suspension-EPSs are already a fraction from sieving from the same



batch of material. However, a pronounced difference in cell size is encountered (cp. Figure 39 b)), the average cell size of extruded EPS is in the range of 300  $\mu\text{m}$ , whereas the suspension-EPS has a cell size of about 60  $\mu\text{m}$ . Also for the cell size, the distribution of extruded EPS is broader compared to the suspension-product.

This difference in cell size is also expected to be encountered in the micro-morphology. Thus, the wall and strut thickness as function of cell size are plotted in Figure 40.

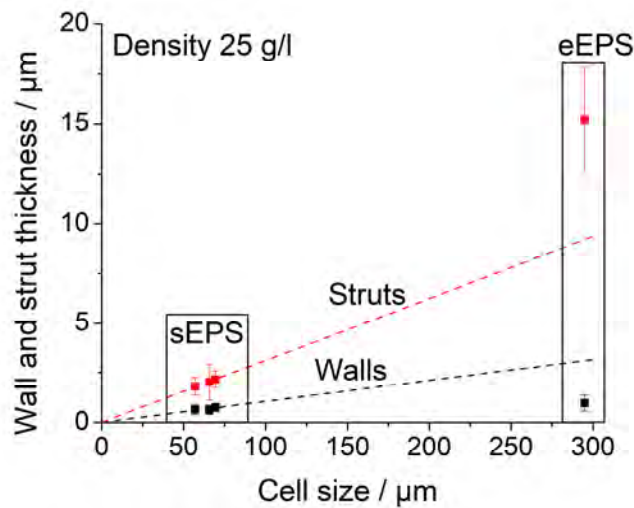


**Figure 40: Wall and strut thickness of sEPS and extrusion EPS as function of cell size with a linear fit through the data points of sEPS. The error bars do not represent the error of quantification but the width of distribution.**

The wall and strut thicknesses of sEPS follow a linear relationship with cell size. In comparison to extrusion EPS, a strong difference is obvious: the wall thickness remains almost constant and is lower than expected from the linear fit, whereas the struts of EPS are significantly thicker than expected from the fit.

From these pronounced differences in morphology, also an effect on the properties is expected. In terms of thermal conductivity, it remains to be seen, if the cell size effect (lower radiative transfer from cell border to cell border) or the effect of too thin cell walls (IR radiation can easily pass through the walls and struts) dominates. In terms of mechanics, the higher fraction of struts could cause a deterioration of mechanics of extrusion EPS.

### 5.1.5 Summary on the morphological features of the studied bead foams

Bead foams possess a complex multi-scale morphology from the meter- down to the micro-meter-range as shown in Figure 41. A studied part of the reference EPS (disc of 30 x 5 cm) is made up of a considerable number of beads, name 750,000 of them. Each bead itself contains 1000 cells, thus 750 million cells are found in the plate. Also, considerable inner surfaces are found in a bead foam part. The interfacial surface area between the beads is about 11 m<sup>2</sup>, whereas the total inner surface of the cells amounts to 235 m<sup>2</sup>. These numbers become even more impressive, when it is considered that the said foam part only weights about 90 g.

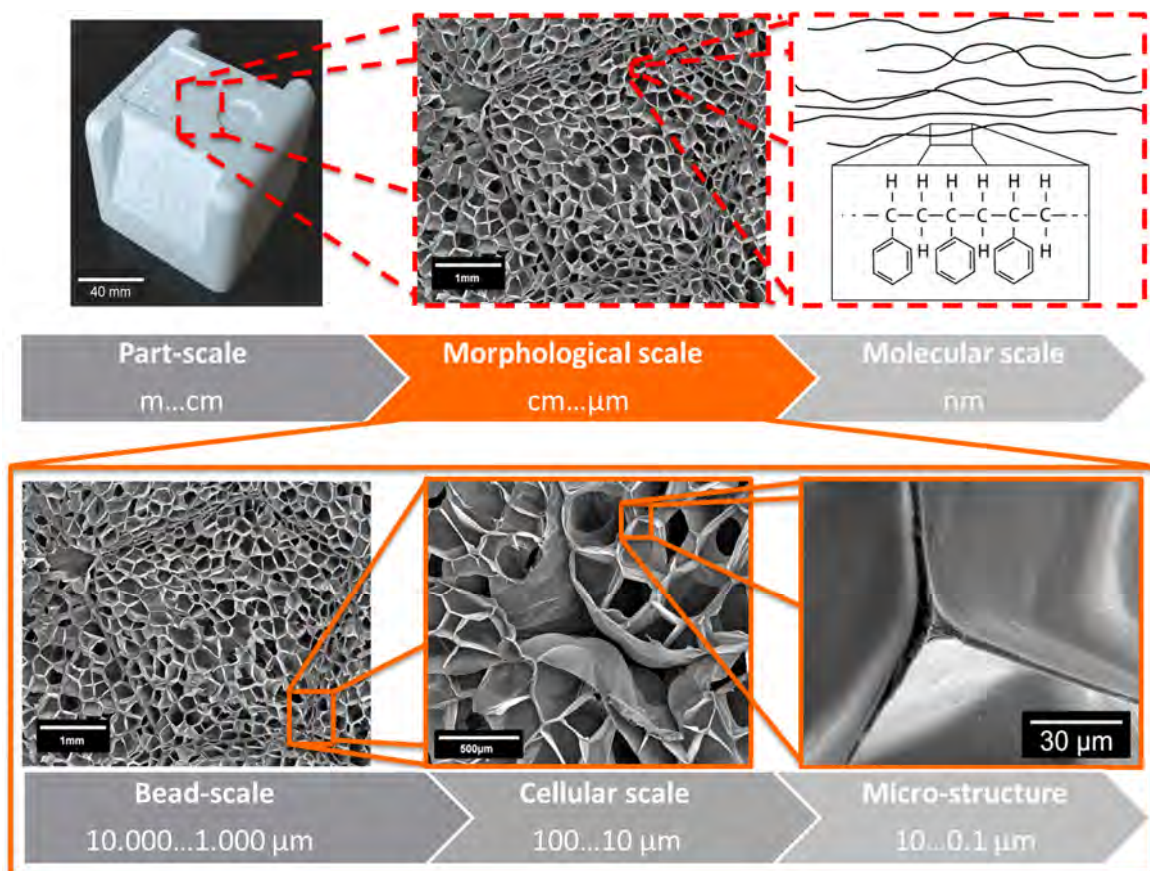


Figure 41: Repetition of Figure 27 to display the multi-scale morphology of bead foams.

Thus, it is very important to study the homogeneity of the part. It was found to be very homogeneous in the lateral dimension for both cell size and density. Only the location at the injector deviates, hence no samples are taken from this location. In contrast, a density gradient along the thickness coordinate is found. However, cell size is not much affected.

Secondly, the interdependencies of the different morphological parameters were studied. A variation of cell size at constant density naturally leads to a change in wall and strut thickness for both EPS and E-Por.

Interestingly, the walls of EPS are thinner than in E-Por and vice versa the struts. When bead size is varied, the morphology of E-Por remains rather constant, only some changes in the micro-morphology are observed. In contrast, EPS exhibits a strong dependency of cell size on bead size: larger beads cause larger cells, which leads to a change in strut thickness, too. When the density is increased by varied pre-foaming conditions, then both cell and bead size become smaller, which also causes a change in the micro-morphology for EPS and E-Por. Thirdly, EPS from suspension polymerisation (sEPS) was compared to EPS produced in extrusion with under-water pelletisation. In terms of bead size both materials are in a comparable range. However, this does not account for the cell size, which is for sEPS only about one fifth of extrusion EPS. Interestingly, the wall diameter remains the same, only the struts of extrusion EPS become thicker.

The changes in macro- (cell and bead size) and micro-morphology (wall and strut thickness) are expected to affect the mechanical and thermal transport properties. A higher fraction of struts can reduce the linear mechanical properties at low density according to the Gibson-Ashby-model but lead to improved insulation capabilities due to improved absorption of IR radiation. Smaller cells are supposed to improve the insulation capabilities. It remains to be seen in the subsequent chapters, whether these hypotheses are correct.

## 5.2 Mechanical and fracture mechanical properties

The following chapter will show how the bead foam's morphology affects the mechanical properties. At first, the fundamental properties under compressive and flexural loading are presented and the mechanisms explained. Subsequently, the fracture toughness in relation to the morphology is discussed.

Again, it is noted, that all samples are named according to the following system:

$$\text{Material\_Density[g/l]\_AverageCellSize[\mu\text{m}]\_AverageBeadSize[mm]}.$$

Additionally, a "REF" at the end denotes the reference samples.

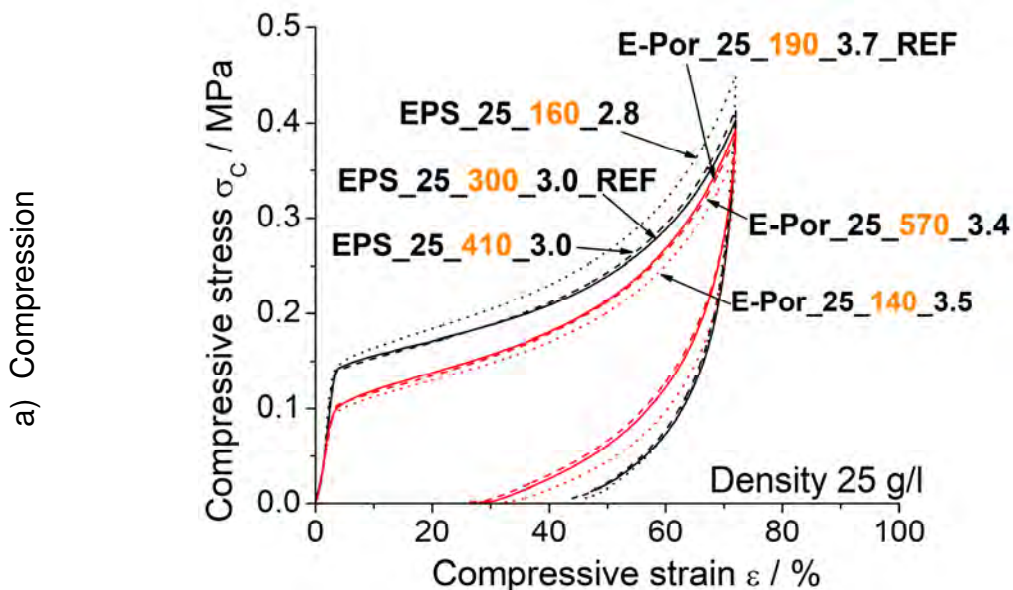
### 5.2.1 Fundamental mechanical characterisation (quasi-static behaviour)

The fundamental mechanics in compression and bending of both EPS and E-Por are presented below. The focus lies on EPS, as we can better deduce the governing mechanisms of this model material.

The morphological parameters are discussed as before from the small length scale to the large, thus at first the cell scale and second the bead scale are presented. Subsequently, the density is presented and discussed, as both bead and cell sizes vary with density.

#### 5.2.1.1 Effect of the micro-morphology by variation of cell size

When the cell size is varied, also the micro-morphology in the shape of the cell walls and cell struts is directly affected. Smaller cells lead to thinner walls and struts as shown before. It is expected, that this also affects the mechanical response of the respective foams. Thus, stress-strain curves for representative samples of EPS and E-Por in compressive and flexural loading are shown in Figure 42.



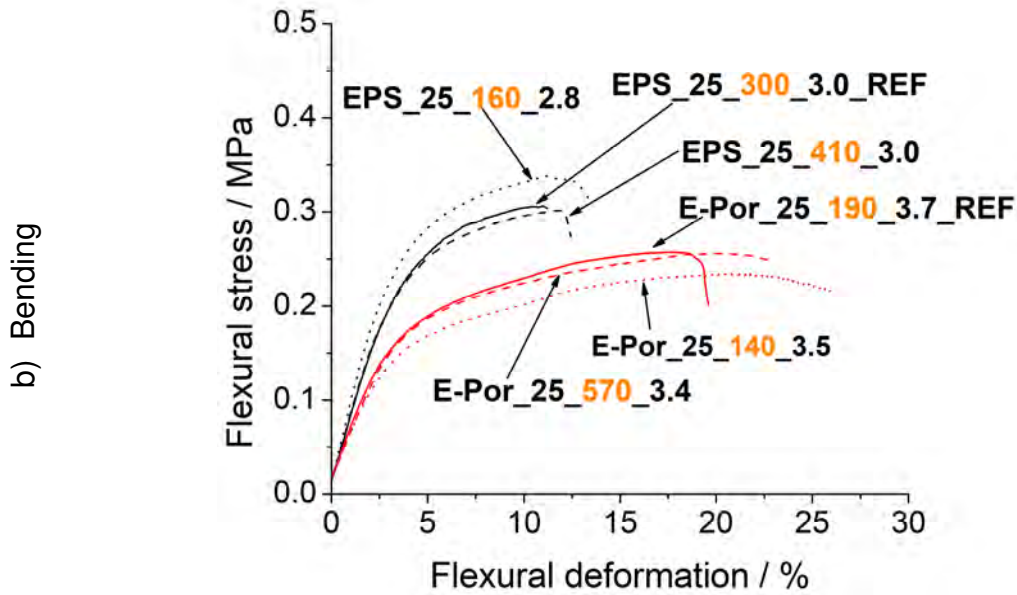


**Figure 42: Stress-strain curves of EPS (black) and E-Por (red) at a density of 25 g/l with various cell sizes (orange number) under a) compressive and b) flexural loading.**

The curves for EPS and E-Por in compression (Figure 42 a)) are typical for low-density foams with thin walls and struts. Three regimes can be distinguished: a) the linear elastic regime (strain < 4 %), the plateau regime (strain > 4 % and < 50 %) and ultimately the regime of densification (strain > 50 %). It is interesting to note, that no stress overshoot after the linear-elastic regime is observed. This indicates a high potential for plastic deformation of the thin cell walls and struts. Also, the stress-strain curves under flexural loading are typical (Figure 42 b)). After a linear-elastic regime, the curves flatten until failure occurs (drop of the stress). When EPS and E-Por are compared, it becomes clear that E-Por is more elastic than EPS. This is reflected in the lower hysteresis area as well as increased recovery in compression (Figure 42 a)) and a higher strain at failure in bending (Figure 42 b)). However, the increased elasticity comes at the cost of lower properties as will be shown below.

From the stress-strain curves, the characteristic values in relation to cell size are extracted. As shown in Figure 43, both the compressive and flexural properties (modulus and strength) of EPS are sensitive towards cell size, whereas no significant trend can be observed for E-Por.

This is attributed to the fact, that the mechanical response of E-Por is distinctly affected by the PE-domains, which are elongated sufficiently for the studied density (25 g/l). The elongation of the PE-domains does not systematically vary with cell size. Similar observations were also made for the fracture toughness and will be discussed in the second part of the chapter (chapter 5.2.2.1, page 90).



In contrast, the mechanical properties of EPS are distinctly dependant on cell size. In the linear regime of deformation both the compressive and flexural modulus increase by about 18 %, when the cell size reduces from 400 to 150  $\mu\text{m}$  (Figure 43 a) and b)). Also, the non-linear regime is affected significantly. Interestingly, the compressive strength increases only by 7%, whereas the flexural strength increases by 19 % when cell size is reduced from 400 to 150  $\mu\text{m}$ . Only the recovery after compression remains unaffected by cell size (*cp.* Appendix: Figure 125). Possible reasons for the observation of better mechanics with smaller cells for EPS will be given below.

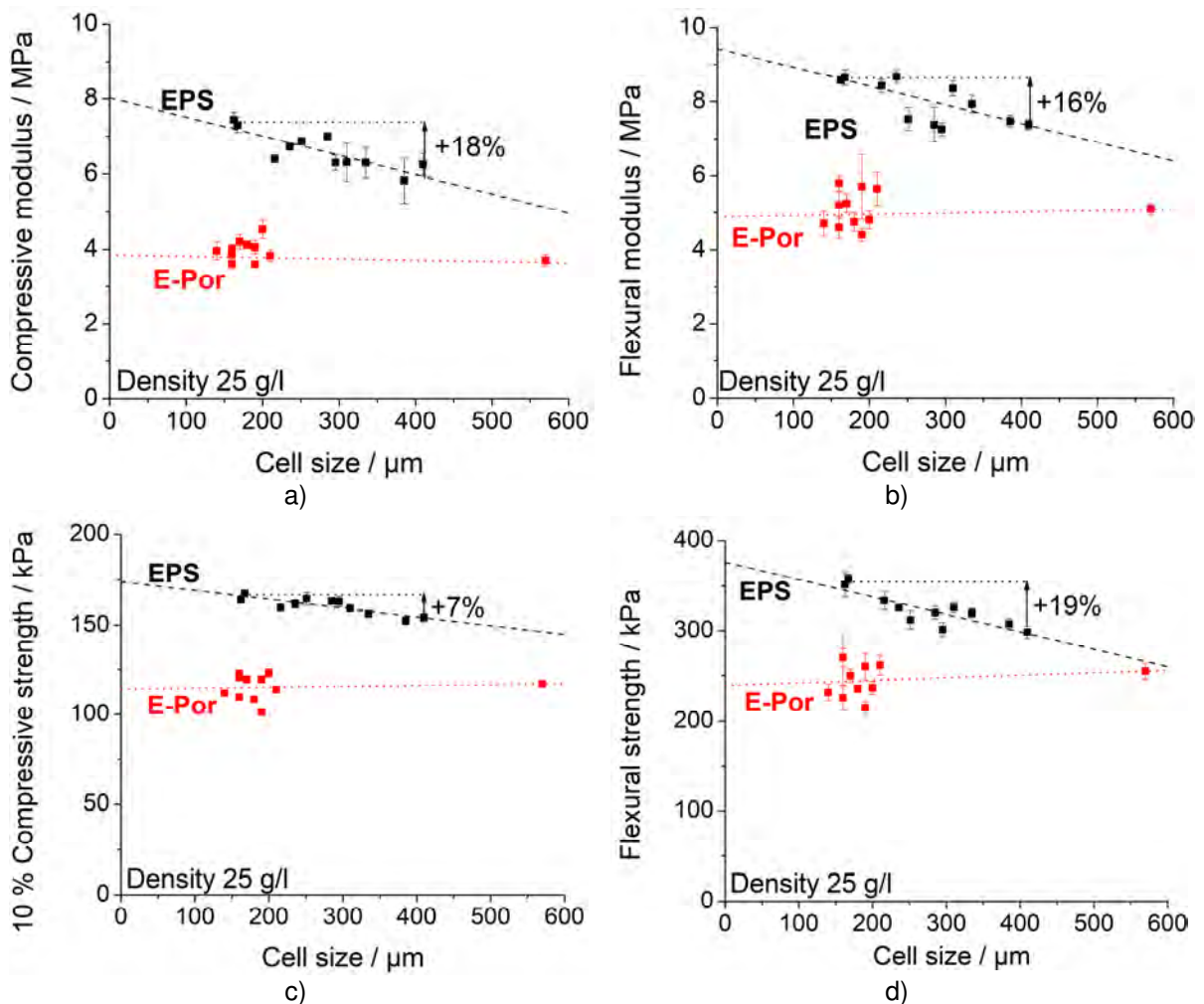


**Figure 43: Characteristic values of EPS and E-Por as function of cell size at a density of 25 g/l. The a) compressive and b) flexural modulus as well as c) the compressive strength at 10 % strain and d) the flexural strength are shown.**

Two origins for the observed behaviour appear possible:

1. Differences in residual orientations
2. Different molecular state of small cells (similar to annealed/tempered PS)

The first reason derives from the foaming process itself. During expansion, the polymer is subjected to equi-biaxial elongation [153], which leads to an orientation of the polymer chains. These orientations are “frozen”, when the polymer undergoes its glass transition upon cooling and loss of dissolved blowing agent. Residual stresses are a consequence of the frozen orientations. These stresses can lead to a pre-loading of the cell walls and struts, which acts as restoring force upon loading with external forces. Thus, the mechanical properties are improved.

Secondly, we can consider the difference in molecular state of the small cells. From literature it is known, that polystyrene, which was annealed, exhibits superior mechanical properties compared to quenched PS, as shown in Figure 44 a) [154]. As both modulus and strength are improved by both annealing and smaller cells, the mechanism can be responsible for both observations. Thus, one should study how similar the foamed samples are to an annealed state.

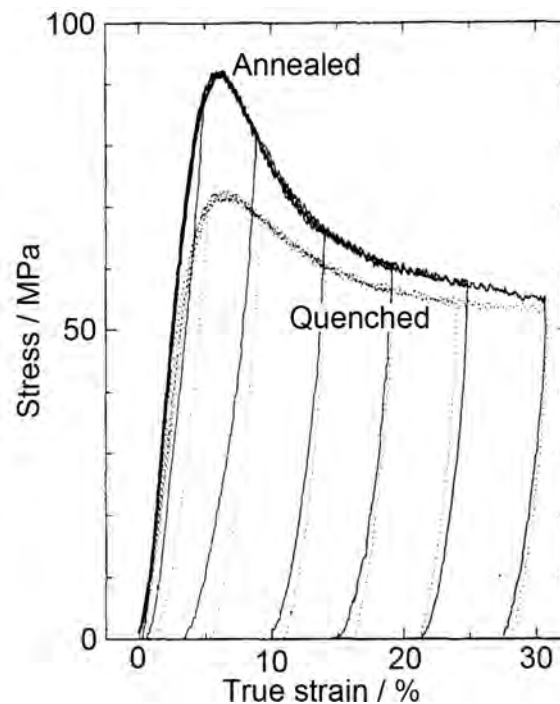


**Figure 44: Stress-strain curve (compression) of annealed and quenched Polystyrene. Graph modified from Hasan et al. [154].**

These two hypotheses were explored with two different experiments. Residual orientations lead to strong restoring forces, when the polymer is heated above its glass transition temperature  $T_G$ .

Thus, EPS beads were put into an oven at various temperatures and their shrinkage was recorded as function of time. If orientation is a function of cell size, the shrinkage speed should be highly dependent on cell size.

In order to obtain further information on the molecular state, DMA experiments (temperature sweeps) with untreated samples and tempered samples (85 °C, 14 days) were carried out. In particular, the shift in  $T_G$  with respect to cell size was noted, as this property represents the difference to tempered samples and thus the potential for better mechanical properties. In the following section, the results of these experiments for a selection of samples are discussed below.

#### **a) Residual orientation measured by shrinkage experiments above $T_G$**

In order to have sufficient temporal resolution, the temperature of the shrinkage test is needed to be sufficiently low. However, low temperatures would lead to long experimentation times. Thus, pre-experiments (not shown here) showed that 120 °C was a suitable temperature.

The relative volume as a function of time is shown in Figure 45 a) for samples with various cell sizes (constant density 25 g/l, almost constant bead size). It can be seen, that two regimes of shrinkage occur. At the beginning, the shrinkage proceeds rather slowly. After about 1000 s a distinct decrease in volume takes place. Three shrinkage mechanisms lead to this behaviour: a) a reduction of the internal free surface, b) the relaxation of residual stresses due to frozen chain orientation and c) a collapse of the foam structure upon heating.

In order to account for this finding, the relative volume as function of cell size was evaluated in the two regimes (4 min and 45 min) as plotted in Figure 45 b). It is observed, that almost no cell size dependency exists at the early stage of shrinkage. In contrast, the second regime is highly dependent on cell size. In this stage, the sample has shrunk significantly, thus the driving force to reduce the internal free surface should be low and the sample is at equilibrium temperature. Thus, the shrinking should be dominated by stress-relaxation.

In summary, the shrinkage experiment indicates, that residual stresses contribute to better mechanical properties within smaller cells. This is also due to the fact that the direction of chain orientation is the expansion direction of the cell walls and struts.



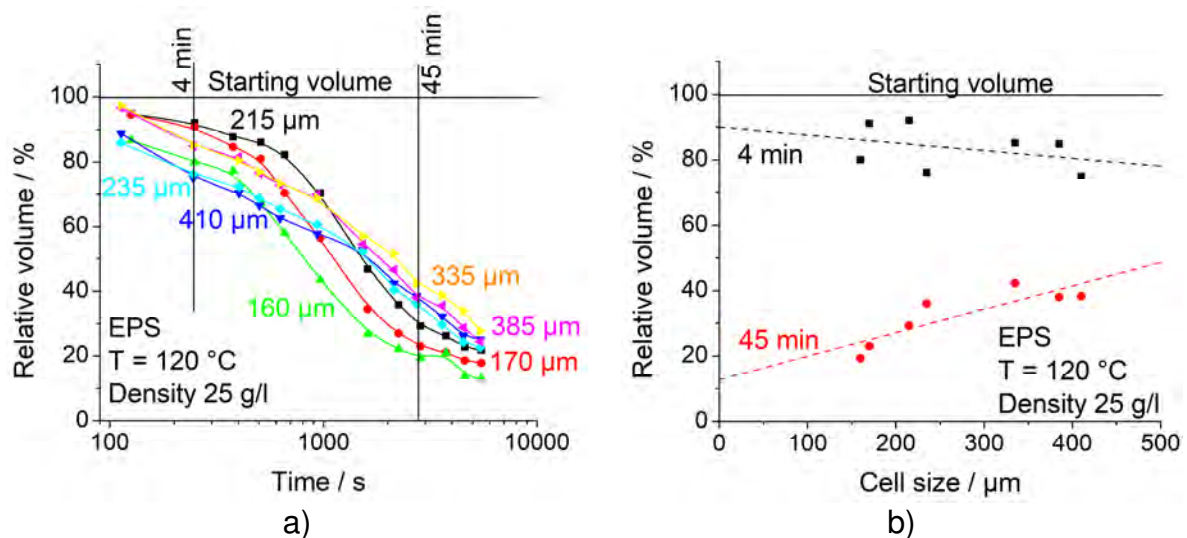


Figure 45: Results from shrinkage experiments at 120°C: a) the transient relative volume for samples with various cell sizes and b) the relative volume as function of cell size after 4 min (240 s) and 45 min (2700 s) heating in an oven at 120 °C.

### b) Shift in the glass transition compared to tempered samples (DMA)

In order to test, how close EPS samples with different cell sizes are to their tempered counterparts, DMA experiments of untreated and tempered samples were conducted. An example curve for the reference EPS is shown in Figure 46 a). The storage modulus of the tempered sample is higher compared to the untreated sample. Furthermore, a shift in  $T_G$  by 6.5 °C occurs. This shift may be caused by residual pentane within the structure. This was tested by TGA-experiments. As  $T_G$  is reduced by about 7 °C per wt-% pentane [64], nearly 1 % pentane should be detectable in the TGA-diagram of the EPS reference sample. However, no weight reduction was detected. Thus, this possibility is discarded.

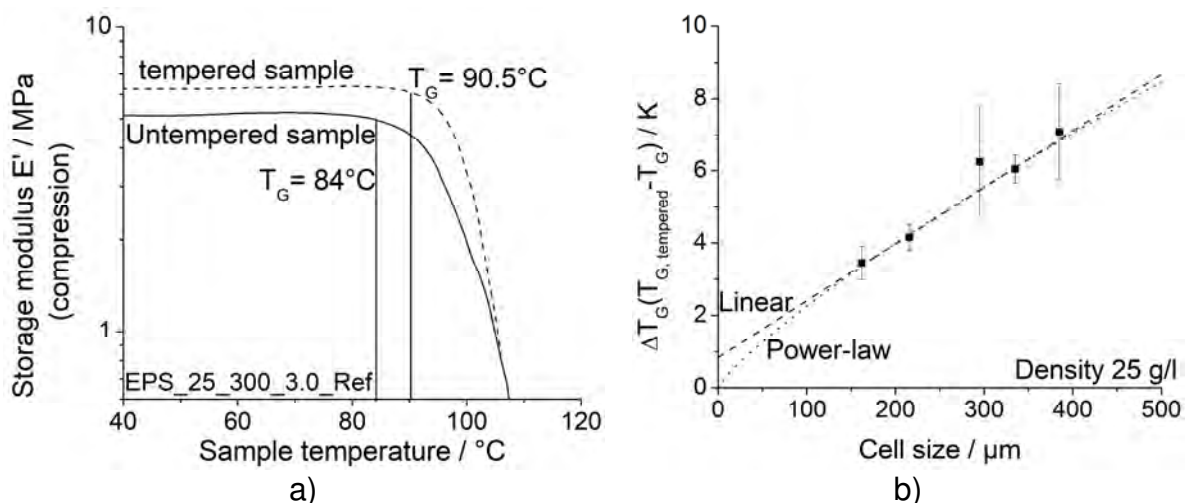


Figure 46: a) DMA curves of an untempered and tempered reference sample shown alongside their respective glass transition temperatures,  $T_G$ . b) Difference in  $T_G$  between untempered state and tempered samples with respect to cell size.

Interestingly, the difference between the tempered  $T_G$  and the “normal”  $T_G$  is a function of cell size as shown in Figure 46 b). A significant trend of  $\Delta T_G$  versus cell size is observed. From the results it is concluded, that foams with smaller cells possess a higher degree of annealing compared to foam with large cells. A reason for this finding could be the lower thermal conductivity of foams with small cells (as shown in the following chapter), which gives the centre of the bead foam more time to cool and thus achieve a higher degree of annealing.

In summary, the DMA experiments strengthen the hypothesis, that smaller cells exhibit a higher degree of annealing and thus possess superior mechanical properties.

### **c) Concluding remarks**

Smaller cells clearly improve the mechanical properties of neat EPS, however not the blend, E-Por. Unfortunately, the available literature does not provide conclusive answers to the “why?”. Thus, the two possibilities “residual stress due to frozen orientation” and the “degree of annealing” were investigated by means of shrinkage experiments and DMA temperature-sweeps. With these fundamentally different experiments, the following statements can be drawn:

- Smaller cells lead to higher residual stress
- Smaller cells increase the degree of annealing.

These two facts can lead to better properties with smaller cells. However, more research should be conducted on this highly interesting and relevant topic in order to be able to transfer the mechanisms to other materials. Also, the free volume could be affected by changes of the cell wall thickness. Positron annihilation lifetime spectroscopy at low energies could be carried out to explore the fractional free volume of the cell walls and struts with respect to cell wall thickness.

#### **5.2.1.2 Effect of inter-bead interfacial area by variation of bead size**

When the bead size is changed, the interfacial area between the beads changes drastically as explained before. The benchmark system, suspension EPS with three different bead sizes, is also presented and discussed, which allows a broader view on the effect of bead size on the mechanical properties.

The respective stress-strain curves of representative samples possessing different bead sizes are shown in the appendix (*cp.* Figure 126). The shapes of the stress-strain curves are not significantly different. However, the characteristic values show interesting trends. Since, the linear and non-linear properties exhibit the same trends, only the

linear values are shown here (*cp.* Figure 47 a) and b)). The non-linear characteristic values are given in the appendix (*cp.* Figure 127).

In general, no universal law for the three materials can be derived. Under compressive loading an optimum bead size exists for EPS (sEPS 2.3 mm, extrusion EPS 3 mm), whereas E-Por shows almost no sensitivity towards bead size fluctuations. In contrast, the flexural properties benefit from larger beads for all three materials, as no maximum is discernible. Interestingly, a trend across all three materials can be seen for the property of recovery after compression. An optimum bead size at about 3.8 mm exists. In compression, similar properties of sEPS and extrusion EPS are found, whereas sEPS delivers superior properties in flexural deformation.

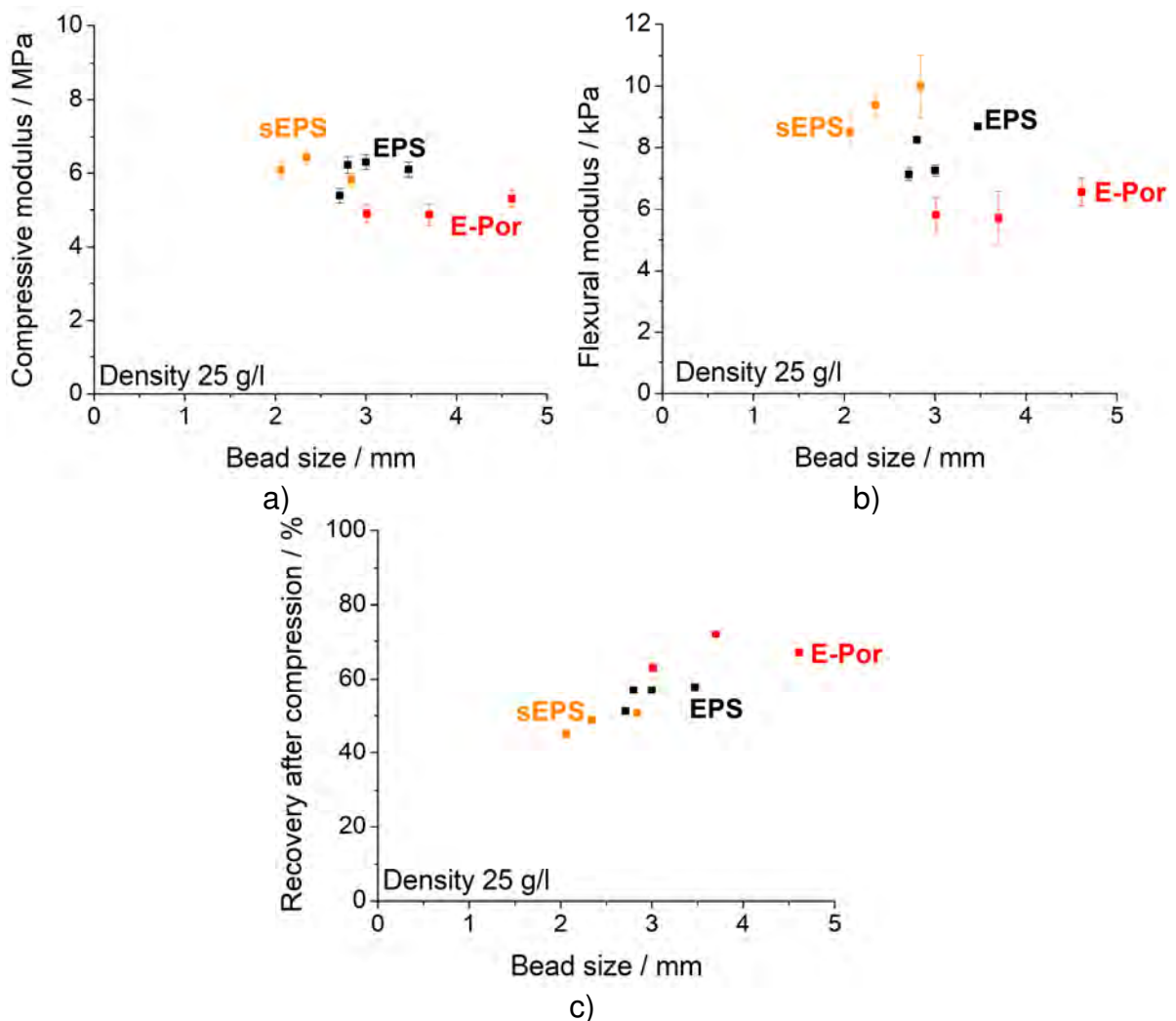


**Figure 47: Characteristic values of EPS and E-Por in dependency of bead size: a) compressive and b) flexural modulus as well as c) the recovery after compression.**

From the results, it is concluded that the bead size affects the moulding quality. Larger beads lead to better moulding due to better energy transfer and less surface that needs to be softened. This improves the mechanical response. However, a negative trend on

the mechanics is expected for beads that are too large, since they cause more macro-porosity, which then diminishes the mechanical properties. The section on the dependency of bead size on the fracture toughness (chapter 5.2.2.2, page 97) will elaborate this topic further.

### 5.2.1.3 Effect of the polymer fraction (foam density) on the fundamental mechanical properties

The variation of density goes hand in hand with a change of both cell and bead size as well as micro-morphology (wall and struts). Therefore, the effect of a combination of changing morphology and density on the properties is observed. As expected, the density is, by far, the most important parameter on the mechanical response of bead foams as can be seen in Figure 48. It can be seen, that the properties of E-Por are shifted towards lower values compared to EPS. Slight differences between EPS and E-Por arise for the compressive modulus. In contrast, EPS and E-Por possess more similar values in flexural deformation.

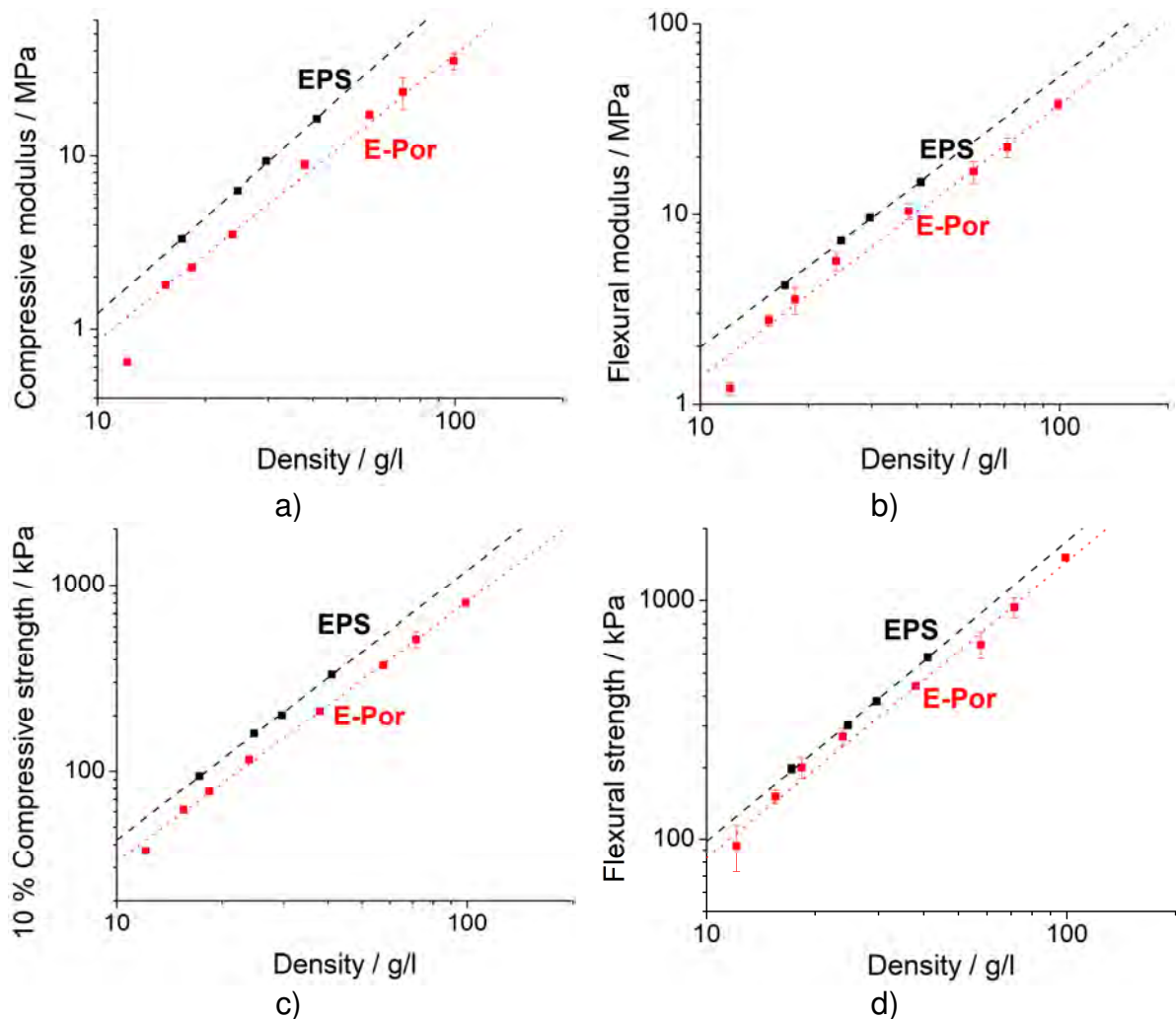


Figure 48: Effect of density on a) compressive and b) flexural modulus as well as c) compressive and d) flexural strength of EPS and E-Por. Both cell and bead size vary with density.

All properties obey power-law statistics ( $y = Ax^n$ ), which is also reported in literature [155]–[157]. The power-law exponent  $n$  represents the sensitivity towards density and is given in Table 5. It can be observed, that  $n$  is higher for compression than bending. In bending,  $n$  is rather similar for strength and modulus, whereas a distinct difference is found for compression. This can be explained by a different sensitivity of deformation mechanisms on density. In bending, the deformation mechanism is the same in the linear and non-linear region (stretching dominated), which is not true for compression (linear region: bending, buckling; non-linear region: plastic hinging, breaking).

**Table 5: The power-law exponent  $n$  of density for the quasi-static properties.**

	<b>Flexural modulus</b>	<b>Flexural strength</b>	<b>Compressive modulus</b>	<b>Compressive strength</b>
<b>EPS</b>	1.44	1.24	1.84	1.45
<b>E-Por</b>	1.43	1.26	1.65	1.40

In all cases, the power-law model was the most suitable, *e.g.* if a linear fit is used for bending, non-physical results arise for low densities as the modulus / strength equal zero at a density above zero. This would mean no mechanical properties below a critical threshold, which does not make sense. The power-law model also yields superior fitting quality compared to a fit with the famous Gibson-Ashby-Model (*cp.* Appendix Figure 130 a) and b)), since this model fails to describe the modulus at low density.

The recovery after compression is also significantly affected by density (*cp.* Appendix Figure 129). As expected, lower density leads to an increased recovery as the aspect ratio of the cell walls and struts increases, which prevents or reduces plastic deformations. However, this is only true for densities  $\geq 20$  g/l. At lower density, the effect of macro-porosity then dominates.

#### **5.2.1.4 Micro-deformation mechanisms in polystyrene bead foams**

The micro-deformation mechanisms were studied *via in-situ* SEM. A standard light-microscope is not suitable due to a low depth-of-field as well as the light-transparent cell walls and struts. With *in-situ* SEM, a miniaturized mechanical testing apparatus is placed into the SEM, which continuously provides SEM micrographs during the slow deformation of the sample. Only a selection of samples was tested due to high experimental effort. For the interpretation of the results it must be considered, that the experiments are conducted under vacuum.



However, this is not deemed problematic, as the experiments are not meant to yield stress-strain curves, which are highly dependent on the cell gas. The deformation is recorded on the surface at the foam, where the surrounding gas has no influence.

The aim of these studies is to clarify where the deformation in compression takes place and whether other structural parameters lead to premature local failure. The results of the reference EPS (EPS\_25\_300\_3.0\_Ref) are presented in Figure 49.

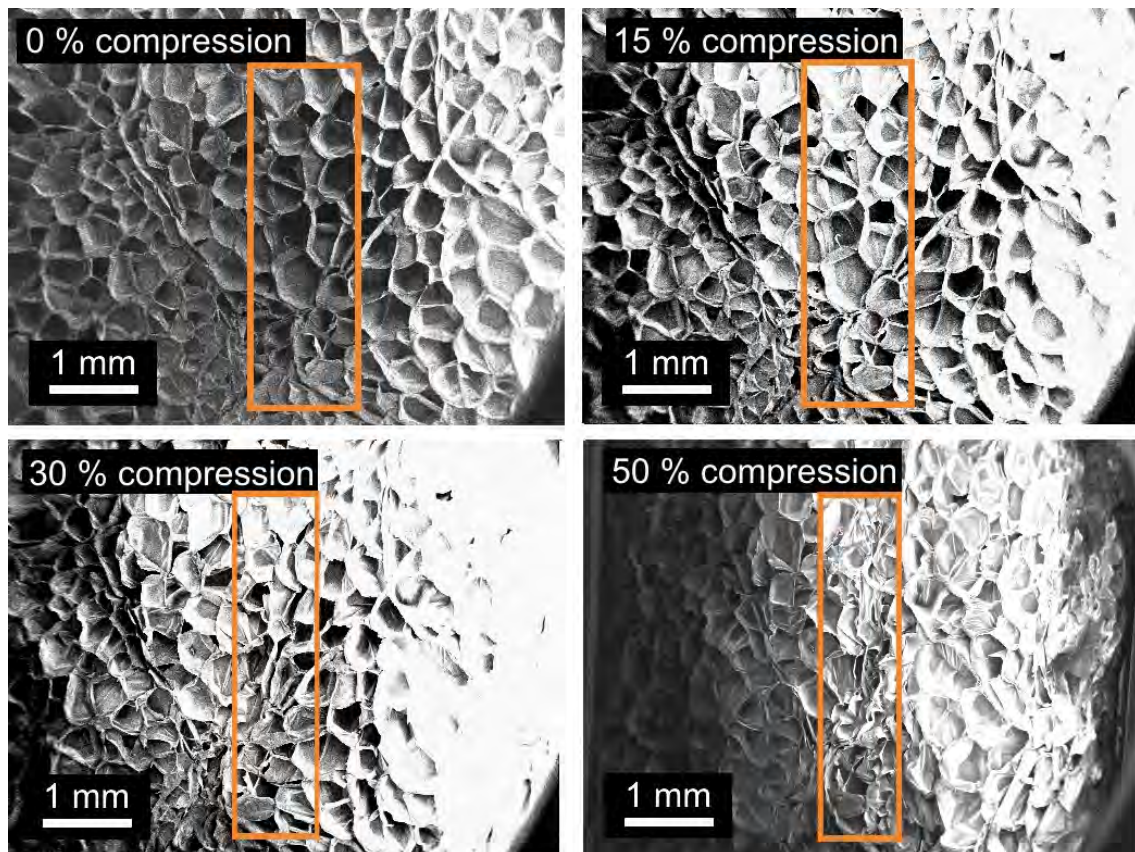


**Figure 49:** *In-situ* SEM micrographs of the reference EPS (EPS\_25\_300\_3.0\_Ref) at various strains in compressive deformation (speed: 10  $\mu\text{m/s}$ ).

During the experiment, the sample shifts, which leads to clipping in a part of the observed area (e.g. the right corner in the micro-graph at 30 % strain). It is observed, that the deformation is highly localised. This was expected as this is well-known for foams in general. When the area, which is highlighted in orange, is considered, it becomes clear, that the deformation starts in the central region of the bead and then “grows” to the outer regions.

In order to obtain information on how the interfacial area affects the deformation pattern, samples from the smallest beads were tested (EPS\_25\_310\_2.7), as they exhibit the worst mechanical properties and thereby should show the mechanisms leading to premature failure in the most pronounced manner. The resulting micrographs at different strains are presented in Figure 50.

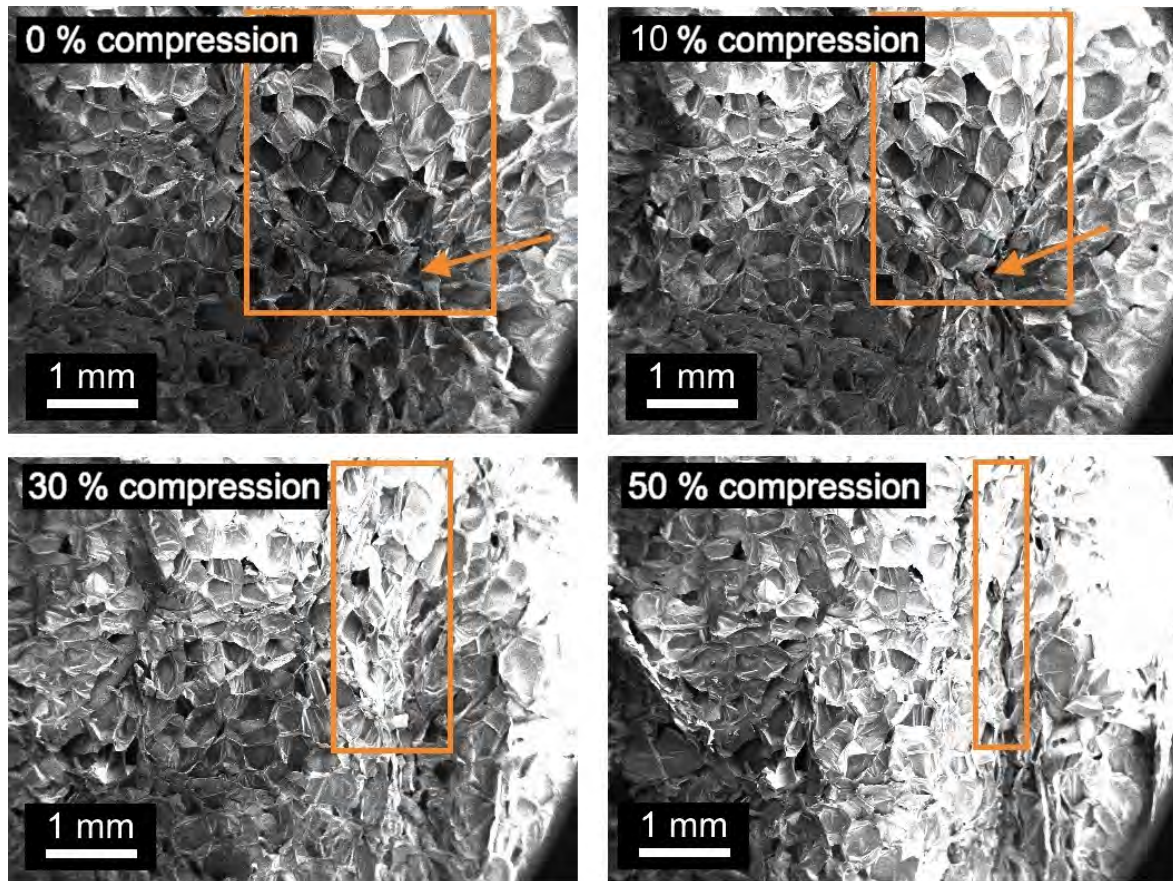


Figure 50: *In-situ* SEM micrographs of the EPS sample made from the smallest beads (EPS\_25\_310\_2.7) at various strains in compressive deformation (speed: 10  $\mu\text{m/s}$ ).

Interestingly, a macro-void is also visible as highlighted by the arrow. It can be seen, that the deformation spreads from this macro-void as it is already quite deformed at low average strains. It is concluded, that the macro-porosity between beads acts as a weak spot in compressive loading. It is observed once more, that especially the central regions of the beads are preferably deformed as shown by the highlighted area.

In summary, it was seen that deformation is highly localized and preferably starts in the central region of the beads, independently on bead size. Furthermore, it is observed, that residual macro-porosity acts as a defect and is responsible for diminished properties of parts made of small beads compared to the reference.



### 5.2.1.5 Effect of the strain rate on the mechanical response and its interdependency with the foam morphology

The effect of strain-rate on the mechanical properties is highly interesting from both a scientific as well as practical viewpoint. The strain-rate affects both mechanical response of the polymer as well as the efficiency of the cell gas in order to provide restoring forces against further deformation. Since EPS is often used for crash-absorbing applications, *e.g.* in helmets, knowledge on the effect of strain rate on the mechanics is a requirement for the efficient design of protective equipment.

It is shown that both EPS and E-Por exhibit a distinct sensitivity of their mechanical response towards strain rate, as shown for E-Por in Figure 51. It is observed, that the non-linear properties are changed pronouncedly: strength is increasing distinctly with increasing strain rate. Furthermore, the recovery after compression is distinctly improved at higher strain rates.

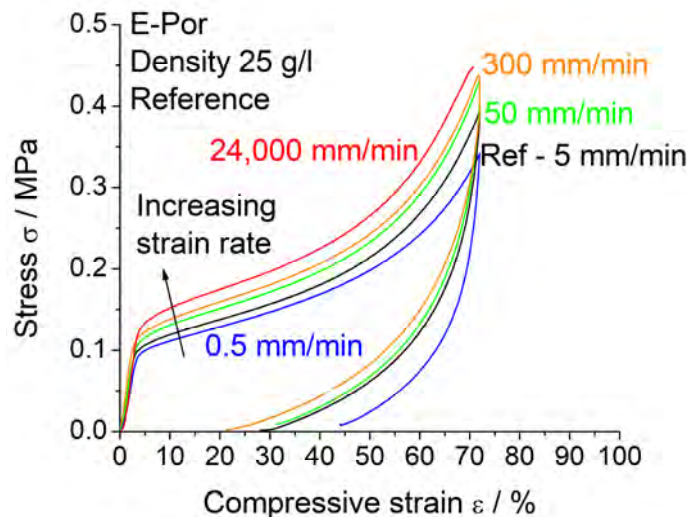


**Figure 51: Stress strain-curves of E-Por (E-Por\_25\_190\_3.7\_Ref) at different strain-rates.**

However, EPS and E-Por show some differences in their individual dependencies on strain rate, which will be discussed here. Therefore, the characteristic values for compression of the reference samples (density 25 g/l) are plotted in Figure 52.

A clear dependency of all characteristic values on strain-rate is observed. The modulus, strength and especially recovery after compression improve with increasing strain-rate. We will first discuss the strain-rate dependency of the modulus and strength and then later discuss the recovery. Interestingly, the dependency of modulus and strength can be quantified using power-law statistics as already seen for the density-dependency ( $y = Ax^n$ ;  $y$ : Modulus or strength,  $x$ : Strain rate,  $A$ :  $y$  at strain rate 1,  $n$ : sensitivity of  $y$  on strain rate). Especially the sensitivity  $n$  is of interest, since it signifies the relative change of mechanical response on strain rate.



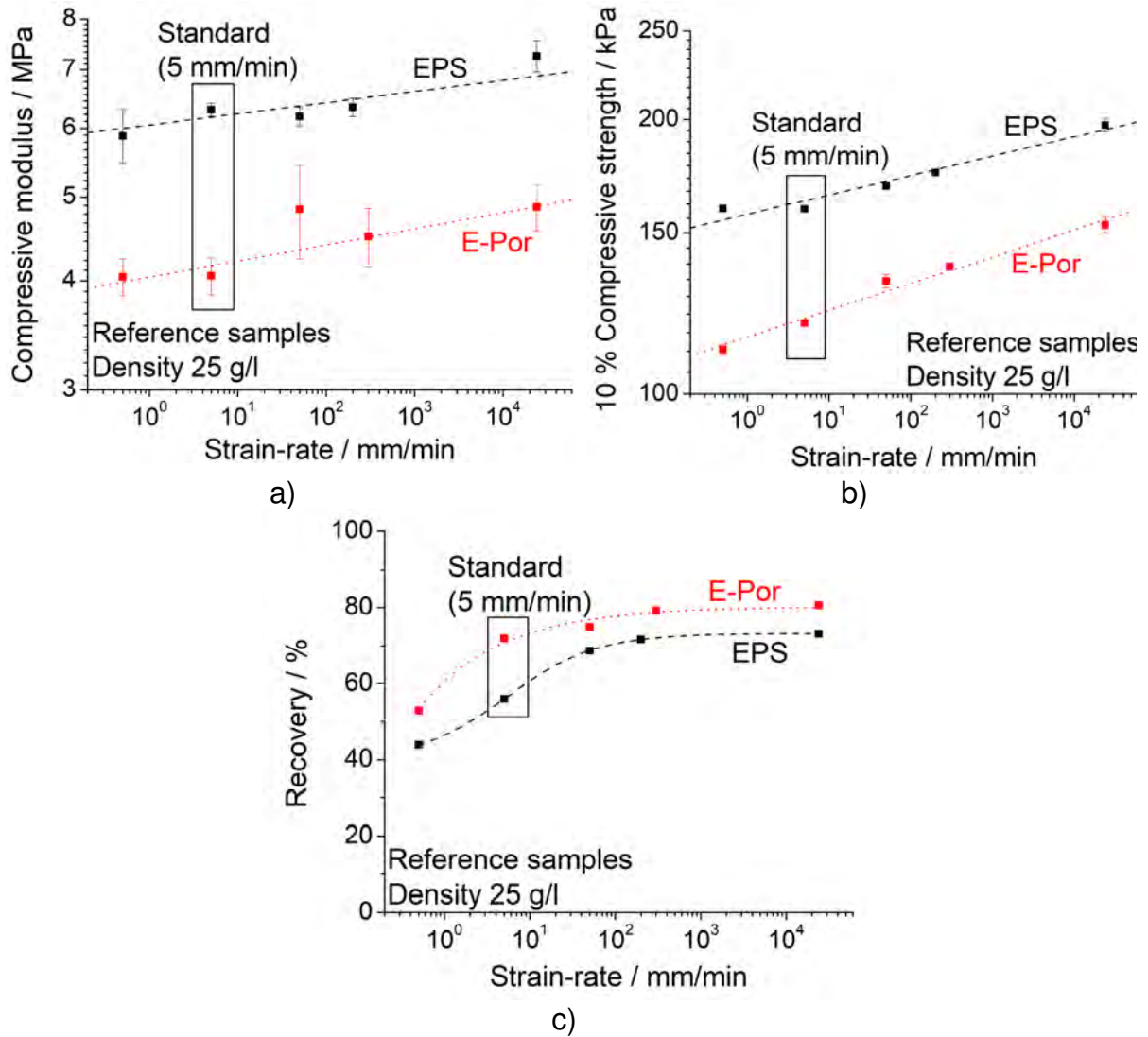


**Figure 52: Dependency of the a) compressive modulus, b) compressive strength and c) recovery after compression on strain-rate for the reference materials eEPS\_25\_300\_3.0\_Ref and EPOR\_25\_190\_3.7\_Ref.**

For EPS,  $n$  of the modulus (at the reference density of 25 g/l) is  $n_{E,EPS} \approx 0.012$ ,  $n$  of the 10%-compression strength is  $n_{S,EPS} \approx 0.021$ . In contrast, E-Por exhibits a distinctly higher sensitivity  $n$  of the modulus of  $n_{E,EPor} \approx 0.018$  as well as for strength  $n_{S,EPor} \approx 0.029$ . This behaviour is attributed to the matrix material. E-Por consists of a blend of PS with a significant amount of PE. At room temperature, the glass transition temperature of PE is exceeded significantly, which is related to a distinct sensitivity of the mechanical response on strain rate in accordance with the relation of experimental time and a characteristic material time (*i.e.* the relaxation time). Analogously, this is described by the Deborah-number  $De$  (relaxation time / time of observation) in rheology.

For PE, the relaxation time must be in the same range of the experimental time or below, which is reasonable as the  $T_G$  is exceeded significantly. For PS, this is not the case, because the experiments were conducted at room temperature, which is around 80 °C below  $T_G$ . Hence no relaxation of the main chains can occur, so no or only a very small dependency of the modulus (and therefore  $n$ ) on strain-rate is expected.

In terms of strength, a higher strain-rate dependency  $n$  for E-Por is expected compared to EPS, which is due to the higher strain-rate sensitivity of the PE-phase (content about 23 vol-%). This is also observed. In general, the strain-rate sensitivity of the strength is higher than for the modulus. This relates to the diffusion of the cell gas out of the foam, which is almost irrelevant in the regime of linear (small) deformations, but not for high deformations. At low strain rates, the cell gas has enough time to diffuse out of the foam during compression thus it cannot contribute to restoring forces (stress). In contrast, a high amount of the cell gas remains “trapped” within the cells at high strain rates and thus is able to cause a restoring force (stress). The effect is similar to the previously described findings of the modulus (characteristic material time vs. time of experiment).

However, the most pronounced effect of strain-rate is observed for the compression set as depicted on Figure 52 c). As described previously, E-Por exhibits a higher recovery after compression than EPS due to more elastic cell walls and struts. Interestingly, both materials reach plateau-behaviour at high strain rates. At low strain rates, the recovery is much less pronounced. This is attributed to two factors: a) the characteristic material time of the polymer matrix, which is especially important for E-Por ( $T_{\text{measurement}} > T_G$  of PE phase) and b) the diffusion of air out of the cellular structure, which changes the recovery at different strain rates distinctly as explained before.

The inter-dependency of  $n$  on the studied morphological properties is schematically shown in Table 6. The fact that only E-Por exhibits sensitivity of the modulus on the morphology is striking. It is found, that larger cells and higher density lead to decreasing strain-rate sensitivity. This is attributed to a reduced effect of the PE phase with larger cells and higher density. Higher density with large cell walls and struts will lead to a reduced degree of PE-stretching (the PE domains are supposedly more spherical), so PE will contribute less to the elastic mechanical response. Larger beads in contrast, have thinner cell walls and struts, which leads to the contrary effect.

**Table 6: Schematic dependency of the strain rate sensitivity exponent  $n$  on the morphology of EPS and E-Por.**

	Modulus		Strength	
	EPS	E-Por	EPS	E-Por
Cell size (smaller)	NA	+	NA	NA
Bead size (larger)	NA	-	NA	NA
Density	NA	-	+	NA

### 5.2.1.6 Summary on the fundamental mechanical properties

The fundamental mechanical properties of polystyrene-based bead foams were studied by bending and compression tests as well as by *in-situ* SEM, in order to observe the micro-deformation mechanisms. In this frame, the understanding of the effect of the morphological features on the mechanics is to be facilitated.

It was found that a smaller cell size leads to improved properties for EPS, but not for E-Por, as the mechanics of E-Por is dominated by the PE-domains. The mechanism behind the cell size dependency of EPS was examined by shrinkage experiments and DMA, which showed that higher orientation and higher potential for annealing with smaller cells are the responsible mechanisms. It is concluded, that EPS exhibits morphology dominated behaviour, whereas E-Por is highly affected by the PE-phase.

In terms of bead size, larger beads lead to better mechanical properties as they improve the moulding quality due to better energy transfer and less surface area, which needs to be softened. However, a negative trend on the mechanics is expected for beads that are too large due to larger macro-voids. EPS from suspension polymerisation was compared to EPS from extrusion. In compression, similar properties were observed, whereas sEPS is superior in flexural deformation.

When density is varied, similar trends for EPS and E-Por are observed. In general, density is the factor with the most pronounced influence on the mechanical properties. As reported in the literature, the dependency of the mechanical properties on density obeys power-law statistics. Density affects the response in compression more than in bending since deformation mechanisms with a higher density-dependency act in compression.

The investigation of the micro-deformation mechanisms showed that deformation is highly localised in the centre of the beads. Furthermore, macro-porosity is a weak site and acts as a defect when deformation in the surrounding area increases.

The effect of strain rate is significant for both EPS and E-Por. The modulus of E-Por is more affected by the strain rate than the modulus of EPS. This is due to molecular effects of the PE-domains in E-Por. Strength is highly dependent on strain rate for both materials, as strain rate determines the amount and inner pressure of the cell gas (restoring force) due to the ratio of strain-rate and diffusion speed.

## 5.2.2 Effect of the bead foam morphology on the fracture toughness and failure mechanism

In the following section, the results on the fracture toughness of both EPS and E-Por are presented. We will focus on EPS, as this model material allows a better deduction of the governing mechanisms.

The morphological parameters are discussed as before from small length scale to the large, thus at first the cell scale and then the bead scale are presented. Subsequently, the density is presented and discussed, as both bead and cell sizes vary with density.

### 5.2.2.1 Effect of the micro-morphology via cell size variation on the fracture toughness

The effect of the micro-morphology on the fracture toughness of EPS is studied for samples with almost constant density and bead size but varying cell size. Through cell size, the wall and strut thickness are also affected. The fracture toughness  $J$  as a function of cell size is plotted in Figure 53. It is clear, that cell size plays a crucial role for the improvement of toughness.

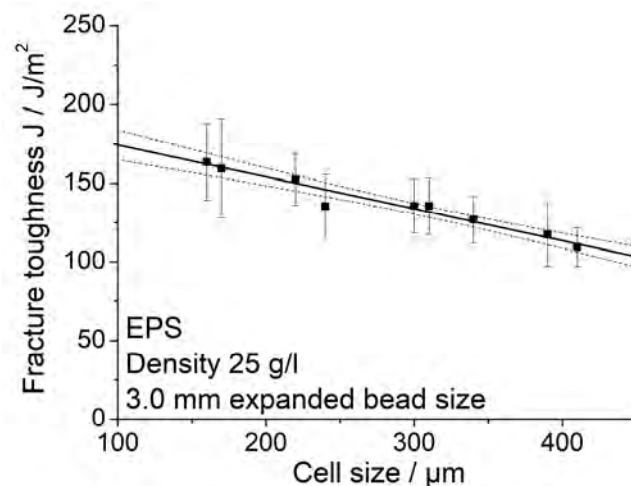


Figure 53: Fracture toughness as function of cell size for EPS with a density of 25 g/l and bead size of 3 mm. The upper and lower line represent the 95 % confidence bands of the fit.

The fracture toughness distinctly increases with a reduction in cell size: at 400  $\mu\text{m}$  cell size,  $J$  reads 110  $\text{J}/\text{m}^2$ , while  $J$  is above 160  $\text{J}/\text{m}^2$  at 150  $\mu\text{m}$  cell size, which equals an improvement of toughness by 45 %. The increase of  $J$  scales perfectly linear with  $J$  for all data-points except one sample (the only point outside of the 95 % confidence interval) with increased talcum concentration, which deviates towards lower values. The reason for this deviation will be explained in detail later on.

Although the data points exhibit rather large error bars, the average value is significant. For a 95 % confidence, a sample size of at least five is necessary, for 99 % confidence at least 9<sup>1</sup>. This sample size was exceeded significantly as 20 samples per data-point were tested.

Two mechanisms could be responsible for this behaviour. The first mechanism would work on the cell scale. The cells lead to crack blunting: the radius of the crack tip is reduced and thus the stress at the tip reduced. However, this mechanism does not explain the dependency of the fracture toughness  $J$  on cell size, as the opposite dependence is expected: larger cells lead to a larger crack tip radius and thus less stress. As such, toughness should increase with cell size. However, the opposite is observed. The reason could be the size difference between cell size and the size of the crack tip in compact polystyrene. Since the cells are much larger than the crack tip, the stress is reduced anyway, and no dependency on cell size would be observed.

The mechanism, which can explain the dependency of toughness on cell size, is coupled with the multi-scale character bead foams (*cp.* Figure 54) since a foam cell is built of thin films - the cell walls.

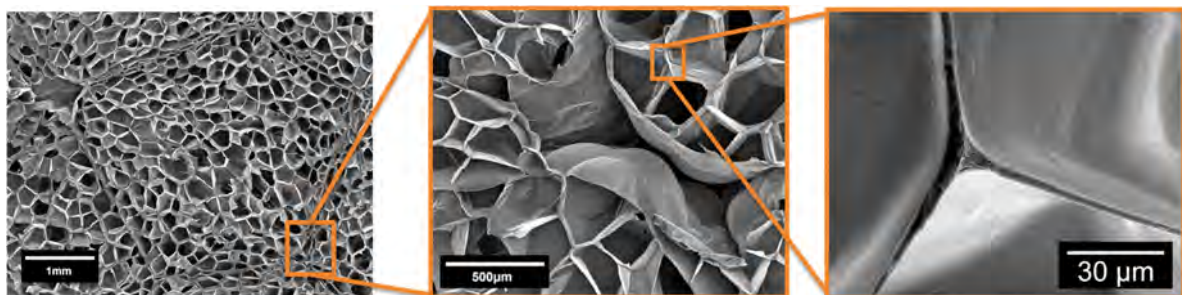


**Figure 54: Multi-scale structure of a bead foam: from left to right: bead scale, cellular scale with macro-porosity between beads and the micro-scale (cell walls and struts).**

As the cell wall thickness scales with cell size to  $t_w \sim d$ , the walls get thinner when the cell size decreases. This thinning of cell walls leads to the enhancement of plastic

<sup>1</sup>  $n \geq \frac{z^2 \sigma^2}{e^2}$  with the absolute error  $e = 45.2$  (value from the data), the variance  $\sigma^2 = 2488$  (value from the data) and the parameter  $z \approx 2$  (95% confidence) or  $z = 2.58$  (99% confidence)

deformation: the cells in front of the crack tip can be stretched plastically before breaking. Thus, more energy is dissipated and the fracture toughness increases.

The size of the plastic zone in front of the crack tip was calculated for compact PS according to Irwin (plane strain conditions) to be 11 to 25  $\mu\text{m}$  and according to the Dugdale-model to be 80 to 190  $\mu\text{m}$ . Both length scales are significantly larger than the typical dimension of a cell wall, which is typically below one  $\mu\text{m}$  as shown in Figure 55.

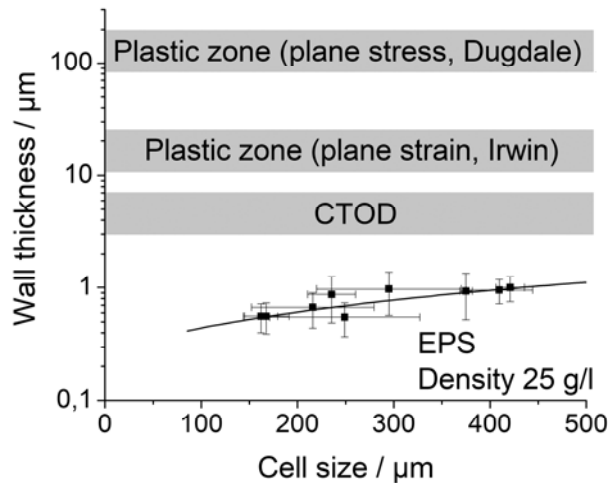


**Figure 55: Thickness of the cell walls as function of cell size. Furthermore, the characteristic regions of the plastic zones as well as the crack-tip-opening displacement are highlighted.**

This value is also below the crack-tip-opening displacement (CTOD), which is in the range of 3.2 to 7.2  $\mu\text{m}$ . From these considerations it is concluded, that the toughness increases at constant foam density due to enhanced plastic deformation when the dimension of the cell walls is reduced. This is achieved by a reduction of cell size.

This mathematical deduction is also confirmed experimentally. For example van der Smanden [158] studied the strain at break of thin PS-films and PS/PE multilayer structures in dependency on PS layer thickness. The respective stress-strain curves are given in Figure 56 a).

It is clearly visible, that the toughness of the sample (area under the stress-strain-curve) increases distinctly for thinner films. Additionally, the strain at break as function of layer thickness is plotted in Figure 56 b). Two regimes are distinguished: (i) for PS layer dimensions above about 3  $\mu\text{m}$  the strain at break is very small and hardly depending on thickness and (ii) the strain at break attains high values and becomes distinctly thickness-dependent for dimensions smaller than 3  $\mu\text{m}$ . The cell walls are in the second regime as their thickness is usually below 1  $\mu\text{m}$  at a density of 25 g/l. From the variation of thickness with cell size and the dependency on strain at break, and thereby toughness, the pronounced correlation of toughness and cell size is explained.

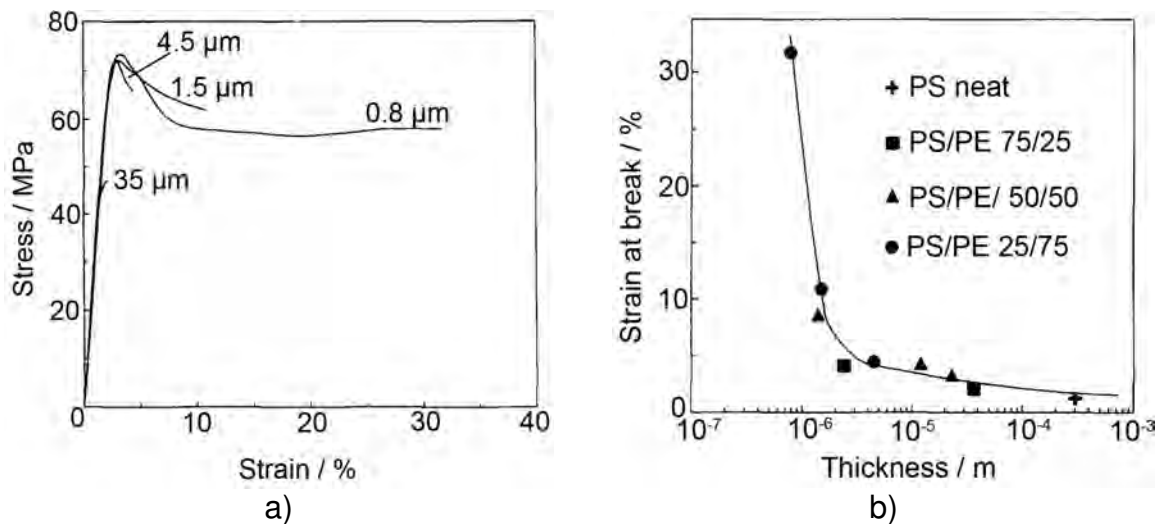
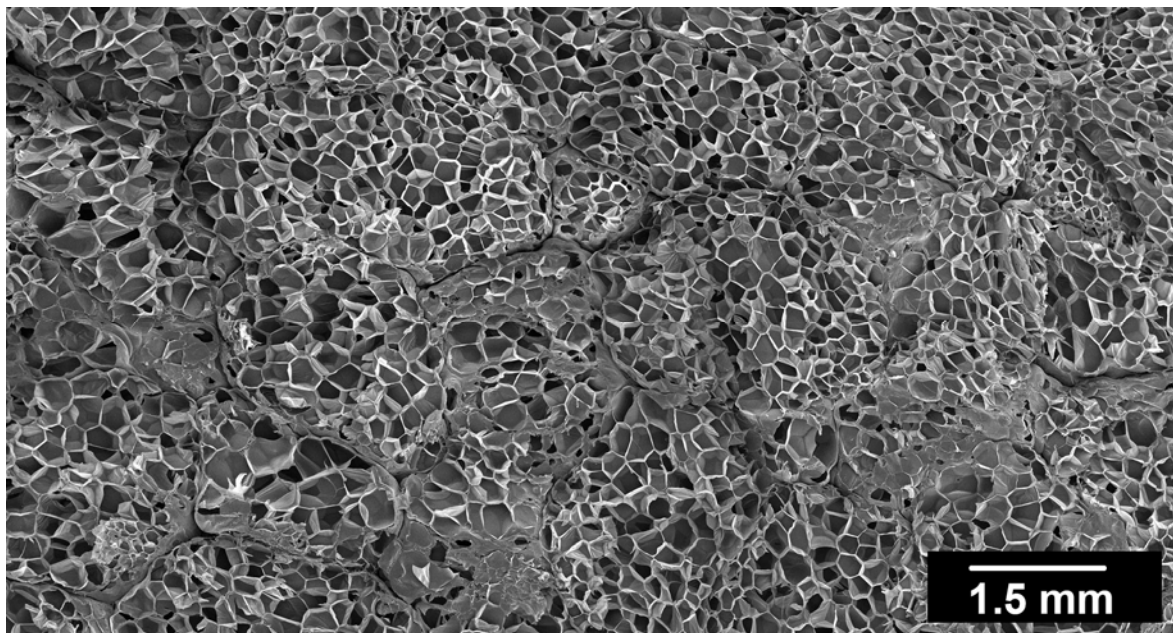


Figure 56: a) Stress-strain-curves of PS films with different thicknesses and b) the strain at break as function of the PS layer thickness. Both curves are slightly modified for better readability from van der Sanden [158].

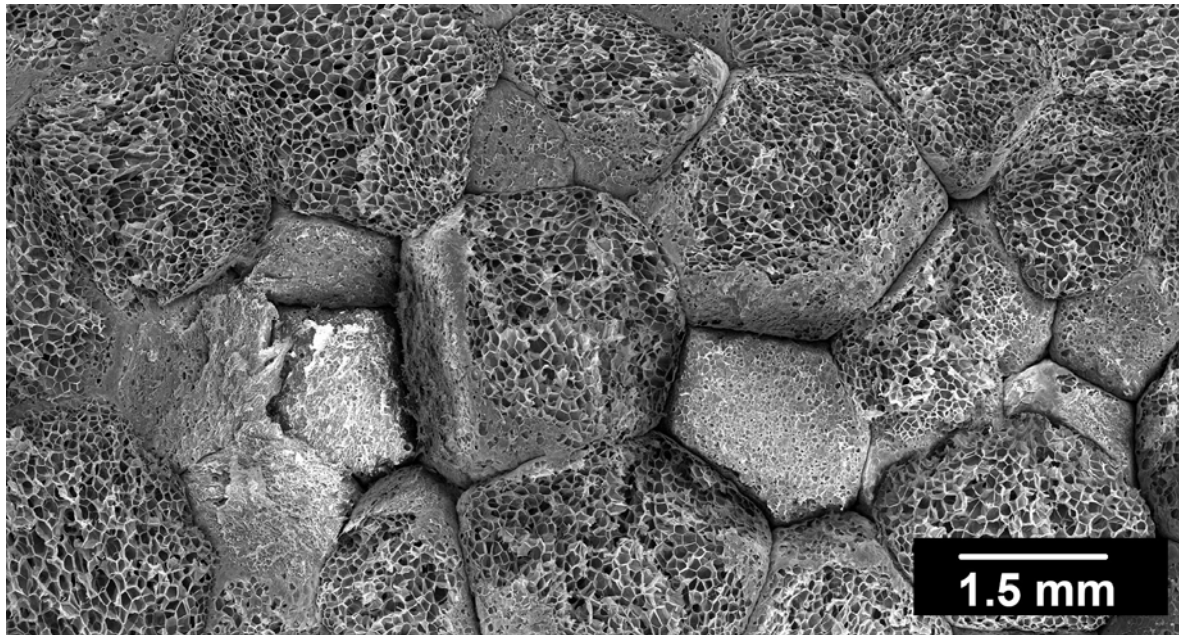
#### Correlation of fracture toughness to the fracture surface

The requirement for the distinct cell size dependency of toughness is intra-bead (cellular) fracture. In order to test this requirement, many SEM-images of the J-Integral sample's fracture surface were combined to complete panoramas. Two panoramas of the reference sample and a sample with fine cells (145 μm average diameter) are shown in Figure 57. It can be observed, that the crack mainly propagates through the beads, thus the requirement of the above-stated hypothesis is fulfilled.



a) EPS\_25\_300\_3.0\_REF





b) EPS\_25\_160\_2.8

**Figure 57: Fracture surface of EPS-samples: a) reference and b) fine cell sample. The crack mainly propagates through the beads (cellular fracture).**

Furthermore, one can observe that the material with the highest fracture toughness does not necessarily have the highest area fraction of cellular fracture (*cp.* Figure 57 a) and b)). According to the available scientific literature, the opposite is expected [43]. Therefore, it is concluded, that the effect of cell size is more pronounced than the mechanism of fracture in the parameter-region studied (cellular fracture dominating: > 90 % intra-bead fracture).

#### Reduction of the fracture toughness by excessive talcum addition

As shown above, the studied materials obey a linear trend of decreasing toughness with increasing cell size due to an enhanced potential for plastic deformation for thinner cell walls. However, one sample deviates from this behaviour as shown in Figure 58. It contains an increased talcum content compared to the other samples.

The addition of talcum is required to ensure successful foaming. By adding more talcum, the cell size is reduced. The reduced cell size is reflected in the fracture toughness until a plateau, where more talcum does not lead to an improvement in fracture toughness (*cp.* Figure 131, Appendix), although the cell size is further decreasing.

It can be concluded, that the addition of talcum leads to opposing effects. Firstly, more talcum leads to a lower cell size, which then leads to improved fracture behaviour as shown. This mechanism is dominant for low and moderate additions of talcum. In contrast, the additive acts as defect at high concentrations.



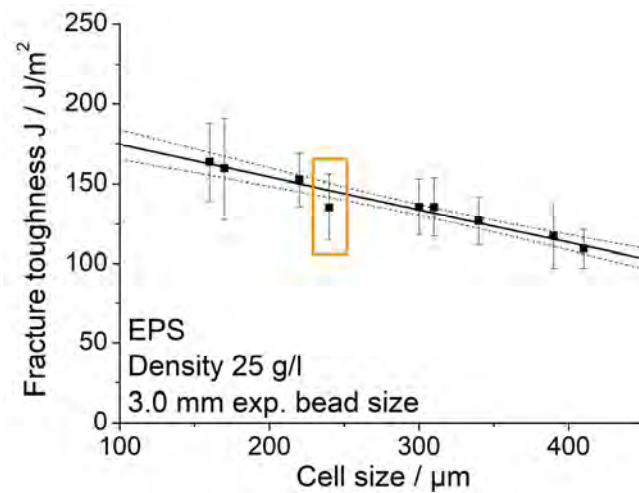


**Figure 58: Fracture toughness of EPS as function of cell size. Only the set of samples with increased talcum content deviates from the expected behaviour and lies out of the 95 % confidence bands.**

Talcum, which is located in the thin cell walls (*cp.* Figure 59), leads to a) less polymer around the talcum particle, b) fluctuations in the shape and c) crack initiation due to stress concentration around the particle (modulus talcum  $\gg$  PS). The latter comes from the fact that adhesion between the particle and the polymeric matrix is weak (requirement for nucleation). These factors drastically reduce the fracture toughness at high concentrations of nucleating agents.

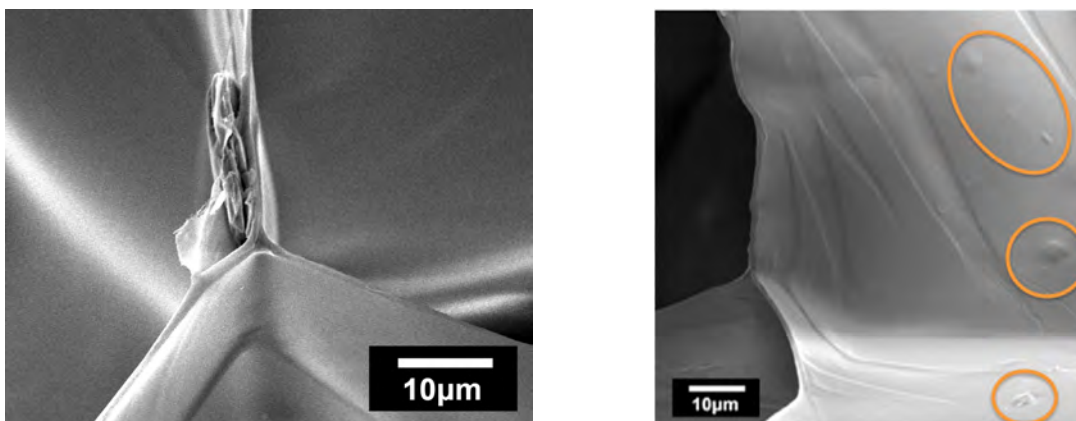


**Figure 59: Highlighted location of talcum in a cell wall (left) and its supposed effect on cell wall thickness.**

#### Further increase of the fracture toughness by reducing the domain size by addition of Polyethylene (E-Por)

The PS/PE-blend E-Por exhibits superior fracture toughness in contrast to EPS. The average fracture toughness of E-Por ( $192 \pm 22 \text{ J/m}^2$ ) is 40 % higher compared to the reference EPS ( $136 \pm 17 \text{ J/m}^2$ ) as shown in Figure 60. Furthermore, it is independent of cell size as the average values of the individual sets of samples do not obey any trend.

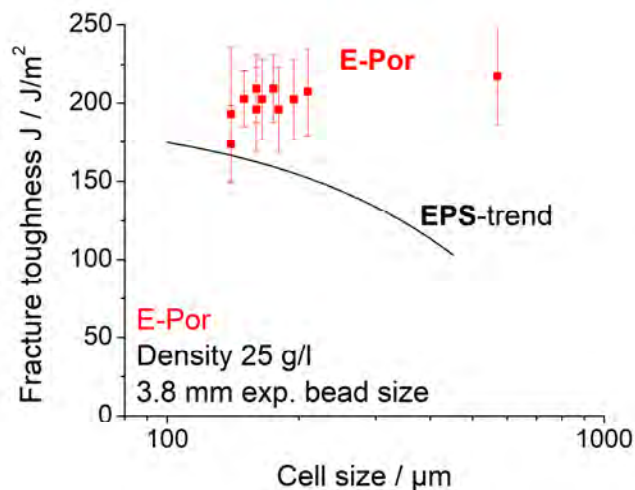


**Figure 60: Fracture toughness of E-Por as function of cell size at a density of 25 g/l. The line of EPS represents the linear dependency of toughness on cell size and is shown for comparative purposes.**

The reason for this distinctly increased toughness is the inner morphology of E-Por, which has one additional length scale as shown in Figure 61. The addition of polyethylene leads to a reduced domain size of polystyrene and thus an enhanced plasticity, as already shown in case of EPS. In this frame, EPS has a domain size (equivalent to the wall thickness) of about 1  $\mu\text{m}$  and 6  $\mu\text{m}$  (cell struts), while E-Por has a domain size of about 0.2  $\mu\text{m}$  in both the cell walls and struts.

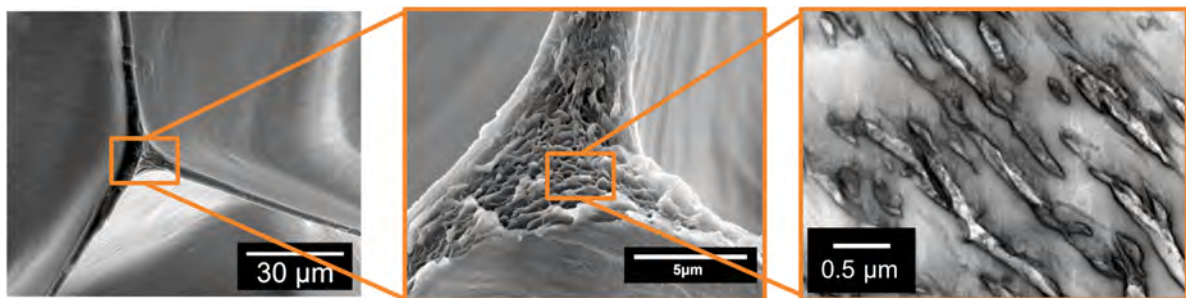


**Figure 61: The additional length scale in E-Por: the introduction of polyethylene leads to smaller domains of PS.**

In summary, it is seen that the domain size of PS is the main factor for an increased fracture toughness of PS-based bead foams at a constant density. From the literature it was found, that the wall thickness has to be below a critical dimension (about 3  $\mu\text{m}$ ) to enable large plastic deformation [158]. In our studies, we found that the addition of PE in E-Por leads to a further reduction of domain size of PS and thus an increased fracture toughness. The principles observed on the model polymer PS herein are likely to hold for extrusion foams as well as foams from other brittle materials.

### 5.2.2.2 Variation of the interfacial surface between the beads by a variation of bead size

When the bead size is varied then the interfacial area changes as well, which needs to be fused in steam-chest moulding. When the moulding is done at the same parameter for beads with different bead sizes (as in this study), a distinct effect on the fracture toughness and failure mechanism is expected.

Indeed, the effect of increasing bead size on the fracture behaviour is distinct. An optimum behaviour can be observed with a maximum at the reference material with a cell size of 295  $\mu\text{m}$  (Figure 62). However, cell size has a pronounced influence on the fracture behaviour as shown above (section 5.2.1.1). For the studied EPS-materials, the cell size is changing distinctly (*cp.* Figure 62, numbers besides the data-points).

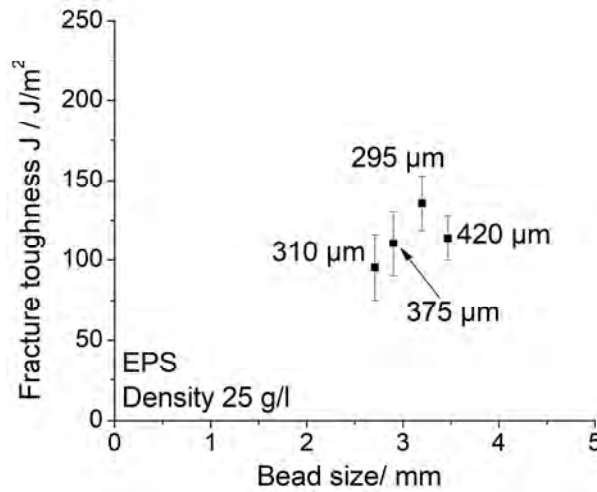


**Figure 62:** Fracture toughness in dependency of bead size. The respective average cell size is shown besides each data-point.

In order to account for this influence, each data point of  $J$  has to be shifted depending on the cell size of the respective material  $d_{c,0}$  in comparison to the cell size of the reference  $d_{c,Ref}$  according to Equation 6.

$$J_{corr} = J_0 + \frac{dJ}{dd_c} (d_{c,0} - d_{c,Ref}) \quad \text{Equation 6}$$

$J_0$  is the fracture toughness of the reference material. The correction requires the derivative of fracture toughness  $J$  on cell size,  $\frac{dJ}{dd_c}$ , which reads  $-204 \text{ kJ/m}^3$ . This procedure requires that there's no secondary interdependency between bead size  $d_B$ , cell size  $d_c$  and fracture toughness ( $\frac{\partial J(d_c, d_B)}{\partial d_c \partial d_B}$ ).

Taking the correction into account, the fracture toughness increases with bead size until a plateau is reached, as seen in Figure 63.

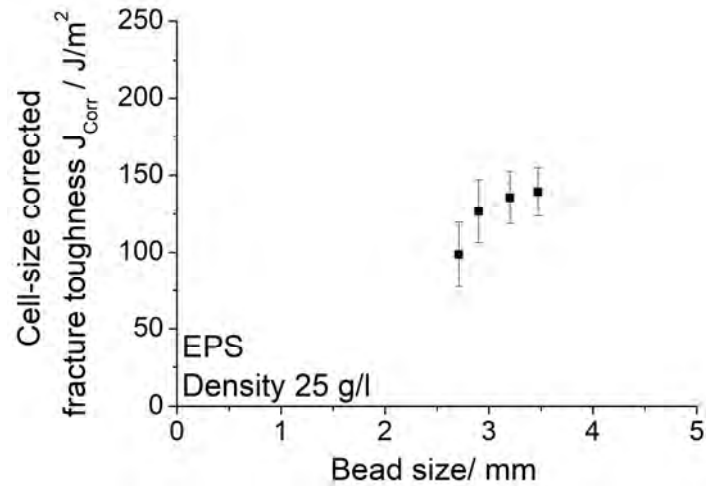


**Figure 63: Fracture toughness corrected for cell size  $J_{corr}$  versus bead size for EPS.**

In contrast to EPS, E-Por does not show a) a strong variation of average cell size with bead size and b) no statistical effect of cell size on the fracture toughness. Thus, no correction has to be applied to the data. The fracture toughness of E-Por as function of cell size is plotted in Figure 64.

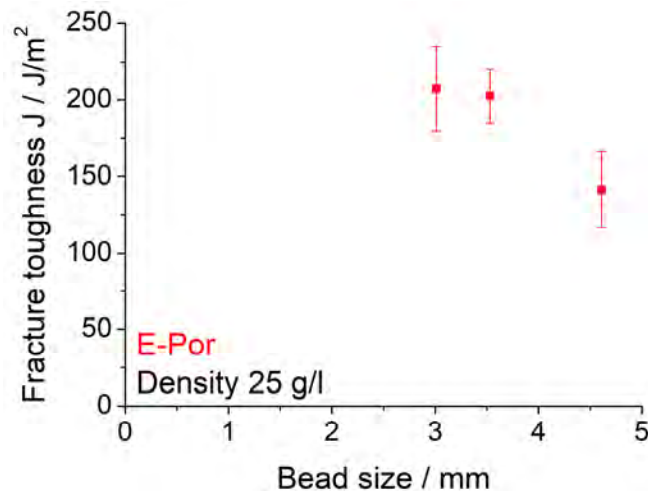


**Figure 64: Fracture toughness as function of bead size for the PS/PE-blend E-Por.**

In comparison to EPS, the opposite behaviour is observed in E-Por. A plateau is observed for a bead size between 3 and 3.5 mm, which drops off for large beads. Although the behaviour of EPS and E-Por appear contradictory at first, other factors must be considered, as will be shown later on.

Correlation of fracture toughness to the fracture surface

SEM-pictures and the analysis of the fractured surfaces are employed to explore the prevailing mechanism of failure. At first EPS is examined and afterwards E-Por.

For EPS it is observed, that the fraction of cellular fracture increases with increasing bead diameter (see Figure 65, fracture surfaces). The quantification of the intra-bead fracture reveals a linear dependency between the failure mechanism and the measured fracture toughness in this range of bead sizes (see Figure 65, graph). This dependency takes both the parameters of cell size as well as bead size into account (J values not corrected). Unfortunately, the fracture mechanism in dependency of bead size alone cannot be determined for EPS due to the distinct cell size variation with bead size.

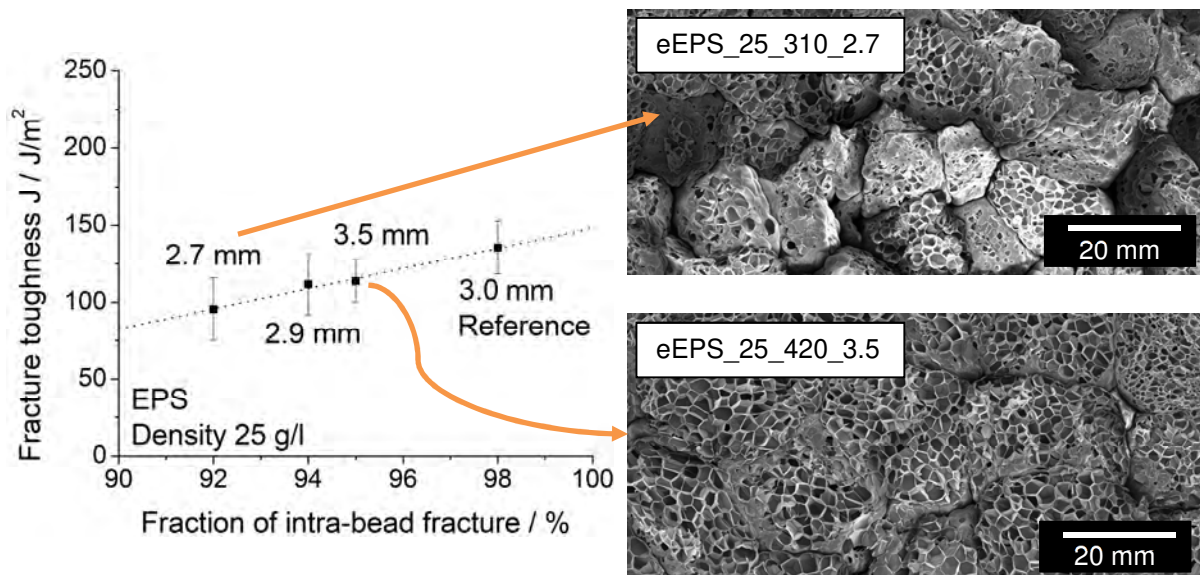


**Figure 65: Fracture toughness as function of the fraction of intra-bead fracture as well as fracture surfaces from J-samples of EPS. Upper picture: small beads (EPS\_25\_310\_2.7), lower picture: large beads (EPS\_25\_420\_3.5).**

Also, E-Por exhibits a distinct dependency of the fracture surface and fracture toughness, where the same trend as EPS is observed. Toughness increases with intra-bead fracture (Figure 66). Hereafter, a comparison to the benchmark system will be drawn, which also has a varying bead size, for us to explain the “bigger picture”.



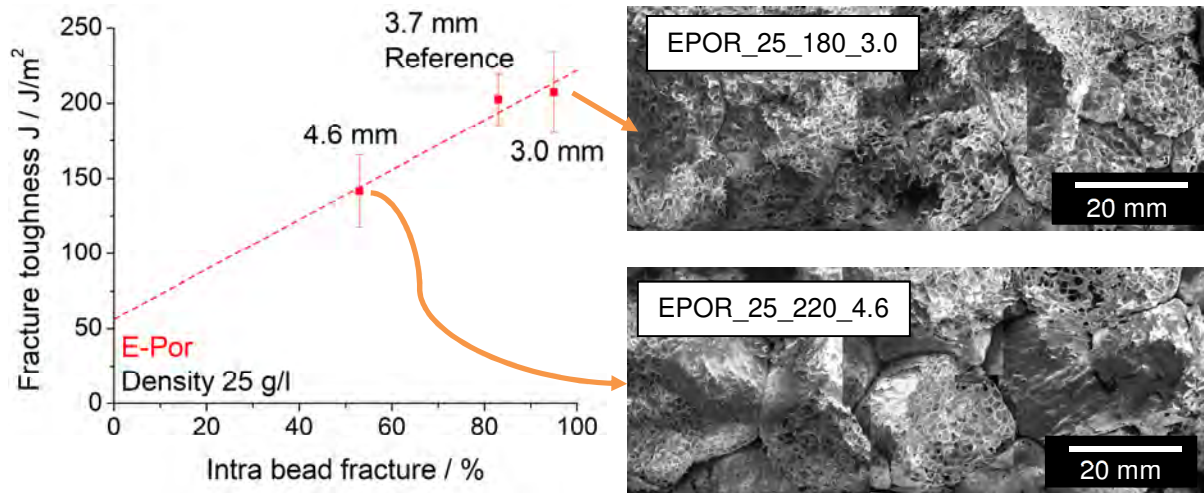


**Figure 66: Fracture toughness as function of the fraction of intra-bead fracture as well as fracture surfaces from J-samples of E-Por. Upper picture: small beads (EPOR\_25\_180\_3.0), lower picture: large beads (EPOR\_25\_220\_4.6).**

Comparison to the benchmark systems

The benchmark systems of EPS produced from suspension polymerisation shows hardly any variation in cell size. Hence, the effect of bead size variation can be studied exclusively. The fracture toughness of all materials is shown in Figure 67 a). Furthermore, the toughness of sEPS with respect to intra-bead fracture is presented in Figure 67 b).

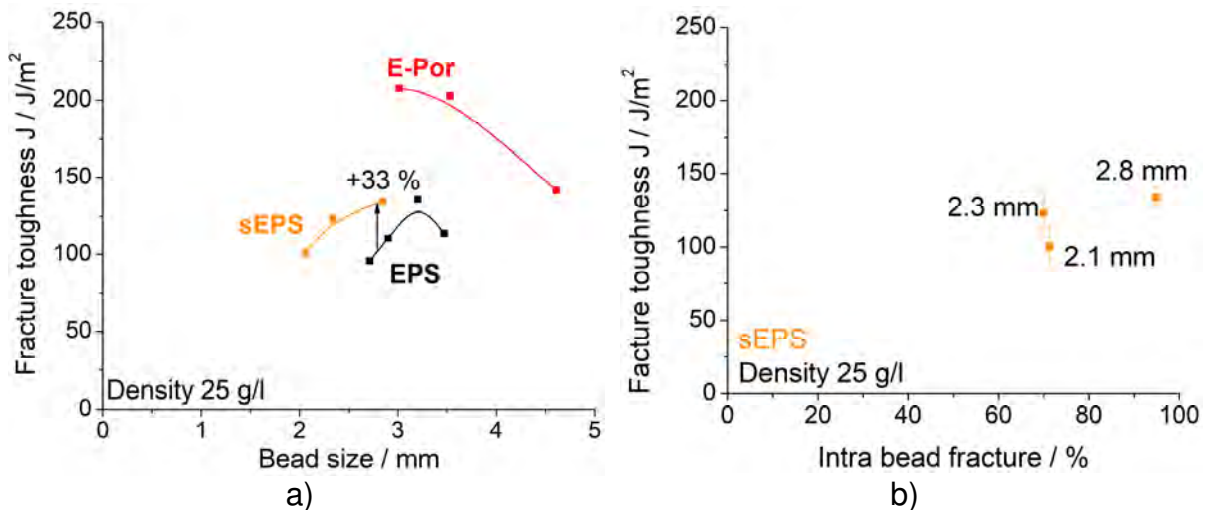


**Figure 67: a) The fracture toughness of the studied systems in dependency on bead size (density 25 g/l). The shown data for EPS are not corrected for cell size. b) The fracture toughness of the benchmark systems sEPS, density 25 g/l, in dependency on the fraction of intra-bead fracture. The numbers besides the data-points indicate the bead size of the respective materials.**

First, it is visible that the toughness of sEPS is much lower compared to E-Por, which was expected. As for EPS the same trends of sEPS of increasing toughness with a) increasing bead size and b) increasing fraction of intra-bead fracture are observed.

Interestingly, sEPS has an about 33 % higher fracture toughness at the same bead size compared to EPS. This is attributed to the significantly lower cell size of sEPS (60  $\mu\text{m}$  (sEPS) vs. 300  $\mu\text{m}$  (EPS)) and by that also smaller cell walls and struts.

The fracture surfaces of the sEPS samples are shown in Figure 68. The surface of fracture appears to be smoother with increasing bead size: both the waviness (topology) of the surface and the increasing cellular fracture contribute to this fact. Hereafter, the presented results are combined to form a “bigger picture”. Furthermore, the physical and technical reasons for it are explained.

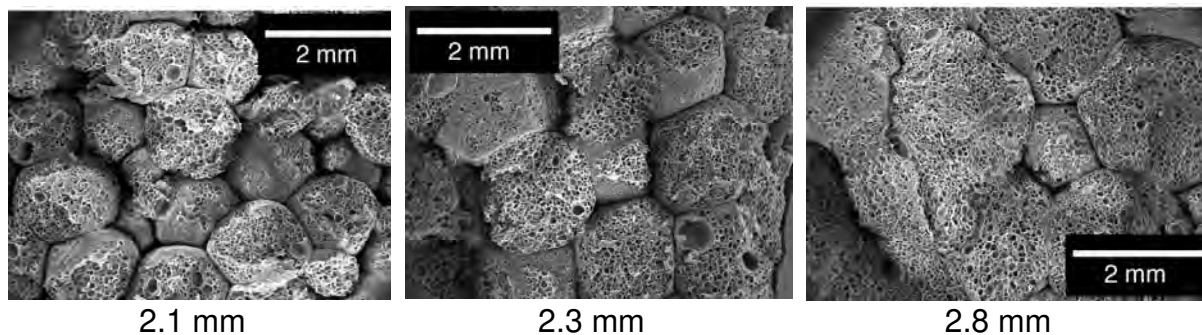


**Figure 68: Fracture surfaces of the benchmark-EPS materials with varying bead size (sEPS, from suspension polymerisation with pentane).**

#### Categorisation of the obtained results to a greater picture

In summary, it was found that for sEPS and EPS fracture toughness increases with increasing bead size. Both materials have small to medium-sized beads. In contrast, E-Por with medium-sized to large beads exhibits the opposite behaviour. In order to allow for a better comparability, the data-points at each bead size are divided by the respective maximum value of either EPS or E-Por (same maximum value for sEPS and EPS). As the cell size of the EPS samples show a significant variation and toughness is highly depending on cell size, this was carried out for the values corrected for cell size. This relative fracture toughness is plotted in Figure 69.

From the data, a distinct optimum-behaviour for beads in the range between 3 and 3.5 mm is found. Smaller or larger beads than this range lead to a reduced fracture toughness. The mechanisms behind this will be explained in the following section. Afterwards, an interpretation of those mechanisms with the available data is given.

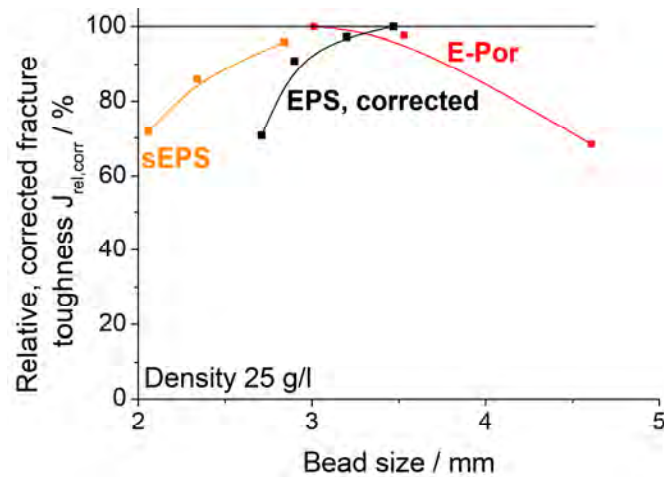


**Figure 69: Relative fracture toughness of sEPS, (extrusion) EPS and E-Por as function of bead size (density 25 g/l).**

#### Origin of the observed dependency of toughness and fracture mechanism on bead size

It is important to note that the following section assumes a constant cell size; only the bead size varies. Thus, the effect of cell size can be excluded for the interpretation. Primary effects and secondary effects can be distinguished. When the bead size affects the crack propagation directly, we speak of primary effects. This is the case when one fracture mechanism is fully dominant (either complete intra bead or inter bead fracture). In contrast, the secondary (or indirect) effects do not change the propagation of the crack directly, but affect the interfacial strength or the fraction and size of macrovoids (interstitial volume).

At first, the primary mechanisms are explained. In earlier studies it was shown that the fraction of intra-bead (cellular) fracture correlates well to the fracture toughness of bead foams [43]. However, also the effect of bead size at complete intra or inter bead fracture, must be considered. If the crack propagates between beads (inter-bead), the bead size is deemed to have an effect, since it might affect crack branching and thus the creation of new surfaces inside the material. A higher rate of generation of free surface leads to higher fracture toughness, since this mechanism dissipates energy. As depicted in Figure 70 a), smaller beads have a higher possibility of crack branching or crack deflection during crack propagation.



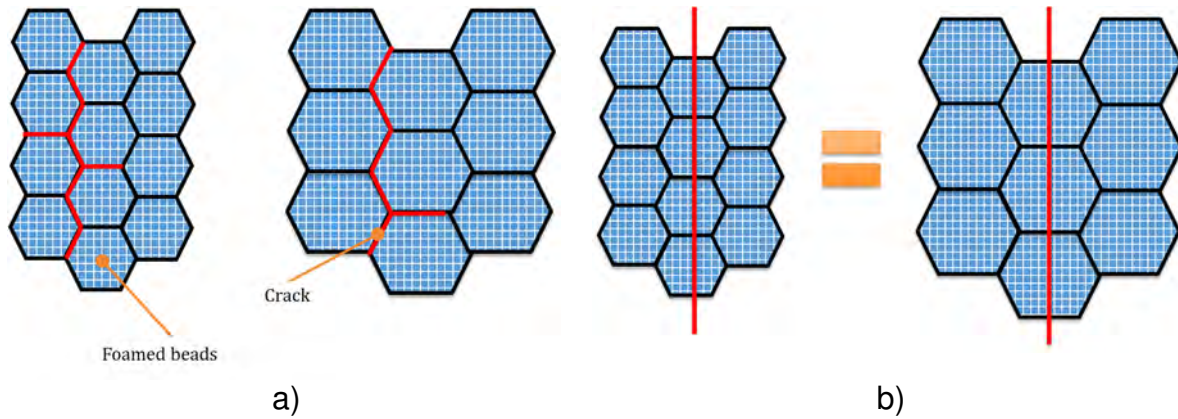


**Figure 70: Schematic representation of the two principle crack propagation mechanisms: a) inter-bead and b) intra-bead failure for small and large beads each.**

In contrast, when intra bead fracture is dominant, the fracture toughness predominantly depends on the cellular morphology and not on bead size (Figure 70 b)). It is noted, that a constant cellular morphology is assumed.

After showing the primary effects, also secondary effects must be considered. That means that the bead size affects the processing (steam-chest moulding) or morphology of the product and thus indirectly the toughness. In this frame, a dependency of the interfacial strength (caused by altered steam-chest moulding quality) on bead size is likely, especially for small beads. Two factors can cause this dependency:

1. Ratio of steam-energy / surface-area is increasing with bead size
2. Change of flow resistance for the steam
3. Diffusion of pentane out of the beads during intermediate storage

The first effect derives from the idea that during steam-chest moulding a given amount of energy is distributed to the surfaces of the beads. Since smaller beads possess a higher surface area for a given mould volume, the ratio energy per surface-area is decreasing. Less thermal energy is available per unit surface area. Thus, the polymer chains obtain less mobility for the inter-diffusion across the bead-bead interface. Hence, the interfacial strength and quality of fusion is reduced.

The second effect addresses the processing in a more direct way. Smaller beads have a higher flow resistance for the steam during steam-chest moulding. Hence, less total energy is available for the moulding process. In detail, the effect works as follows: in steam-chest moulding, a pressure difference for the passing steam is set. Consequently, the flow-rate of the steam varies depending on the pressure-difference and bead size. The effective flow rate as a function of pressure and bead size then determines the energy transfer of the steam to the beads' surfaces. Thus, the state of inter-diffusion of the polymer chains between neighbouring beads and thereby the interfacial

strength is changed. If the interfacial strength is lower than the rupture strength of the bead, the bead will mainly fail in inter-bead mode, otherwise intra-bead fracture will dominate.

A relation between the pressure drop, the bead size and the resulting flow rate is given by the well-known Kozeny-Carman-equation. In this equation, the volumetric flow rate at a constant pressure drop scales to the square of the bead diameter,  $\dot{V} \sim d_p^2$ . Consequently, more steam passes through the mould for larger beads and more energy can be transferred to the beads. It is important to note, that this equation is valid for laminar flow with a Reynolds number  $Re < 10$  only. In steam-chest moulding, the flow through the mould is turbulent. However, the equation helps to better understand the underlying phenomena. Possibly the two factors even act synergistically, leading to a more pronounced effect compared to each independently. It is concluded that they give a sensible explanation of the encountered phenomena and the inter-dependency between processing and bead morphology.

A further effect is the depletion of pentane, which is dependent on bead size. Since smaller beads possess a higher surface area, more pentane can diffuse out both during the storage of expandable beads and the intermediate storage between pre-foaming and steam-chest moulding. This affects the quality of fusion in a distinct way as both intimate contact and the inter-diffusion of polymer chains are reduced. If pentane diffuses out of the beads, the pressure between the beads is reduced, thus reducing the intimate contact. Furthermore, chain mobility is reduced with lower pentane content, since pentane is an effective plasticising agent [159].

In contrast to the previously described phenomena, which are mainly interesting for small beads, the now outlined effect mainly applies to parts made of large beads. This effect is macro-porosity. Where multiple beads meet, their expansion might not be enough to fill out all the interstitial volume of the bead fill. From geometrical considerations, it can be seen that, at the same volumetric expansion (assuming the same residual pentane concentration), large beads do not expand by the same absolute diameter compared to small beads. This principle is shown schematically in Figure 71.

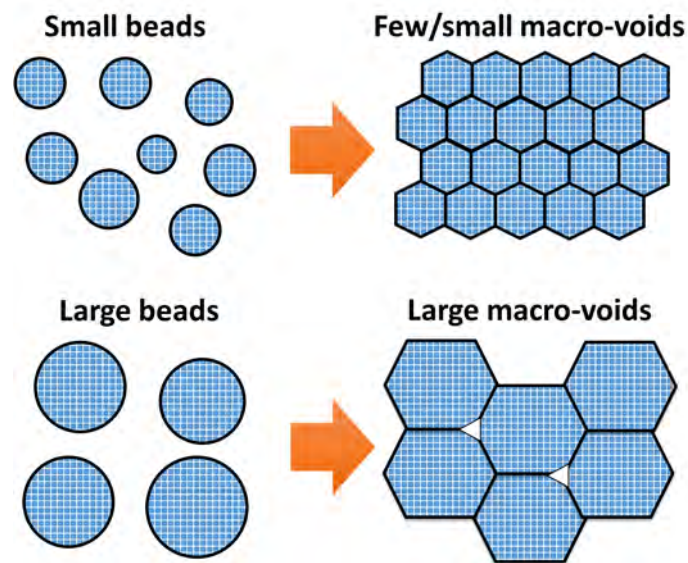


**Figure 71: Schematic representation of the residual interstitial volume after moulding for small and large beads.**

The fraction and size of the remaining macro-porosity is deemed to have a pronounced effect on crack initiation as large cavities enhance crack initiation and propagation due to small crack radii at their corners (see also Figure 72 a)). As visible on the fracture surfaces in Figure 72 b), this mechanism indeed seems to be responsible for an increase of intra-bead failure for E-Por with very large beads.

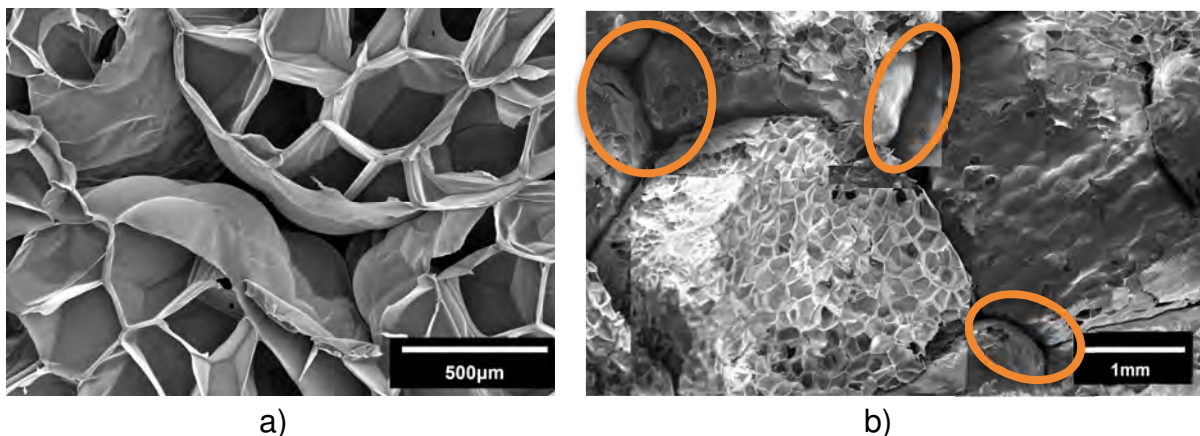


**Figure 72: SEM micrographs of the sample with the largest bead size (EPOR\_25\_220\_4.6). a) Macro-porosity from SEM-sample for cell size analysis; b) extended macro-porosity as crack initiation site from fracture surface from bending tests.**

The findings of the section on bead size are summarised graphically in Figure 73. For both small and large beads, the crack propagates along the bead boundary to a significant amount. The reason for this is reduced quality of fusion for the small beads and macro-porosity between the beads acting as defect and crack initiator for the large beads. In medium sized beads, the crack mainly propagates through the beads and not along them, which leads to the maximum plateau in fracture toughness.

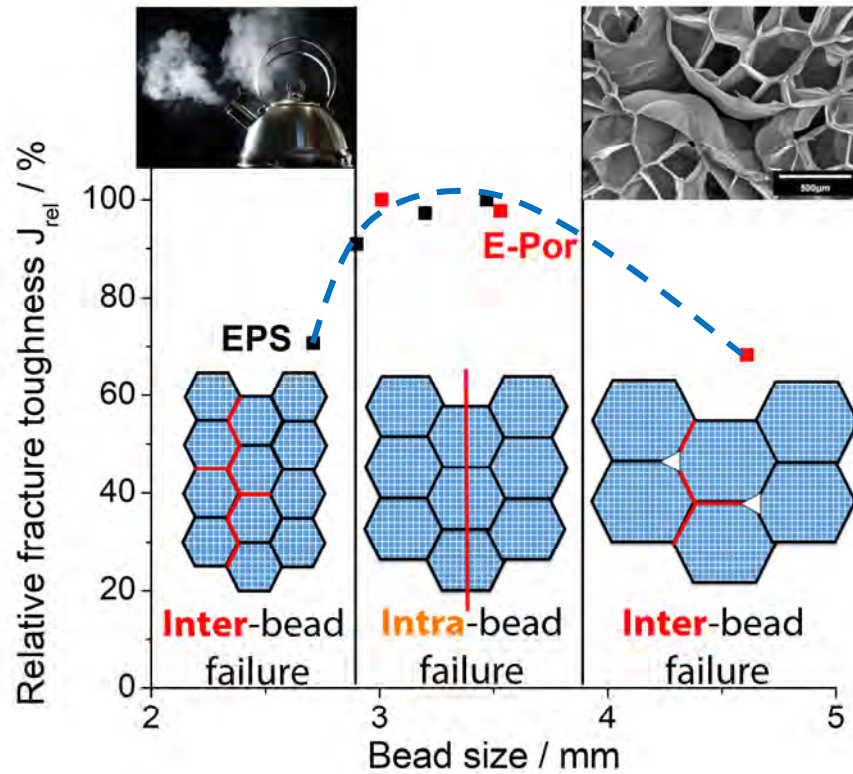


Figure 73: Graphical summary of the mechanisms behind the fracture of EPS and E-Por as function of bead size.

### 5.2.2.3 Effect of density on the fracture toughness of bead foams

As mentioned, the density distinctly affects the morphological properties of both EPS and E-Por. Besides the higher amount of polymer needed to be ruptured, also cell and bead size effects need to be considered. The three mentioned effects cannot be separated, since non-linear dependencies and interactions of the aforementioned parameters cannot be ruled out experimentally with the materials at hand.

The fracture toughness as function of density is plotted for EPS and E-Por in Figure 74. In general, it is observed, that increasing density also increases the fracture toughness quite distinctly. However, EPS and E-Por exhibit different behaviours. For EPS, the toughness increases almost linearly, whereas E-Por seems to have two regimes as shown in the figure. This finding will be addressed later.

Furthermore, the question arises, whether the fracture toughness does simply scale to the amount of fractured material available (the polymer volumetric fraction) within the foam. Therefore, the fracture toughness of a hypothetical high-impact polystyrene (HIPS) [161], [162] at 40 g/l is also plotted in Figure 74. As J-Integral values for PS were not available in literature, the value of HIPS was used. The value at 40 g/l is simply scaled linearly from the original density of HIPS.



It is observed that both EPS and E-Por are significantly above the value of HIPS, which shows the importance of the cellular morphology on fracture toughness; the fracture toughness does not simply depend on the amount of material, through which the crack has to propagate.

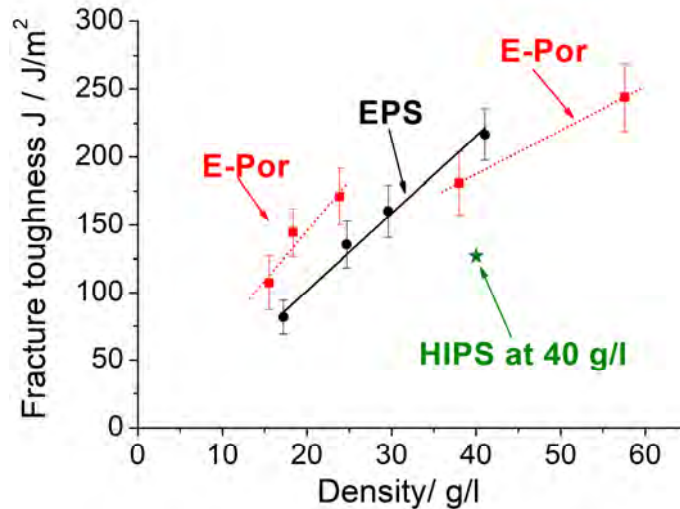


**Figure 74: Fracture toughness as function of density for EPS, E-Por and a hypothetical HIPS at 40 g/l (linear scaling with density assumed).**

The reason for the increasing fracture toughness with density is the increasing rupture strength of the individual beads. If more solid is contained in each bead, more force is required to break it apart. Besides the increase of rupture strength, it is probable that also the previously shown cell size effect is of distinct importance and, at least partially, is responsible for the increase of toughness of EPS. For EPS, the failure mechanism is mainly of intra-bead (cellular) type as shown in Figure 75 and remains independent on density in the studied range.

In contrast, the fracture pattern for E-Por correlates well with the failure mechanisms as the cellular fracture reduces with increasing density. This is sensible as the probability for the rupture of a bead reduces with increasing strength.

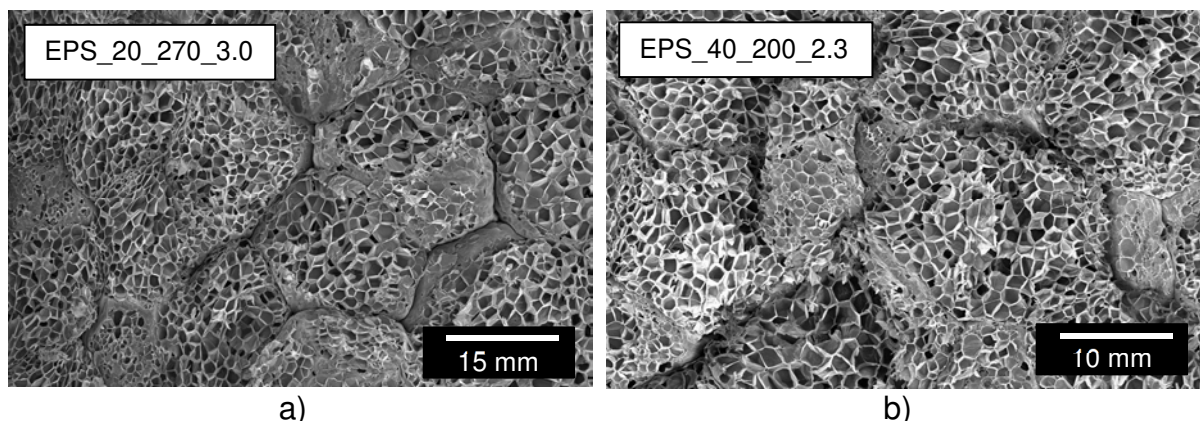


**Figure 75: Fracture surface of EPS with different densities: a) 20 g/l and b) 40 g/l.**

As mentioned before, a jump in fracture toughness is observed between 25 and 40 g/l (cp. Figure 74). A similar trend is also observed in the fraction of intra bead fracture (cp. Figure 76). The jump is attributed to the structure of E-Por as a blend, namely the elongation and orientation of the toughening PE-domains (as shown in Figure 61). The orientation of the PE-phase will be parallel to the direction of the cell walls and struts due to the elongation of these during foam expansion. Different aspect ratios arise from different levels of expansion. The higher the expansion (the lower the density), the higher the elongation. The higher the elongation, the higher their toughening effect. From the available data it is concluded, that a critical expansion exists, below which no toughening effect can be achieved. This expansion lies between 25 and 40 g/l. Aspect ratios below the critical are even counterproductive for fracture toughness, since the not sufficiently elongated PE-phase acts as a defect, leading to premature fracture and toughness even below EPS. Since EPS has no toughening second phase, no jump is observed.

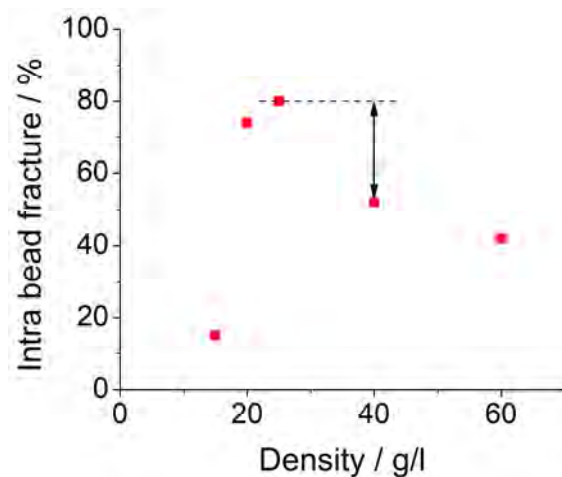


**Figure 76: Fraction of intra bead (cellular) fracture for E-Por as function of density.**

#### **5.2.2.4 Summary on the fracture mechanics of bead foams**

Cell size proved to have a distinct effect on the fracture toughness EPS, but no significant effect for E-Por. This was attributed to different toughening mechanisms for the materials. The toughness of EPS depends on the thickness of the cell walls and struts. Thinner cell walls promote an increased effect of plastic yielding and increased elongation at break. Both effects lead to improved fracture toughness. Thus, a transition of plane strain and plane stress occurs. Furthermore, a strong effect of talcum (nucleating agent) concentration was found for EPS. Talcum leads to increased toughness at low concentrations due to the reduction of cell size. Above a critical concentration talcum acts as a defect in the foam structure and the effect of reduced cell size is not dominant anymore. This leads to reduced fracture toughness. In contrast to EPS, E-Por is inherently tough due to its blend structure of polystyrene (PS) and polyethylene (PE). The addition of PE reduces the characteristic thickness of PS (EPS: wall thickness, E-Por: distance between PE-phases), which then increases the toughness of the foam.

Bead size proved to have a pronounced effect on both EPS and E-Por. An optimum of toughness for bead sizes between 3 and 3.5 mm is found. The crack tends to propagate more along the bead-bead boundary for both too small and too large beads. In contrast, the crack propagates mainly through the beads at the optimum. This is attributed to the interdependency of moulding quality for small beads (< 3 mm) as the steam energy has to be distributed to a larger surface area. Furthermore, smaller beads have a higher flow resistance for the steam, which leads to a reduced energy transfer and thus lower interfacial strength. Large beads (> 3.5 mm) exhibit a higher amount of macro-porosity, which acts as a defect thus reducing the fracture toughness.

Finally, density is, as expected, the most important parameter affecting the fracture toughness of bead foams. A distinct effect for both EPS and E-Por was found as increased density leads to improved toughness. This derives from increased rupture strength of the beads with higher density. EPS exhibited a linear dependency on density, whereas two regimes were observed for E-Por. This change is attributed to different expansion levels resulting in a different elongation of the toughening phase and thereby a changed toughening effect thereof. For a strong toughening effect, the PE-phase needs to be sufficiently elongated; otherwise it acts as a defect.

### 5.3 Interplay of the bead foam structure with its thermal conductivity

Heat conductivity in homogeneous foams is an already very complex matter. However, for bead foams this is increasingly true as the morphological feature of the bead interfaces and its associated length scale possibly come into play. In contrast to earlier studies, the phenomenon of cell size is studied at constant density in this work. Furthermore, the effects of changing bead size and the effect of a density gradient within a part are addressed.

#### 5.3.1 Influence of the cell size on the insulation properties by reducing the radiative energy transport inside the foam

The influence of cell size is highly dependent on the range of foam density being investigated. Especially at lower densities, foam cell size is one of the determining factors for the thermal transport properties as will be shown below. Additionally, the heat conduction by the entrapped gas can strongly depend on the cell size, especially when the free path length of a molecule of the cell gas and the cell size are in the same order of length scale (Knudsen effect). However, the investigated range of cell sizes does not lead to the Knudsen effect. This would typically require small cells with cell diameters below 10  $\mu\text{m}$  [163]. The following section aims to clarify experimentally, how influential the radiative contribution is, how it can be controlled by cell size and how it depends on temperature. Figure 77 shows the thermal conductivity of foam samples as a function of cell size.

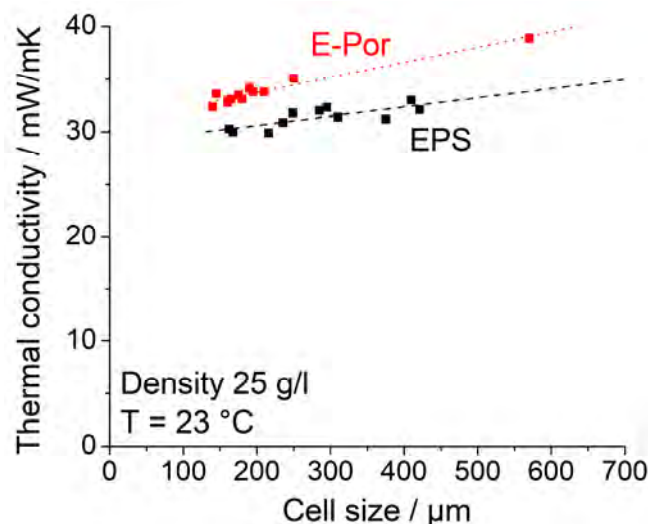


Figure 77: Dependency of thermal conductivity on cell size at constant foam density of 25 g/l for both EPS and E-Por. An enlarged section is shown in the Appendix (Figure 132).



Two observations can be made: (1) smaller cells lead to a reduced thermal conductivity in a linear manner and (2) EPS has a lower thermal conductivity than E-Por.

Observation (1) is attributed to the dependency of radiative heat transfer on cell size, at least at the low density of 25 g/l. Smaller cells cause a lower radiative energy transfer between two opposing sides. A smaller temperature difference (for smaller cells) leads to a lower net radiative energy transport (emission minus absorption) along the temperature gradient according to the Stefan-Boltzmann law. Furthermore, in smaller cell foams, the higher number of phase interfaces leads to more reflection of the IR photons [134]. On the other hand, cell walls and struts are thicker in foams with large cells at a constant foam density, which is supposed to decrease the transparency for infrared radiation and thereby reduce the total energy transfer. This matter will be discussed in more detail, when EPS from extrusion is compared to sEPS. The observed effect of cell size on thermal conductivity is conclusive compared to the computational model from Ferkl et al. [134], [146], who reasoned that this is due to hindered radiative energy transport by smaller cells. The different slope of the dependency can be due to a different cell size distribution, which is generally wider for E-Por.

Observation (2) comes from the differences in the matrix material and thereby a different intrinsic thermal conductivity. In contrast, to standard EPS, E-Por consists of about 70 % polystyrene and 30 % polyethylene. Polystyrene has a thermal conductivity of 156 mW/mK [164], whereas polyethylene has 330 mW/mK [165]. Thus a combined value of 208 mW/mK yields for E-Por assuming a parallel setup. This is 33 % more than the standard EPS.

### **5.3.2 Interdependency between temperature and cell-size – the dependency of radiation on the length scales of the cells**

In order to further explore the topic of the radiative contribution, experiments at higher temperatures were conducted for EPS in order to promote radiation, which scales to  $T^4$  for ideal black bodies. Thus, the thermal conductivity of EPS as function of temperature is plotted for four examples of cell sizes in Figure 78.

To better understand the underlying phenomena, the total thermal conductivity was separated into its components by calculating the solid and gaseous conduction,  $\lambda_{sol}$  and  $\lambda_{gas}$  respectively and by subtracting them from the total conductivity in order to obtain the radiative contribution  $\lambda_{rad}$ .

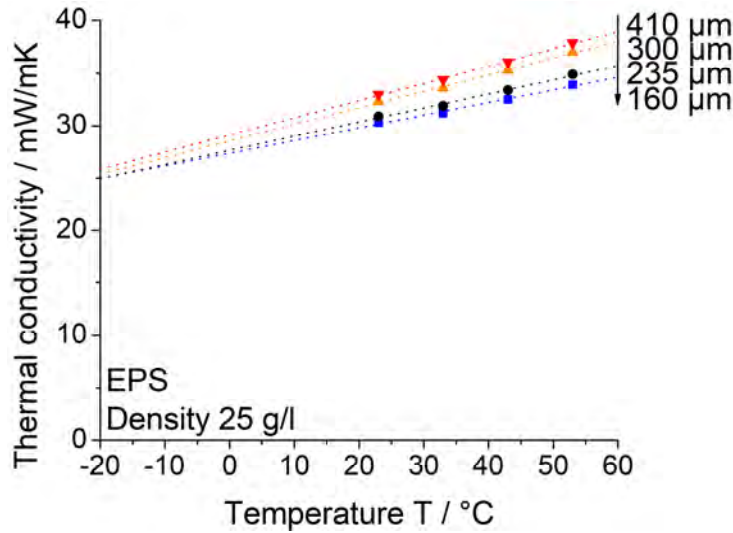


**Figure 78: Thermal conductivity as function of temperature for four different cell sizes of EPS. An enlarged section is shown in the Appendix (Figure 133).**

The gaseous conduction was calculated by obtaining the fraction of each phase (solid and gas) from the relative foam density ( $\rho_{rel}$ ). This method was used in literature [166]. The thermal conductivity of air  $\lambda_{air}$  in dependency of temperature was fitted by a 2<sup>nd</sup> order polynomial with data from the CRC Handbook of Chemistry and Physics [167]. The conduction from the solid matrix  $\lambda_{sol}$  requires a calculation in a more complex manner according the IKP-model [166]. This model is based on a cubic unit cell taking the volume fraction of cell walls  $\phi_W$  and cell struts  $\phi_S$  into account. The latter quantities were obtained using a dodecahedron as unit cell with a volume calculated from the measured cell size. The cell struts and walls are located at the corners and faces of the dodecahedron. From the function of cell strut and wall thickness versus density, their respective volume fractions were determined. The density-averages yielded  $\phi_W = 0.73$  and  $\phi_S = 0.27$ .

For the conductivity of compact polystyrene  $\lambda_{PS}$ , a value of 156 mW/mK was used [164]. The radiative contribution  $\lambda_{rad}$  was then calculated by subtracting the combined solid and gaseous components from the total thermal conductivity ( $\lambda_{tot}$ ) as seen in Equation 7, Equation 8 and Equation 9.

$$\lambda_{sol} = \rho_{rel} \left( \frac{2\phi_W + \phi_S}{3} \right) \lambda_{PS} \quad \text{Equation 7}$$

$$\lambda_{gas} = (1 - \rho_{rel}) \lambda_{air}(T) \quad \text{Equation 8}$$

$$\lambda_{rad} = \lambda_{tot} - (\lambda_{sol} + \lambda_{gas}) \quad \text{Equation 9}$$

The total thermal conductivity and its respective contributions are plotted in Figure 79. It becomes clear, that the slope of the total conductivity is higher than the slope of the “gaseous + solid” ( $\lambda_{sol} + \lambda_{gas}$ ) contribution. This implies, that the radiative contribution increases with temperature, which is expected and is reflected in Figure 79. Furthermore, the radiative contribution increases with smaller cells, which is coherent with simulations [146].

Furthermore, it is important to note, that smaller cells have a significantly lower radiative contribution. For example, the 160  $\mu\text{m}$  cell have a 53 % lower radiative conductivity than 410  $\mu\text{m}$  cells at 23  $^{\circ}\text{C}$  (2.8 versus 5.3 mW/mK).

In summary, it is concluded, that the cell size is an important factor to control the thermal radiation of foams. In general, the total thermal conductivity scales almost linearly with cell size in the region of 150 to 600  $\mu\text{m}$  cell as shown in Figure 77.

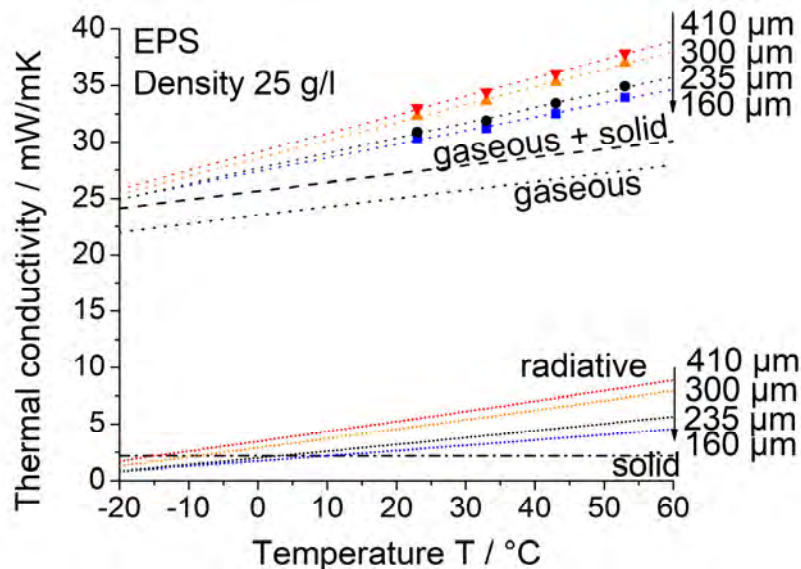


**Figure 79: The total thermal conductivity and its gaseous, solid and radiative contribution in dependency of temperature for four cell sizes at a constant density of 25 g/l.**

However, when the cell size is reduced further, deviations from this linear trend are observed, as shown in the comparison of EPS from extrusion and sEPS in Figure 80. The three sEPS materials deviate in their whole from the linear trend with almost no scatter. The mechanism behind this derives from the ratio of the cell wall and strut thickness compared to the wavelength at the maximum of the spectral radiant emittance of a black body at a given temperature (Figure 81).

When the cell size becomes smaller at a given density, the cell walls and struts naturally also become thinner. Thick walls and struts, which are larger than the wavelength at the maximum emittance, have a higher probability of photon absorption, whereas thin walls and struts smaller than the maximum have a high chance of photon transmission, which leads to a larger “effective cell size”. Thus, the radiative contribution is enhanced, when the cell walls and struts become too thin to effectively absorb radiation. This is true for sEPS as can be observed in Figure 81: the cell walls and struts of sEPS (orange bars) are much smaller than the wavelength at the maximum at 300 K. In contrast, EPS from extrusion has thicker cell walls and especially struts, which are close to the maximum at 300 K (grey bars). For the sake of completeness, the analogous graph for E-Por is given in the Appendix in Figure 135.

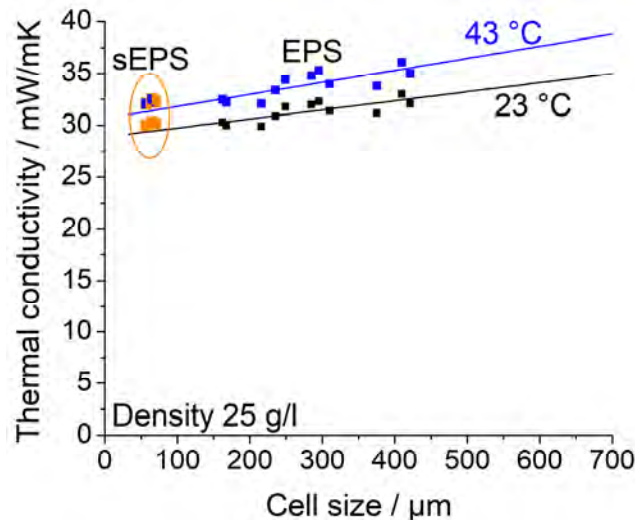


**Figure 80: Comparison of the total thermal conductivities versus cell size of sEPS and EPS at 23 and 43 °C temperature. An enlarged section is shown in the Appendix (Figure 134).**

This behaviour is the reason, why IR absorbing and scattering additives as graphite are used for low-density foams for thermal insulation with small cells as for example Neopor or Styrodur C (both by BASF SE).

In summary, it was seen that smaller cells lead to better insulation properties for low-density foams below 30 g/l, which can be attributed to a lower radiative energy transport. Temperature is a major factor affecting the radiative transport in foams and thus the thermal conductivity. Furthermore, small cells showed less sensitivity of the thermal conductivity towards temperature changes as their spacial temperature gradient is lower. However, too small cells with too thin walls and struts lead to a change in transmittance for the infrared radiation and thus a larger “effective cell size”.

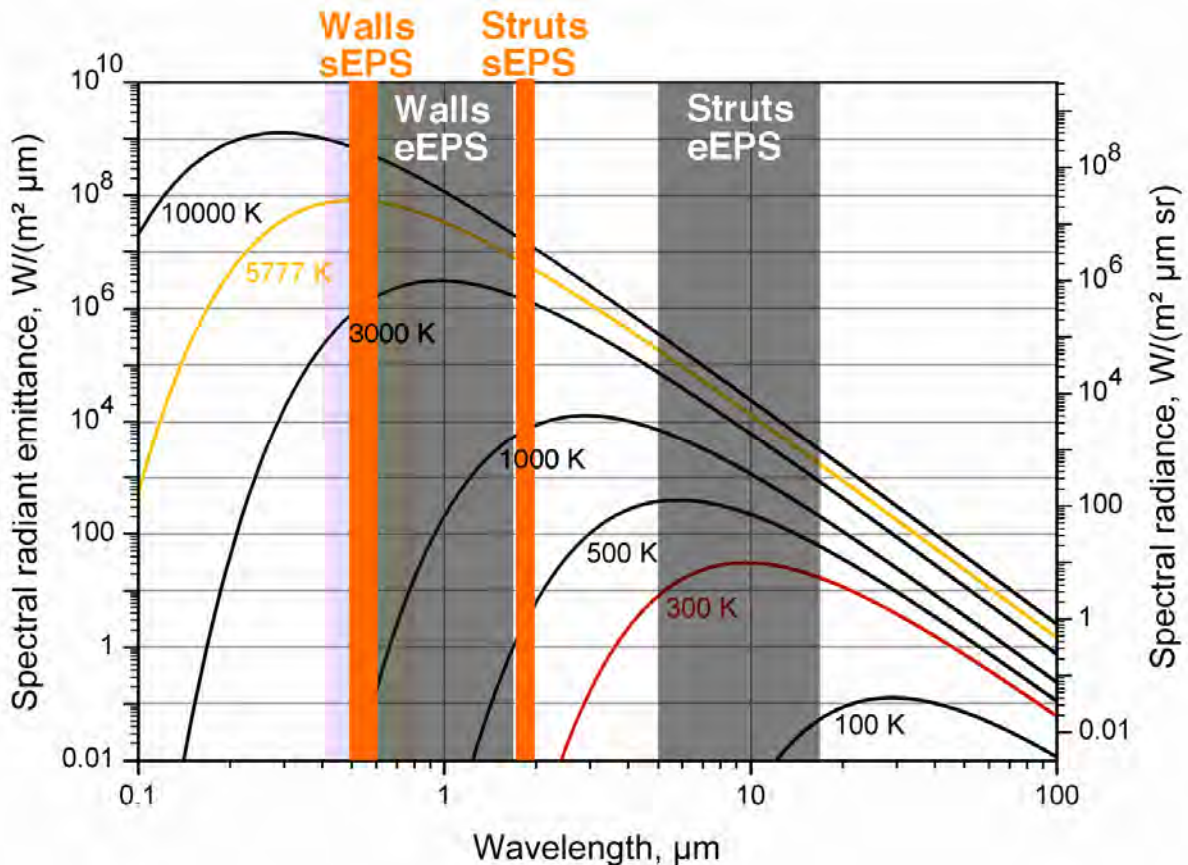


Figure 81: Comparison of the emission spectra of thermal radiation of a black body with the typical dimensions of the cell walls and struts of sEPS (orange) and EPS (grey) (Spectra used from [168]).

### 5.3.3 Effect of the foams internal interface on the insulation properties by variation of the bead size

When the bead size is changed for EPS and E-Por, no clear trend of the thermal conductivity can be observed (*cp.* Figure 82). E-Por only exhibits an almost negligible trend of decreasing conductivity with increasing bead size, whereas the opposite trend is observed for EPS.

The reason for this observation for EPS is rather clear as the cell size significantly increases with bead size. This leads to an increased thermal conductivity as shown in the previous section. For E-Por the reason is not directly tangible, since the average cell size is constant for the three different bead sizes of E-Por. However, differences arise in the cell size distribution as the cell sizes at the bead boundaries and in the centre of the beads are slightly varying. In the larger beads, the cellular structure is more homogenous and the cell walls and struts are also thinner, which should theoret-

ically increase the radiative heat transfer. However, this must be outweighed by another factor, which might be in this case the homogeneity of the cell size distribution. However, it must be stated that the observed change is rather a trend.

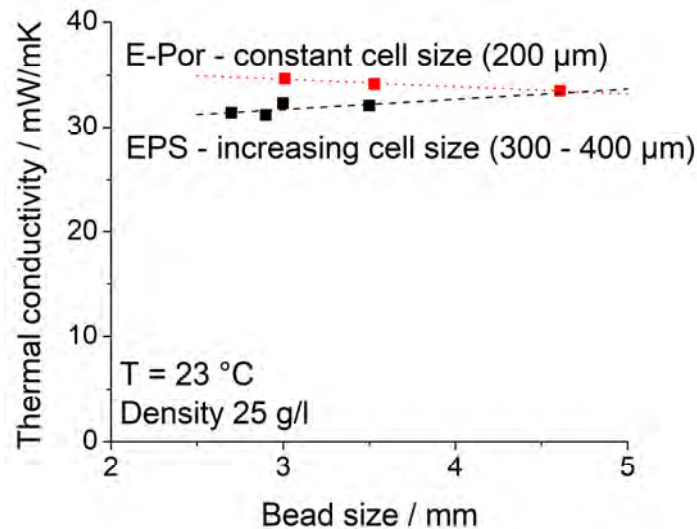


**Figure 82: Thermal conductivity of EPS and E-Por in dependency on bead size. Please note, that EPS exhibits increasing cell size with larger bead size, whereas the E-Por materials have an almost constant cell size.**

In summary, a changing bead size does not directly affect the thermal transport in bead foams. However, indirect effects as a changing cell size or cell size distribution or probably macro-porosity lead to a change in insulation behaviour.

### 5.3.4 Effect of polymer fraction (density) on the thermal transport at varying cell and bead size

Following the independent analyses of the influence of both cell size and bead size on the thermal conductivity at a constant density of 25 g/l, the combined effects of density and foam morphology are discussed in the following.

The effect of density on the thermal properties of polymer foams has been extensively studied in the literature. The main challenge in these works is, that by changing the foam density, all morphological features of the foam are affected as well. Figure 83 shows the heat conductivity of EPS and E-Por samples as function of density. It can be seen, that the insulation properties of both EPS and E-Por are distinctly affected by density. Since the density range for E-Por is more extended and the governing mechanisms of thermal transport are the same for both materials, the focus is put to E-Por in the following.



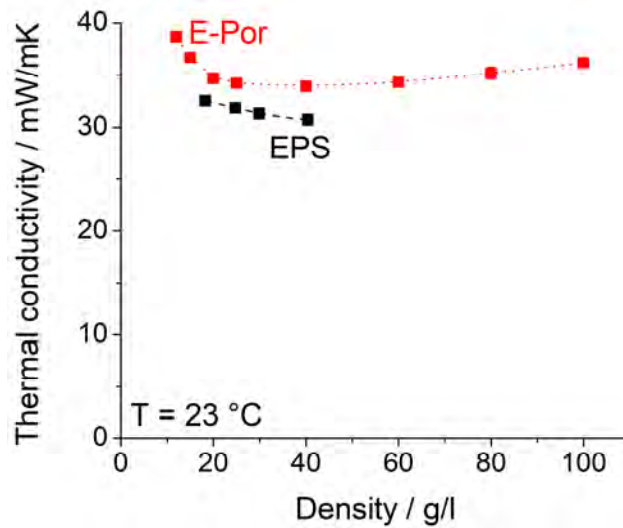


Figure 83: Thermal conductivity of E-Por versus foam density for EPS and E-Por.

The thermal conductivity as function of density indeed exhibits text-book-behaviour with its typical U-shaped curve. To make the underlying phenomena more understandable and clear, the total thermal conductivity was separated into its components as shown previously. Due to the fact, that E-Por is a blend-system consisting of polystyrene and polyethylene, an average thermal conductivity for the solid contribution was calculated,  $\lambda_{PS-PE}$  as shown before.  $\lambda_{PS-PE}$  reads 208 mW/mK. The resulting individual components of foam thermal conductivity are shown in Figure 84.

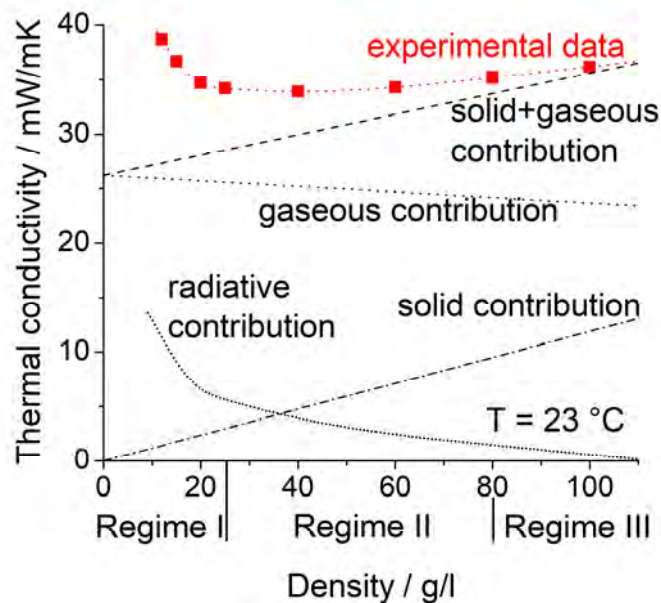


Figure 84: Separation of total thermal conductivity of E-Por into the contributing fractions, namely solid and gaseous conduction and radiation as function of density.



Three regimes of heat conductivity with regards to foam density are observed in Figure 84. A fourth can be derived from the extrapolation of the solid and gaseous contribution. The first regime (densities below 25 g/l) is governed by infrared radiation and gaseous conduction. Since the density is very low in this regime, heat conduction through the polymer matrix (about 2 mW/mK) can be almost neglected compared to the other components, as clearly visible in Figure 84. The conduction of the cell gas is almost constant over density for this range of highly expanded foams. Therefore, the change of the thermal conductivity with density is related to IR radiation at very low densities. The increase in IR radiation at very low foam densities is due to large cells as well as the thin cell struts and walls at this low-density range. A minor contribution to the high conductivity of low-density foams might be also attributed to the large bead sizes, as already shown in the previous sections.

The second regime corresponds to moderate foam densities (about 40 g/l) in which the lowest thermal conductivity is reached. In this regime, the solid conduction is still low, while the cellular morphology allows for only a small contribution of radiative heat flux. In this regime, gaseous conduction is the dominating mechanism for thermal transport.

At higher foam densities above 60 g/l (third regime), the solid conduction becomes increasingly important, since more material can contribute to heat conduction. However, the gaseous contribution is still dominating the total value. For densities above 80 g/l, it is observed that radiation becomes less important, because the cell sizes are continuously reduced and the cell walls/struts are much thicker. Those two factors lead to a low temperature gradient over a single cell and a lower transparency for infrared radiation, respectively. The fourth region at densities above about 180 g/l is dominated by solid conduction. Gaseous convection can be neglected for cells smaller than 3 mm [134]

As a conclusion, with respect to density, four regimes of heat conductivity were observed for E-Por foams:

- **Regime I - Low density** (*shape dominated by radiation*): large foam cells significantly enhance the heat conductivity through radiation.
- **Regime II - Moderate density** (*shape dominated by gaseous conduction*): small cell sizes lead to low radiative heat flux and density is still low to ensure low conduction through the polymeric matrix. Therefore, the heat conductivity is at its minimum.

- **Regime III - Increased density** (*shape dominated by solid dominated regime*): Thermal conductivity is proportional to density; gaseous conduction is still the most important factor.
- **Regime IV - High density** (*solid dominated regime*): Thermal conductivity is dominated by the polymer.

### 5.3.5 Effect of the macroscopic density gradient in a moulded part

Another factor, which has so far been neglected in literature, is the effect of the density gradient within a bead foam part. The expansion of the beads near the mould surface is hindered, which leads to a density gradient along the part thickness (*cp.* visualisation in the Appendix, Figure 136). In order to study the effect of the density gradient, an example study on selected samples of E-Por was conducted. Therefore, samples including the surface layer and from the central part of the foam plate (and thus different density gradients and average densities) are studied and compared. Figure 85 shows the influence of the sample origin for foams with different cell sizes and foam densities. The bead size was not studied as no effect on E-Por was observed previously.

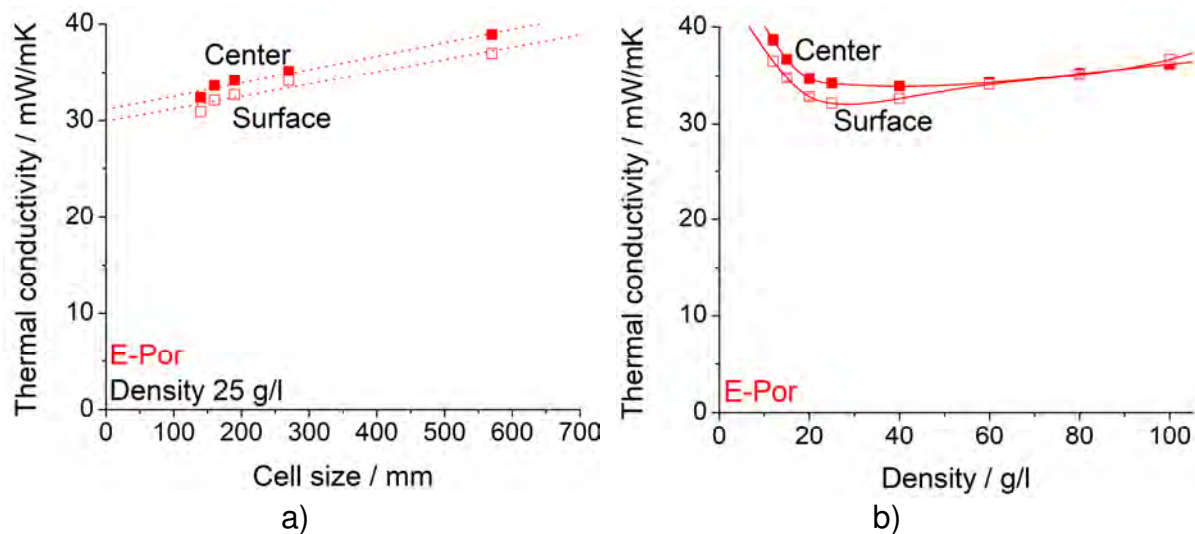


**Figure 85: Heat conductivity of E-Por samples measured in the centre of a part and at the edge with skin as a function of a) cell size and b) foam density.**

At the constant density of 25 g/l, the influence of the sample origin is significant and constant for all cell sizes. Samples including the surface exhibit a reduction of thermal conductivity by almost 5 %. At this average density, the samples from the surface layer possess a density closer to the optimum density, which is higher than the average density. Thus, the thicker cell walls and struts of the denser parts cause a shielding effect for radiation, thereby decreasing the thermal conductivity at the surface. This is

a further indication for the importance of radiative heat transfer on the thermal conductivity of foams.

When the foam density is taken to consideration, a more complex pattern is observed as shown in Figure 85 b). For low and moderate densities, samples from the surface have a significantly lower thermal conductivity due to the same effect as explained before. At densities below 60 g/l of the part, the density of the surface is closer to the optimum density. However, at densities above 60 g/l the thermal conductivity of samples from the outer layer is higher compared to the samples from the centre. In this case, the denser outer layer possesses a less optimal density than the core. It is noteworthy, that cell size analysis did not show a significant variation of cell size along the sample's thickness coordinate.

### **5.3.6 Summary of the dependency of the thermal conductivity on the bead foam morphology**

The morphological changes have a profound impact on the thermal transport properties. From literature it is known, that gaseous convection can be neglected for cells smaller than 3 mm [134]. However, smaller cells are beneficial for the insulating capabilities of the foam, since they help to reduce the potency of infrared radiation. It is known from literature, that thinner walls and struts should have the opposite effect. However, this is only true for walls and struts smaller than the wavelength at the maximum of the spectrum of a black body as for sEPS.

In contrast, bead size does not alter the thermal transport directly; it rather affects it indirectly through other factors. One factor is the change of cell size with bead size as for extrusion EPS, another factor is the homogeneity of the cell size distribution as for E-Por. Interestingly, the homogeneity of cell size outweighs a reduction of cell wall and strut thickness with larger beads.

The thermal conductivity is affected distinctly by density. Three regimes of thermal conductivity are identified, a fourth becomes apparent when the solid and gaseous contribution are extrapolated. At low densities below 20 g/l, gas-conduction dominates the total thermal transport, whereas the shape is dominated by infrared radiation. In this range, large cells as well as thin walls and struts facilitate radiative energy transport. At moderate densities around 40 g/l, gaseous conduction is the dominating mechanism for the shape of the curve. There, the cell size is distinctly smaller compared to foams with a very low density, which leads to a low radiative heat flux. Furthermore, the density is still low resulting in a small contribution of conduction through

the polymeric matrix. For high-density foams above 80 g/l, conduction through the polymer matrix becomes increasingly important leading to an almost linear dependency on density. Radiation is only a minor contribution, since the cell walls and struts are thick and the cells themselves are small. However, gaseous conduction is still dominating. This changes in regime four at densities larger than about 180 g/l.

Furthermore, the skin of a bead-foamed part is an important factor to consider. For the samples with densities below 25 g/l, the thermal conductivity of samples from the centre of the moulded plate is higher than those from the surface. However, at a density above 60 g/l, this behaviour turns. This is attributed to the density gradient within a part. In the case of low average density, the density at the skin is closer to the optimum. In the case of high average density, a less optimal density is found near the skin compared to the centre.

## Part II: Creation and exploration of a novel length scale in EPS: a thick skin around the beads

### 5.4 The unknown morphological parameter of a thick bead skin

#### 5.4.1 Motivation for a thick bead skin

The motivation to study a skin around EPS bead is two-fold. First, no knowledge about this structural parameter exists. Secondly the questions arises whether this property could not be harvested to create foams with enhanced mechanical properties. Here, the second motivator comes to play. From sandwich structures it is well known, that a combination of a foam core and high-modulus face sheets leads to superior stiffness. With a solid skin around the beads, this concept would be realised on a micro-structural level as shown in Figure 86. Thus, it was hoped to facilitate an internal sandwich effect.

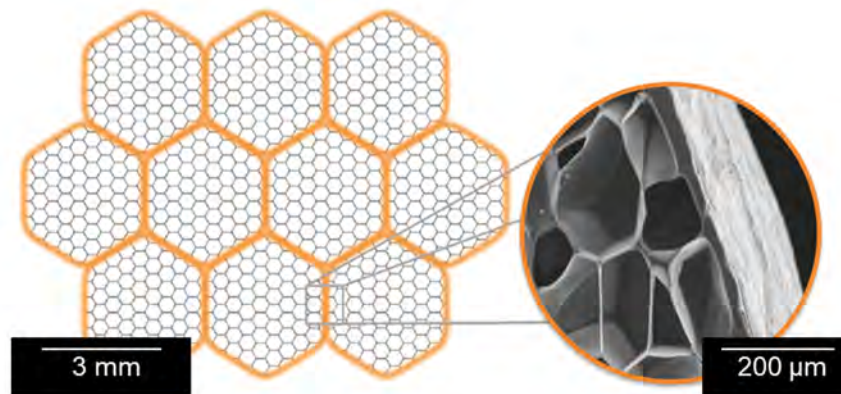


Figure 86: Visualisation of the internal sandwich in a bead foam part.

#### 5.4.2 Fundamental idea to create a thick bead skin

The basic approach to realise this concept is based on a simple principle idea. If a sufficient amount of blowing agent (pentane) is removed locally from a finite surface layer of the beads, they would only expand in the still pentane-rich centre during pre-expansion. This can be simply achieved by storing the expandable beads below, but close to, their glass transition temperature. This approach is shown in Figure 87, where a virgin bead (not depleted of pentane) is compared to a pre-treated (locally pentane-depleted) one. The virgin bead would not form a solid skin, whereas the treated bead forms a skin in pre-expansion.

This approach has the charm that the density of both types of beads can be set to the same level by an appropriate variation of the pre-expansion conditions (steam-temperature and pre-expansion time).

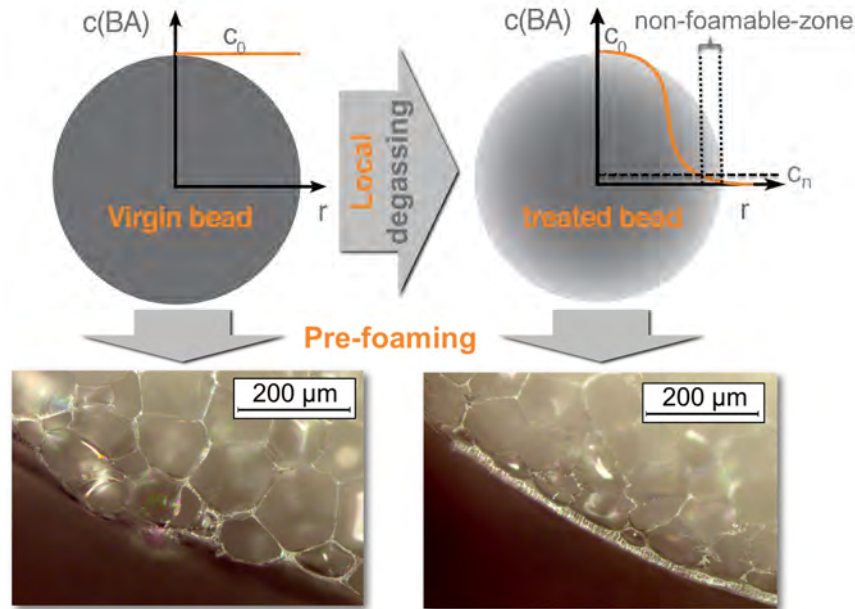


Figure 87: Concept of the fundamental idea how to create a skin around EPS-beads.

In order to study the effect of the skin on the mechanical properties, a two-step approach is followed. At first, the fundamental concept is evaluated in lab-scale to test its applicability. Subsequently, it is up-scaled from the lab to industrial machinery to create larger amounts for steam-chest moulding. The moulded parts are then evaluated regarding their structure-property-relationships. This approach is depicted in Figure 88.



Figure 88: Approach for the methodological development of the method to create a solid skin around EPS-beads.

### 5.4.3 Aims for the creation of a thicker skin

The aims of this part of the work are two-fold. 1) Process-wise, the method must allow the effective control of the skin thickness (*e.g. via* storage time and/or temperature) and be scalable from lab-scale to industry-sized machinery to process quantities > 10 kg of EPS beads. 2) In terms of morphology it is aimed to increase the skin thickness by at least one order of magnitude to > 5  $\mu\text{m}$  as compared to untreated beads (about 0.5  $\mu\text{m}$  skin thickness). Furthermore, the skin needs to be rather homogeneous, meaning it should not be ruptured or possess too severe fluctuations in thickness.

### 5.5 Development of a process to create beads with a thick skin

#### Validation of the concept

A similar approach as the proposed one was tried by Kumar und Weller [169]. They saturated Polycarbonate (PC) with  $\text{CO}_2$  and stored the saturated samples for certain times at ambient conditions. Thus, a locally  $\text{CO}_2$ -depleted boundary was achieved, which did not foam. The described experiment was successfully reproduced using Lexan 121 by DSM as shown in Figure 89. The thickness of the unfoamed boundary layer increases with desorption time: longer desorption times lead to thicker skins.

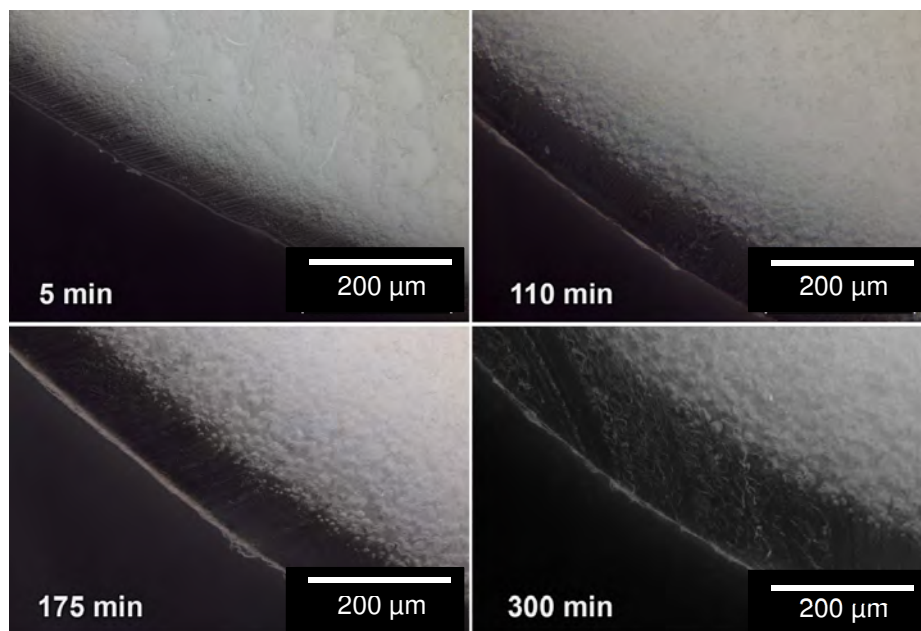


Figure 89: Reproduction of the skin formation in [169] during foaming of Polycarbonate by local depletion of  $\text{CO}_2$  by storage at ambient conditions prior to foaming.



### 5.5.1 Establishment of the fundamental concept in lab-scale

#### Desorption of pentane in EPS

In order to quantify the transient pentane-loss, isothermal TGA experiments were conducted on the expandable EPS beads. The total pentane content can be estimated from the material datasheet. EPS contains about 6 wt-% pentane. Due to the pentane-loading the glass transition temperature ( $T_G$ ) is reduced by about 7 °C per wt-% pentane [64]. Thus it was decided to run the experiments at 60 °C to ensure a not too fast diffusion with the aim that the local depletion can be accurately controlled by oven-storage time. Furthermore, a temperature below the  $T_G$  does not yet lead to foaming, which is also a necessity for the local pentane-depletion.

The resulting transient mass is plotted in Figure 90. At the beginning of the experiment a pronounced loss of pentane takes place, which levels off in the course of the experiment. After 1 h about 0.4 wt-% left the sample, after 3 h 0.5 % and after 5 h 0.9 %, which equals about 15 % of the total pentane content.

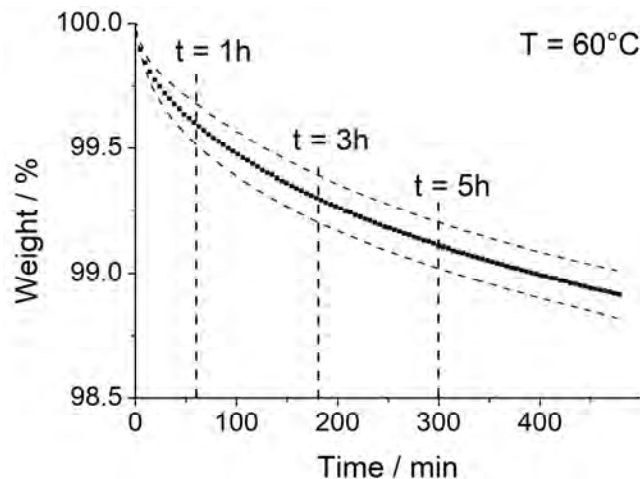


**Figure 90: Averaged transient pentane loss at isothermal conditions (60°C, average of 8 measurements). The dashed lines denote the standard deviation of the experiments.**

Based on the TGA experiments, initial oven storage trials with a duration of 1, 3 and 5 h are carried out. Due to the pentane loss at the border and thus an increased glass transition temperature, higher pre-foaming temperatures compared to the virgin material are expected and will be trialled as well (virgin EPS is usually pre-foamed with steam temperatures between 80 and 120 °C [170], [171]).

### Process-development for EPS

In order to validate the approach for EPS and get an understanding for the time-scale, expandable beads taken directly from an EPS-barrel are placed in a convection oven at 60 °C for 1 h, 3 h and 5 h. These times were selected from the TGA results in a way that not too much pentane diffused out of the beads as they still have to foam in the core to a low density. Subsequently, these beads and some untreated beads (for reference) were foamed inside a glycerine-bath at 120 °C for 10 s. Cross-sections of the pre-foamed beads were studied using a light-microscope and are shown in Figure 91.

It is clearly visible, that it is possible to control the beads' skin thickness *via* a local pentane depletion induced by a storage at elevated temperature. For example, the compact skin of the 3 h – 60 °C sample is many times thicker compared to the virgin reference bead. It can also be seen, that the storage time has a direct correlation with the skin thickness as was hypothesised.

However, the skin especially of the 3 h and the 5 h samples is rather inhomogeneous. This could be due to an uneven distribution of temperature inside the oven. In order to test this hypothesis, the beads were degassed inside a tempered water-bath. However, this approach did not lead to a thick compact skin and was thus discarded.

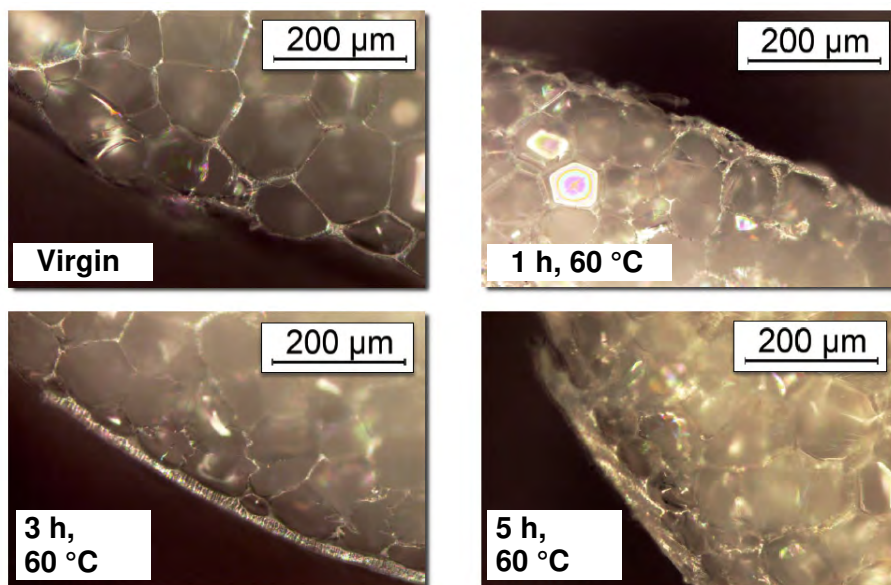


**Figure 91: Cross-sections of a pre-foamed virgin reference bead and pre-foamed beads, which were pentane depleted at 60 °C for 1, 3 and 5 h. The beads were pre-foamed at 120 °C for 10 s.**

In order to study the effect in more detail, SEM images of the surfaces of the beads were taken (Figure 92, upper images). These images clearly show unfoamed areas of polystyrene for the stored beads. In comparison, the shape of the cellular structure is

visible on the surface of virgin (not pentane-depleted) beads. This effect can also be observed in the cross sections (Figure 92, lower images), where steep hills of PS are observed. However, unfoamed areas of PS are clearly visible, which underlines the viability of the approach.

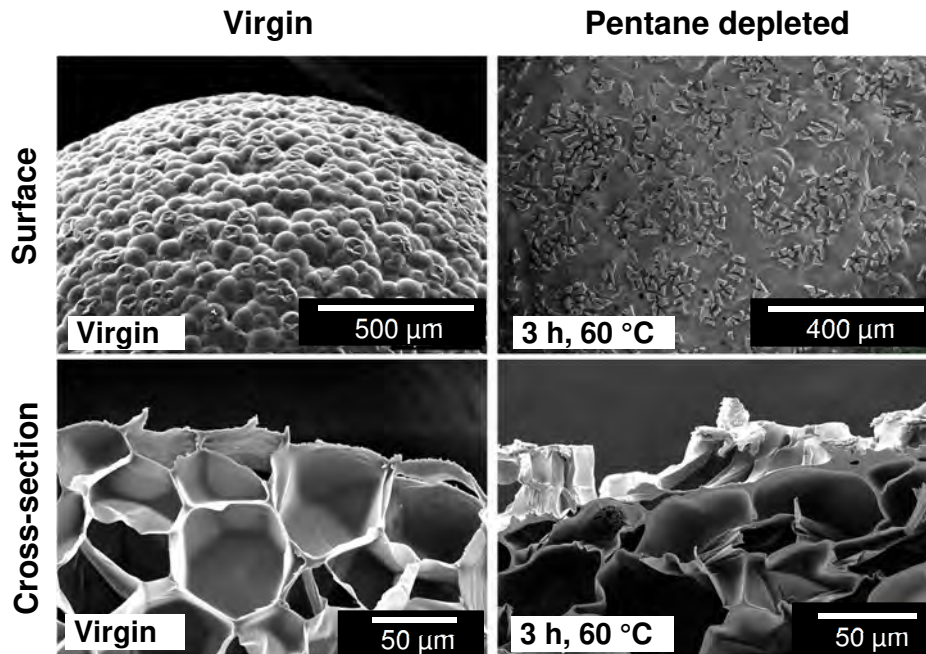


**Figure 92: Surfaces and cross-sections of virgin beads (left) and the pentane-depleted beads (3 h, 60 °C). The beads were pre-foamed at 120 °C for 10 s.**

In order to shed more light into the inhomogeneities, the surface with a special focus on the “hills” is depicted in higher magnifications in Figure 93. It appears, that the pentane-depleted region does not flow sufficiently during pre-foaming, but rather break up and rupture until a layer with sufficiently low viscosity (due to low amounts of residual pentane) is reached, which can ultimately flow.

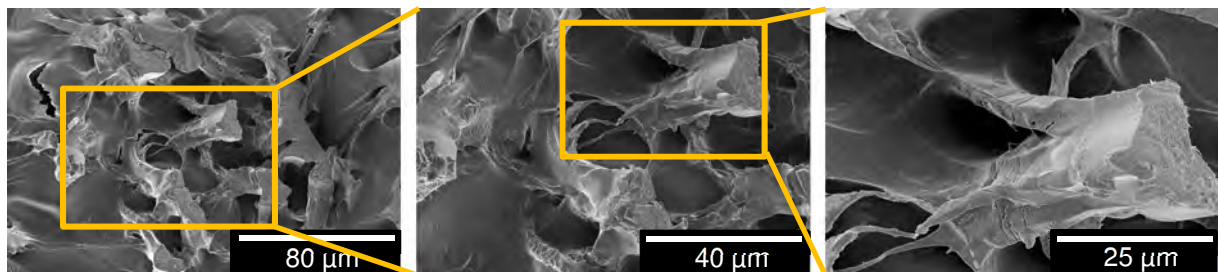


**Figure 93: Surface of beads stored for 3 h at 60 °C. The beads were pre-foamed at 120 °C for 10 s.**

Improvement of the flowability of the pentane-depleted layer

In order to facilitate the flowability two approaches were tested: 1) increase of the pre-foaming temperature and 2) plasticisation of the boundary layer by a non-foaming solvent.

The variation of the pre-foaming temperature up to 180 °C ultimately eliminated the hills. However, no compact skin was observed at this elevated temperature and thus this approach was discarded. In contrast, lower temperatures than 120 °C did not lead to a sufficient level of foaming of the beads. Hence, the following experiments were carried out at a pre-foaming temperature of 120 °C.

The second approach aims to plasticise the pentane-depleted outer layer to obtain sufficient flowability so that a compact and homogeneous skin forms during pre-foaming. Therefore, the beads were washed in a solvent for 30 min, dried and subsequently pre-foamed. Ethanol (boiling point 78 °C), 2-butanon (boiling point 80 °C) and toluene (boiling point 110 °C) as high-boiling solvent were tested.

Both 2-butanon and toluene quickly dissolve the polystyrene such that foaming was not possible. In contrast, ethanol does not dissolve EPS. The foamed beads treated with ethanol did not display a ruptured skin. However, no increase of skin thickness could be noted. Based on this result it was hypothesised, that the ethanol treatment either leads to the diffusion of pentane to the outer layer and/or to nucleation and foaming in the outer layer (ethanol acts as blowing agent) and/or enables the foaming of small amounts of residual pentane in the outer layer.

**Table 7: Summary of the observations from the study of the effect of washing time in ethanol after the oven storage.**

<b>Duration of ethanol treatment</b>	<b>Condition of the skin</b>
<b>0 s</b>	Inhomogeneous skin-thickness, locally thicker skin, skin-rupture
<b>10 s</b>	Semi-homogeneous skin-thickness, <b>thick skin</b> , skin-rupture
<b>30 s</b>	<b>Homogeneous</b> skin-thickness, <b>thick skin</b> , <b>no rupture</b>
<b>60 s</b>	<b>Homogeneous</b> skin-thickness, <b>thick skin</b> , <b>no rupture</b>
<b>5 min</b>	<b>Homogeneous</b> skin-thickness, thin skin, <b>no rupture</b>
<b>15 min</b>	<b>Homogeneous</b> skin-thickness, thin skin, <b>no rupture</b>
<b>30 min</b>	<b>Homogeneous</b> skin-thickness, thin skin, <b>no rupture</b>

In order to find a balance between the plasticising effect to suppress skin-rupture and the foaming of the pentane-depleted layer, the effect of washing time was studied. The summarised results are given in Table 7. It can be clearly observed, that the ethanol-storage time is the deciding factor for skin homogeneity as well as skin thickness. Only with the correct treatment time, the aim of a thick skin with a homogeneous thickness can be achieved. In order to shed more light into the effect of ethanol storage time, 3 h, 60 °C-samples without and with ethanol treatment were studied using SEM-imaging.

A comparison between only pentane-depleted beads and pentane-depleted, ethanol treated beads is shown in Figure 94. The beads not treated with ethanol clearly exhibit skin rupture. In contrast, the 30 s ethanol treatment effectively prevents the rupture of the skin (smooth surface) by the softening effect, while allowing the skin to flow and form a compact and thick layer.

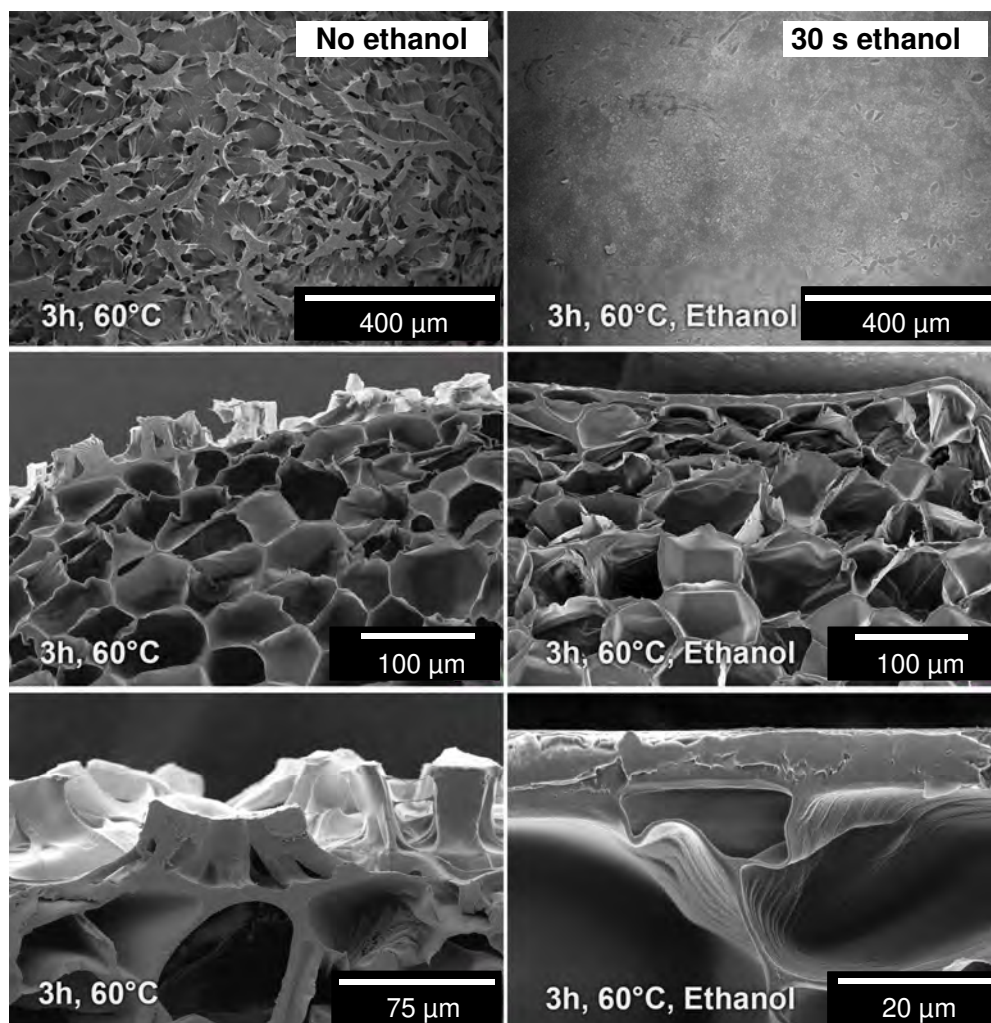
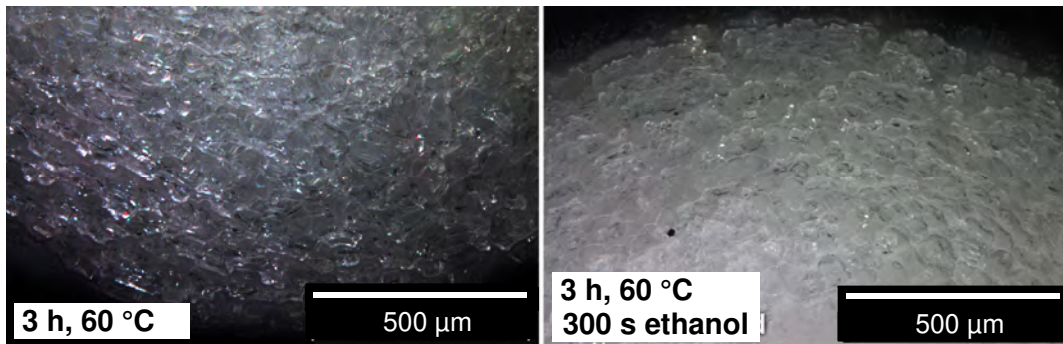


Figure 94: SEM-images from pre-foamed, pentane-depleted beads (3 h, 60 °C) without (left side) and with a 30 s ethanol treatment (right side).



However, also, the removal of anti-static additives or processing aids could be a decisive mechanism. Especially, the latter are known to facilitate skin rupture for a lower cycle time in steam-chest moulding [172]. In order to test this possibility, beads were washed in ethanol for 5 min before the oven storage, so only the additives on the surface are washed away. The absorbed ethanol evaporates during oven storage. The surface of the resulting beads is shown Figure 95. No distinct difference between the reference beads and the ethanol treated beads can be observed, both exhibit surface fracture, which can be seen from the solid polystyrene hills. The ethanol treated skin is slightly less fractured, which could also be attributed to fluctuations in the process. Furthermore, no homogeneously thicker skin forms.



**Figure 95: Pre-foamed EPS-beads, which were subjected to a 3 h oven storage at 60 °C without (left) and with (right) 5 min ethanol washing prior to oven storage.**

It is noteworthy, that the removal of additives by washing with ethanol supports the formation of a solid skin in the best case, but is not the main mechanism. Also, the thickness of the skin cannot be affected by removing surface additives.

#### Final method for the production of EPS-beads with a thick skin in lab-scale

In summary, it was found that the skin thickness is indeed controllable *via* oven storage time at 60 °C, which leads locally reduced pentane concentration at the surface and prevents foaming in this part. However, the ability for flow of the pentane-depleted polystyrene layer is not sufficient (pre-foaming temperature below the glass transition temperature), hence rupture of this layer during expansion is encountered. This problem was solved by a pre-treatment of washing the expandable beads for 30 s with ethanol after the oven storage and before the pre-foaming. This leads to a sufficient plasticisation of the pentane-depleted layer, which can thus be stretched. As a result, a solid, smooth and homogeneously thick skin is obtained. Ultimately, a homogeneous bead skin with a thickness of  $9.5 \pm 2.4 \mu\text{m}$  (3h, 60 °C) was achieved, which is 19 times

the thickness of the virgin beads ( $0.5 \pm 0.1 \mu\text{m}$ ). It is noteworthy, that the removal of surface additives is not responsible for preventing skin fracture. A schematic summary of the final process is given in Figure 96.

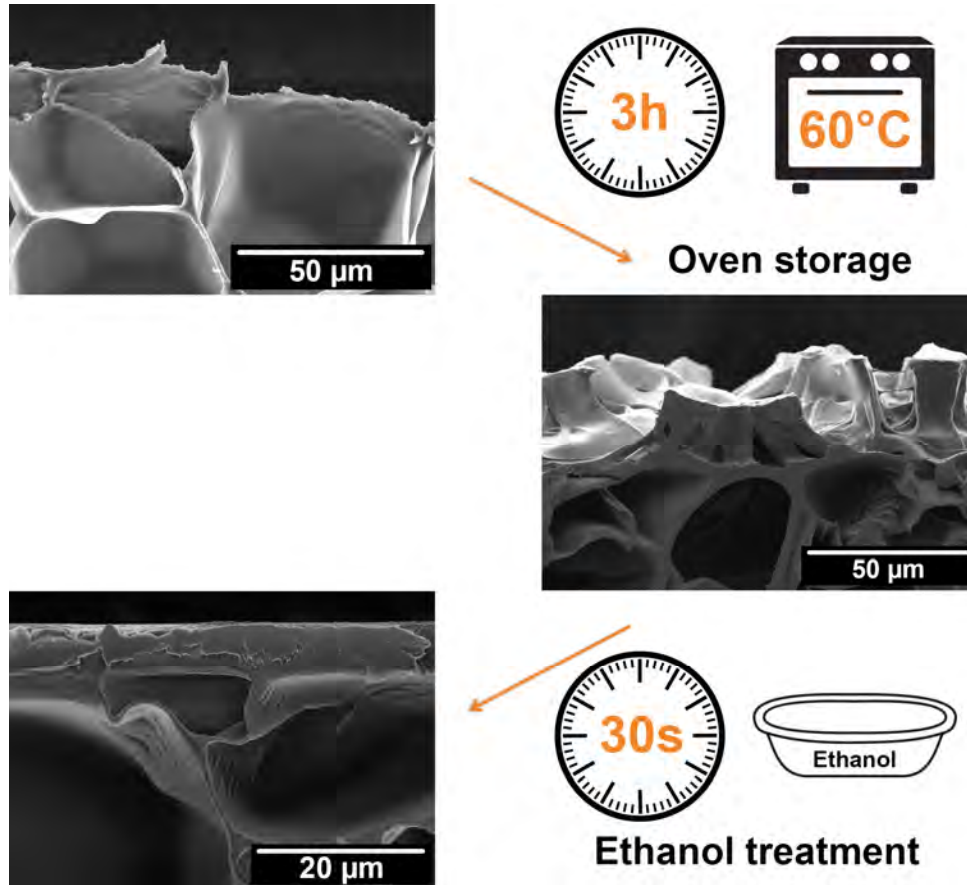


Figure 96: Schematic summary of the process for the formation of a solid skin around EPS.

### 5.5.2 Up-scale of the process to industrial pre-foaming machines

The previous lab-scale process must be up-scaled to industrial pre-foaming machines in order to a) test its applicability beyond pure science and b) to obtain enough beads (15 – 20 kg per material variation) for steam-chest moulding and ultimately mechanical testing. The target bulk density for pre-foaming was 40 g/l.

At the beginning of this subchapter problems and solutions of the up-scaled process in comparison to the lab-scale approach are studied and discussed, such as the degassing process of the beads in the oven or the waiting intervals between the processing steps. Since the energy for pre-foaming is supplied *via* steam in comparison to the lab-scale in a glycerine bath, the effect of steam pressure on the skin has to be investigated. Ultimately, a comparison to the lab scale approach is drawn and further insight into the effect of oven storage time provided.



Effect of the time-intervals between the individual processing steps

For the degassing in a convection oven for lab-scale, a single layer of beads is put on a metal plate and mixed at fixed intervals to provide the same heat transfer to all beads, which leads to reproducible results. For the up-scaled process the beads are filled into a pre-heated tub with a maximum filling level of 10 cm, the tub is located in the oven in such a way that the hot air flows directly onto the beads. Furthermore, the beads are mixed at fixed intervals.

In the lab-scale the time differences between the steps oven-storage, ethanol treatment and pre-foaming are very short, whereas they are significant for the industrial scale (e.g. by transportation times). This might affect the concentration-profile of pentane and thus the skin formation. The time difference between ethanol treatment and pre-foaming is also supposed to be of influence, as the presence of ethanol would facilitate the diffusion of pentane back to the outer layer. These time intervals are schematically shown in Figure 97.

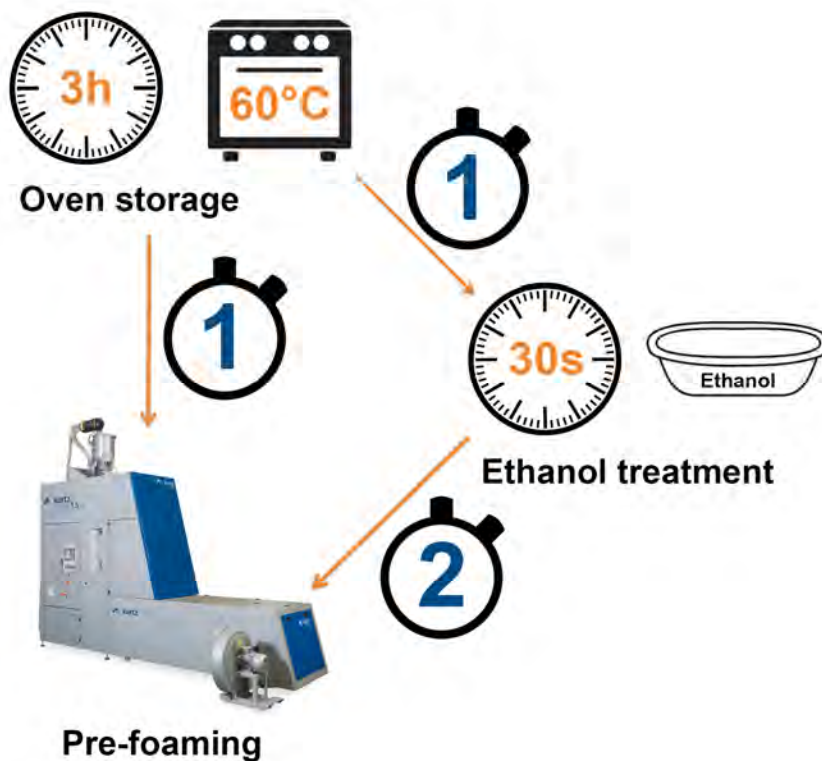


**Figure 97: Schematic of possible affecting times intervals in the industrial scale process to create thick skins.**

Regarding the duration between oven storage and pre-foaming or ethanol treatment (Figure 97, clocks showing (1) ), an interval of 4 h was found to be uncritical, if the

beads are stored at ambient conditions. If stored in a fridge at -18 °C, durations up to 24 h did not impede the resulting bead skin, although a thicker skin was observed at a storage time of 5 d (although not in a reproducible manner). In contrast, the time between the ethanol treatment and pre-foaming is more critical as it should not exceed 15 min. Otherwise the skin becomes rough.

For the following trials, the beads were treated in a convection oven as described above for a given time and subsequently frozen. In the following day, up to 500 g of beads were put between two sieves and submerged into ethanol for 30 s. Pressurized air was blow into the setup to remove residual ethanol. The pre-foaming is then conducted using 1 kg of such prepared beads.

#### Influence of the steam pressure on the skin formation

In industrial scale pre-foaming, the steam-pressure plays a significant role on the quality and thickness of the skin. Thus, it was studied in more detail. Therefore, the conditions a) virgin beads at 150 mbar steam pressure, b) pentane depleted beads (3 h, 60 °C) at 100, 150, 200 and 300 mbar steam pressure (30 s ethanol treated) and c) pentane depleted beads (6 h, 60 °C) at the optimum steam pressure of b) as test for the ethanol treatment (not ethanol treated) were studied.

The resulting bead skin thicknesses in dependency on steam pressure in pre-foaming are plotted in Figure 98 as well as a comparison to lab-scale results (glycerine bath) and virgin beads. The target bulk density for pre-foaming was  $40 \pm 3$  g/l.

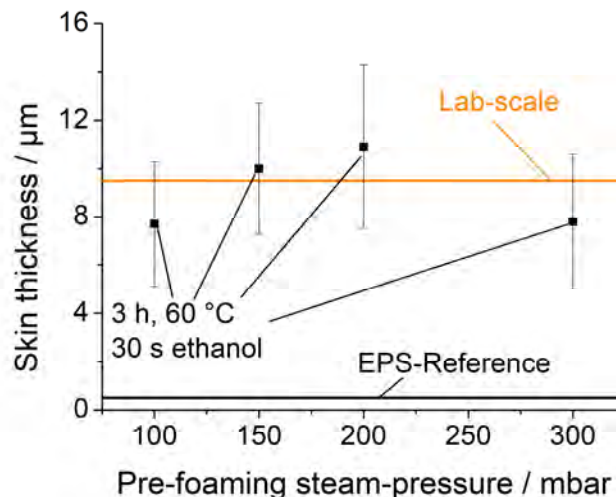


**Figure 98: Resulting bead skin thickness of 3 h, 60 °C (30 s ethanol treated) beads in dependency on the steam pressure in pre-foaming. Virgin reference EPS and the lab scale result are shown for comparison. The target bulk density for pre-foaming was  $40 \pm 3$  g/l.**

It is obvious, that the steam-pressure is a decisive factor for the formation of a solid skin around the beads. Clearly, an optimum behaviour is observed as too low and too high steam pressures lead to unsatisfactory results (thinner skin thicknesses).

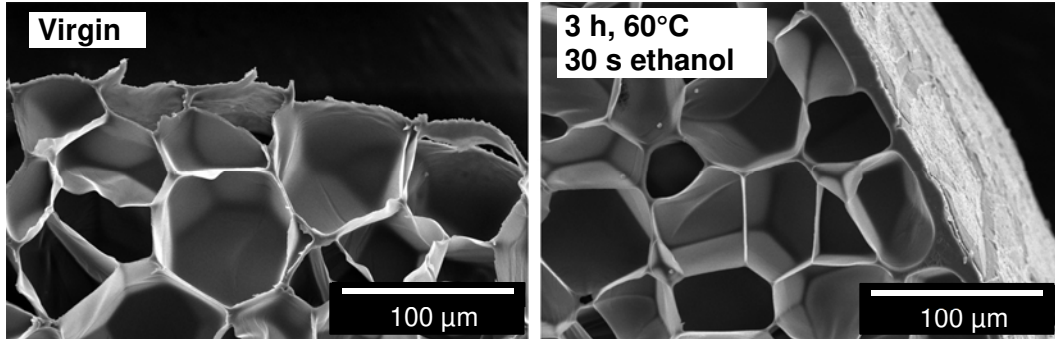


**Figure 99: SEM micrographs of cross sections of beads from industrial pre-foaming. Left: a virgin reference bead. No distinct difference between skin and cell wall thickness is found. Right: the oven stored (3 h, 60 °C) and ethanol treated (30 s) bead has a thick skin.**

The maximum skin thickness of about 11 μm was obtained at 200 mbar. This is 20 times the thickness of the skin compared to virgin EPS. Furthermore, the industrial scale approach allows similar skin thickness as compared to the lab scale method.

SEM images of cross-sections of beads pre-foamed with 100, 200 and 300 mbar are shown in Figure 100. In addition to lower skin thicknesses at a low steam pressure (100 mbar), also heavy rupture of the skin is observed. The mechanism behind this phenomenon will be discussed in the paragraph “*Effect of steam-pressure and ethanol-treatment on the foaming time*” (page 135). In contrast, the samples at 200 and 300 mbar exhibit a rather smooth skin with hardly any break-up. Only some shallow lines as a pre-stage to rupture are observed. However, the average skin thickness is significantly reduced at high pressure (300 mbar). A higher steam pressure results in enhanced energy transfer and higher temperature, which can lead to nucleation closer to the surface and thus a thinner skin.

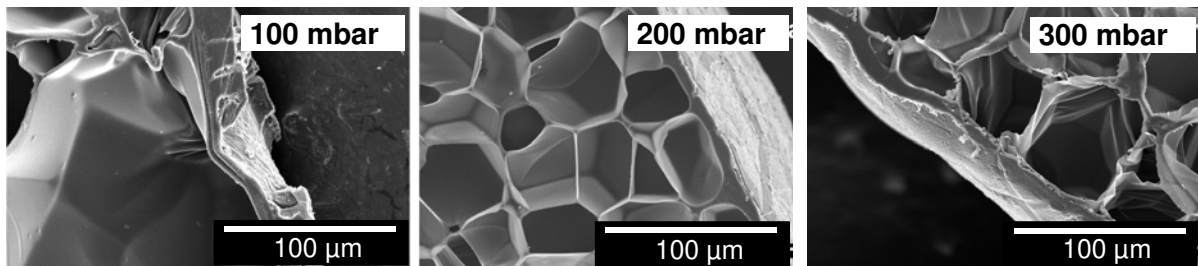


**Figure 100: SEM micrographs of cross sections of pre-expanded, pentane depleted (3 h, 60 °C) and ethanol treated (30 s) beads at steam pressures of 100, 200 and 300 mbar, respectively.**

Due to the very different nature of the pre-foaming methods in lab-scale and industrial-scale (glycerine bath vs. hot steam), the possibility exists, that the ethanol treatment is not necessary anymore for the industrial scale approach.

Therefore, also oven-stored beads, which were not treated with ethanol, were pre-foamed in industrial scale at optimum conditions (200 mbar). SEM images of cross-sections of the resulting beads can be observed in Figure 101. It can be concluded, that the plasticisation by an ethanol treatment is a necessity.

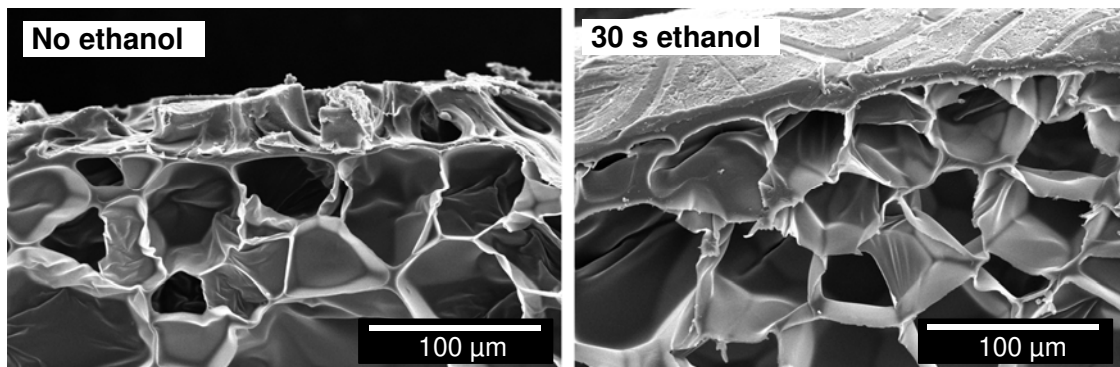


**Figure 101: SEM micrographs of cross-sections of pre-expanded, pentane depleted (3 h, 60 °C) beads without (left) and with 30 s ethanol treatment (right) foamed at 200 mbar steam pressure.**

#### Effect of steam-pressure and ethanol-treatment on the foaming time

The beads are pre-expanded until the expansion reaches the desired level (density). When reaching this set level, the steam supply is stopped to stop further expansion. The necessary steaming time for a certain expansion can give valuable information on both the effect of steam-pressure as well as ethanol treatment and thus the governing expansion mechanism. The respective steaming times for the oven-treated beads with and without ethanol treatment are given in Table 8.

**Table 8: Effect of ethanol treatment and steam pressure on the required pre-foaming time.**

Process	Time t (100 mbar) / s	Time t (200 mbar) / s
3 h, 60 °C	100	15
3 h, 60 °C, ethanol-treated	150	10-13

As expected, the pre-foaming time decreases, when the steam pressure / temperature is increased as more energy is transferred per unit time. This leads to faster foaming. It is interesting to note, that the pre-foaming time at low steam pressure (100 mbar) is significantly higher with ethanol than without. However, they are in a similar range at 200 mbar steam pressure.

These observations can be explained with the ratio of the time required for ethanol diffusion and the process time (similar to the Deborah-number in rheology). At low steam pressure, the beads only heat up slowly (much slower than the ethanol treatment of 30 s). Thus, the ethanol has enough time to diffuse out of the bead. The following vaporisation dissipates significant levels of energy, which leads to longer expansion time compared to the untreated material (150 s vs. 100 s). Thus, ethanol cannot plasticise the boundary anymore and skin rupture occurs as shown in Figure 100. In contrast, ethanol cannot diffuse out of the beads and vaporise at optimum steam pressure. Thus, it can act as plasticiser and thus accelerate the foaming compared to the untreated beads (15 s untreated vs. 10-13 s treated).

#### Validation of the final steam pressure for longer oven times

Ultimately, the developed procedure was validated for beads with even higher oven storage time (6 h vs. 3 h). The resulting skin thicknesses are plotted in Figure 102.

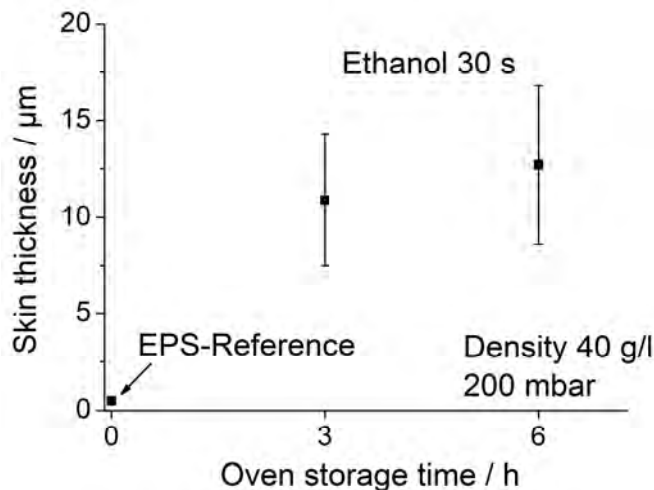


**Figure 102: Bead skin thickness at different oven times (60 °C storage). Both samples were ethanol treated (30 s) and pre-foamed with 200 mbar steam to a bulk density of  $40 \pm 3$  g/l.**

With doubled oven storage time, the skin thickness increases by 18 % from 11  $\mu\text{m}$  to almost 13  $\mu\text{m}$ . Both samples display smooth skins without rupture. Due to a lower pentane concentration, the expansion rate is reduced. Due to that, the pre-foaming time increased by a factor of 2 - 3 compared to the 3 h beads. Ultimately, it is concluded, that the developed method can be successfully transferred even to rather extended oven storage times.

As already shown in Figure 98, both lab-scale and industrial approach ultimately can result in comparable skin thicknesses. The skin thickness is even slightly higher at 150 and 200 mbar compared to lab-scale. Both surfaces display similar surface-homogeneity as shown in Figure 103.

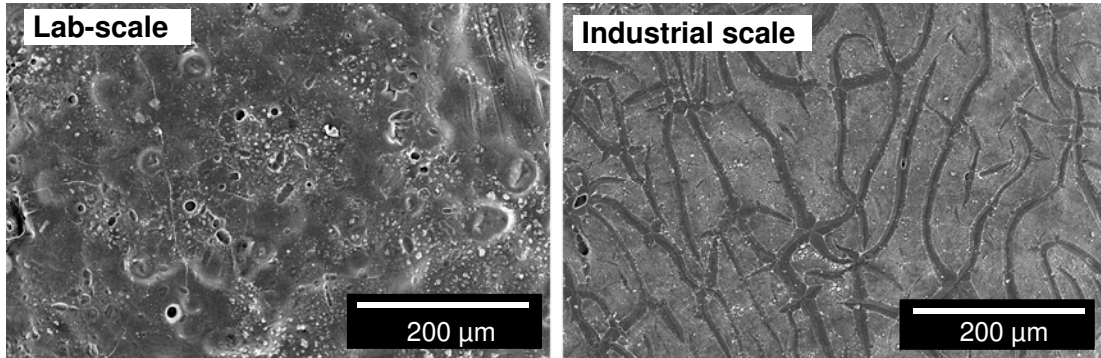


**Figure 103: Surface of a lab-scale (left) and an industrially pre-foamed bead (right). Both samples were stored at 60 °C for 3 h and treated with ethanol for 30 s.**

### 5.5.3 Summary of process to create beads with a thick skin

In order to create compact skins around EPS-beads the idea to locally deplete pentane in order to cause local suppression of foaming was followed. This local depletion was achieved by the storage of the expandable beads in a convection oven at elevated temperature below the glass transition to prevent foaming. At first, the principle was tested and a method in lab-scale was developed. It was found, that only the local depletion of pentane at the bead's surface leads to ruptured skin as the beads are foamed below or only around the glass transition temperature of pentane-depleted polystyrene.

This problem was solved by local plasticisation of the skin using ethanol. It is noteworthy, that only moderate treatment times around 30 s lead to the desired effect and smooth skins. If the treatment time is too short, not sufficient plasticisation is achieved. In contrast, if the treatment time is too long, the pentane diffusion back to the skin is promoted.

Subsequently, the lab-scale method was up-scaled to an industry-sized pre-foamer. The up-scale of the oven storage proved not to be a problem. However, the intervals between storage, ethanol treatment and pre-foaming must be sufficiently short.

Furthermore, the establishment of the pre-foaming process had to be studied in more detail. A focus was set to the effect of steam pressure, where an optimum value of 200 mbar was found. Higher or lower values lead either to a thin skin (too high pressure) or to skin rupture (too low pressure). The reason for the latter is, that the time-scale for the diffusion of ethanol out of the bead is shorter than the heating of the

beads; thus the softening effect of ethanol is removed. If the steam pressure is too high, the expansion proceeds too rapidly and enhances nucleation in the outer layer.

With the thus described method, a bead skin thickness of up to 13  $\mu\text{m}$  was achieved, which equals a relative increase by a factor of more than 20. A detailed analysis of the skin thickness in dependency of the oven storage time will be given in the following chapter.

## **5.6 Interplay between the bead skin thickness and the morphology**

With the developed process, another length scale was introduced to the bead foam. Besides, the normal length scales of the part (m - cm), beads (mm), cells (mm -  $\mu\text{m}$ ) and cell walls and struts (sub- $\mu\text{m}$ ), also the bead skin comes into play. It has a scale between the cells (600 – 60  $\mu\text{m}$ ) and the cell walls and struts (0.5 – 3  $\mu\text{m}$ ), as the bead skin can be up to 14  $\mu\text{m}$  thick. The following section will thus describe in detail, how the skin thickness varies with oven time and how it affects the morphological length scales of the beads and cells.

### **5.6.1 Analysis of the variation of the bead skin thickness by oven storage time**

According to the developed process, samples with different oven storage times and thus different bead skin thicknesses were produced and analysed. The dependency of bead skin thickness on oven storage time is plotted in Figure 104. A sigmoidal dependency of the skin thickness on oven storage time can be observed. Especially between 2 and 3 h a distinct increase in skin thickness is observed, which levels off at storage times greater than 4 h.

Although a skin thickness of about 10  $\mu\text{m}$  might not appear much, this small layer represents a significant fraction of the polymer within the whole bead. In order to emphasise this matter, the relative mass fraction in dependency on the average skin thickness was calculated and is tabulated with the experimentally obtained skin thicknesses in Table 12. As basis for the calculation, a diameter of the foamed beads of 2.2 mm (as measured) and a bead (not bulk) density of 68 g/l (40 g/l bulk density at 60 % occupied volume) was used.



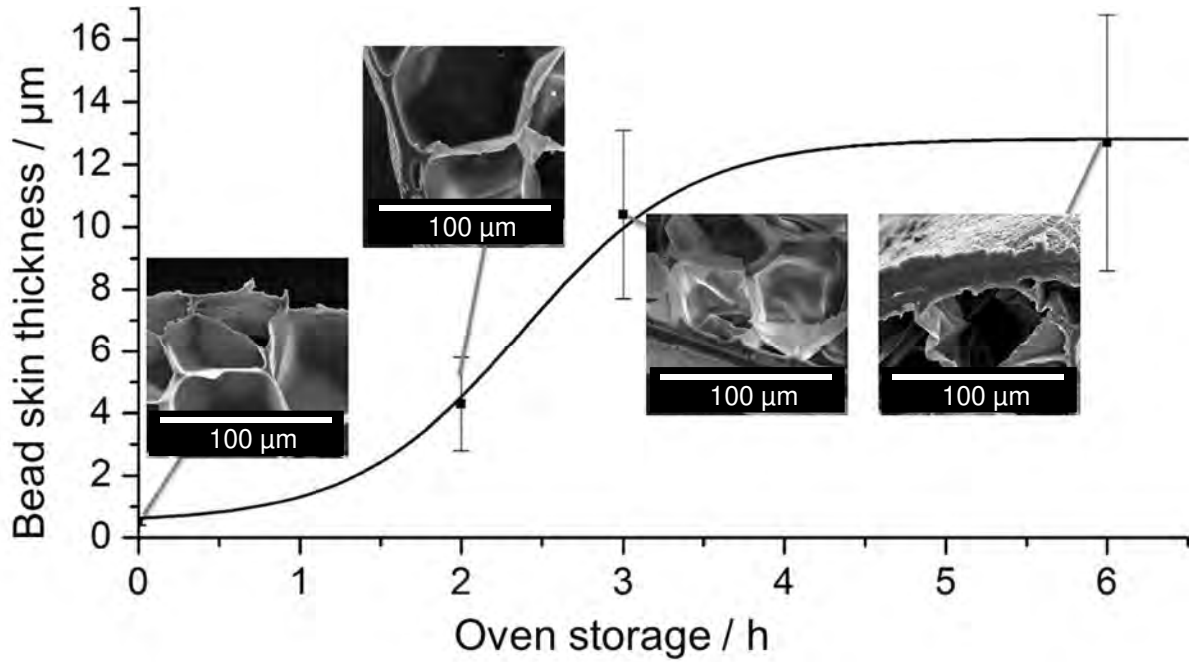


Figure 104: Dependency of the bead skin thickness on oven-storage time (industrial scale process) with representative SEM micrographs of the respective bead skins.

Beads with thin skin (*e.g.* the virgin beads) only have negligible fractions of polymer in their skin. However, when the skin thickness increases, significant fractions of the total polymer are now located in the skin. The beads with 6 h oven storage time have the majority (above 50 %) of polymer located in the skin. Also, the theoretical maximum skin thickness can be calculated, which yields a skin thickness of only 24.4  $\mu\text{m}$ . In this case, the bead assumes the structure of a Ping-Pong ball, which only consists of skin and “cell-gas” in its centre.

Table 9: skin thickness and calculated mass fraction of the skin in dependency on the oven storage time.

Duration of oven storage / h	Skin thickness / $\mu\text{m}$	Calculated mass fraction of the skin / %
0	0.5 ± 0.1	2
2	4.3 ± 1.5	18
3	10.4 ± 2.7	42
6	12.7 ± 4.1	52
Maximum theoretical value	24.4	100

Besides, the mainly technical dependency of skin thickness and oven time, another highly interesting observation was made. The skin of pentane depleted, ethanol treated and pre-foamed beads are analysed in SEM at extremely high magnifications. A number of beads exhibits nano-sized holes in the skin (*cp.* Figure 105). These holes have a diameter  $< 50$  nm. It is safe to assume, that the depth of these holes is much smaller compared to the bead skin thickness, thus their effect on the quality of fusion can be neglected. The holes must result from the diffusion and evaporation processes of ethanol in the skin layer. Possibly, this phenomenon could also be applied to produce membranes in an effective manner by simply saturating a polystyrene film and subjecting it to a flow of hot steam in order to facilitate the diffusion and evaporation of the ethanol. By an appropriate ethanol treatment time, steam pressure and steaming time also the control of the holes size appears viable.

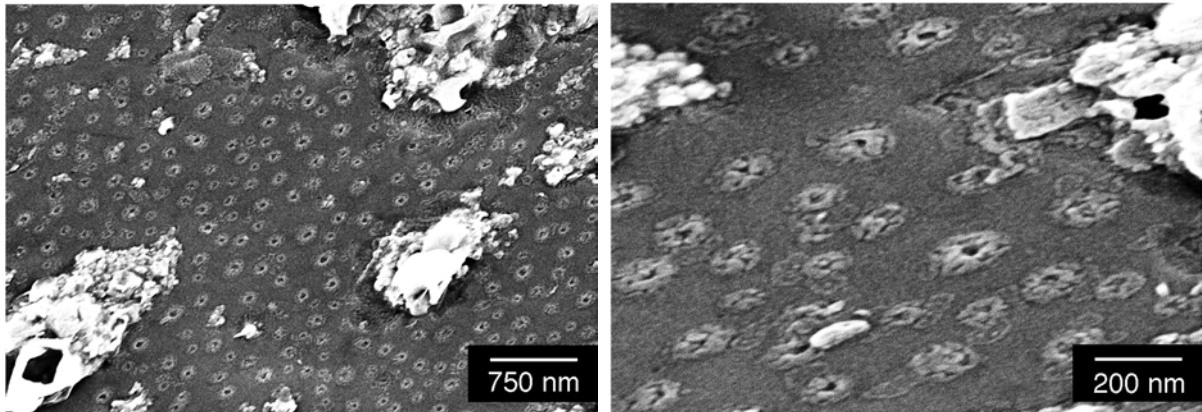


**Figure 105:** High magnification SEM micrographs of the bead skin of pre-foamed beads (3 h, 60°C, 30 s ethanol treated). Nano-sized holes in the skin can be observed, which derive from the evaporation of ethanol from the pentane depleted skin.

### **5.6.2 Effect of the thick skin on the evolution of the bead size during the processing cycle**

In the following, the evolution of the bead diameter over the process cycle (*i.e.* pre-foaming and steam-chest moulding) in dependency on oven storage time is considered. As reference and starting point, the bead size distribution of the expandable beads is given in Figure 106. A symmetrical distribution with an average value of 1.05 mm yields. Since only slight weight fractions of pentane are removed from the beads, no effect of oven storage time on the expandable bead size is expected.

When the beads are pre-expanded, the oven storage time comes into play (*cp.* Figure 106). The average diameter remains constant at about 2.2 mm, the widths of the symmetrical distributions increase with oven storage time and thus skin thickness.

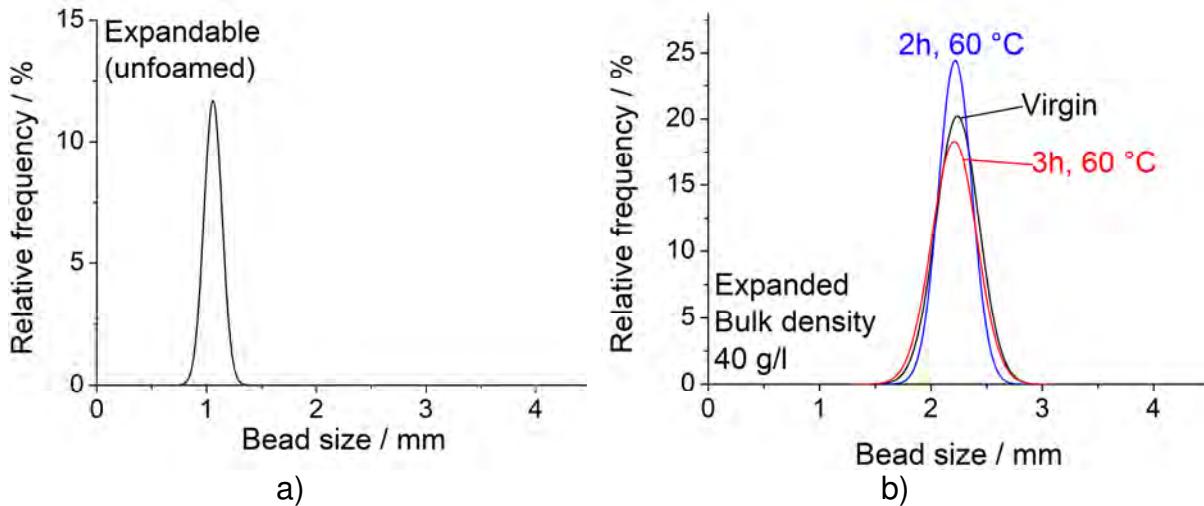


**Figure 106: Bead size distribution of a) expandable (unfoamed) and b) expanded (pre-foamed) beads.**

After steam-chest moulding the beads are not present in a spherical shape any more as the expansion is locally limited. Due to that, the beads assume polyhedral shapes (*cp.* fracture pattern in Figure 124). The equivalent diameter to a sphere is shown in Figure 107. It can be seen, that the effect of oven storage time is even more pronounced, as the distributions of the beads with a thick skin are significantly wider compared to the reference beads. However, the centres of the distributions of the three materials are rather close to each other.

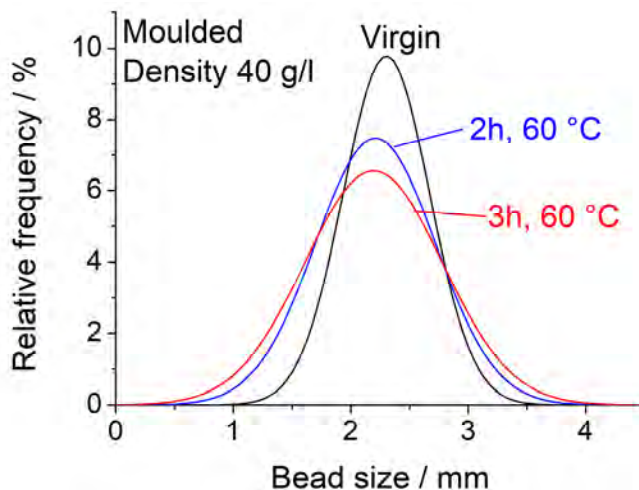


**Figure 107: Bead size distribution of the equivalent diameter after steam-chest moulding.**

From the different distributional widths, it can be hypothesised that the skin affects the fusion process of the beads. This matter will be examined in closer detail in the section on the effect of the bead skin on the mechanical properties.

### 5.6.3 Impact of a thicker skin on the cellular morphology

As the cell size has an important role on the mechanical properties, as shown before, it has to be considered closely. It is expected, that the cell size increases when the bead skin gets thicker as less material has to expand to a higher degree (constant nucleation density assumed). The distribution of the cell diameters of moulded parts from beads with three different skin thicknesses is plotted in Figure 108. As can be observed, the expectation is true indeed: thicker skins come with an increased average cell size. The measured cell sizes were also compared to the theoretically calculated ones in Table 10. The same trend between measured and calculated value is observed. However, the calculation underestimates the measured value.

**Table 10: Comparison of the experimentally determined and the calculated cell size in dependency of skin thickness.**

Oven storage / h	Skin thickness / $\mu\text{m}$	Calculated average cell size / $\mu\text{m}$	Measured average cell size / $\mu\text{m}$
0 (virgin)	0.5	42	42
2	4.3	44	49
3	10.4	50	58

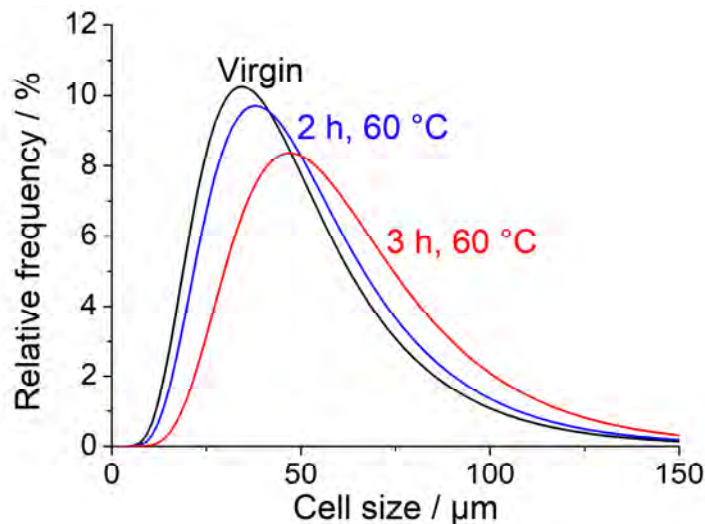


**Figure 108: Cell size distribution after steam-chest moulding (density 40 g/l).**

If the volumetric fraction of the skin and ultimately the bead skin thickness are calculated from the experimentally determined cell size, much thicker skins yield (*cp.* Table 11).

**Table 11: Comparison of the experimentally determined and the calculated skin thickness.**

Oven storage / h	Measured skin thickness / $\mu\text{m}$	Calculated skin thickness from cell size / $\mu\text{m}$
2	4.3	9.3
3	10.4	15.2

Besides the cell size, also the dimensions of the cell walls and struts are important. Therefore, SEM images of cell walls and struts are depicted in Figure 109.

No statistically significant changes of wall and strut thickness are observed in the SEM images. However, the 3 h sample appears to exhibit thinner walls. This is expected as the available polymer for foaming drastically becomes less with increasing skin thickness.

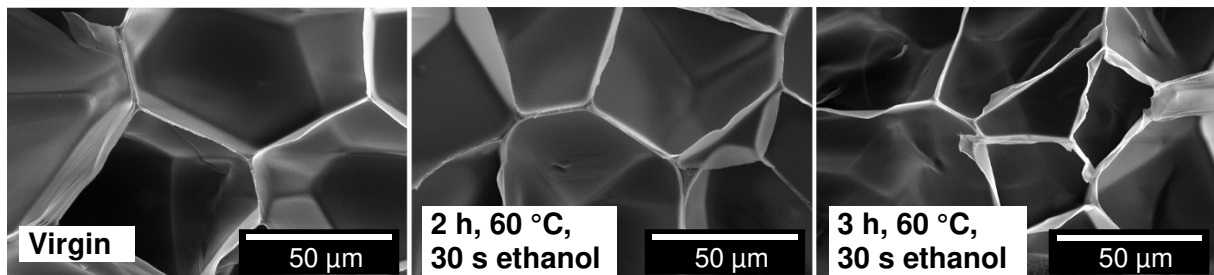


**Figure 109: SEM micrographs of the micro-morphology of virgin reference and pentane-depleted, ethanol treated beads (2 and 3 h oven storage at 60°C).**

#### 5.6.4 Evolution of the thick bead skin during steam-chest moulding

A different moulding behaviour is expected with increasing bead skin thickness. This derives from the fact, that a) a transition from nano- to micro-scale takes place (standard skin thickness compared to the novel beads) and b) the thick skin might not endure the post-expansion process during moulding without rupture as its potential for plastic deformation is decreased (as previously shown for the dependency of fracture toughness on cell size). Thus, cross sections of moulded parts were analysed regarding their fusion quality. The resulting SEM images can be observed in Figure 110.

Partial and not complete moulding can be observed in all three materials in form of porosity in the joints between the beads. During moulding, the formerly homogeneous skin of the 2 h and 3 obtained, at least partially, fluctuations in skin thickness as can be observed on Figure 110, left corner of the red circle (2h, 60 °C, 30 s ethanol). This stems from the post-expansion during moulding, as the expansion in this step is not homogeneous (low at points where beads already touch and high in the interstitial voids). Furthermore, the beads are not uniformly moulded, which can be seen from residual porosity in the bead-bead interfaces (not the interstitial volume).



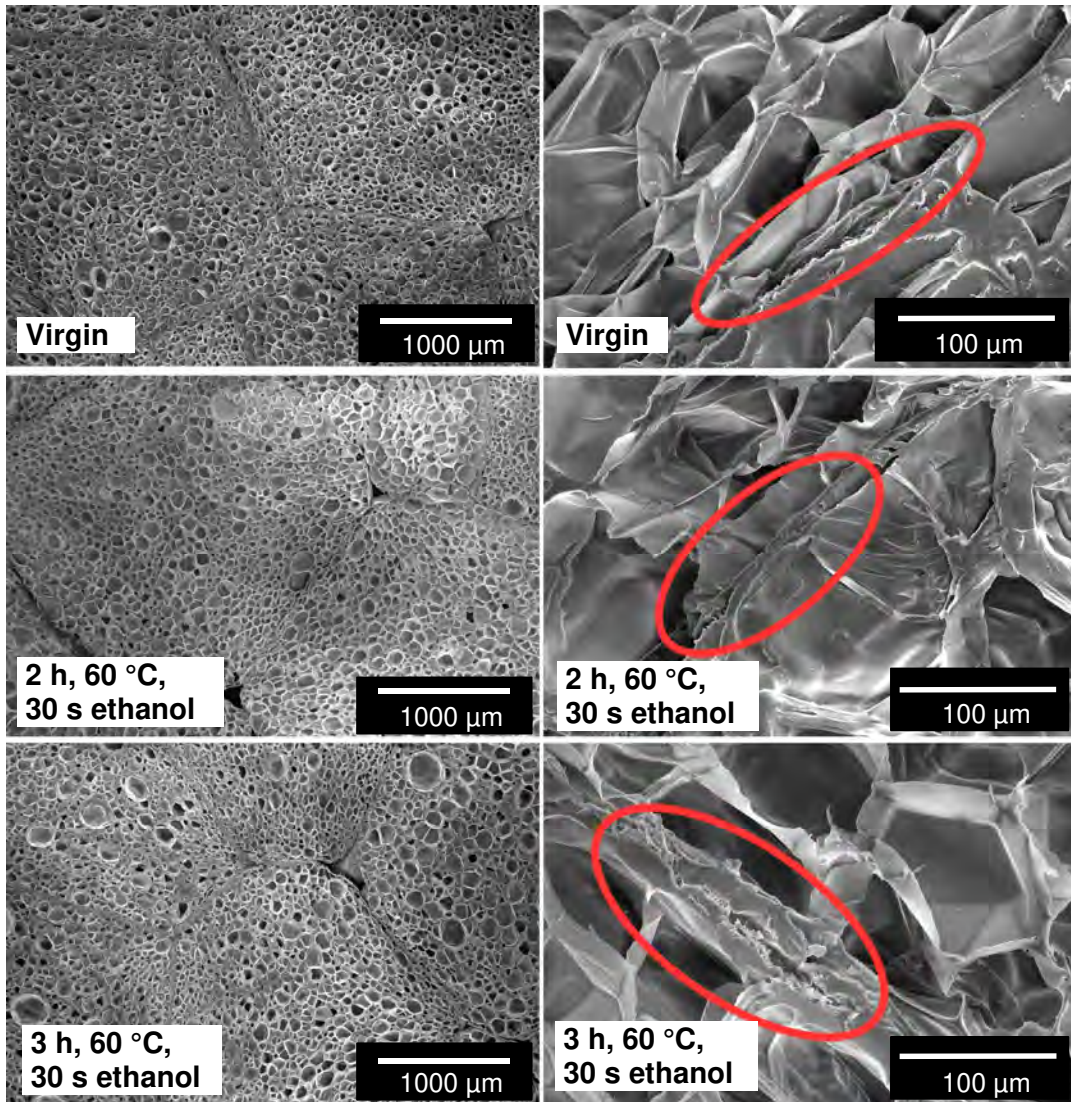


**Figure 110: SEM micrographs of cross-sections of moulded parts made of beads with different oven storage time as well as the reference virgin beads. The red circles highlight the fusion line between the beads. The same moulding conditions are applied for the three materials.**

Besides the inhomogeneous skin thickness and not complete moulding, beads with a thick skin also exhibit fracture of the skin, which is most pronounced in the interstitial volume due to high expansion as shown in Figure 111.

A similar process as in the previous experiments, where bead skins ruptured during pre-foaming, takes place. However, this is not a severe phenomenon, which greatly affects the mechanical response as will be shown later. A possible solution to prevent skin rupture is a second plasticisation of the skin. This approach will be briefly discussed in the outlook of the chapter.

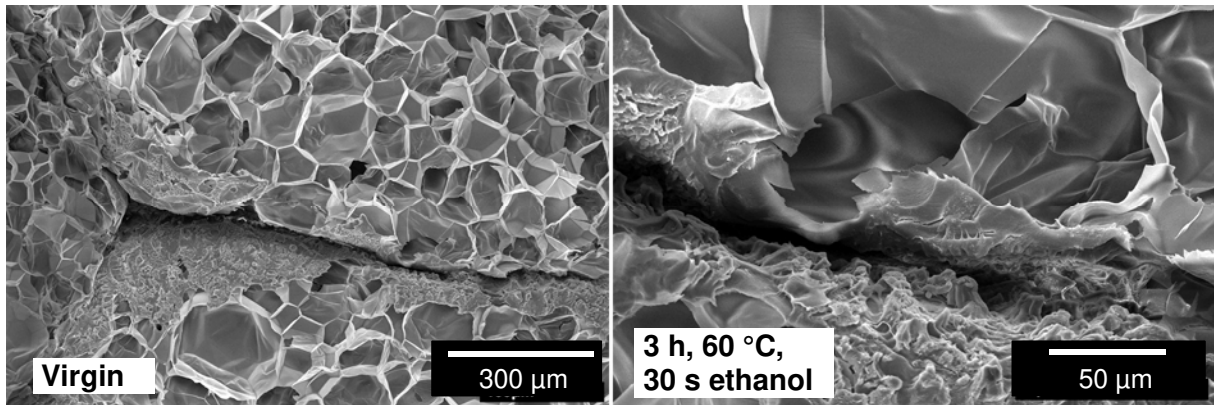


**Figure 111: SEM micrograph of interstitial volume in a moulded part made of beads with 3 h oven storage time and ethanol treatment (60 °C). The same moulding conditions are applied for the materials.**

### **5.6.5 Summary of the effect of a thick bead skin on the other morphological features**

In summary, it was shown, that the bead skin thickness can be effectively controlled by the oven storage conditions. At the same time density remains constant as it is controlled by the pre-foaming-conditions. After 3 h oven treatment at 60 °C, a skin thickness above 10 µm could be realised, which corresponds to a mass fraction of more than 40 % of the total polymer of the bead. For the given material, a maximum skin thickness of about 23 µm was calculated (similar to a Ping-Pong ball: only skin, no foam in the centre). In terms of bead morphology, no severe impact of the bead skin thickness was found. Only a minor broadening of the bead size distribution is observed. In contrast, its impact on the cells is more pronounced. With increasing skin thickness, the cell size increases since fewer cells have to expand more (constant nucleation density in the pentane-rich areas). Furthermore, the cell walls reduce in thickness.

During the moulding process, the skin deteriorates as its homogeneity decreases and rupture occurs, especially at locations with high deformation as in the interstitial volume.



## 5.7 Effect of the bead-skin thickness on the mechanical properties

In the subsequent chapter, the effect of a thick skin on the basic mechanical properties (*i.e.* compressive and flexural deformation) will be discussed at first for single beads, afterwards for moulded parts.

### 5.7.1 Effect on the compressive properties

#### 5.7.1.1 Compression of a single bead – isolated effect of the bead skin

Previously it was shown that the bead skin became inhomogeneous and even ruptured during moulding. In order to reduce the complexity of the research, this phenomenon is taken out of the equation by testing single beads with a compact and intact skin before investigating moulded samples with the shown characteristics.

Therefore, single bead compression tests were conducted in a rotational rheometer due to its high accuracy in terms of normal force and gap. Before, the compression test, each bead is analysed regarding its mass and diameter, from which the individual density is then calculated. The “stress” is calculated from the ratio of the normal force and the cross-section of the beads and the strain from the height of the gap and the cross section. Thus, the stress (at a given strain) versus density data-points are plotted. The data-points are then fitted using a second order polynomial fit as shown exemplarily in Figure 112, which shows the results for the virgin beads.

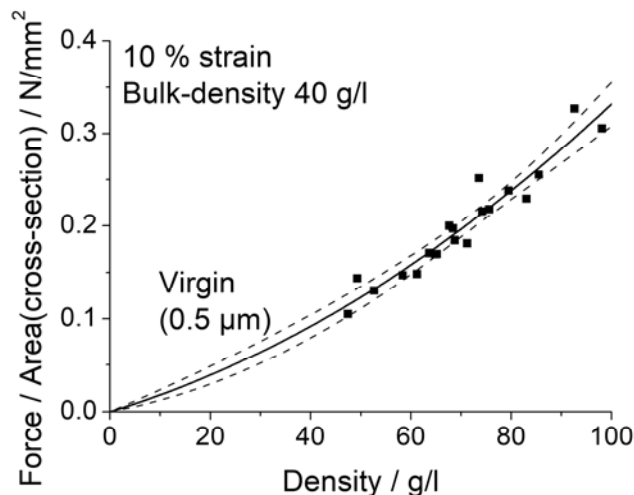


**Figure 112: Single-bead compression test of virgin pre-foamed beads: force per cross-section area at 10 % strain versus density. The dashed lines represent the 95 % confidence intervals.**

As expected, the mechanical properties scale significantly with density. Furthermore, the second order polynomial fits the data-points well. In order to keep clarity in the graphs, only the fits and the 95 % confidence bands of the reference sample are shown in Figure 113 for “strains” of 10 and 50 % (5 and 25 % *cp.* Appendix Figure 137).

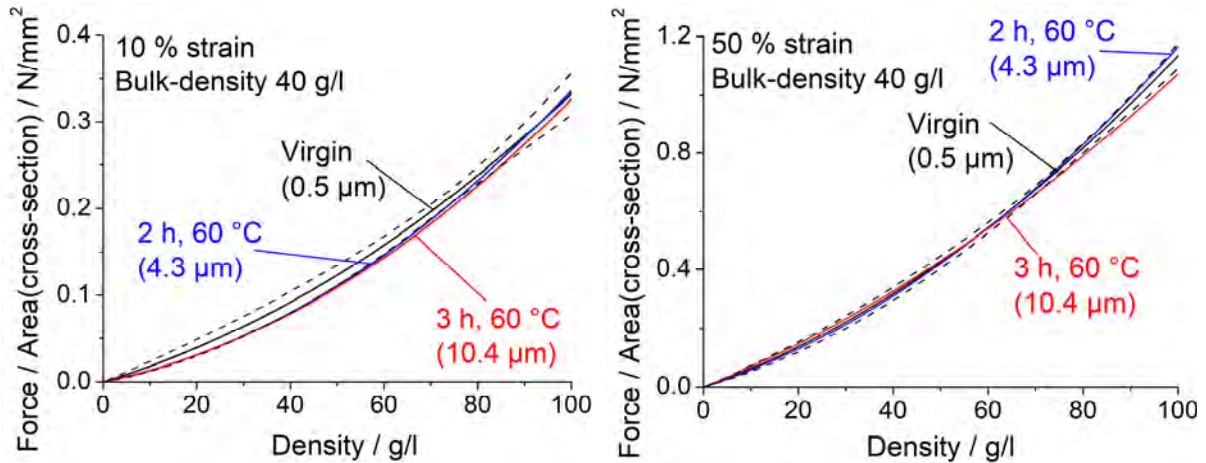


**Figure 113: Force per cross-section area as function of density in single-bead compression for 10 % and 50 % strain (cp. Appendix Figure 137 for 5 and 25 %). The dashed lines represent the 95 % confidence intervals of the virgin reference.**

From the diagrams in Figure 113 it can be concluded, that

- no significant effect of the bead skin thickness for single beads is found as the confidence bands of the fits overlap
- density is the most important factor as shown in Part I.

However, the trend that a more homogeneous distribution of the polymer within the beads is advantageous for the compressive properties in the relevant regimes of density can be observed. In the following, this finding will be studied using moulded plates.

### **5.7.1.2 Compression of moulded parts – combined effects of the skin and moulding**

Hardly any effect of a thick bead skin was observed for single beads. Thus, it is of interest, whether the same is true for moulded parts, especially since the thick skin both fractures as well as affects moulding. It is noteworthy, that the data on the bead skin thickness always refers to the skin thickness of the pre-foamed, but not yet moulded beads. Thus, a bead skin thickness of 0.5 µm represents the virgin reference beads, a skin thickness of 4.3 µm represents the pentane-depleted for 2 h at 60°C and a skin thickness of 10.4 µm stands for 3 h oven treatment. The latter two were also treated with ethanol. The resulting stress-strain-curves in compression are plotted in Figure 114.

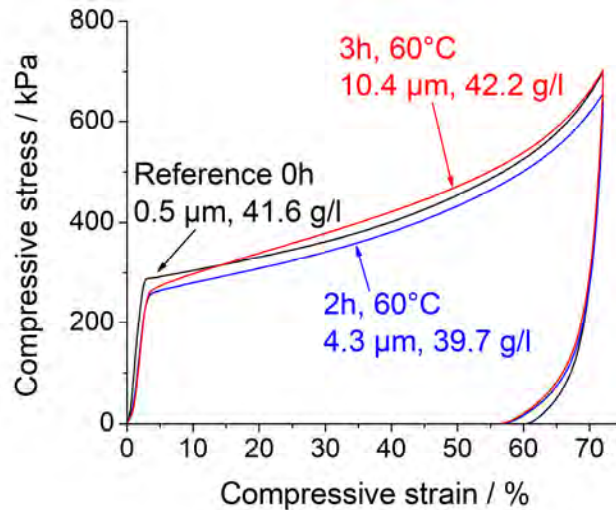


**Figure 114: Representative stress-strain-curves under compressive loading for steam-chest moulded parts with different bead skin thickness.**

It is observed, that the sample without bead skin displays better mechanics in the loading curve than the sample with 4.3  $\mu\text{m}$  skin thickness. Interestingly, the sample with thick skin shows superior properties in the region between 15 and 60 % strain as the plateau is region is steeper. Furthermore, all samples with thicker skin exhibit better recovery. Apparently, the thick skin partially prohibits cell gas from diffusing out of the beads, which then contributes to a higher restoring force.

From the stress-strain-curves the characteristic properties are evaluated. The compressive modulus as function of bead skin thickness is plotted in Figure 115. Although the density varies, no dependency of bead skin thickness on the compressive properties in the linear region is observed.

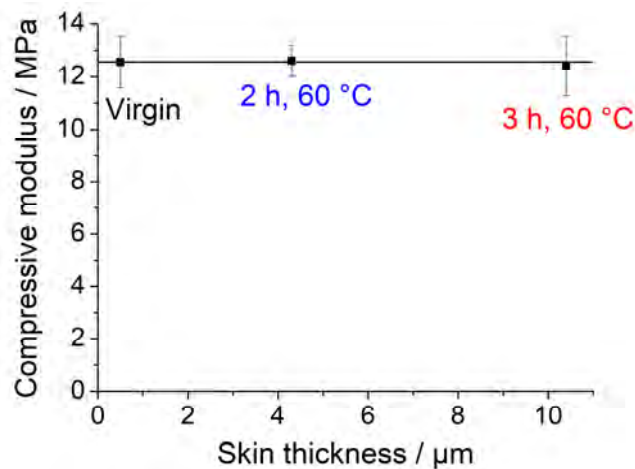


**Figure 115: Compressive modulus as function of bead skin thickness. The beads with a thicker skin were ethanol treated. The density was  $40 \pm 3$  g/l.**

Part II: Creation and exploration of a novel length scale in EPS: a thick skin around the beads

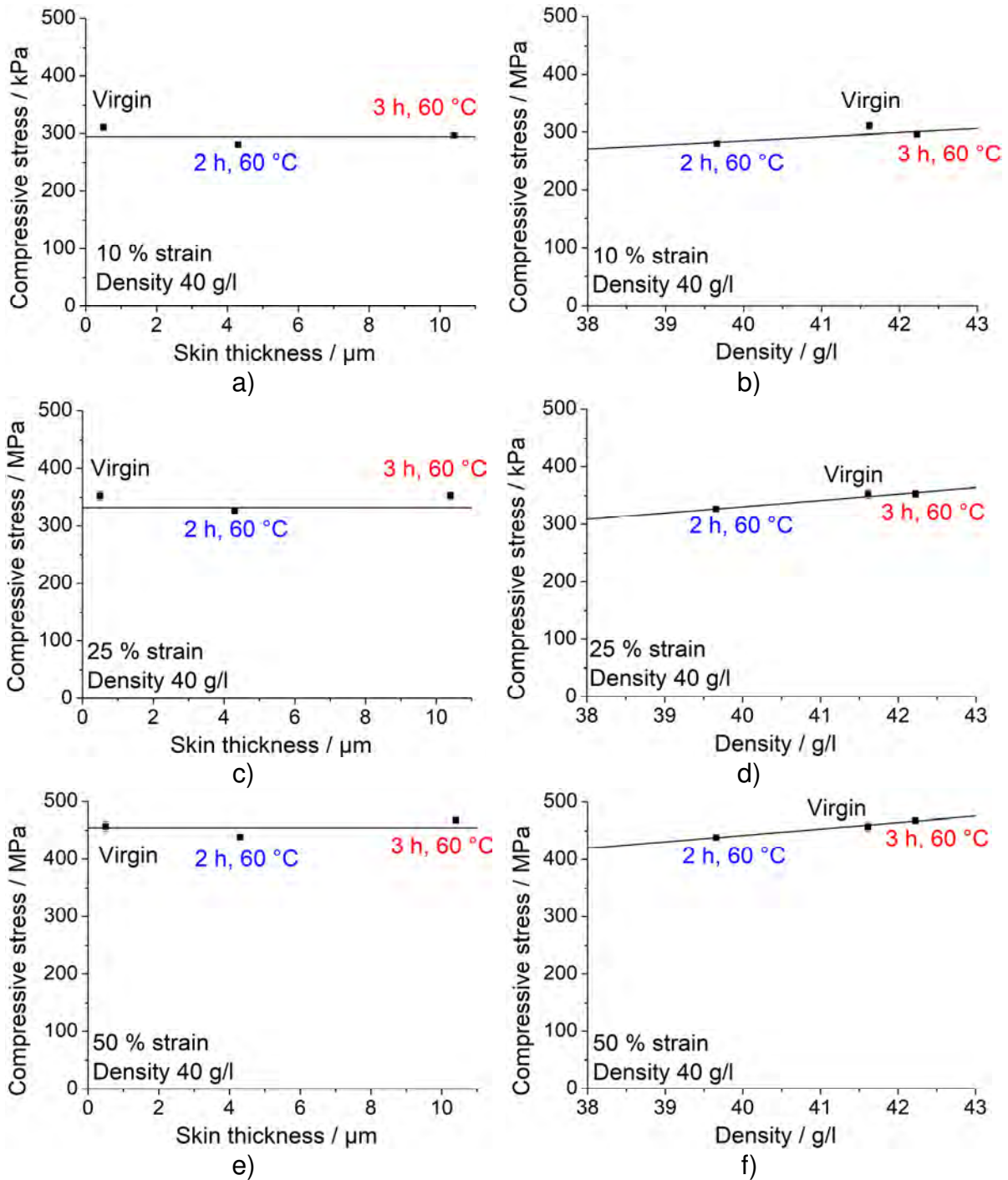


Figure 116: Characteristic compressive properties in dependency of the bead skin thickness (left column) and density (right column). The beads with a thicker skin were ethanol treated.

The strengths at different strains are plotted as function of density in Figure 116 a), c) and e). It is observed, that that the strengths at different strains exhibit a slightly U-shaped curve as function of bead skin thickness. The linear fits are constant, though. However, taking the multitude of parameters into account, definitive statements have to be drawn carefully. For example, density was already shown to be the single most important parameter for the mechanical properties of EPS. It varies in the range of 5 %

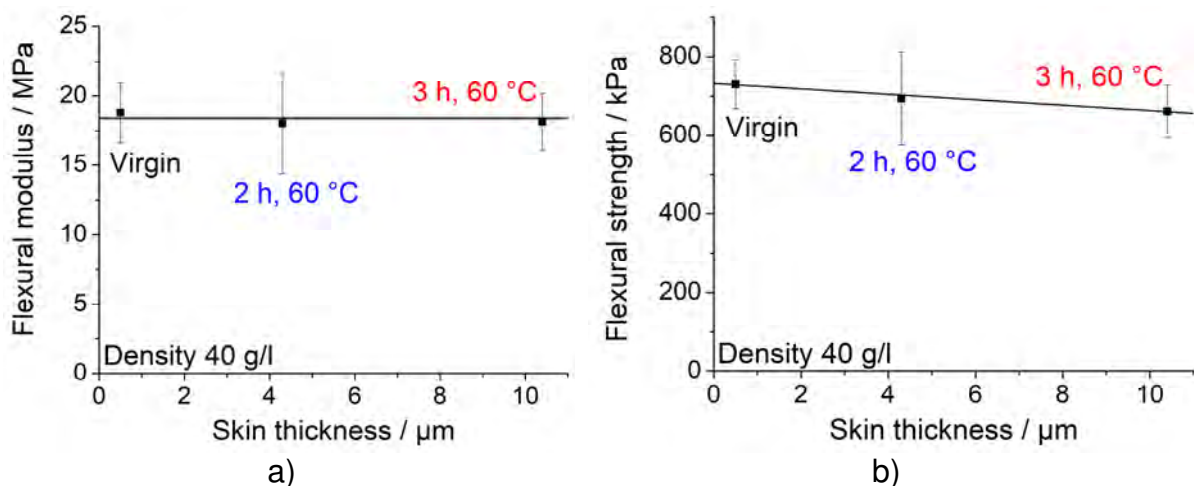
for the different moulded parts. Thus, the stress was also plotted as function of density in Figure 116 (right column) and the data points are fitted to a quadratic fit through the origin. In contrast to the modulus, the skin becomes more important at the beginning of the plateau region (10 % strain) as the sample from virgin beads (0.5  $\mu\text{m}$  skin thickness) lies significantly above the fit running through the beads with a thick skin (Figure 116 b)). However, the reference value becomes closer to the values with thick skins at higher strains above 25 % compared to the 10 % strain (*cp.* Figure 116 b) with d) and f)). This means, that the skin becomes less disadvantageous at higher strains.

In summary it can be stated, that a thicker bead skin leads to slightly deteriorated properties especially in the plateau region for both pre-expanded beads as well as moulded parts produced with them. Thus, the initial hope to create an internal sandwich effect, which positively affects the compressive properties, was not fulfilled. However, the local pentane depletion does not impede the material quality in a significant manner; thus, a stable process is demonstrated.

### 5.7.2 Effect of skin thickness on the quality of fusion

In order to study the effect of the thick skin on the fusion of the beads, bending tests are a suitable method as they also allow the study of the fracture pattern, which then can be well correlated to fusion quality.

The characteristics of the materials in flexural deformation in dependency of the bead skin thickness are plotted in Figure 117. Similar to compressive deformation, no dependency of the modulus (linear deformation) is found. However, in the non-linear region correlations are encountered as both flexural strength and maximum flexure show a dependency on the bead skin. The former is slightly reduced, whereas the latter shows a trend of increasing with skin thickness.



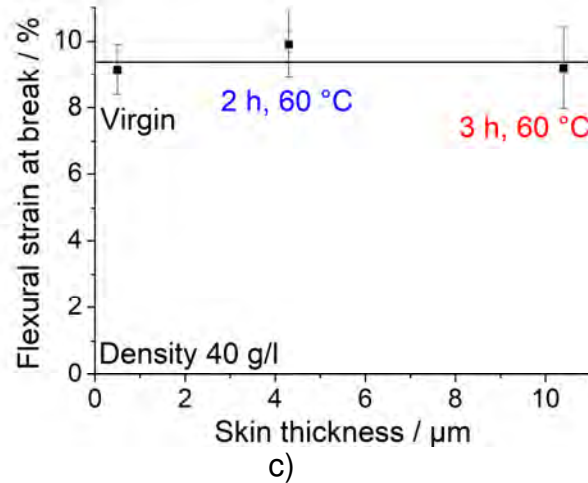
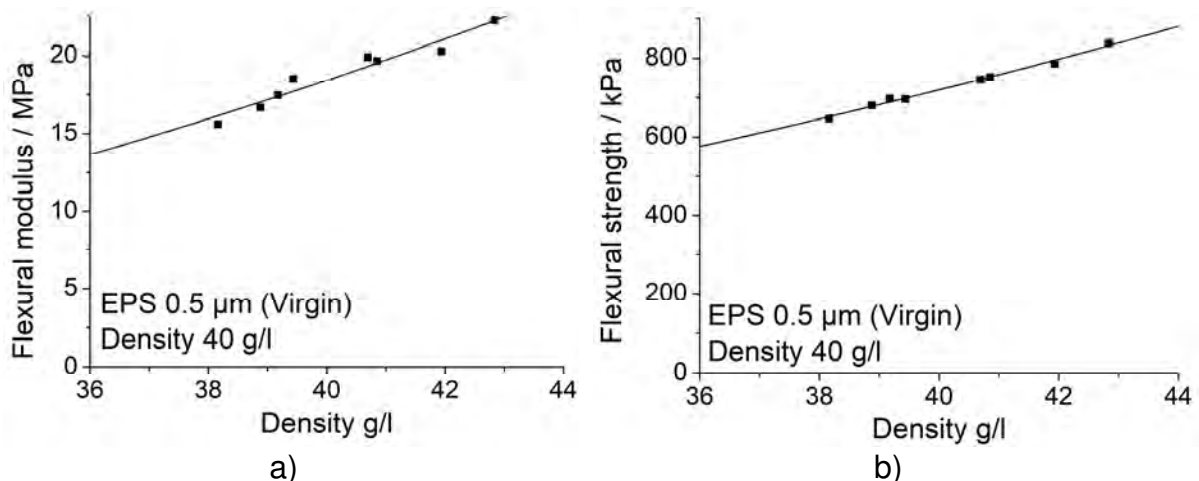


Figure 117: Characteristic properties from bending tests: a) flexural modulus, b) flexural strength and c) maximum flexural strain. The density was  $40 \pm 3$  g/l.

However, a drawback of the measurements is the pronounced experimental error of up to 20 % relative deviation for the modulus. In order to shed some light into this topic, the characteristic values of each sample were plotted as function of density in Figure 118. Here, the origin for the large errors becomes eminent: already small variations in density by  $\pm 2$  g/l at an average of 40 g/l lead to a distinct response in the mechanical properties. The respective data-points were fitted linearly through the origin. This fit is reasonable as not only compressive stresses are present in bending, but also tensile and shear stresses. A single linear fit appears suitable for the reference sample for both the modulus and strength (cp. Figure 118 a) and b)), but not for the samples with increased bead skin thickness. For these, two regions (and thus two fits) can be distinguished: a region with lower properties (Figure 118 c), d), e) and f), black fits) and a region with distinctly higher properties (Figure 118 c), d), e) and f), red fits). The relative differences between the two regions are given in the plots. They are up to 29 %.





Part II: Creation and exploration of a novel length scale in EPS: a thick skin around the beads

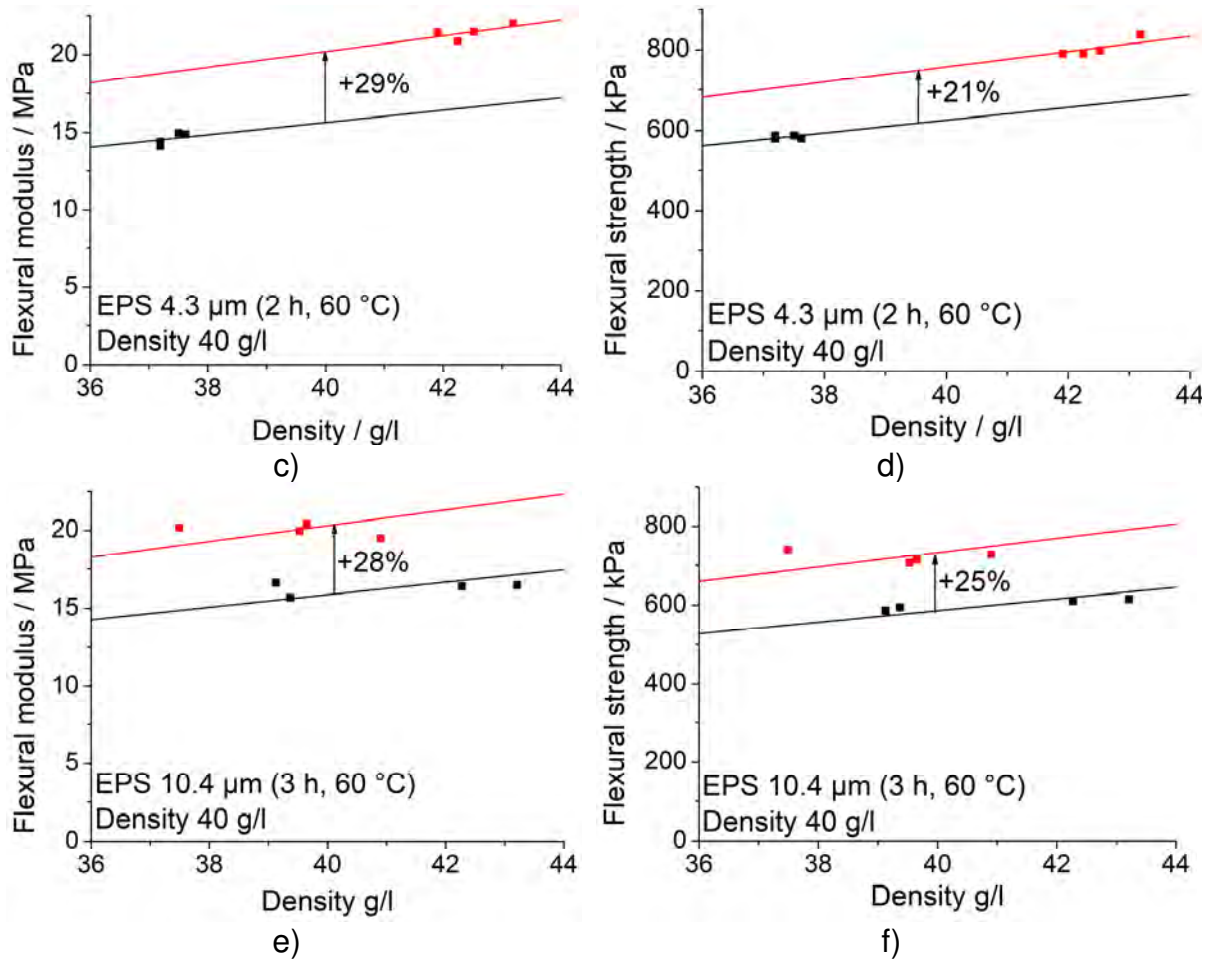


**Figure 118: Flexural modulus (left column) and flexural strength (right column) as function of density for beads with three different skin thicknesses. Two sets of samples are observed for the moulded plates from beads with a thick skin: samples with high modulus (red) and rather low modulus (black).**

When moulded parts from beads with different skin thickness are compared, again a slight deterioration of properties is observed. The data of the high-property regime is used for the comparison as it represents the potential of the material. So, the modulus decreases at a density of 43 g/l from 25 MPa (0.5 μm skin thickness) to 23.5 MPa (both 4.3 μm and 10.4 μm skin thickness) and the strength from 0.84 MPa (0.5 μm skin thickness) to 0.81 MPa (4.3 μm skin thickness) and to 0.79 MPa (10.4 μm skin thickness), respectively.

From these observations it becomes clear, that the bead skin leads to inhomogeneous fusion during moulding, as shown in Figure 110 and Figure 111. However, also macroscopic inhomogeneities within the part are expected to occur, which could be responsible for different mechanical responses within one part.



In order to explore this phenomenon, samples from a plate were categorised before mechanical testing (*cp.* Figure 119 a)). It is possible that either gravity in combination with a wider bead size distribution (small beads travel to the bottom) of the modified beads leads to a difference between the upper and the lower samples (dark blue versus light blue) or a premature closing of the steam path due to a difference between the first and second cross-steaming (difference between front and back samples, lower sketch: light blue versus yellow) is responsible. Especially the latter appears highly probable.

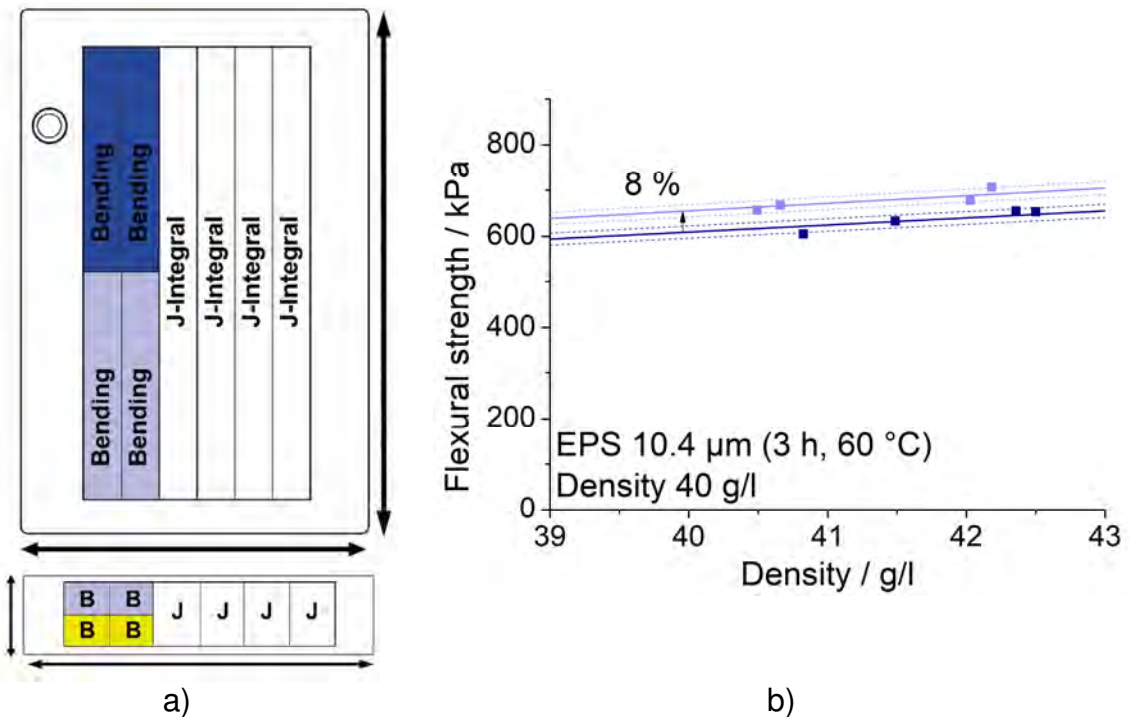


Figure 119: a) Locations of the tested samples in the moulded plate as well as b) the resulting flexural strength as function of density from a reproduction test using 10.4 µm-skin beads.

In contrast to the expectation, no dependency on the steam direction (yellow versus light blue samples) was observed (no two regimes). In contrast, two regimes from samples from a different height of the moulded plate (light blue versus dark blue) are observed (plotted in Figure 119 b)). The dotted lines represent a 90 % confidence interval. As they do not overlap, two regimes can be distinguished with higher significance. The samples with better mechanical properties (light blue) are taken from the bottom, whereas the sample with reduced properties (dark blue line) are taken from the upper part of the plate (dark blue). Thus, it is concluded, that the filling process of the beads with thicker skins is affected more by gravity or the skin itself in comparison to virgin beads (friction effects).

### 5.7.3 Fracture toughness

The fracture toughness was determined using the method of the J-Integral as shown on page 55 . In contrast to the bending test, no effect of sample height takes place as the crack propagates always in the same height relative to the moulded plate.

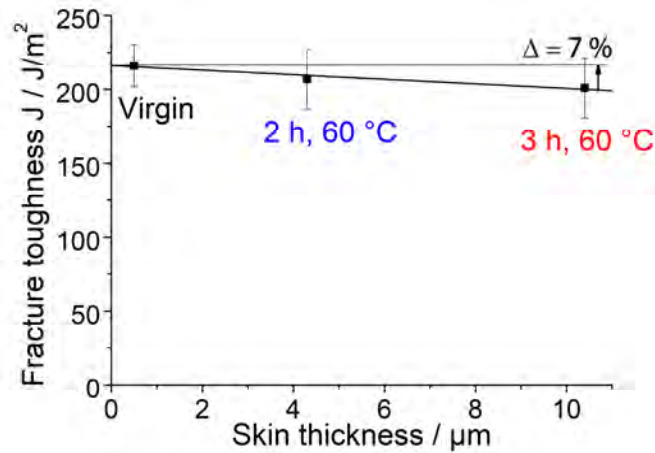
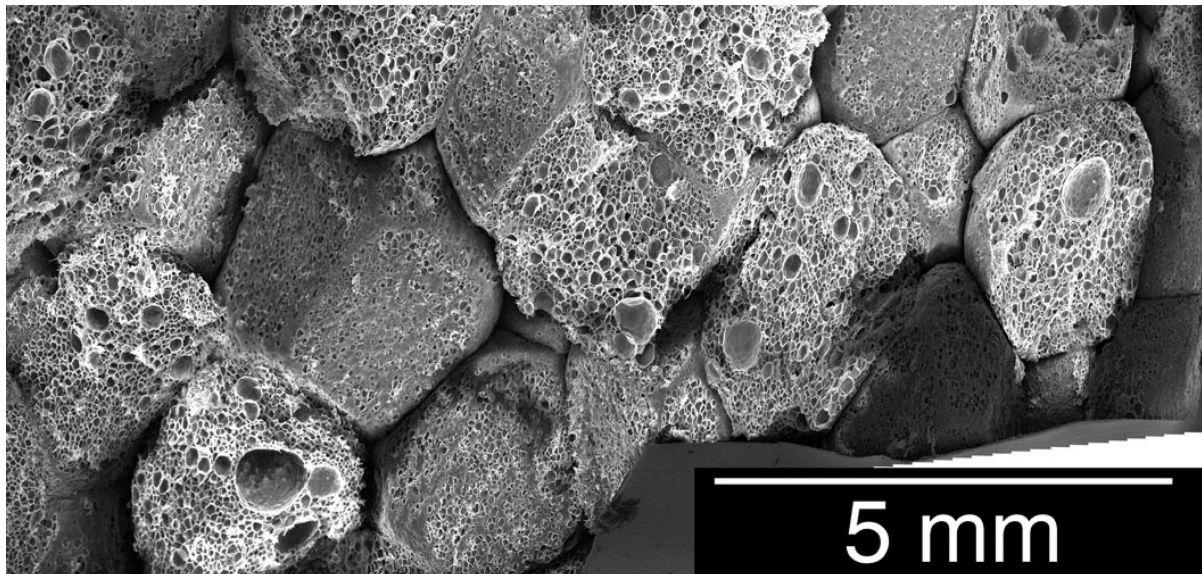


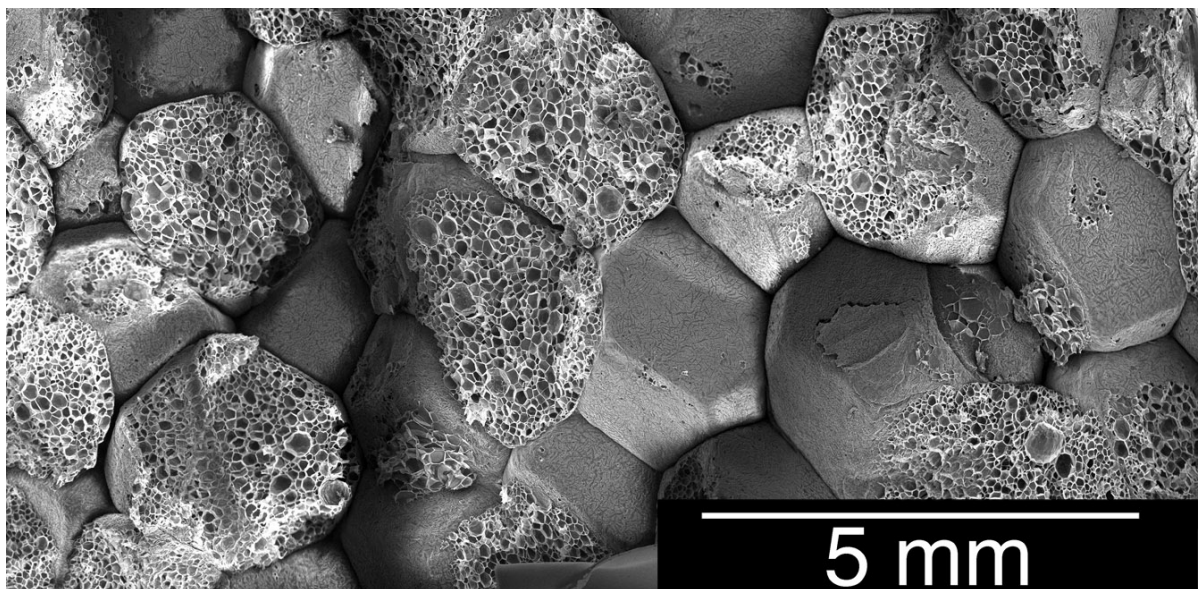
Figure 120: J-Integral in dependency on bead skin thickness. The density was  $40 \pm 3 \text{ g/l}$ .

Similar to the compressive and flexural properties, a trend of decreasing fracture toughness is observed. J decreases by 7 % for the 10  $\mu\text{m}$ -skin beads compared to the reference virgin beads. Three factors change the fracture toughness compared to the virgin beads: a) a thicker skin promoting brittle inter-bead fracture (possibly by a reduced moulding quality), b) a distinct reduction of density within the bead and c) a reduction of cell wall and strut thickness. The factors a) and b) would lead to a reduced fracture toughness, whereas c) would facilitate plastic deformation of the cell walls, thus causing higher energy dissipation and fracture toughness. Obviously, the first two effects dominate as the toughness values are reduced. However, the reduction is significantly smaller as could be expected. For example, the reduction in the foam bulk density from 40 g/l to 20 g/l for a skin of 10  $\mu\text{m}$  (about 50 % of polymer in the bead skin) would account for a reduction of fracture toughness of about 55 %. The energy dissipated for the rupture of the skin and the higher fracture toughness improve this value significantly.

In order to clarify the effect of a thicker skin on the failure mechanism, SEM panoramas of fracture surfaces were constructed. They are shown in Figure 121.



a) 0 h – Virgin reference (0.5  $\mu\text{m}$  skin)



b) 3 h oven time (10  $\mu\text{m}$  skin)

**Figure 121: Fracture surfaces of parts from beads with two different oven times: a) virgin reference beads (0 h, 0.5  $\mu\text{m}$  skin thickness) and b) beads stored at 60 °C for 3 h , (10  $\mu\text{m}$  skin thickness).**

It can be seen, that a thick skin facilitates inter-bead (interfacial) fracture. This is reasonable, since a higher stress is required to rupture a thicker skin. At constant moulding conditions then the probability of interfacial failure increases. However, when the reference sample is regarded, one observes also a rather high amount of intra-bead failure or at least failure close to the surface as the bead structure and topology can still clearly be seen for numerous beads.

It is concluded, that the promotion of inter-bead failure with thicker skin is a reason for reduced fracture properties.

#### **5.7.4 Summary on the effect of a thick bead skin on mechanical properties**

A thicker bead skin leads to deteriorated properties in general as compression, bending and the fracture toughness all exhibit a trend of decreasing with increasing skin thickness. However, the results cannot be only reduced to the skin thickness as the effect of density is even more pronounced. Interestingly, introducing a thick bead skin leads to locally inhomogeneous samples after moulding. Both the effect of gravity and the wider bead size distribution lead to the formation of two regimes of sample properties: samples located lower in the mould exhibit better properties compared to the samples at the top. In terms of fracture toughness, smaller effects as expected are found. Apparently, the bead skin dissipates more energy during fracture than expected although inter-bead fracture is promoted by thicker skins.

#### **5.8 Summary of the novel length scale of bead skin thickness**

Besides cell size and bead size, a compact skin around beads is another possible morphological feature of bead foams. However, it is completely unstudied in current scientific literature. Not even its formation is described. However, it could promote a kind of internal sandwich effect in a moulded part.

Thus, the work aimed to create homogeneous, thick skins around EPS beads with a thickness at least one order of magnitude higher than “standard” beads. Furthermore, the developed method is aimed to be suitable also for industrial scale pre-foamers.

The basic idea to create this feature is a local depletion of pentane below a critical concentration required for foaming. This is done by storage in a convection oven below, but close to, the glass transition temperature of expandable EPS beads before pre-foaming. By variation of oven time, the thickness of the pentane depleted layer can be controlled and thus also the resulting skin thickness. Ultimately, beads with a homogeneous skin thickness 20 times thicker than “standard” beads could be created. However, a plasticisation step by washing the beads in ethanol directly before pre-foaming is necessary to prevent the rupture of the pentane-depleted layer. Also, the up-scale to industrial pre-foamers was conducted successfully. The parameter of steam-pressure proved to be crucial to achieve a skin without rupture.

The subsequent morphological analysis showed, that skin with a thickness up to 13  $\mu\text{m}$  could be realised. This corresponds to about 50 % of the total polymer of a bead being located within the skin. Interestingly, the plasticisation by a treatment with ethanol led to nano-sizes holes in the skin of some particles. This finding could be used for

the creation of membranes. In terms of bead size, the introduction of a thick bead skin broadened the bead size distribution and led to an increased cell size as fewer cells have to expand more for a constant bead density. In contrast, the wall and strut thickness decreases according to mathematical models. Unfortunately, the thick bead skin partially ruptured during moulding, especially in regions with high strains as the interstitial volume (*e.g.* the macro-porosity).

Initially, it was desired to achieve improved mechanical properties by the introduction of a thick skin around foamed beads *via* an internal sandwich effect. Unfortunately, this hope could not be fulfilled, as a slight deterioration of properties was observed with thicker skins. Furthermore, the mechanical properties display a more pronounced dependency on foam density than skin thickness. Also, the homogeneity of moulded parts suffered, when beads with thick skins were steam-chest moulded. This was attributed to the broader bead size distribution, which promotes a “demixing” of bead with different sizes during filling.

### **5.9 An experimental outlook: Improvement of the steam-chest moulding process by a second ethanol treatment**

As previously shown, the beads exhibited skin rupture during steam-chest moulding. In order to prevent this effect, the beads were treated with ethanol a second time just before moulding. However, this requires the usage of another mould, which can be filled manually (hereafter titled “mould 2”). In order to obtain comparable results, the reference mould of the previous experiment was used as well (hereafter titled “mould 1”). This is necessary, as a new batch of beads was used, which could have a slightly different pentane content and thus expansion behaviour. For the trials with “mould 2”, two types of beads (virgin and 2 h oven time) and with or without the second ethanol treatment were conducted. The surfaces of the moulded beads from these trials are shown in Figure 122. From these pictures, classifications of the surface quality were made. Thus, beads with a “rough” surface exhibit a significant degree of rupture (*e.g.*

Figure 122 a), b) and e)), whereas a “medium” surface rather exhibits some holes without or little surface break-up (*e.g.* Figure 122 (c)). In contrast, beads with a smooth surface exhibit neither or only minimum break-up (*e.g.* Figure 122 (e) and (f)).

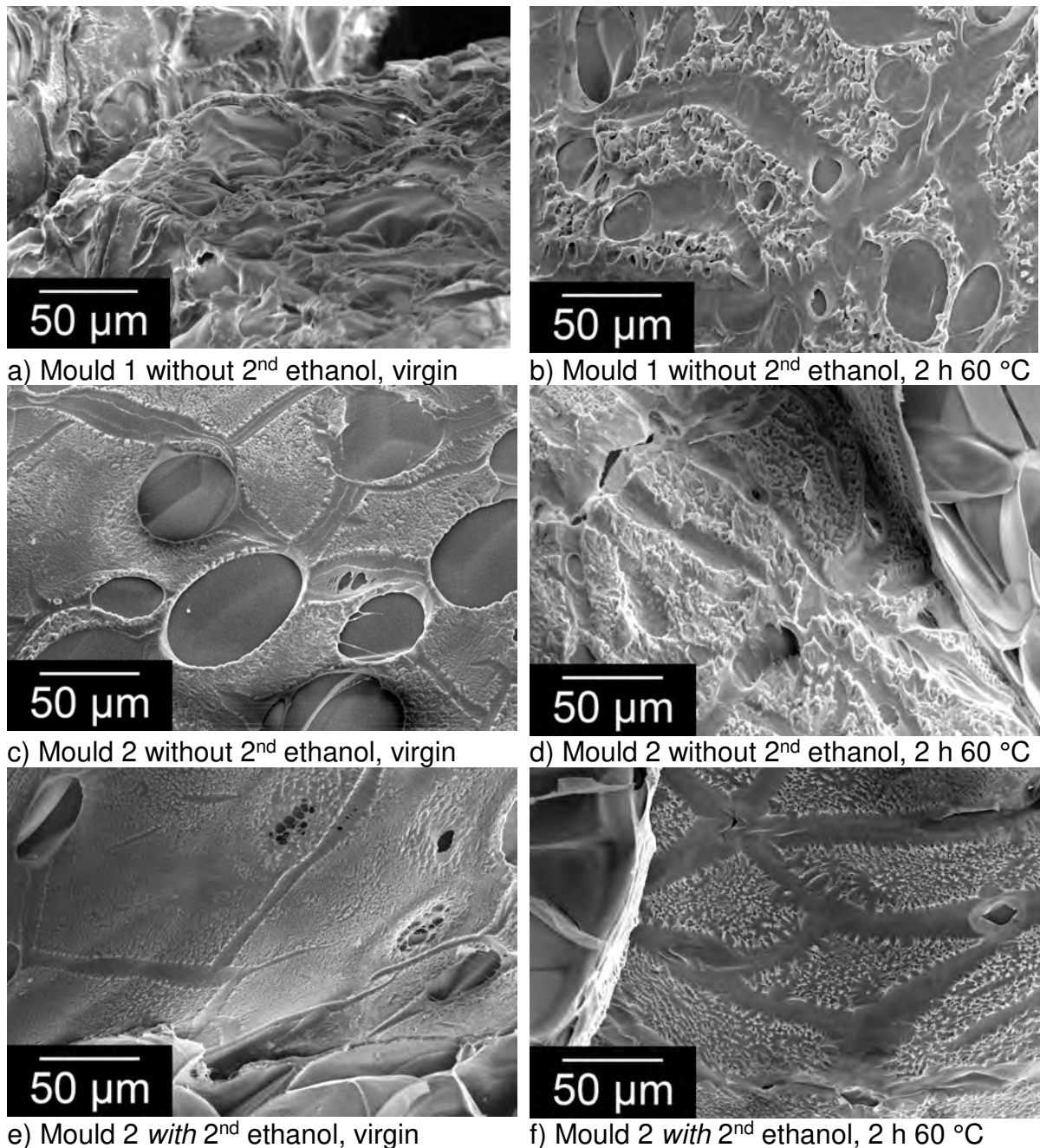


**Figure 122: Surface of the moulded beads at the interstitial volume between beads (macro-porosity). This represents the areas with the highest expansion of the bead skin (worst case).**

The results of all trials (mould 1 and 2, 0 to 4 h oven storage, with and without ethanol treatment of the foamed beads) are tabulated in Table 12. It can be seen, that generally better surfaces can be achieved in mould 2. However, the surface quality is still not completely satisfactory without a second ethanol treatment of the beads. In contrast, the second ethanol treatment leads to smooth surfaces independently of oven storage time. Thus, the idea of a second plasticisation step was successfully validated.



**Table 12: Effect of the oven storage time, mould and ethanol treatment of the foamed beads on the surface roughness of the moulded beads after steam-chest moulding (SCM).**

Oven storage time	Reference (mould 1, no ethanol)	Mould 2 No ethanol	Mould 2 Ethanol treatment of the foamed beads before moulding
0	Rough	Medium	Smooth
1	Medium	Medium	Smooth
2	Rough	Rough	Smooth
3	Rough	Medium	Medium
4	Rough	Rough	Smooth

The resulting density and flexural strengths as function of oven time for the three materials are plotted in Figure 123. The density of the ethanol treated pre-foamed beads with a smooth skin is slightly higher compared to the untreated foamed beads. It is interesting to note, that at low oven storage time (0 h) for mould the density significantly lower compared to the untreated beads (30 vs. 40 g/l). However, the mechanical properties in terms of strength are slightly better.

That means that the second ethanol treatment has the potential to significantly improve the mechanics in bending. Furthermore, the mould has a pronounced effect on the mechanics, as mould 1 delivers significantly lower mechanical properties compared to mould 2.

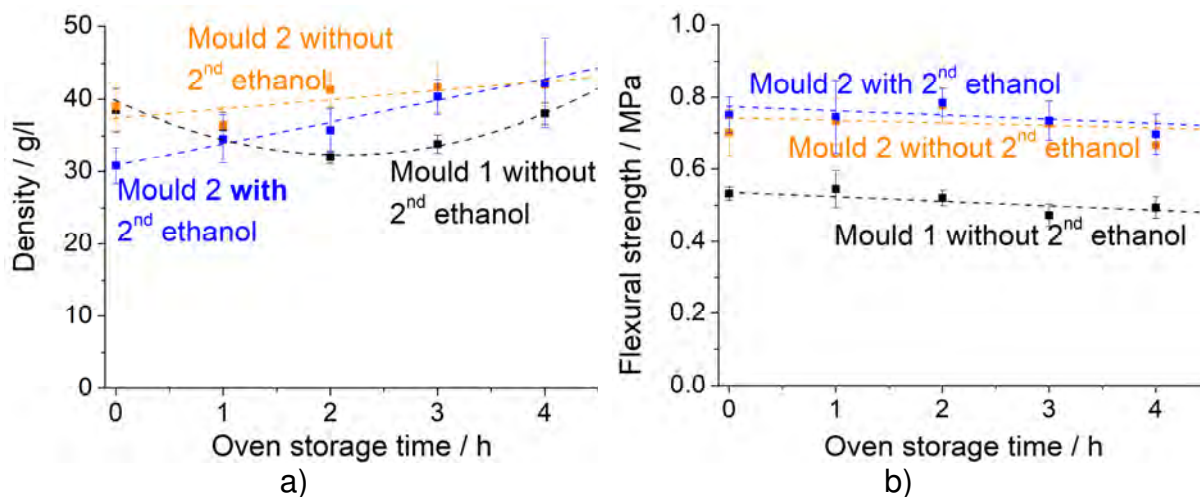


**Figure 123: a) Resulting density and b) flexural strength as function of oven time for the three different moulding procedures.**



Also, the fracture surfaces of ethanol treated pre-foamed beads were compared to non-treated pre-foamed beads (*cp.* Figure 121). They are shown in Figure 124. For the virgin beads an ethanol treatment before moulding appears beneficial as intra-bead fracture is promoted. In contrast, no improvement of the fracture behaviour is observed for the samples with a thicker bead skin as similar fractions of inter-bead fracture occur. These findings agree directly to the mechanical properties in bending as presented just before.

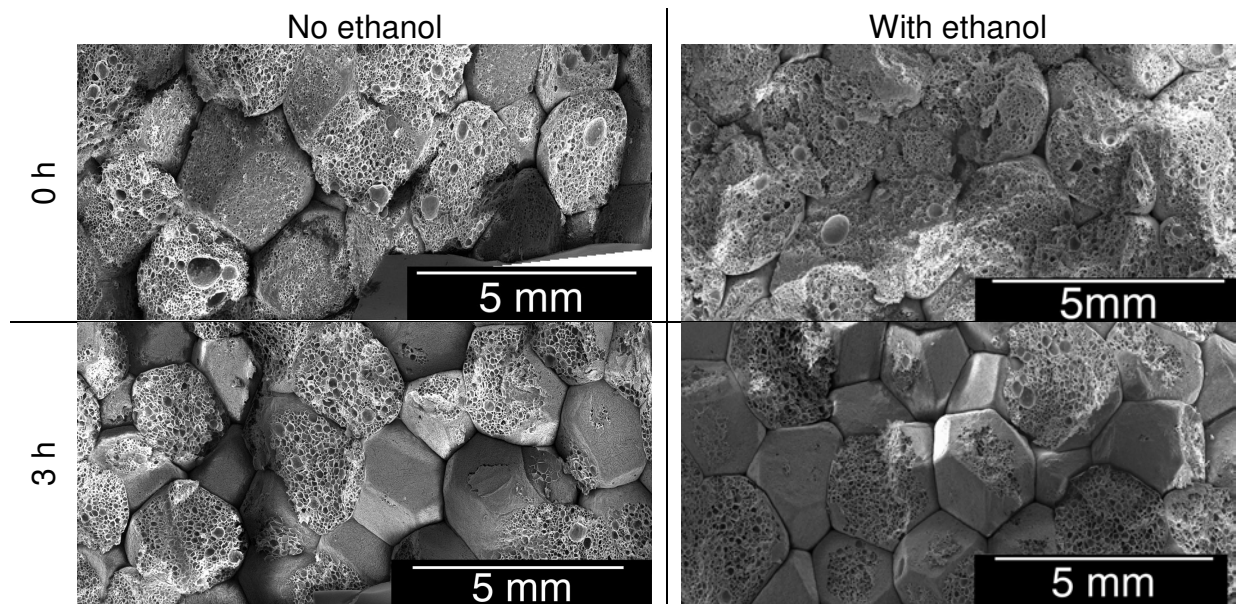


**Figure 124: Fracture surfaces of beads with different skin thickness as well as with and without an ethanol-treatment of the pre-foamed beads before moulding (mould 2).**

However, an ethanol treatment before moulding can not only be beneficial for the surface quality and mechanics, but also other benefits might be achievable with this method, which are deemed to be highly relevant for beads in general or bead foams made of technical thermoplastics. For example, a reduction of steaming time and pressure is possible due to a faster softening surface and polymer chains with higher mobility (similar to the already shown effect on pre-foaming). Thus, energy savings are possible and by that monetary savings as well. Furthermore, this approach could enable the mouldability of high-temperature thermoplastics (as PEI) since the glass transition temperature is reduced significantly due to local plasticisation.

## 6 Summary

Expandable polystyrene, EPS, is a widely used foam material. It accounts for one quarter of the current foam production in terms of volume. Although it has been used for decades, it remains a rather under-studied material in the scientific literature as many knowledge gaps could be identified. For example, the effect of the foam morphology on the mechanical properties of EPS has never been studied in literature to the best knowledge of the author.

Thus, it was the aim of this study to fill these gaps in knowledge by investigating the structure-property relationships of EPS. Therefore, three different polystyrene-based bead foams were investigated, namely EPS made by suspension polymerisation in the presence of pentane (benchmark material), EPS made by extrusion and E-Por (PS/PE-blend bead foam). These materials possess different morphological properties in terms of cell size, bead size and density.

It was shown, that bead foams possess a complex multi-scale morphology. The moulded parts were found to be very homogeneous in the lateral dimension for both cell size and density. A variation of cell size at constant density naturally leads to a change in wall and strut thickness for both EPS and E-Por. Interestingly, the walls of EPS are thinner in comparison to E-Por at the same density and vice versa for the struts. This affects both the mechanics and thermal conductivity. When the density is increased, then both cell and bead size become smaller, which also causes a change in the micro-morphology of both EPS and E-Por. The cell size of EPS from suspension polymerisation is significantly smaller compared to EPS produced in extrusion with under-water pelletisation.

In terms of the fundamental mechanics, smaller cells lead to improved mechanical properties for EPS, which originates from a higher orientation of the polymer chains and a higher potential for annealing with smaller cells. In contrast, E-Por does not exhibit a correlation between the mechanical properties and cell size. In contrast, the domain-size of polystyrene in E-Por is governed by the blend morphology, which did not show a systematic variation with cell size for the studied materials. In terms of bead size, larger beads show better mechanical properties due to better energy transfer during steam-chest moulding. However, a negative effect is found in large beads (> 5mm) due to the increasing presence and size of macro-voids.

In general, density has the most pronounced influence on the mechanical properties, which shows a power-law dependency on modulus and strength. The investigation of the micro-deformation mechanisms proved that deformation is highly localised in the centre of the beads and that macro-porosity between the beads acts as a weak site and stress-concentrator. This can be seen from locally increased deformation in the surroundings of macro-porosity. The effect of strain rate is significant for both EPS and E-Por. However, increased strain rate causes more distinct changes in the regime of non-linear deformation compared to the linear regime.

The fracture toughness was investigated by means of non-linear fracture mechanics, namely the J-integral. The cell size proved to have a distinct effect for EPS, but no significant effect for E-Por. This was attributed to different toughening mechanisms in both materials. The characteristic length scale for the toughness of EPS is the thickness of the cell walls and struts. Smaller cells with thinner cell walls and struts allow increased plastic deformation and thereby higher toughness. In contrast to EPS, E-Por is inherently tougher than EPS due to a reduction of the domain size of polystyrene by the introduction of polyethylene. The bead size proved to show an optimum of toughness for bead sizes between 3 and 3.5 mm. For both very small and very large cells the crack tends to propagate more along the bead boundaries, which is caused by a deterioration of moulding quality for beads that are too small (bead diameter  $< 2.5 - 3$  mm) as well as a higher amount of macro-porosity with larger beads (bead diameter  $> 4 - 4.5$  mm). As expected, density is the most important parameter for the fracture toughness of bead foams. Increased density leads to improved toughness as the rupture strength increases with higher density.

The morphological changes have a profound impact on the thermal transport properties as well. It is observed, that smaller cells are highly beneficial for the insulating capabilities of the foam, since they help to reduce the potency of infrared radiation. However, this is only true if the cell walls and struts are not too thin (below the wavelength of the IR radiation), thereby showing possible challenges for nano-cellular foams. In this frame, cells smaller than  $50 \mu\text{m}$  do not appear beneficial, if no modifications like IR-reflecting graphite particles as in grey EPS are introduced. A change of bead size does not affect the thermal transport directly.

In contrast, density affects the thermal conductivity distinctly. The thermal conductivity as function of density exhibits a U-shaped behaviour. Three regimes of thermal conductivity are identified, a fourth becomes apparent when the solid and gaseous contribution are extrapolated: 1) a pronounced decrease in thermal conductivity with decreasing density at low density ( $< 20$  g/l) strongly affected by radiative heat transfer, 2) an optimum at around 40 g/l, which should be aimed at in insulation applications, and 3) a slow increase in thermal conductivity with increasing density at high density ( $> 80$  g/l), which is still dominated by conduction through the gas. In regime 4), at a density above 180 g/l, thermal conductivity is ultimately dominated by conduction through the polymeric matrix. In the case of E-Por, the introduction of PE leads to reduced insulation capabilities compared to EPS due to the higher thermal conductivity of PE and thinner cell struts.

Besides cell size and bead size, a compact skin around the beads is another possible morphological feature of bead foams. It was expected to introduce an internal sandwich-effect due to the thick compact skin around the beads. The underlying idea to create this feature is a local depletion of pentane below the critical concentration required for foaming. This depleted layer is not foaming during pre-expansion of the beads and only stretched out. The size of the depleted layer and thereby the thickness of the bead skin can be controlled by the storage at elevated temperature. Ultimately, a method was developed to create beads with a homogeneous thickness more than 20 times thicker than conventional beads. Furthermore, the up-scale to an industrial pre-foamer was conducted successfully, showing that an appropriate steam-pressure is of utmost importance. The subsequent morphological analysis showed, that bead skins with a thickness up to 13  $\mu\text{m}$  could be realised. This corresponds to about 50 % of the total polymer of a bead being located within the skin. A thicker bead skin leads to an increased cell size and a lower wall and strut thickness. In the studies, the skin ruptured during moulding, especially in regions with high strains as the interstitial volume (*e.g.* the macro-porosity). Moreover, the expected internal sandwich was not observed, as a very slight deterioration of properties was found in foams with thicker skins. Overall, it was found that the mechanical properties display a more pronounced dependency on foam density than skin thickness.

In summary, it can be seen that the polystyrene-based bead foams need to be tailored for their respective application in terms of density and morphology, which is especially true for the important application as insulation material.

## 7 Outlook

### Local description of the free volume in the micro-morphological scale

As in every scientific work, questions are not only answered, but also new ones are raised. This is true for the effect of cell size on the mechanical properties of PS-based bead foams, which was studied in a macroscopic manner. Therefore, more sophisticated methods to study the local properties of cell walls and struts are required. For example, positron annihilation lifetime spectroscopy could give valuable information of the free volume as function of the thickness coordinate of a cell wall for different cell sizes. Thus, the increased plasticity with decreasing cell size could also be studied.

It is possible, that foams with very small cells possess a significant fraction of more ductile material at the surface of the cell walls. In this frame, micro-mechanical studies using AFM are a promising approach as they allow the determination of the mechanical properties as function of the thickness coordinate of a cell wall or strut.

### Further testing

In terms of testing methods, the topic of fatigue in EPS was not presented in the frame of this work, as it would exceed the scope of this study. Furthermore, the effect of ageing on the mechanical properties of EPS and thermoplastic foams in general is interesting, but remains unstudied in literature. Due to the foam structure with an inherently large inner surface, the ageing rate is expected to be significantly higher compared to compact samples. Also, different ageing mechanisms are possible due to the small diffusion length scales and thus promoted thermo-oxidative degradation. To the best knowledge of the author, only studies on the effect of ageing on the thermal conductivity have been carried out [173], [174], and therefore opens the door to study the effect of ageing on a wide range of mechanical properties. Besides ageing, weathering is also of interest (e.g. the effect of incident radiation).

### Studies of the bead-bead interface

The already mentioned ideas focus on structure-property relationships. However, the bead-bead boundary is both a relevant and challenging scientific playground. Especially semi-crystalline bead foams and bead foams of blends are interesting as both crystallinity and blend morphology might change drastically during processing and thus affect the properties. The current studies on the interface mainly follow an empirical approach: the steam-chest moulding conditions are varied, which leads to different mechanical responses and to a different fracture pattern.

However, this is only a macroscopic parameter. Hence, the microscopic features of the bead-bead interface have been ignored (an exception for semi-crystalline EPP is the work by Gensel et al. [102]). In order to understand the mechanisms of inter-bead bonding, it appears of high importance to study also the microscopic features of the interface.

### The effect of the glass transition temperature and crystallinity on the deformation behaviour

Another interesting topic is a comparison between fundamentally different bead foams: it is not known, whether the same deformation mechanisms or dependencies on foam morphology apply above the glass transition temperature, e.g. for the semi-crystalline foams EPP or soft bead foams (ETPU). In this frame, the presence of crystals below the glass transition should be studied as well, for example using EPBT.

### Further studies on the effect of a thick bead skin

Also the topic of the thick bead skin can be explored further. For example, the effect of the thick skin on thermal conductivity is of interest as a thick skin might promote heat transfer by conduction through the thick skin and by that nullify small cell sizes within the bead. Furthermore, the ethanol treatment before moulding and its effect on the smoothness of the bead surface is also highly promising subject for further studies.

### Transfer of the work's results to novel amorphous bead foams

Finally, it would be reasonable to transfer the generated knowledge of the morphology to other amorphous bead foams. Especially, the maximum service temperature of EPS is too low for many applications. Thus, bead foams such as E-PC or E-PEI can smoothly round up the existing products. However, the moulding of such bead foams is challenging as steam chest moulding requires an extremely high steam pressure of about 20 bar. This is both challenging from a technical as well as safety perspective.

A contribution to the solution to this problem was also developed in the frame of this work. For example, a plasticising agent such as ethanol could be applied to the bead before moulding in order to soften their surface and locally reduce the glass transition temperature of the material. Possibly, this technique could enable the moulding of high-temperature thermoplastics using conventional EPP moulding machines.

## 8 Ausführliche deutsche Zusammenfassung

Expandierbares Polystyrol (EPS, ugs. je nach Region “Styropor”, “Unicell”, “Styrofoam”) ist einer der meist genutzten Schäume. Ein Viertel der weltweiten Schaumproduktion bezogen auf das Volumen besteht aus EPS. Der Grund hierfür liegt im geringen Preis von EPS, dessen guter Transportierbarkeit (es wird nur Mikrogranulat und kein geschäumtes Material den Verarbeitern geliefert) und den allgemeingültigen Vorteilen von Partikelschäumen (Kombination von geringer Dichte und freier Formgebung). Dies ist durch die einzigartige Herstellungs- und Verarbeitungsrouten bedingt. Im Falle von EPS wird zuerst expandierbares Mikrogranulat hergestellt, welches beim Verarbeiter vorgeschäumt wird (expandiertes Granulat) und anschließend im Formschaumprozess zu Teilen verarbeitet (verschweißt) wird.

Im Gegensatz zu angesagten Forschungsthemen, wie z.B. Nanokompositen, ist die Literatur über Partikelschäume eher beschränkt. Hauptsächlich wird die Auswirkung der Formschaumbedingungen auf die mechanischen Eigenschaften untersucht. Dabei führt bessere Verschweißung erwartungsgemäß zu besserer Mechanik, wie beispielsweise verbessertem Verhalten unter schlagartiger Belastung oder höherer Bruchzähigkeit. Im Allgemeinen wird die Verschweißungsqualität aus Bruchbildern bestimmt, genauer aus dem Verhältnis von inter- und intra-partikulärem Bruch. Im Falle von teilkristallinem EPP wird häufig angenommen, dass ein doppelter Schmelzpeak die Voraussetzung für gute Verschweißbarkeit ist. Deswegen wird die Entstehung und Auswirkung dieses Merkmals in vielen Publikationen eingehend untersucht. Die geschieht auch mit dem Ziel das erlangte Wissen auf andere teilkristalline Polymere wie zum Beispiel PLA zu übertragen.

Bisweilen wird EPS als Modellmaterial, z.B. zur Erforschung der Isolationseigenschaften von zellulären Materialien, genutzt. Trotzdem gibt es nur vergleichsweise wenige wissenschaftliche Veröffentlichungen über EPS. Mehr Informationen lassen sich hingegen in den technischen Broschüren von Materialherstellern wie der BASF SE finden. In diesen wird das Thema der Dämm- bzw. Isolationseigenschaften zum Teil näher betrachtet. Jedoch fehlt den Informationen wissenschaftlicher Tiefgang, wohingegen verfügbare experimentelle wissenschaftliche Veröffentlichungen teils nicht schlüssig sind, da wichtige Einflussgrößen vermischt und/oder gemeinsam betrachtet werden (z.B. Zell- und Partikelgröße bei veränderlicher Dichte). Eine ähnliche Schlussfolgerung lässt sich für die Studien über das mechanische Verhalten von EPS treffen, da hauptsächlich der Einfluss der Formschaumparameter auf das Bruchbild untersucht



wird. Allerdings beschäftigt sich keine der Arbeiten mit dem Einfluss der Morphologie bei unverändertem Formschaumprozess. Demzufolge fehlt eine umfassende Grundlage für weitergehende Untersuchungen.

Als Partikelschaum hat EPS eine mehrskalige Morphologie aus Zellwänden und -steigen, den Zellen selbst, den Schaumpartikeln und schließlich dem gesamten Bauteil. In diesem Zusammenhang bedingt eine Änderung der Partikelgröße auch eine Änderung der zu verschweißenden Fläche, wohingegen kleinere Zellen zu einer anderen Mikromorphologie (Zellstege und -wände) führen. Jedoch ist der Wirkzusammenhang zwischen Morphologie und der Schaumteileigenschaften noch nicht umfassend untersucht worden. Neben Zell- und Partikelgröße ist auch eine kompakte Randschicht um die Partikel herum vorstellbar, ähnlich einem geschäumten Tischtennisball. Dieser Morphologieparameter ist bis dato komplett unerforscht; es existiert auch keine Methode um diesen gezielt zu erzeugen.

Das Ziel der Arbeit ist es, ein umfassendes Verständnis des Einflusses der Morphologie von Partikelschäumen auf deren Eigenschaften zu erlangen. Damit soll zur Beantwortung der offenen Fragestellungen zu EPS ein Beitrag geleistet werden. In diesem Rahmen sollen Struktur-Eigenschaftsbeziehungen etabliert werden. Dafür müssen charakteristische Merkmale (wie Zell- und Partikelgröße sowie Dichte), welche einen starken Einfluss auf das mechanische Verhalten und das Dämmverhalten der fertigen Teile haben, jeweils anwendungsspezifisch identifiziert werden. In diesem Zusammenhang ist zu beachten, dass die vorliegende Arbeit nicht die Untersuchung des Einflusses des Formschaumprozesses einschließt, da dieser bereits Gegenstand zahlreicher Untersuchungen war. Aus praktischer Erfahrung ist bekannt, dass der Zusatz eines Blendpartners zu höherer Elastizität führt, was für besonders für Verpackungsanwendungen wichtig ist. Deshalb soll der Mechanismus hinter dieser Beobachtung exemplarisch für einen Polystyrol/Polyethylen-Blend (PS/PE-Blend; E-Por®) im Vergleich zu EPS aufgeklärt werden.

Schließlich ist eine kompakte Randschicht um die Partikel von besonderem wissenschaftlichem Interesse. In diesem Zusammenhang muss eine Methode entwickelt werden, mit welcher sich eine homogene Randschicht gezielt erzeugen lässt. Diese Randschicht soll mindestens eine Größenordnung dicker als die „Haut“ nicht modifizierter Partikel sein. Es wird davon ausgegangen, dass sich eine dicke Randschicht auf die

restlichen morphologischen Eigenschaften und schlussendlich der Mechanik auswirkt, da sich die Materialverteilung innerhalb der Partikel ändert.

Entsprechend der Ziele ist die Arbeit zweigeteilt. Teil I widmet sich der Untersuchung von Bauteilen aus nicht modifizierten Partikel ohne dickere Randschicht. Es wird der Zusammenhang zwischen mechanischem Verhalten sowie Dämmverhalten und den morphologischen Einflussgrößen (Partikel- und Zellgröße sowie Dichte) betrachtet. Diese Einflussgrößen bestimmen 1) die Grenzflächen zwischen den Partikeln innerhalb des Bauteils, 2) die Mikromorphologie in Form von Zellwänden und –stegen sowie 3) den Anteil Polymer in der Schaumstruktur (Dichte). Daneben soll ein PS/PE-Blend (E-Por®) im Vergleich zu EPS untersucht werden.

In diesem Zusammenhang ist zu beachten, dass nur die Herstellparameter der Partikel angepasst wurden, um unterschiedliche Partikelmorphologien in den Bauteilen zu erhalten. Die Vor- und Formschäumparameter wurden jedoch (bis auf die variable Dichte) konstant belassen.

Um die Morphologie der Bauteile zu beschreiben, werden deren Homogenität und die Zusammenhänge zwischen Dichte, Partikelgröße, Zellgröße und Mikromorphologie (Wand- und Stegdicke) näher untersucht. Die Untersuchung der Mechanik in Abhängigkeit der Morphologie erfolgt in Druck- und Biegedeformation. Daneben wird der Einfluss der Deformationsgeschwindigkeit sowie die lokale Deformation unter Druckbelastung untersucht. Die bruchmechanische Charakterisierung erfolgt durch Messung des J-Integrals als Zähigkeitsparameter sowie der Untersuchung der Bruchflächen. Schlussendlich wird das Dämmverhalten in Abhängigkeit der Morphologie betrachtet.

Teil II der Arbeit erforscht die bisher unbekannte Größe der dicken Randschicht um Partikel. In diesem Rahmen wird zuerst eine Labormethode entwickelt und diese anschließend auf den industriellen Maßstab übertragen, um Bauteile für die weitergehenden Untersuchungen zu erhalten. Die Wechselbeziehung zwischen Randschichtdicke und den anderen Morphologieparametern wird in diesem Zusammenhang betrachtet. Schlussendlich erfolgt die Untersuchung des Einflusses der Randschichtdicke auf die mechanischen Eigenschaften.

Partikel und Bauteile für die Untersuchungen in Teil I wurden von der BASF SE zur Verfügung gestellt. Basis der untersuchen für Teil II war expandierbares Mikrogranulat, welches auch von der BASF SE bereitgestellt wurde.

## **Zusammenfassung zu Teil I**

### Morphologische Grundcharakterisierung

Bauteile aus Partikelschäumen besitzen eine komplexe mehrskalige Morphologie vom Meter-Maßstab bis hin in den Mikrometerbereich. Standardmäßig werden zylindrische Platten mit der Dimension 300 x 50 mm (Durchmesser x Höhe) untersucht. Diese bestehen aus rund 750.000 Einzelpartikeln. Jeder dieser Partikel selbst enthält circa 1.000 Schaumzellen bei einem Zelldurchmesser von 300 µm. Auch die Grenzfläche zwischen den Partikeln ist beachtlich, nämlich circa 11 m<sup>2</sup>. Diese Zahlen sind umso beeindruckender, wenn man auch die geringe Masse der Platte von nur 90 g bei einer Dichte von 25 g/l bedenkt.

Demzufolge ist es notwendig vor weiteren Untersuchungen die Homogenität der Platte zu betrachten. Es zeigte sich, dass die Platten hinsichtlich Dichte und Zellgröße in lateraler Richtung homogen sind. Nur am Injektor zeigen sich erwartungsgemäß Abweichungen. Im Gegensatz dazu haben die Platten einen Dichtegradienten in Dickenrichtung mit einem Minimum im Zentrum der Platte. Jedoch zeigen sich keine signifikanten Abhängigkeiten der Zellgröße.

Des Weiteren wurden die Abhängigkeiten der verschiedenen Morphologiegrößen untereinander untersucht. Kleinere Zellen führen erwartungsgemäß zu dünneren Zellwänden und -stegen für EPS und E-Por. Die Zellwände von EPS sind dünner als in E-Por, die Zellstege entsprechend dicker. Bei der Variation der Partikeldichte zeigt sich für EPS eine starke Abhängigkeit der Zell- und Mikromorphologie. Größere Partikel besitzen größere Zellen. Im Gegensatz zu EPS ändert sich die Zellmorphologie von E-Por nicht signifikant mit der Partikelgröße. Die Änderung der Dichte wird durch die Vorschäumbedingungen (Zeit und Temperatur) bestimmt. Höhere Dichte bedingt kleinere Partikel und gleichzeitig kleinere Schaumzellen, da die Nukleierungsdichte für die Schaumzellen konstant bleibt. Diese müssen aber weniger expandieren.

Auch wurde EPS, welches in Extrusion mit Unterwassergranulierung hergestellt wurde, mit EPS aus der Suspensionspolymerisation („sEPS“) mit Pentan verglichen. Im Hinblick auf die Partikelgröße sind beide Varianten vergleichbar. Unterschiede ergeben sich jedoch für die Zellgröße, welche bei sEPS nur circa ein Fünftel von EPS aus der Extrusion mit Unterwassergranulierung beträgt. Interessanterweise sind die Wanddicken der Mikromorphologie vergleichbar, nur die Zellstege von EPS aus der Extrusion sind dicker.

Die Untersuchung der Zellmorphologie erfolgte auch im Hinblick auf die Endeigenschaften. Es wird erwartet, dass die Änderungen in der Makro- (Partikel- und Zellgröße) und Mikromorphologie (Wand- und Stegdicke) sich auf die Mechanik und die Wärmeleitfähigkeit auswirken. Ein höherer Anteil an Zellstegen führt laut dem Modell von Gibson und Ashby zu geringeren Kennwerten in der (linearen) Mechanik. Jedoch wird erwartet, dass dickere Stege die Isolationsleistung verbessern, da diese besser IR-Strahlung absorbieren. Auch kleinere Zellen sollten sich positiv auf die Dämmleistung auswirken.

### Mechanische Grundcharakterisierung

Die grundlegenden mechanischen Eigenschaften wurden in Druck- und Biegeversuchen ermittelt. In-situ Druckversuche im REM wurden durchgeführt, um die mikroskopischen Deformationsmechanismen zu untersuchen.

Kleinere Schaumzellen verbessern im Allgemeinen die Eigenschaften von EPS, jedoch nicht von E-Por, da die Mechanik von E-Por von den PE-Domänen bestimmt wird, welche nicht systematisch mit der Zellgröße variieren. Der Mechanismus hinter der Zellgrößenabhängigkeit von EPS wurde durch Schrumpfungsversuche bei erhöhter Temperatur und dynamisch mechanischer Analyse (DMA) näher untersucht. Dabei zeigte sich, dass eine stärkere Orientierung der Polymerketten sowie ein höherer Grad an Wärmeauslagerung bei kleineren Zellen für verbesserte Eigenschaften verantwortlich sind.

Im Hinblick auf den Einfluss der Partikelgröße zeigte sich, dass größere Partikel zu besserer Mechanik führen, da bei diesen eine bessere Verschweißungsqualität vorliegt. Dies liegt an besserem Energietransfer des Dampfes an die Partikel während des Formsäumens sowie einer geringeren Gesamtpartikeloberfläche. Jedoch zeigt sich für zu große Partikel eine Umkehr des Verhaltens, da bei diesen vermehrt Makroporosität („Zwickel“) zu beobachten ist. Diese wirken als Defekt und beeinflussen dann die Mechanik.

Wird die Dichte der Partikel und des Formteils geändert, zeigen sich für E-Por und EPS ähnliche Trends. Insgesamt ist die Dichte die wichtigste Einflussgröße auf die mechanischen Eigenschaften. Wie in der Literatur dargestellt, folgt die Dichteabhängigkeit der mechanischen Kennwerte dem Potenzgesetz. Unter Druckbelastung wird die Mechanik jedoch stärker von der Dichte beeinflusst als unter Biegebelastung. Dies liegt darin begründet, dass die Deformationsmechanismen unter Druckbelastung eine höhere Dichteabhängigkeit aufweisen als unter Zugbelastung, welche auch in Biegung

auftritt. Bei der Untersuchung der Mikrodeformationsmechanismen zeigte sich, dass die Deformation lokal stärker im Zentrum der Partikel stattfindet. Des Weiteren fungiert die Makroporosität als Schwachstelle zwischen den Partikeln, was zu lokal erhöhter Deformation und damit Versagen um den Zwickel führt.

#### Morphologie- und Dichteabhängigkeit der bruchmechanischen Eigenschaften

Die Bruchzähigkeit von EPS wird stark von der Zellgröße beeinflusst, jedoch gibt es keinen Zusammenhang für E-Por. Dies wird auf verschiedene zähigkeitsbestimmende charakteristische Größen zurückgeführt.

Die Bruchzähigkeit von EPS hängt stark von der Dicke der Zellwände und -stege ab. So fördern dünnere Strukturen die Verformbarkeit bis zum Versagen. Es tritt ein Übergang vom ebenen Dehnungszustand in den ebenen Spannungszustand auf. In diesem Zusammenhang zeigt sich auch ein starker Effekt der Nukleierungsmittelkonzentration (Talkum). Bei niedriger Konzentration führt Talkum zu kleineren Zellen und damit dünneren Stegen und Wänden. Dies hat eine erhöhte Bruchzähigkeit zur Folge. Steigt die Talkumkonzentration jedoch über einen kritischen Wert, wirkt Talkum jedoch als Defekt in der Schaumstruktur; die Bruchzähigkeit sinkt in diesem Fall. Der Effekt der verkleinerten Zellen wird in diesem Fall von der erhöhten Defektdichte in der Polymermatrix überwogen. Im Gegensatz zu EPS ist E-Por durch seine Blendstruktur „inhärent zäh“. Der Zusatz von PE zu PS führt zu einer geringeren charakteristischen Dicke der PS-Domänen (vgl. charakteristische Größe EPS: Steg- und Wanddicke), was zähigkeitssteigernd wirkt.

Auch die Partikelgröße hat einen starken Einfluss auf die Bruchzähigkeit. So wurde eine optimale Partikelgröße im Bereich 3 bis 3,5 mm gefunden. In diesem Bereich läuft der Riss hauptsächlich durch die Partikel. Sowohl für kleinere wie auch größere Partikel breitet sich der Riss eher entlang der Partikel-Partikel-Grenzfläche aus. Für kleine Partikel wird dies auf schlechtere Verschweißung zurückgeführt, da sich die Energie des Dampfes beim Formschäumen auf eine größere innere Fläche verteilen muss. Daneben hat eine Schüttung aus kleineren Partikel einen größeren Strömungswiderstand gegenüber dem Dampf während des Formschäumprozesses, was zu schlechterem Energieaustausch führt. Im Gegensatz dazu haben Bauteile aus großen Partikeln mehr Zwickel, welche als Defekt bzw. Rissinitiator wirken und damit die Bruchzähigkeit senken.

Die Dichte ist die wichtigste Einflussgröße auf die Bruchzähigkeit. Höhere Dichte führt erwartungsgemäß zu höherer Bruchzähigkeit, da die Festigkeit der Einzelpartikel entsprechend steigt. EPS zeigt eine lineare Abhängigkeit, wohingegen E-Por zwei Bereiche aufweist. Bei niedriger Dichte fungiert das PE zähigkeitssteigernd, da es gedehnt vorliegt und die PS-Domänen effektiv voneinander separiert. Bei hoher Dichte liegt es kugelförmiger vor und fungiert als Defekt.

#### Morphologie- und Dichteabhängigkeit der Wärmeleitfähigkeit

Wie auch bei der Bruchzähigkeit hat die Schaummorphologie auch einen starken Einfluss auf die Wärmeleitfähigkeit. Kleine Zellen sind für die Dämmeigenschaften sowohl von EPS als auch E-Por förderlich, obwohl die dünneren Stege und Wände mit kleineren Zellen transparenter für IR-Strahlung sein sollten. Der entscheidende Faktor bei EPS aus Extrusion ist der Temperaturunterschied zwischen den Enden der Zelle (und damit die Zellgröße bei gegebenem Temperaturgradienten), was den Nettowärmetransport durch Strahlung in einer Zelle festlegt.

Jedoch ist dieser Mechanismus nur wirksam, wenn die Wände und Stege dicker sind als die Wellenlänge der emittierten IR-Strahlung bei gegebener Temperatur. Ansonsten werden die Wände zunehmend transparent für IR Strahlung; eine größere „effektive Zellgröße“ liegt dann vor. Dieser Fall ist bei sEPS zu beobachten, welches trotz sehr kleiner Zellen eine schlechtere Dämmwirkung als EPS aus der Extrusion aufweist.

Im Gegensatz dazu beeinflusst die Partikelgröße die Wärmeleitfähigkeit nur indirekt. Ein Faktor ist die Änderung der Zellgröße mit der Partikelgröße wie im Fall von EPS aus der Extrusion mit Unterwassergranulierung, was zu den oben beschriebenen Phänomenen führt.

Die Dichte beeinflusst auch die Wärmeleitfähigkeit stark. Drei Bereiche der Wärmeleitfähigkeit in Abhängigkeit von der Dichte lassen sich direkt identifizieren, ein vierter Bereich wird ersichtlich, wenn man den Dichtebereich und damit den Anteil an Polymer bzw. Zellgas am Gesamtsystem weiterdenkt. Bei Dichten kleiner 20 g/l dominiert die Wärmeleitung durch das Zellgas die Gesamtwärmeleitfähigkeit, die Änderung mit der Dichte wird aber durch IR-Strahlung determiniert, da große Zellen mit dünnen Stegen und Wänden eine hohe IR Durchlässigkeit aufweisen. Bei mittlerer Dichte um 40 g/l liegt ein Minimum in der Wärmeleitfähigkeit vor. In diesem Dichtebereich sind die Zellen noch klein genug für geringe Temperaturunterschiede zwischen den beiden Zellseiten, damit für geringen Wärmetransport durch Strahlung, und die Dichte niedrig genug um nur wenig Energietransport durch die Matrix zu ermöglichen. Für Schäume

höherer Dichte im Bereich 80 g/l wird die Wärmeleitung durch die Polymermatrix immer wichtiger, der Strahlungsanteil wird vernachlässigbar, da die Zellwände trotz kleiner Zellgrößen dick sind. Die Wärmeleitung durch das Zellgas ist trotzdem weiterhin der dominante Faktor. Dies ändert sich erst in Bereich vier bei einer Dichte größer 180 g/l. In diesem Bereich beherrscht dann die Matrix die Wärmeleitfähigkeit des Schaumes.

## **Zusammenfassung zu Teil II**

### Erforschung eines Prozesses für Partikel mit dicker Randschicht

Neben der Zell- und Partikelgröße ist eine kompakte Randschicht eine weitere mögliche morphologische Einflussgröße. Die Motivation für eine dickere Randschicht um die Partikel ist es, eine Art von internem Sandwicheffekt hervorzurufen. Jedoch ist die Randschicht bisher vollständig unerforscht in der wissenschaftlichen Literatur. Es ist ein Ziel der Arbeit eine Randschicht mit mindestens der zehnfachen Dicke von „normalen“ Partikel zu erhalten, welche eine homogene Dicke aufweist. Des Weiteren muss die Methode auch für den industriellen Maßstab anwendbar sein.

Die grundlegende Idee um eine kompakte Randschicht um die Partikel zu erzeugen ist die lokale Absenkung des Treibmittelgehaltes (Pentan) am Rand des Mikrogranulats vor dem Vorschäumen, so dass die Expansion nur vom „unberührten“ Teil in der Mitte mit genug Treibmittel herrührt. Diese lokale Absenkung des Pentangehaltes wurde durch Auslagerung des Mikrogranulates in einem Konvektionsofen bei einer Temperatur unterhalb der Glasübergangstemperatur  $T_G$  von PS/Pentan erreicht.

Dieses Prinzip wurde zuerst exemplarisch geprüft und anschließend eine Labormethode zur Kontrolle der Randschichtdicke für EPS entwickelt. Die lokale Entnahme des Treibmittels führte allerdings beim Vorschäumen zu Rissen in der Randschicht sowie einer inhomogenen Randschichtdicke, da der Vorschäumvorgang bei einer Temperatur um den  $T_G$  von reinem PS stattfindet. Dieses ist dadurch nicht verformbar genug. Das Problem ließ sich durch eine lokale Plastifizierung mit Ethanol lösen, was schlussendlich zu einer glatten und homogen dicken Randschicht führt.

Bei der Maßstabsvergrößerung der Methode auf einen industriellen Vorschäumer zeigte sich, dass das Zeitintervall zwischen Ofenauslagerung, Ethanolbehandlung und Vorschäumen hinreichend klein sein muss. Des Weiteren mussten die Auswirkung der Prozessparameter des Vorschäumens näher untersucht werden. Es zeigte sich, dass der optimale Dampfdruck bei 200 mbar liegt. Höhere oder geringere Dampfdrücke führen wiederum zu Rissen in der Partikelrandschicht. Der Grund hierin liegt im Verhältnis



der Zeitskalen für die Diffusion des Ethanols aus der Randschicht einerseits und der Erhitzung des Mikrogranulats andererseits.

Schlussendlich konnten Randschichten um die Partikel mit einer Dicke von maximal 13  $\mu\text{m}$  erreicht werden, was einer Erhöhung der Dicke um den Faktor 20 entspricht (ausgehend von expandierten Partikeln aus unbehandeltem Mikrogranulat). Die Dicke bei konstanter Dichte lässt sich sehr gut über die Ofenauslagerungszeit steuern.

Bei einer Ofenauslagerung von 3 h bei 60 °C resultierte eine Randschichtdicke um die Partikel von mehr als 10  $\mu\text{m}$ , was einem Massenanteil der Randschicht von mehr als 40 % an der Gesamtmasse des Partikels entspricht. Als Obergrenze für die Randschichtdicke wurden 23  $\mu\text{m}$  berechnet. Die resultierenden Partikel wären dann mit einem Tischtennisball vergleichbar, bestehend nur aus einer Hülle ohne Schaumkern.

#### Effekt der Randschichtdicke auf die Morphologie und Mechanik

Insgesamt hat die Einführung einer kompakten Randschicht keine starke Auswirkung auf die Partikelmorphologie. Es lässt sich eine leichte Verbreiterung der Partikelgrößenverteilung beobachten sowie eine Zunahme der Zellgrößen, da weniger Zellen nun mehr expandieren müssen um eine gegebene Partikeldichte zu erreichen. Dies bedingt auch eine Reduktion der Zellwand- und Zellstegdike. Während des Formschäumprozesses verschlechtert sich allerdings die Homogenität der Randschicht, da diese besonders in Bereichen starker Deformation reißt.

Eine dickere Randschicht um die Partikel führt im Allgemeinen zu verschlechterten Eigenschaften in Druck- und Biegedeformation sowie einer geringeren Bruchzähigkeit. Jedoch können die verschlechterten Eigenschaften nicht nur auf die Randschicht zurückgeführt werden, sondern auf lokal inhomogene Formteilen, die nur bei Partikeln mit dicker Randschicht entstehen. Es zeigt sich, dass Proben vom unten Teil der Form weisen bessere mechanische Eigenschaften auf als Proben vom oberen Teil. Die Bruchzähigkeit wird nur wenig von der Randschichtdicke beeinflusst. Jedoch erhöht eine dickere Randschicht leicht den Anteil an Bruch entlang der Partikel-Partikel-Grenzen. Insgesamt zeigt sich leider, dass sich die Motivation des internen Sandwicheffektes nicht einstellte.

## **Ausblick**

Im Rahmen der vorliegenden Dissertation wurden nicht nur Fragen beantwortet, sondern auch weitere Fragestellungen aufgeworfen und potentielle Forschungsfelder identifiziert, welche in Zukunft näher betrachtet werden sollten. Dies trifft besonders auf den Einfluss der Zellgröße auf die Mechanik zu, der weitergehend untersucht werden sollte und in der vorliegenden Arbeit „nur“ makroskopisch untersucht wurde. Beispielsweise erlauben PALS-Messung (engl. für positron annihilation lifetime spectroscopy) die Quantifizierung des lokalen freien Volumens in Zellstegen und –wänden als Funktion der Dickenrichtung. Damit könnte die stärkere plastische Verformbarkeit mit dünner werden Wänden und Stegen (kleinere Zellen) näher untersucht werden. Möglicherweise besitzen Schäume mit sehr kleinen Zellen einen höheren Anteil an potentiell duktilem Material an der Oberfläche der Zellwände. In Diesem Rahmen können auch mikromechanische Untersuchungen mit Rasterkraftmikroskopen weitere Erkenntnisse liefern.

Neben der weiteren Aufklärung der verbesserten Mechanik mit kleineren Zellen sind auch Alterungsphänomene und der Einfluss von Bewitterung in Abhängigkeit der Schaummorphologie sowohl wissenschaftlich als auch wirtschaftlich interessant.

Neben den genannten für Schäume allgemeingültigen Themen sind besonders für Partikelschäume die Eigenschaften und Vorgänge an den Partikel-Grenzflächen spannend. Das betrifft insbesondere Partikelschäume aus teilkristallinen Materialien und Blends, da sowohl die Kristallinität als auch die Blendmorphologie an dieser Stelle erhebliche Auswirkungen haben sollten. Bisherige Studien legen ihren Schwerpunkt eher auf den Einfluss des Formschäumens und dessen makroskopisch beobachtbare Auswirkungen, jedoch nicht auf materialspezifische und/oder mikroskopische Effekte.

Sinnvollerweise sollten die in dieser Arbeit erhaltenen Erkenntnisse auch auf neuartige Typen von amorphen Partikelschäumen übertragen werden. Vorstellbar ist hier beispielsweise E-PEI bzw. das zur K 2019 von der Covestro AG vorgestellte E-PC.

## Appendix

Chapter 5.2.1 (page 74 ff.)

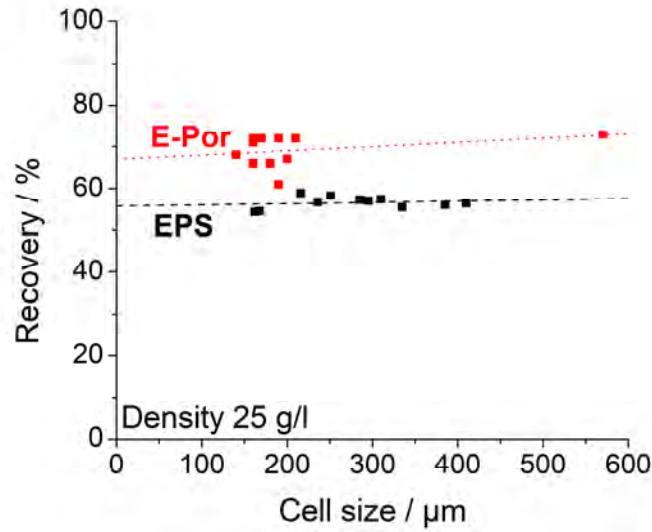


Figure 125: Recovery after compression as function of cell size.

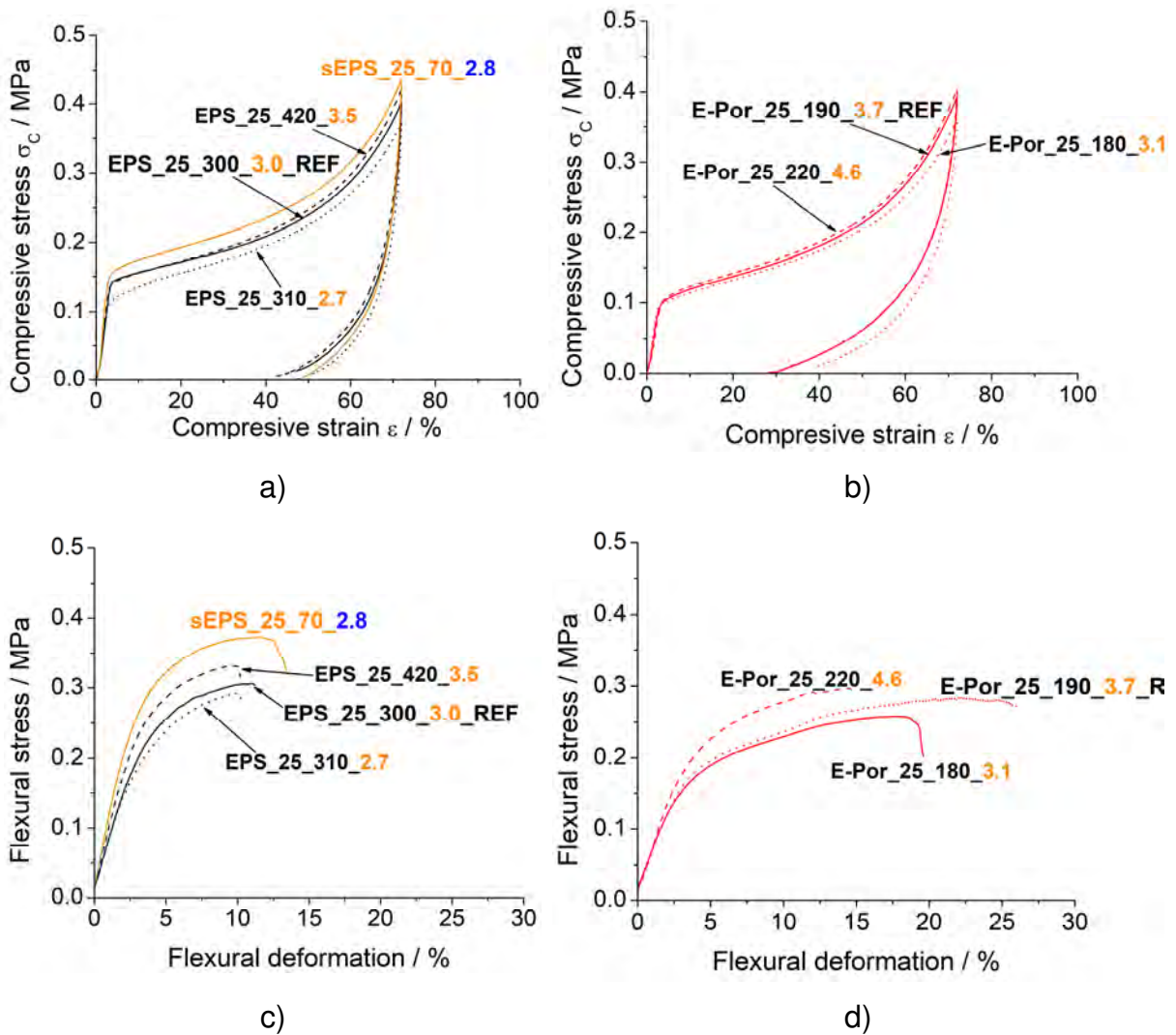


Figure 126: Stress-strain curves of EPS (black), sEPS (orange) and E-Por (red) with different bead sizes under compressive (a) and b)) and flexural loading (c) and d)).

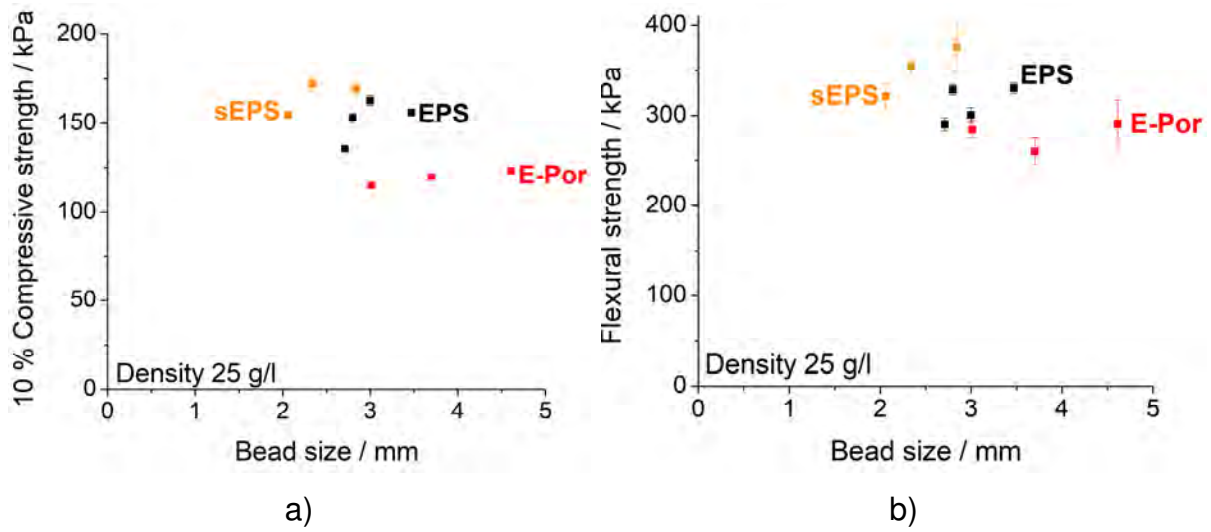


Figure 127: a) Compressive strength at 10 % strain and b) flexural strength as function of bead size.

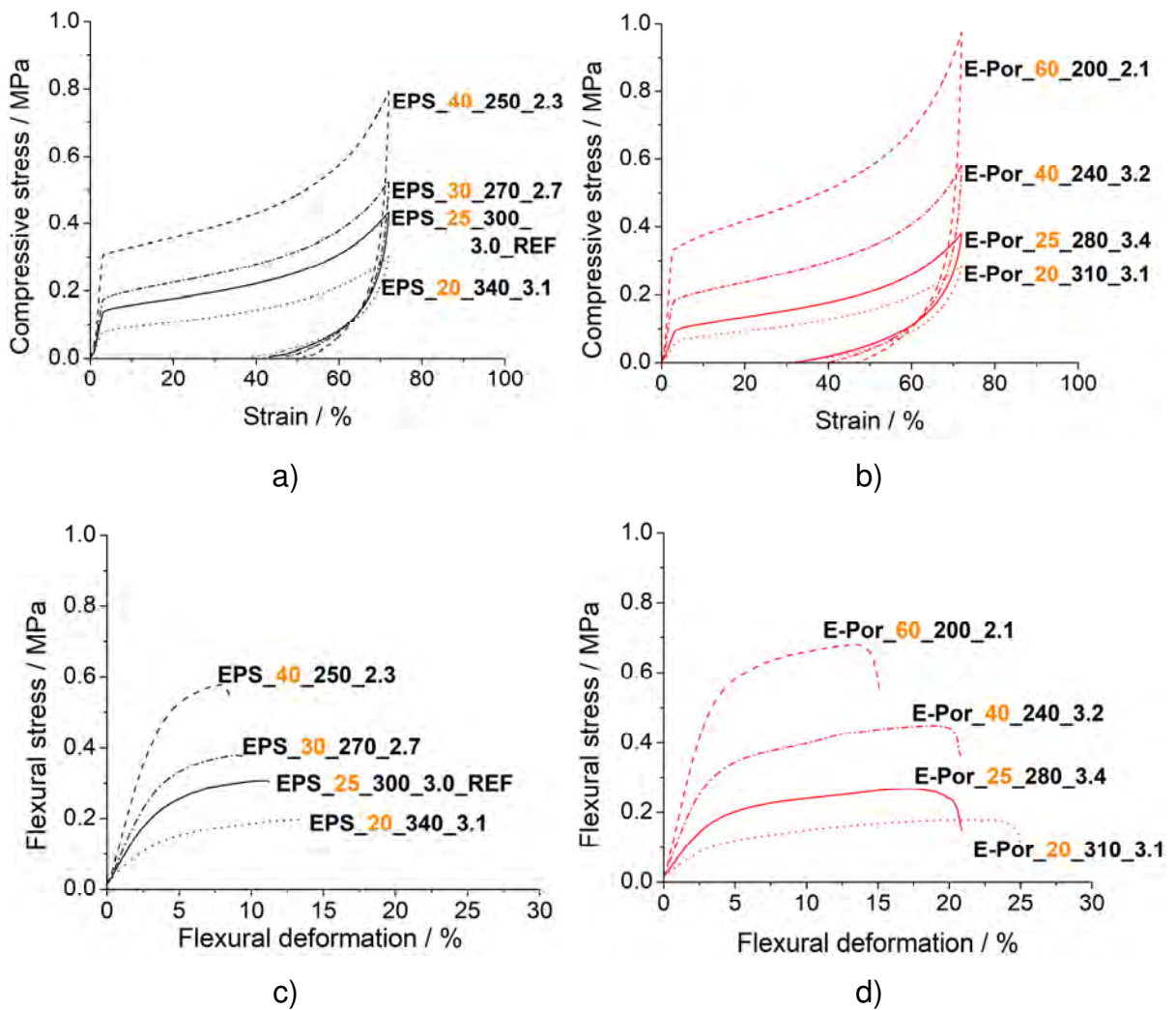


Figure 128: Stress-strain curves of EPS (black) and E-Por (red) with different densities under compressive loading (a and b) as well as flexural loading (c and d)).

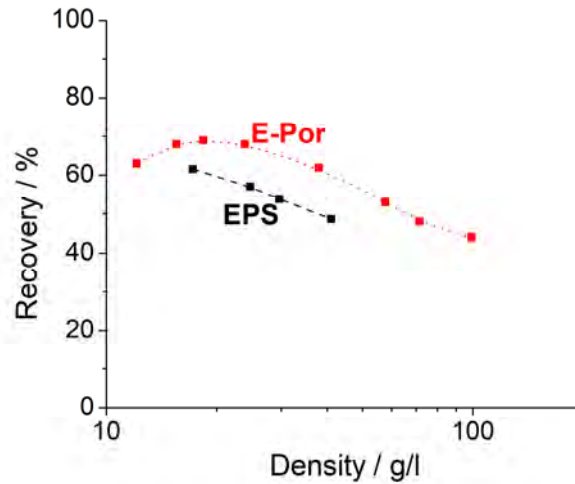


Figure 129: Recovery after compression as function of density for E-Por and EPS.

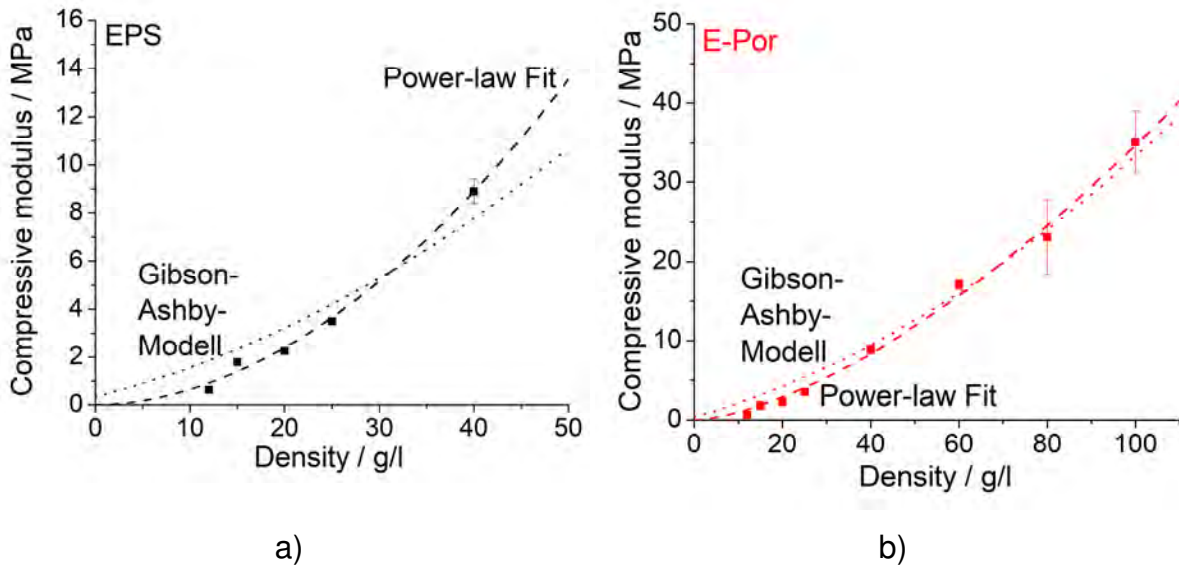


Figure 130: Comparison of the Gibson-Ashby model with a power-law-fit for a) EPS and b) E-Por.

Chapter 5.2.2 (page 90 ff.)

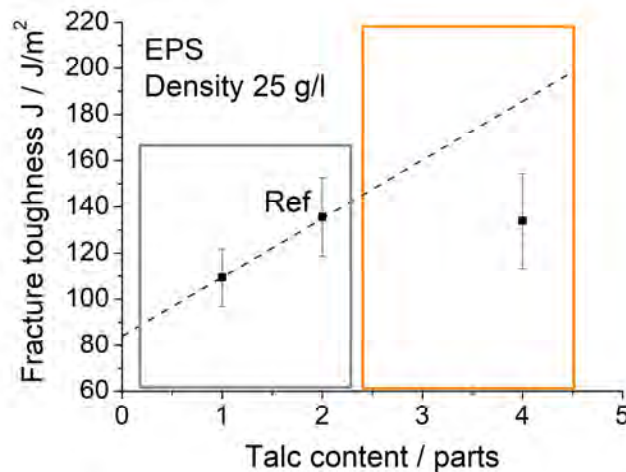


Figure 131: Effect of talcum addition on the fracture toughness of EPS. The reference material is processed with a talc content of 2 parts.

Chapter 5.3 (110 ff.)

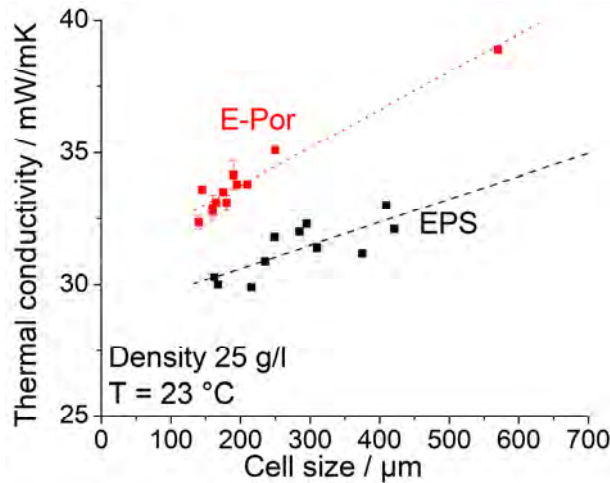


Figure 132: Dependency of thermal conductivity on cell size at constant foam density of 25 g/l for both EPS and E-Por. Zoomed graph.

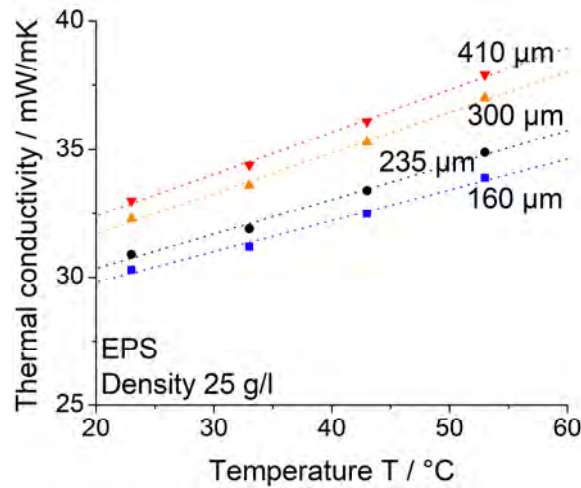


Figure 133: Thermal conductivity as function of temperature for four different cell sizes of EPS. Zoomed graph.

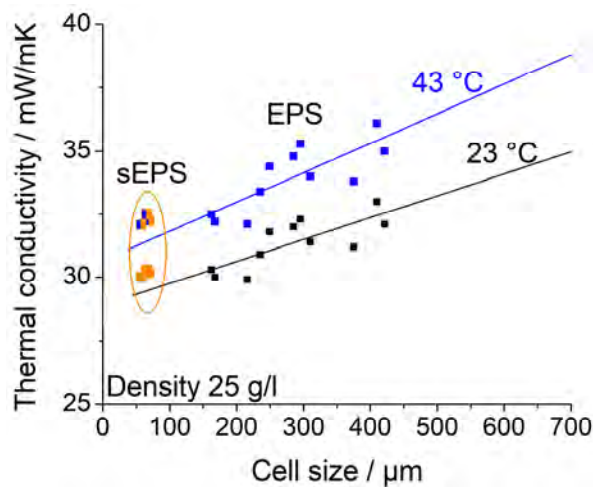


Figure 134: Enlarged comparison of the total thermal conductivities of sEPS and EPS from extrusion at 23 °C and 43 °C.



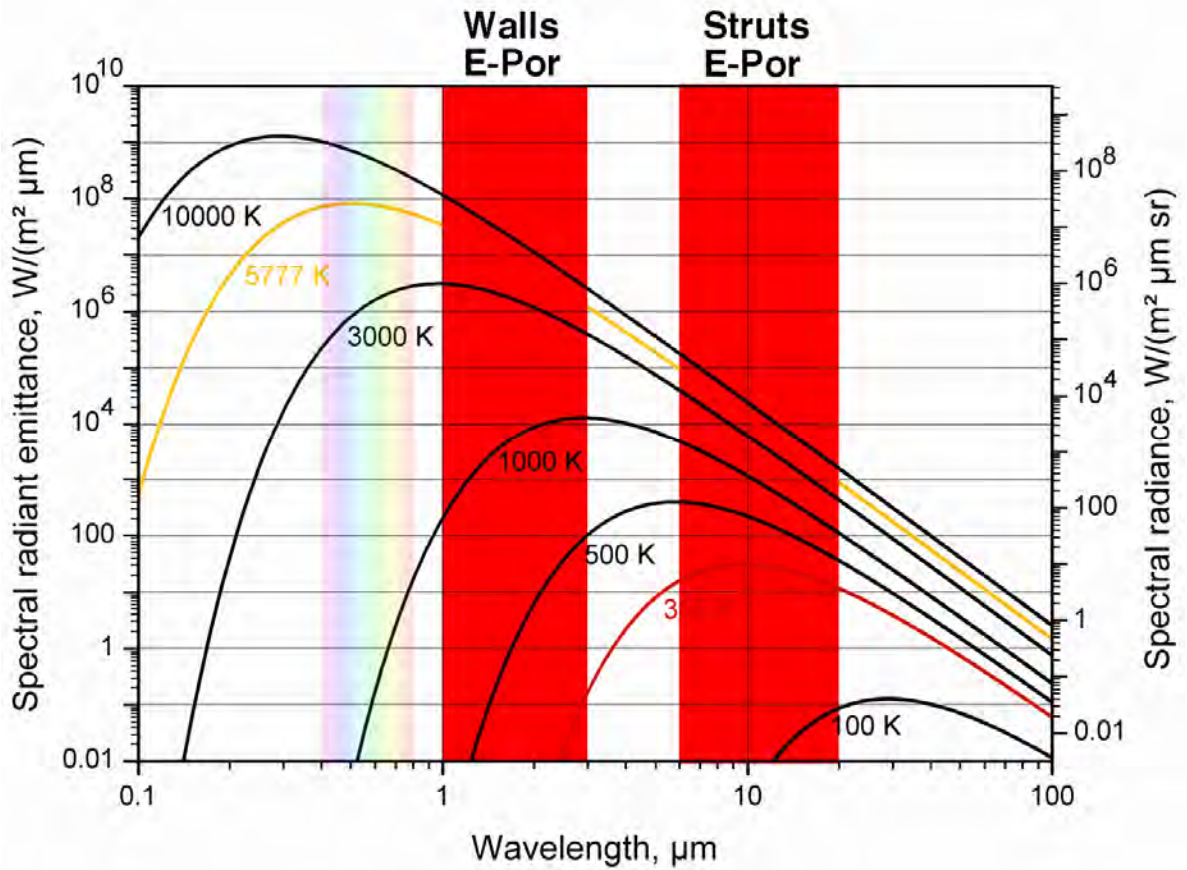


Figure 135: Comparison of the emission spectra of thermal radiation of a black body with the typical dimensions of the cell walls and struts of E-Por (Spectra used from [168]).

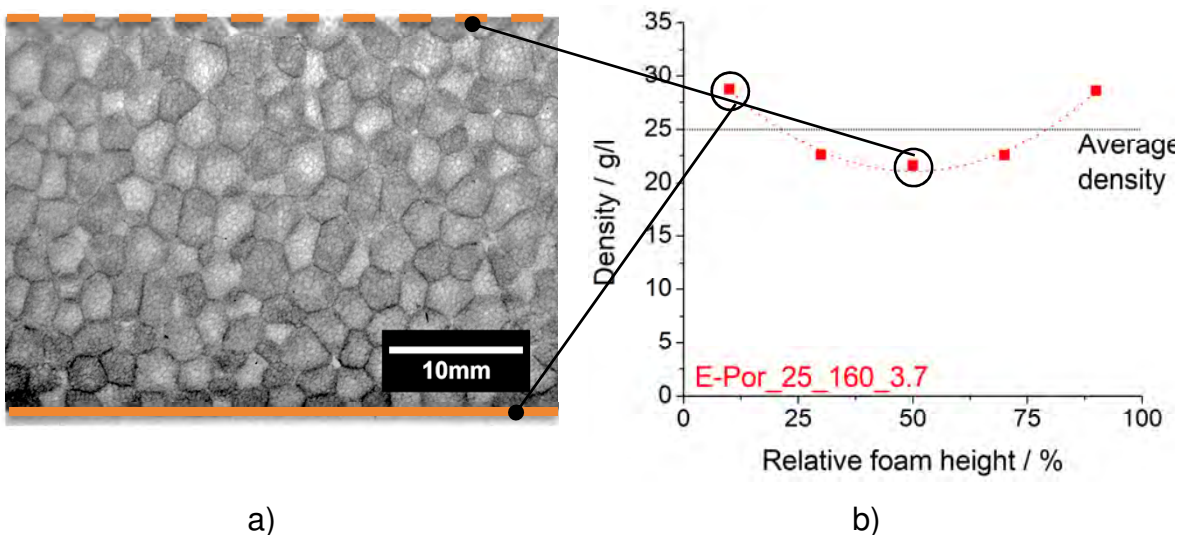


Figure 136: a) Visualisation of the skin region (solid line) and the middle region (dashed line) of a part, b) density distribution over the sample thickness (average density 25 g/l).



## Chapter 5.7 (page 146 ff.)

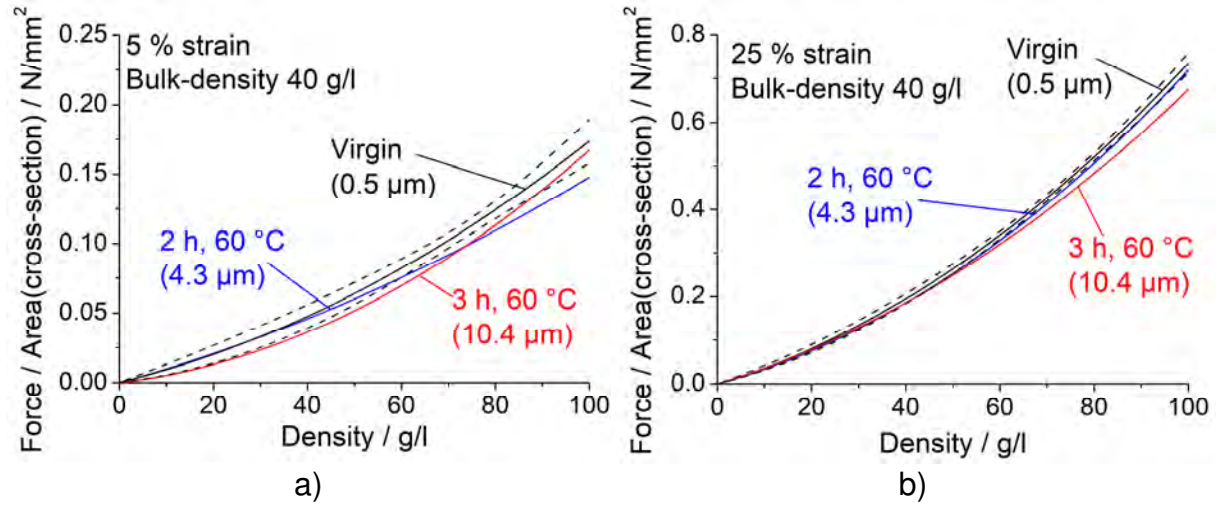


Figure 137: "Stress"-strain curves in single-bead compression for 5 and 25 % strain.

---

**References**

- [1] MarketsandMarkets Research Private Ltd., “Polymer Foam Market by Type (PU, PS, PO, PVC, Phenolic, Melamine), End-Use Industry (Building & Construction, Packaging, Automotive, Furniture & Bedding, Footwear, Sports & Recreational), and Region - Global Forecast to 2022,” publicly visible information, 2017.
- [2] Grand View Research, “Expanded Polystyrene (EPS) Market Analysis By Product, By Application (Construction, Automotive, Packaging), By Region (North America, Europe, Asia Pacific, Central & South America, MEA), And Segment Forecasts, 2014 - 2025,” publicly visible information, 2017.
- [3] R. Coquard, D. Baillis, and D. Quenard, “Heat transfer in low-density eps foams,” *12èmes Journées Internationales de Thermique*, pp. 291–294, 2005.
- [4] W. Eicke-Henning, “Grenfell Tower- Nun kommt die Wahrheit heraus,” Energieinstitut Hessen, 2018.
- [5] C. Trassl and H. Wörthwein, “Klasse statt Masse,” *Kunststoffe*, vol. 12, pp. 134–137, 2010.
- [6] M. Khodai and N. Parvin, “Pressure measurement and some observation in lost foam casting,” *J. Mater. Process. Technol.*, vol. 206, no. 1–3, pp. 1–6, 2008.
- [7] P. Kannan, J. J. Biernacki, and D. P. Visco, “A review of physical and kinetic models of thermal degradation of expanded polystyrene foam and their application to the lost foam casting process,” *J. Anal. Appl. Pyrolysis*, vol. 78, no. 1, pp. 162–171, 2007.
- [8] X. J. Liu, S. H. Bhavnani, and R. A. Overfelt, “Simulation of EPS foam decomposition in the lost foam casting process,” *J. Mater. Process. Technol.*, vol. 182, no. 1–3, pp. 333–342, 2007.
- [9] J. Schellenberg and M. Wallis, “Dependence of Thermal Properties of Expandable Polystyrene Particle Foam on Cell Size and Density,” *J. Cell. Plast.*, vol. 46, no. 3, pp. 209–222, 2010.
- [10] E. Placido, M. C. Arduini-Schuster, and J. Kuhn, “Thermal properties predictive model for insulating foams,” *Infrared Phys. Technol.*, vol. 46, no. 3, pp. 219–231, 2005.
- [11] S. T. Lee and N. S. Ramesh, *Polymeric Foams - Mechanisms and Materials*. CRC Press, 2004.
- [12] V. Altstädt and A. Mantey, *Thermoplast-Schaumspritzgießen*. Carl Hanser Verlag GmbH & Co. KG, 2011.

- 
- [13] P. Kundra, S. R. Upreti, A. Lohi, and J. Wu, "Experimental Determination of Composition-Dependent Diffusivity of Carbon Dioxide in Polypropylene," *J. Chem. Eng. Data*, vol. 56, no. 1, pp. 21–26, 2011.
- [14] Y. Sato, T. Takikawa, S. Takishima, and H. Masuoka, "Solubilities and diffusion coefficients of carbon dioxide in poly(vinyl acetate) and polystyrene," *J. Supercrit. Fluids*, vol. 19, no. 2, pp. 187–198, 2001.
- [15] D. Raps, T. Köppl, A. R. de Anda, and V. Altstädt, "Rheological and crystallisation behaviour of high melt strength polypropylene under gas-loading," *Polymer (Guildf)*, vol. 55, no. 6, pp. 1537–1545, 2014.
- [16] Q. Zhang, M. Xanthos, and S. K. Dey, "Parameters Affecting the In-Line Measurement of Gas Solubility in Thermoplastic Melts during Foam Extrusion," *J. Cell. Plast.*, vol. 37, no. 4, pp. 284–292, 2001.
- [17] J. S. Colton and N. P. Suh, "Nucleation of microcellular foam: Theory and practice," *Polym. Eng. Sci.*, vol. 27, no. 7, pp. 500–503, 1987.
- [18] A. Wong and C. B. Park, "A visualization system for observing plastic foaming processes under shear stress," *Polym. Test.*, vol. 31, no. 3, pp. 417–424, 2012.
- [19] A. Wong, R. K. M. Chu, S. N. Leung, C. B. Park, J. H. Zong, "A batch foaming visualization system with extensional stress-inducing ability," *Chem. Eng. Sci.*, vol. 66, no. 1, pp. 55–63, 2011.
- [20] S. N. Leung, A. Wong, L. C. Wang, and C. B. Park, "Mechanism of extensional stress-induced cell formation in polymeric foaming processes with the presence of nucleating agents," *J. Supercrit. Fluids*, vol. 63, pp. 187–198, 2012.
- [21] P. Spitael and C. W. Macosko, "Strain hardening in polypropylenes and its role in extrusion foaming," *Polym. Eng. Sci.*, vol. 44, no. 11, pp. 2090–2100, 2004.
- [22] D. Raps, T. Köppl, L. Heymann, and V. Altstädt, "Rheological behaviour of a high-melt-strength polypropylene at elevated pressure and gas loading for foaming purposes," *Rheol. Acta*, vol. 56, no. 2, 2017.
- [23] G. Liu, H. Sun, S. Rangou, K. Ntetsikas, A. Avgeropoulos, and S.-Q. Wang, "Studying the origin of 'strain hardening': Basic difference between extension and shear," *J. Rheol.*, vol. 57, no. 1, p. 89, 2013.
- [24] M. H. Wagner, H. Bastian, P. Hachmann, J. Meissner, S. Kurzbeck, H. Münstedt and F. Langouche "The strain-hardening behaviour of linear and long-chain-branched polyolefin melts in extensional flows," *Rheol. Acta*, vol. 39, no. 2, pp. 97–109, 2000.
-

- 
- [25] C. Gabriel and H. Münstedt, "Strain hardening of various polyolefins in uniaxial elongational flow," *J. Rheol.*, vol. 47, no. 3, p. 619, 2003.
- [26] H. Münstedt, "Rheological properties and molecular structure of polymer melts," *Soft Matter*, vol. 7, no. 6, p. 2273–2283, 2011.
- [27] F. J. Stadler, J. Kaschta, H. Münstedt, F. Becker, and M. Buback, "Influence of molar mass distribution and long-chain branching on strain hardening of low density polyethylene," *Rheol. Acta*, vol. 48, no. 5, pp. 479–490, 2008.
- [28] F. J. Stadler, A. Nishioka, J. Stange, K. Koyama, and H. Münstedt, "Comparison of the elongational behavior of various polyolefins in uniaxial and equibiaxial flows," *Rheol. Acta*, vol. 46, no. 7, pp. 1003–1012, 2007.
- [29] S. H. Tabatabaei, P. J. Carreau, and A. Aji, "Rheological properties of blends of linear and long-chain branched polypropylenes," *Polym. Eng. Sci.*, vol. 50, no. 1, pp. 191–199, 2010.
- [30] S. Hwan Lee, E. Cho, and J. Ryoung Youn, "Rheological behavior of polypropylene/layered silicate nanocomposites prepared by melt compounding in shear and elongational flows," *J. Appl. Polym. Sci.*, vol. 103, no. 6, pp. 3506–3515, 2007.
- [31] M. Okamoto, P. H. Nam, P. Maiti, T. Kotaka, N. Hasegawa, and A. Usuki, "A House of Cards Structure in Polypropylene/Clay Nanocomposites under Elongational Flow," *Nano Lett.*, vol. 1, no. 6, pp. 295–298, 2001.
- [32] M. Okamoto, P. H. Nam, P. Maiti, T. Kotaka, T. Nakayama, M. Takada, M. Ohshima, A. Usuki, N. Hasegawa, and H. Okamoto, "Biaxial Flow-Induced Alignment of Silicate Layers in Polypropylene/Clay Nanocomposite Foam," *Nano Lett.*, vol. 1, no. 9, pp. 503–505, 2001.
- [33] S. Bhattacharya, R. K. Gupta, M. Jollands, and S. N. Bhattacharya, "Foaming behavior of high-melt strength polypropylene/ clay nanocomposites," *Polym. Eng. Sci.*, vol. 49, no. 10, pp. 2070–2084, 2009.
- [34] J. S. Hong, K. H. Ahn, and S. J. Lee, "Strain hardening behavior of polymer blends with fibril morphology," *Rheol. Acta*, vol. 45, no. 2, pp. 202–208, 2005.
- [35] F. Stastny and R. Gaeth, "Verfahren zur Herstellung poroeser Massen aus Polymerisaten," German patent DE845264, 1950.
- [36] BASF SE, "Plasticsportal.net - Neopolen P." [Online]. Available: [https://www.plasticsportal.net/wa/plasticsEU~de\\_DE/portal/show/content/products/foams/neopolen\\_p](https://www.plasticsportal.net/wa/plasticsEU~de_DE/portal/show/content/products/foams/neopolen_p). [Accessed: 08-Aug-2017].
-

- 
- [37] Kurtz Ersa GmbH, "EPP-Vorschäumer." [Online]. Available: <http://www.kurtzrsa.de/moulding-machines/produkte/schaumstoffmaschinen/vorschaeumer/produkt-details/epp-vorschaeumer.html>. [Accessed: 08-Aug-2017].
- [38] BASF SE, "Infinergy® - The first expanded TPU (flyer)." [Online]. Available: [http://www.polyurethanes.basf.com/pu/solutions/en/function/conversions:/publish/content/group/News\\_und\\_Medien/Polyurethan/Infinergy\\_Flyer\\_EN.pdf](http://www.polyurethanes.basf.com/pu/solutions/en/function/conversions:/publish/content/group/News_und_Medien/Polyurethan/Infinergy_Flyer_EN.pdf). [Accessed: 09-Jan-2020].
- [39] adidas AG, "adidas launches ambitious Sub2 programme with the introduction of its adizero Sub2 marathon shoe," 2017. [Online]. Available: <http://news.adidas.com/global/Latest-News/adidas-launches-ambitious-sub2-programme-with-the-introduction-of-its-adizero-sub2-marathon-shoe/s/cbcfed7b-b3bb-4a77-bcff-73a3927bddb9>. [Accessed: 09-Aug-2017].
- [40] Reuters, "Kipsang misses world record in Tokyo Marathon win." [Online]. Available: <http://www.reuters.com/article/us-athletics-marathon-tokyo-idUSKBN16502L>. [Accessed: 09-Aug-2017].
- [41] T. Köppl, D. Raps, and V. Altstädt, "E-PBT - Bead foaming of poly(butylene terephthalate) by underwater pelletizing," *J. Cell. Plast.*, vol. 50, no. 5, 2014.
- [42] W. Zhai, Y.-W. Kim, D. W. Jung, and C. B. Park, "Steam-Chest Molding of Expanded Polypropylene Foams. 2. Mechanism of Interbead Bonding," *Ind. Eng. Chem. Res.*, vol. 50, no. 9, pp. 5523–5531, 2011.
- [43] P. R. Stupak, W. O. Frye, and J. A. Donovan, "The Effect of Bead Fusion on the Energy Absorption of Polystyrene Foam. Part I: Fracture Toughness," *J. Cell. Plast.*, vol. 27, no. 5, pp. 484–505, 1991.
- [44] J. Rossacci and S. Shivkumar, "Bead fusion in polystyrene foams," *J. Mater. Sci.*, vol. 8, no. 38, pp. 201–206, 2003.
- [45] P. R. Stupak and J. A. Donovan, "The Effect of Bead Fusion on the Energy Absorption of Polystyrene Foam. Part II: Energy Absorption," *J. Cell. Plast.*, vol. 27, no. 5, pp. 506–513, 1991.
- [46] N. Hossieny, A. Ameli, and C. B. Park, "Characterization of Expanded Polypropylene Bead Foams with Modified Steam-Chest Molding," *Ind. Eng. Chem. Res.*, vol. 52, no. 24, pp. 8236–8247, Jun. 2013.
-

- 
- [47] J. Schellenberg and M. Wallis, "Dependence of properties of expandable polystyrene particle foam on degree of fusion," *J. Appl. Polym. Sci.*, vol. 115, no. 5, pp. 2986–2990, 2010.
- [48] D. Raps, N. Hossieny, C. B. Park, and V. Altstädt, "Past and present developments in polymer bead foams and bead foaming technology," *Polymer (Guildf)*, vol. 56, pp. 5–19, 2014.
- [49] U. E. Ozturk and G. Anlas, "Hydrostatic compression of anisotropic low density polymeric foams under multiple loadings and unloadings," *Polym. Test.*, vol. 30, no. 7, pp. 737–742, 2011.
- [50] M. Avalle, G. Belingardi, and R. Montanini, "Characterization of polymeric structural foams under compressive impact loading by means of energy-absorption diagram," *Int. J. Impact Eng.*, vol. 25, no. 5, pp. 455–472, 2001.
- [51] S. Doroudiani and M. T. Kortschot, "Polystyrene foams. III. Structure-tensile properties relationships," *J. Appl. Polym. Sci.*, vol. 90, no. 5, pp. 1427–1434, 2003.
- [52] S. Doroudiani and M. T. Kortschot, "Polystyrene foams. II. Structure-impact properties relationships," *J. Appl. Polym. Sci.*, vol. 90, no. 5, pp. 1421–1426, 2003.
- [53] H. Liu, C. Han, and L. Dong, "Study on the cell structure and compressive behavior of biodegradable poly( $\epsilon$ -caprolactone) foam," *Polym. Eng. Sci.*, vol. 48, no. 12, pp. 2432–2438, 2008.
- [54] W. Gong, J. Gao, M. Jiang, L. He, J. Yu, J. Zhu, "Influence of cell structure parameters on the mechanical properties of microcellular polypropylene materials," *J. Appl. Polym. Sci.*, vol. 122, no. 5, pp. 2907–2914, 2011.
- [55] E. K. Lee, "Novel Manufacturing Processes for Polymer Bead Foams," Dissertation, University of Toronto, 2010.
- [56] S. Doroudiani, C. B. Park, and M. T. Kortschot, "Effect of the crystallinity and morphology on the microcellular foam structure of semicrystalline polymers," *Polym. Eng. Sci.*, vol. 36, no. 21, pp. 2645–2662, 1996.
- [57] R. Britton, *Update on Mouldable Particle Foam Technology*. Smithers Rapra Technology, 2009.
- [58] J. Scheirs and D. Priddy, Eds., *Modern Styrenic Polymers*. John Wiley & Sons Ltd, 2003.
-

- 
- [59] J. Wagner, "Halogenfreie Flammenschutzmittelmischungen für Polystyrol-Schäume," Dissertation, Ruprecht-Karls-Universität Heidelberg, 2012.
- [60] P. Eyerer, T. Hirth, and P. Elsner, *Polymer Engineering*. Springer-Verlag Berlin Heidelberg, 2008.
- [61] T. Köppl, "Halogenfrei flammgeschütztes Polybutylenterephthalat und dessen Verarbeitung zu Polymerschäumen," Dissertation, University of Bayreuth, 2014.
- [62] P. Nising, "Flexible foam production," *Sulzer Tech. Rev.*, vol. 2, pp. 4–7, 2012.
- [63] P. R. Stupak, W. O. Frye, and J. A. Donovan, "The Effect of Bead Fusion on the Energy Absorption of Polystyrene Foam. Part I: Fracture Toughness," *J. Cell. Plast.*, vol. 27, no. 5, pp. 484–505, 1991.
- [64] J. Scheirs and B. P. Duane, *Modern Styrenic Polymers: Polystyrenes and Styrenic Copolymers*. John Wiley & Sons Ltd, 2003.
- [65] C. Doriat, "Den gordischen Knoten durchschlagen," *Kunststoffe*, vol. 2, pp. 55–58, 2017.
- [66] BASF SE, "Styropor® 426 C - Technical Leaflet," 2006. [Online]. Available: <https://www.styropor.com/portal/load/fid1223281/Styropor%C2%AE%20P426%20C.pdf>. [Accessed: 11-Feb-2020].
- [67] G. Mennig and K. Stoeckert, *Mold-Making Handbook*, 3rd Edition. Carl Hanser Verlag GmbH & Co. KG, 2013.
- [68] BASF SE, "Neopolen - General Technical information," 2016. [Online]. Available: <https://products.basf.com/documents/pim;save/en/8810969835989.Neopolen%C2%AE.pdf>. [Accessed: 11-Feb-2020].
- [69] "Cellular Polymers: Conference Proceedings" Forum Hotel, London, UK, 20-22 March 1991," Rapra Technology Ltd, 1991.
- [70] BASF SE, "Datasheet Neopolen® P 8220 K." 2010. [Online]. Available: <https://products.basf.com/documents/pim;save/en/8799338441173.Neopolen%C2%AE%20P%208220%20K.pdf>. [Accessed: 10-Feb-2020].
- [71] BASF SE, "Neopolen P - Designed for New Ideas." 2012. [Online]. Available: <https://products.basf.com/documents/pim;save/de/8798511704533.Neopolen%C2%AE%20%E2%80%92%20Designed%20for%20New%20Ideas.pdf> [Accessed: 10-Feb-2020].
- [72] R. B. Allen, B. M. Kim, and I. D. S. Miller, "Expanding thermoplastic resin beads with very high frequency energy." European patent EP 0425886 A2, September 16, 1990.
-



- 
- [73] P. Eyerer, *Polymers - Opportunities and Risks I: General and Environmental Aspects: Chances and Risks*. Springer-Verlag Berlin Heidelberg, 2010.
- [74] I. Sen, E. Dadush, and D. Penumadu, "Microwave-assisted foaming of expandable polystyrene beads," *J. Cell. Plast.*, vol. 47, no. 1, pp. 65–79, 2011.
- [75] J. Zhou, J. Song, and R. Parker, "Structure and properties of starch-based foams prepared by microwave heating from extruded pellets," *Carbohydr. Polym.*, vol. 63, no. 4, pp. 466–475, Mar. 2006.
- [76] J. Zhou, J. Song, and R. Parker, "Microwave-assisted moulding using expandable extruded pellets from wheat flours and starch," *Carbohydr. Polym.*, vol. 69, no. 3, pp. 445–454, 2007.
- [77] X. Peng, J. Song, A. Nesbitt, and R. Day, "Microwave foaming of starch-based materials (I) dielectric performance," *J. Cell. Plast.*, vol. 49, no. 3, pp. 245–258, 2013.
- [78] X. Peng, J. Song, A. Nesbitt, and R. Day, "Microwave foaming of starch-based materials (II) thermo-mechanical performance," *J. Cell. Plast.*, vol. 49, no. 2, pp. 147–160, 2013.
- [79] V. Romanov, "Device and method for producing a particle foam part" International patent WO 2017/125412, July 27, 2017.
- [80] P. Svec, *et al.*, *Styrene Based Plastics and Their Modifications*. Ellis Horwood Ltd, 1990.
- [81] R. Pop-Iliev, G. M. Rizvi, and C. B. Park, "The importance of timely polymer sintering while processing polypropylene foams in rotational molding," *Polym. Eng. Sci.*, vol. 43, no. 1, pp. 40–54, 2003.
- [82] R. Pop-Iliev, "Manufacture of Integral Skin PP Foam Composites in Rotational Molding," *J. Cell. Plast.*, vol. 42, no. 2, pp. 139–152, 2006.
- [83] C. T. Bellehumeur and J. S. Tiang, "Simulation of non-isothermal melt densification of polyethylene in rotational molding," *Polym. Eng. Sci.*, vol. 42, no. 1, pp. 215–229, 2002.
- [84] N. J. Mills, *Polymer Foams Handbook*. Elsevier, 2007.
- [85] S. Nakai, K. Taki, I. Tsujimura, and M. Ohshima, "Numerical Simulation of a Polypropylene Foam Bead Expansion Process," *Polym. Eng. Sci.*, vol. 48, no. 1, pp. 107–115, 2008.
-

- 
- [86] W. Zhai, Y.-W. Kim, and C. B. Park, "Steam-Chest Molding of Expanded Polypropylene Foams. 1. DSC Simulation of Bead Foam Processing," *Ind. Eng. Chem. Res.*, vol. 49, no. 20, pp. 9822–9829, 2010.
- [87] M. Sands, "An Analysis of Mold Filling and Defect Formation in Lost Foam Castings," M.Sc. thesis, Worcester Polytechnic Institute, 1998.
- [88] Holger Deutges, "Understanding the Formation of a Solid Skin Around EPS-Beads and its Effect on the Properties of the Foamed Part," M.Sc. thesis, University of Bayreuth, 2016.
- [89] F. Yang and R. Pitchumani, "Healing of Thermoplastic Polymers at an Interface under Nonisothermal Conditions," *Macromolecules*, vol. 35, no. 8, pp. 3213–3224, 2002.
- [90] R. P. Wool, B.-L. Yuan, and O. J. McGarel, "Welding of polymer interfaces," *Polym. Eng. Sci.*, vol. 29, no. 19, pp. 1340–1367, 1989.
- [91] C. A. Butler, R. L. Mccullough, R. Pitchumani, and J. W. Gillespie, "An Analysis of Mechanisms Governing Fusion Bonding of Thermoplastic Composites," *J. Thermoplast. Compos. Mater.*, vol. 11, no. 4, pp. 338–363, Jul. 1998.
- [92] M. Bousmina, H. Qiu, M. Grmela, and J. E. Klemberg-Sapieha, "Diffusion at Polymer/Polymer Interfaces Probed by Rheological Tools," *Macromolecules*, vol. 31, no. 23, pp. 8273–8280, 1998.
- [93] S. Prager, "The healing process at polymer–polymer interfaces," *J. Chem. Phys.*, vol. 75, no. 10, p. 5194, 1981.
- [94] Y. H. Kim and R. P. Wool, "A theory of healing at a polymer-polymer interface," *Macromolecules*, vol. 16, no. 7, pp. 1115–1120, 1983.
- [95] H. J. Kim, K.-J. Lee, and H. H. Lee, "Healing of fractured polymers by interdiffusion," *Polymer (Guildf.)*, vol. 37, no. 20, pp. 4593–4597, 1996.
- [96] H. Qiu and M. Bousmina, "Determination of Mutual Diffusion Coefficients at Nonsymmetric Polymer/Polymer Interfaces from Rheometry," *Macromolecules*, vol. 33, no. 17, pp. 6588–6594, 2000.
- [97] H. Qiu, M. Bousmina, and J. M. Dealy, "Coupling between flow and diffusion at polymer/polymer interfaces: large amplitude oscillatory shear experiments," *Rheol. Acta*, vol. 41, no. 1–2, pp. 87–92, 2002.
- [98] M. Nofar, Y. Guo, and C. B. Park, "Double Crystal Melting Peak Generation for Expanded Polypropylene Bead Foam Manufacturing," *Ind. Eng. Chem. Res.*, vol. 52, no. 6, pp. 2297–2303, 2013.
-

- 
- [99] J. B. Choi, M. J. Chung, and J. S. Yoon, "Formation of Double Melting Peak of Poly(propylene-co-ethylene-co-1-butene) during the Preexpansion Process for Production of Expanded Polypropylene," *Ind. Eng. Chem. Res.*, vol. 44, no. 8, pp. 2776–2780, 2005.
- [100] M. Nofar, A. Ameli, and C. B. Park, "Expanded polylactide bead foaming - A new technology," *AIP Conf. Proc.*, vol. 1664, pp. 1–6, 2015.
- [101] A. Patel and M. K. Farooqui, "Processing and Characterization of Autoclave-based EPP Beads," M.Eng. Project Report, University of Toronto, 2010.
- [102] J. Gensel, C. Pawelski, and V. Altstädt, "Welding Quality in Polymer Bead Foams : an in situ SEM Study," *AIP Conference Proceedings*, vol. 1914, 060001, 2017.
- [103] N. J. Mills and A. Gilcrist, "Shear and Compressive Impact of Polypropylene Bead Foam," *Cell. Polym.*, vol. 18, no. 3, pp. 157–174, 1999.
- [104] D. Klempner and V. Sendjarevic, *Handbook of Polymeric Foams and Foam Technology*. Carl Hanser Verlag GmbH & Co. KG, 2004.
- [105] N. J. Mills, "Time Dependence of the Compressive Response of Polypropylene Bead Foam," *Cell. Polym.*, vol. 16, no. 3, pp. 194–215, 1997.
- [106] S. Nakai, K. Taki, I. Tsujimura, and M. Ohshima, "Numerical simulation of a polypropylene foam bead expansion process," *Polym. Eng. Sci.*, vol. 48, no. 1, pp. 107–115, 2008.
- [107] C.-T. Yang and S.-T. Lee, "Dimensional Stability Analysis of Foams Based on LDPE And Ethylene-Styrene Interpolymer Blends," *J. Cell. Plast.*, vol. 39, no. 1, pp. 59–69, 2003.
- [108] G. Frederick, G. A. Kaepf, C. M. Kudelko, P. J. Schuster, F. Domas, U. G. Haardt, W. Lenz, "Optimization of Expanded Polypropylene Foam Coring to Improve Bumper Foam Core Energy Absorbing Capability," *SAE Technical Paper 950549*, 1995.
- [109] A. Mahapatro, N. J. Mills, and G. L. A. Sims, "Experiments and modelling of the expansion of crosslinked polyethylene foams," *Cell. Polym.*, vol. 17, no. 4, pp. 252–270, 1998.
- [110] I. Beverte, "Elastic constants of monotropic plastic foams. 2. Deformation parallel to foam rise direction. Numerical calculations," *Mech. Compos. Mater.*, vol. 34, no. 2, pp. 115–122, 1998.
-

- [111] L. J. Gibson and M. Ashby, *Cellular solids*. Cambridge, 1999.
- [112] S. Deschanel, L. Vanel, N. Godin, E. Maire, G. Vigier, and S. Ciliberto, "Mechanical response and fracture dynamics of polymeric foams," *J. Phys. D. Appl. Phys.*, vol. 42, no. 21, p. 214001, 2009.
- [113] J. L. Grenestedt, "Influence of wavy imperfections in cell walls on elastic stiffness of cellular solids," *J. Mech. Phys. Solids*, vol. 46, no. 1, pp. 29–50, 1998.
- [114] J. L. Grenestedt and F. Bassinet, "Influence of cell wall thickness variations on elastic stiffness of closed-cell cellular solids," *Int. J. Mech. Sci.*, vol. 42, no. 7, pp. 1327–1338, 2000.
- [115] J. L. Grenestedt and K. Tanaka, "Influence of cell shape variations on elastic stiffness of closed cell cellular solids," *Scr. Mater.*, vol. 40, no. 1, pp. 71–77, 1998.
- [116] L. Sorrentino, M. Aurilia, and S. Iannace, "A simple method to predict high strain rates mechanical behavior of low interconnected cell foams," *Polym. Test.*, vol. 26, no. 7, pp. 878–885, 2007.
- [117] R. P. Juntunen, V. Kumar, J. E. Weller, and W. P. Bezubic, "Impact strength of high density microcellular poly(vinyl chloride) foams," *J. Vinyl Addit. Technol.*, vol. 6, no. 2, pp. 93–99, 2000.
- [118] C. Barlow, V. Kumar, B. Flinn, R. K. Bordia, and J. Weller, "Impact Strength of High Density Solid-State Microcellular Polycarbonate Foams," *J. Eng. Mater. Technol.*, vol. 123, no. 2, p. 229, 2001.
- [119] L. Di Landro, G. Sala, and D. Olivieri, "Deformation mechanisms and energy absorption of polystyrene foams for protective helmets," *Polym. Test.*, vol. 21, no. 2, pp. 217–228, 2002.
- [120] N. J. Mills and A. S. I. Moosa, "Impacts of Hemispherical Strikers on Polystyrene Bead Foam," *J. Cell. Plast.*, vol. 35, pp. 289–310, 1999.
- [121] P. R. Stupak and J. A. Donovan, "The Effect of Bead Fusion on the Energy Absorption of Polystyrene Foam. Part II: Energy Absorption," *J. Cell. Plast.*, vol. 27, no. 5, pp. 506–513, 1991.
- [122] P. Viot, D. Bernard, and E. Plougonven, "Polymeric foam deformation under dynamic loading by the use of the microtomographic technique," *J. Mater. Sci.*, vol. 42, no. 17, pp. 7202–7213, 2007.

- 
- [123] P. Viot, E. Plougonven, and D. Bernard, "Microtomography on polypropylene foam under dynamic loading: 3D analysis of bead morphology evolution," *Compos. Part A Appl. Sci. Manuf.*, vol. 39, no. 8, pp. 1266–1281, 2008.
- [124] C. Motz and R. Phippan, "Fracture behaviour and fracture toughness of ductile closed-cell metallic foams," *Acta Mater.*, vol. 50, no. 8, pp. 2013–2033, 2002.
- [125] L. Marsavina and T. Sadowski, "Dynamic fracture toughness of polyurethane foam," *Polym. Test.*, vol. 27, no. 8, pp. 941–944, 2008.
- [126] E. E. Saenz, L. A. Carlsson, and A. Karlsson, "Characterization of fracture toughness ( $G_c$ ) of PVC and PES foams," *J. Mater. Sci.*, vol. 46, no. 9, pp. 3207–3215, 2011.
- [127] E. E. Saenz, L. A. Carlsson, and A. M. Karlsson, "In situ analysis of crack propagation in polymer foams," *J. Mater. Sci.*, vol. 46, no. 16, pp. 5487–5494, 2011.
- [128] M. E. Kabir, M. C. Saha, and S. Jeelani, "Tensile and fracture behavior of polymer foams," *Mater. Sci. Eng. A*, vol. 429, no. 1–2, pp. 225–235, 2006.
- [129] E. M. Wouterson, F. Y. C. Boey, X. Hu, and S.-C. Wong, "Fracture and Impact Toughness of Syntactic Foam," *J. Cell. Plast.*, vol. 40, no. 2, pp. 145–154, 2004.
- [130] D. Arencón, M. Antunes, A. B. Martínez, and J. I. Velasco, "Study of the fracture behavior of flexible polypropylene foams using the Essential Work of Fracture (EWF)," *Polym. Test.*, vol. 31, no. 2, pp. 217–225, 2012.
- [131] P. Thiyagasundaram, J. Wang, B. V. Sankar, and N. K. Arakere, "Fracture toughness of foams with tetrakaidecahedral unit cells using finite element based micromechanics," *Eng. Fract. Mech.*, vol. 78, no. 6, pp. 1277–1288, 2011.
- [132] S. Choi and B. V. Sankar, "A micromechanical method to predict the fracture toughness of cellular materials," *Int. J. Solids Struct.*, vol. 42, no. 5–6, pp. 1797–1817, 2005.
- [133] N. J. Mills and P. Kang, "The Effect of Water Immersion on the Mechanical Properties of Polystyrene Bead Foam Used in Soft Shell Cycle Helmets," *J. Cell. Plast.*, vol. 30, no. 3, pp. 196–222, 1994.
- [134] P. Ferkl, R. Pokorný, M. Bobák, and J. Kosek, "Heat transfer in one-dimensional micro- and nano-cellular foams," *Chem. Eng. Sci.*, vol. 97, pp. 50–58, 2013.
- [135] D. Hansen and G. A. Bernier, "Thermal conductivity of polyethylene: The effects of crystal size, density and orientation on the thermal conductivity," *Polym. Eng. Sci.*, vol. 12, no. 3, pp. 204–208, 1972.
-

- 
- [136] D. Hansen and C. C. Ho, "Thermal conductivity of high polymers," *J. Polym. Sci. Part A Gen. Pap.*, vol. 3, no. 2, pp. 659–670, 1965.
- [137] C. L. Choy, F. C. Chen, W. H. Luk, and I. I. Arle, "Thermal Conductivity of Oriented Crystalline Polymers," vol. 18, pp. 1187–1207, 1980.
- [138] S. S. Sundarram and W. Li, "On thermal conductivity of micro- and nanocellular polymer foams," *Polym. Eng. Sci.*, vol. 53, no. 9, pp. 1901–1909, 2013.
- [139] T. Xie, Y.-L. He, and Z.-J. Hu, "Theoretical study on thermal conductivities of silica aerogel composite insulating material," *Int. J. Heat Mass Transf.*, vol. 58, no. 1–2, pp. 540–552, 2013.
- [140] A. Kaemmerlen, C. Vo, F. Asllanaj, G. Jeandel, and D. Baillis, "Radiative properties of extruded polystyrene foams: Predictive model and experimental results," *J. Quant. Spectrosc. Radiat. Transf.*, vol. 111, no. 6, pp. 865–877, 2010.
- [141] C. Tseng and K. Kuo, "Thermal radiative properties of phenolic foam insulation," *J. Quant. Spectrosc. Radiat. Transf.*, vol. 72, no. 4, pp. 349–359, 2002.
- [142] R. Caps, U. Heinemann, J. Fricke, and K. Keller, "Thermal conductivity of polyimide foams," *Int. J. Heat Mass Transf.*, vol. 40, no. 2, pp. 269–280, 1997.
- [143] R. Coquard, D. Rochais, and D. Baillis, "Experimental investigations of the coupled conductive and radiative heat transfer in metallic/ceramic foams," *Int. J. Heat Mass Transf.*, vol. 52, no. 21–22, pp. 4907–4918, 2009.
- [144] R. C. Progelhof, J. L. Throne, and R. R. Ruetsch, "Methods for predicting the thermal conductivity of composite systems: A review," *Polym. Eng. Sci.*, vol. 16, no. 9, pp. 615–625, 1976.
- [145] R. Coquard and D. Baillis, "Numerical investigation of conductive heat transfer in high-porosity foams," *Acta Mater.*, vol. 57, no. 18, pp. 5466–5479, 2009.
- [146] P. Ferkl, R. Pokorný, and J. Kosek, "Multiphase approach to coupled conduction–radiation heat transfer in reconstructed polymeric foams," *Int. J. Therm. Sci.*, vol. 83, pp. 68–79, 2014.
- [147] BASF SE, "Neopor® Downloads." [Online]. Available: [https://www.plasticsportal.net/wa/plasticsEU~de\\_DE/portal/show/content/products/foams/neopor\\_downloads](https://www.plasticsportal.net/wa/plasticsEU~de_DE/portal/show/content/products/foams/neopor_downloads). [Accessed: 02-Sep-2017].
- [148] R. Coquard, D. Baillis, and D. Quenard, "Experimental and theoretical study of the hot-wire method applied to low-density thermal insulators," *Int. J. Heat Mass Transf.*, vol. 49, no. 23–24, pp. 4511–4524, 2006.
-

- 
- [149] C. Y. Zhao, S. A. Tassou, and T. J. Lu, "Analytical considerations of thermal radiation in cellular metal foams with open cells," *Int. J. Heat Mass Transf.*, vol. 51, no. 3–4, pp. 929–940, 2008.
- [150] C. Schips, K. Hahn, M. Hofmann, H. Ruckdäschel, J. Assmann, G. Janssens, G. Gräbel, J. Lambert, and C. Zylla, "Elastic particle foam based on polyolefin/styrene polymer mixtures," U.S. patent US 8729143 B2, 2014.
- [151] K. Hahn, G. Ehrmann, J. Ruch, *et al.*, "Method of producing expandable polystyrene mixtures," European patent EP 1694753 B1, 2010.
- [152] F.-J. Dietzen, G. Ehrmann, B. Schmied, *et al.*, "Method for producing expandable polystyrene" U.S. patent US 7776244 B2, 2010.
- [153] D. Raps, T. Köppl, L. Heymann, and V. Altstädt, "Rheological behaviour of a high-melt-strength polypropylene at elevated pressure and gas loading for foaming purposes," *Rheol. Acta*, vol. 56, no. 2, pp. 95–111, 2017.
- [154] O. A. Hasan and M. C. Boyce, "Energy storage during inelastic deformation of glassy polymers," *Polymer (Guildf.)*, vol. 34, no. 24, pp. 5085–5092, 1993.
- [155] N. J. Mills, R. Stämpfli, F. Marone, and P. A. Brühwiler, "Finite element micromechanics model of impact compression of closed-cell polymer foams," *Int. J. Solids Struct.*, vol. 46, no. 3–4, pp. 677–697, 2009.
- [156] A. P. Roberts and E. J. Garboczi, "Elastic moduli of model random three-dimensional closed-cell cellular solids," *Acta Mater.*, vol. 49, pp. 189–197, 2001.
- [157] S. Deschanel, L. Vanel, N. Godin, E. Maire, G. Vigier, and S. Ciliberto, "Mechanical response and fracture dynamics of polymeric foams," *J. Phys. D. Appl. Phys.*, vol. 42, no. 21, p. 214001, 2009.
- [158] M. C. M. van der Sanden, H. E. H. Meijer, and P. J. Lemstra, "Deformation and toughness of polymeric systems: 1. The concept of a critical thickness," *Polymer (Guildf.)*, vol. 34, no. 10, pp. 2148–2154, 1993.
- [159] R. Gendron and M. F. Champagne, "Effect of Physical Foaming Agents on the Viscosity of Various Polyolefin Resins," *J. Cell. Plast.*, vol. 40, no. 2, pp. 131–143, 2004.
- [160] F. Dresel, "Macro- and Microdeformation Phenomena of Bead Foams in Dependency of their Morphology," M.Sc. Thesis, University of Bayreuth, 2016.
- [161] P. Antich, A. Vázquez, I. Mondragon, and C. Bernal, "Mechanical behavior of high impact polystyrene reinforced with short sisal fibers," *Compos. Part A Appl. Sci. Manuf.*, vol. 37, no. 1, pp. 139–150, 2006.
-



- 
- [162] C. Lee, M.-L. Lu, and F. Chang, "Fracture toughness of high-impact polystyrene based on three j-integral methods," *J. Appl. Polym. Sci.*, vol. 47, no. 10, pp. 1867–1880, 1993.
- [163] B. Notario, J. Pinto, E. Solorzano, J. A. de Saja, M. Dumon, and M. A. Rodríguez-Pérez, "Experimental validation of the Knudsen effect in nanocellular polymeric foams," *Polymer (Guildf.)*, vol. 56, pp. 57–67, 2015.
- [164] E. A. Algaer, M. Alaghemandi, M. C. Böhm, and F. Müller-Plathe, "Anisotropy of Thermal conductivity of amorphous polystyrene in supercritical carbon dioxide studied by reverse nonequilibrium molecular dynamics simulations.," *J. Phys. Chem. A*, vol. 113, no. 43, pp. 11487–94, 2009.
- [165] VDI e.V. (Hrsg.), *VDI-Wärmeatlas*, Springer-Verlag Berlin Heidelberg, 2013.
- [166] K.-E. Wagner, "Simulation und Optimierung des Wärmedämmvermögens von PUR-Hartschaum," Dissertation, Universität Stuttgart, 2002.
- [167] D. R. Lide, Ed., *CRC Handbook of Chemistry and Physics. 84th Edition*. CRC Press, 2003.
- [168] "Black-body spectrum for temperatures between 300 K and 10,000 K in a log-log diagram ", [Online] Available: [https://commons.wikimedia.org/wiki/File:BlackbodySpectrum\\_loglog\\_150dpi\\_en.png](https://commons.wikimedia.org/wiki/File:BlackbodySpectrum_loglog_150dpi_en.png). [Accessed: 10-Feb-2020].
- [169] V. Kumar and J. E. Weller, "A model for the unfoamed skin on microcellular foams," *Polym. Eng. Sci.*, vol. 34, no. 3, pp. 169–173, Feb. 1994.
- [170] M. F. J. Berghmans, K. C. Bleijenberg, J. Teubert, and A. C. G. Metsaars, "Process for processing expandable polymer particles and foam article thereof" U.S. patent US7358280 B2, 2008.
- [171] "Production process of EPS (Expanded Polystyrene) plate," Chinese patent CN102825716 A, 2012.
- [172] B.-K. Ahn, S.-H. Baek, K.-H. Yoo, J.-U. Lee, and J.-C. Won, "Process for preparing expandable polystyrene resin and expandable polystyrene resin composition," International patent WO2006038751 A1, 2005.
- [173] D. A. Brandreth and H. G. Ingersoll, "Accelerated Aging of Rigid Polyurethane Foam," *J. Cell. Plast.*, vol. 16, no. 4, pp. 235–238, 1980.
- [174] D. W. Reitz, M. A. Schuetz, and L. R. Glicksman, "A Basic Study of Aging of Foam Insulation," *J. Cell. Plast.*, vol. 20, no. 2, pp. 104–113, 1984.
-

## Curriculum Vitae

### Personal data

*Name* Daniel Raps

*Address* Kurt-Schumacher-Ring 109  
D-51377 Leverkusen  
Germany

*Phone* +49 157 54177541  
*E-Mail* daniel.raps@gmx.net

*Date of birth* 03.01.1988  
*Place of birth* Reichenbach i.V.



### Professional career

*11/2011 – 03/2012* Internship at **Colormatrix** (Liverpool, UK)

*02/2013 – 10/2017* **Scientific member** at the Chair of Polymer Engineering,  
University of Bayreuth

*11/2017 – 12/2019* **Laboratory Head for Thermal Analysis**  
*From 01/2020* **Laboratory Head in Polyurethane Product Research**  
at Covestro Deutschland AG

### Schooling and higher education

*08/1994 - 06/2007* Primary school and **Gymnasium** (Degree: Abitur (A-level equivalent))

*10/2007 – 01/2013* **“Materials science and engineering”** at the  
University of Bayreuth, Germany (Degree: Dipl.-Ing.  
(Master-equivalent))  
**Diploma-thesis:** „Quantification of blowing agent  
influence on the rheological properties during foaming  
of high melt strength Polypropylene“

## List of publications

### 2014

- D. Raps, T. Köppl, A. Rios De Anda, V. Altstädt, "Rheological and crystallisation behaviour of high melt strength polypropylene under gas-loading," *Polymer*, 2014
- T. Köppl, D. Raps, V. Altstädt, "E-PBT - Bead foaming of Poly(butylene terephthalate) by underwater pelletizing," *J. Cell. Plast.*, 2014
- D. Raps, N. Hossieny, C. B. Park, V. Altstädt, "Past and present developments in polymer bead foams and bead foaming technology," *Polymer*, 2014

### 2015

- C. Okolieocha, D. Raps, K. Subramaniam, V. Altstädt, "Microcellular to nanocellular polymer foams: Progress (2004 – 2015) and future directions – A review," *Eur. Polym. J.*, 2015
- D. Raps, A. Fathi, V. Altstädt, "Bead Foams: Current Trends and Developments in Progress", *FOAMS 2015 – Conference Proceedings*, 2015

### 2016

- D. Raps, S. A. Sanchez-Vazquez, L. Heymann, V. Altstädt, "Exploring the rheology and crystallisation of Polypropylene with dissolved CO<sub>2</sub> using a pressure cell," *GIT Laborjournal*, 2016

### 2017

- D. Raps, T. Köppl, L. Heymann, V. Altstädt, "Rheological behaviour of a high melt strength polypropylene at elevated pressure and gas-loading for foaming purposes," *Rheologica Acta*, 2017
- T. Moss, I. Paulus, D. Raps, V. Altstädt, Greiner, "Ultralight scaffolds of poly(para-xylylene) by template assisted chemical vapour deposition," *e-Polym.*, 2017

### 2018

- H. Goodarzi Hosseinabadi, R. Bagheri, T. Gigl, C. Hugenschmidt, D. Raps, V. Altstädt, "On the mismatch of applied strain field and free volume distribution: clues to uncover the unknown origin of post-yield softening in polymers," *Expr. Polym. Lett.*, 2018

### 2019

- C. Keilholz, D. Raps, T. Köppl, V. Altstädt, "Influence of nucleating agent type on the morphology of extruded polyetherimide foam for printed circuit boards," *J. Cell. Plast.*, 2019

- S. A. Sanchez-Vazquez, C. Bethke, D. Raps, G. Bakis, S. Bard, Du Ngoc Uy Lan, V. Altstädt, "Effect of Resin and Blocked/Unblocked Hardener Mixture on the Production of Epoxy Foams with CO<sub>2</sub> Blocked Hardener in Batch Foaming Process," *Polymers*, 2019
- Du Ngoc Uy Lan, D. Raps, V. Altstädt, *et al.*: "Viscoelastic Epoxy Foams by Aqueous Emulsion Foaming Process," *J. Cell. Plast.*, 2019
- S. A. Sanchez-Vazquez, M. Demleitner, D. Raps, G. Bakis, T. Pflock, A. Chalupka, V. Altstädt, "Dielectric analysis monitoring of thermoset curing with ionic liquids: from modelling to the prediction in the resin transfer moulding process," *Polym. Comp.*, 2019

## 2020

- D. Raps, N. Weingart, M. Lu, L. Endner, V. Altstädt: "Comparison of the Foamability of Linear and Long-Chain Branched Polypropylene: The Legend of Strain-Hardening as a Requirement for Good Foamability," *Polymers*, 2020
- N. Weingart, D. Raps, J. Kuhnigk, V. Altstädt: "Expanded Polycarbonate (EPC) - A New Generation of High-Temperature Engineering Bead Foams," *Polymers*, 2020

## Book chapters

- Contributions to ULLMANN'S Encyclopedia of Industrial Chemistry, chapter Foamed Plastics, Wiley-VCH Verlag GmbH & Co. KGaA, 2016
- Contributions to the Polypropylene Handbook, chapter "Foams", Springer, 2019

## Patents

- "Expanded polyamide pellets and method for manufacturing molded components using them", International patent WO 2016030333 A1